

# CONTRACTOR REPORT

RS-8232-2/ 70179

8524

SAND89-7067  
Unlimited Release  
UC-721



8232-2//070179



00000001 -

## Analysis of the Fluid-Pressure Responses of the Rustler Formation at H-16 to the Construction of the Air-Intake Shaft at the Waste Isolation Pilot Plant (WIPP) Site

John D. Avis, George J. Saulnier, Jr.  
INTERA Inc.  
6850 Austin Center Blvd., Suite 300  
Austin, TX 78731

Prepared by Sandia National Laboratories Albuquerque, New Mexico 87185  
and Livermore, California 94550 for the United States Department of Energy  
under Contract DE-AC04-76DP00789

Printed March 1990

Issued by Sandia National Laboratories, operated for the United States Department of Energy by Sandia Corporation.

**NOTICE:** This report was prepared as an account of work sponsored by an agency of the United States Government. Neither the United States Government nor any agency thereof, nor any of their employees, nor any of their contractors, subcontractors, or their employees, makes any warranty, express or implied, or assumes any legal liability or responsibility for the accuracy, completeness, or usefulness of any information, apparatus, product, or process disclosed, or represents that its use would not infringe privately owned rights. Reference herein to any specific commercial product, process, or service by trade name, trademark, manufacturer, or otherwise, does not necessarily constitute or imply its endorsement, recommendation, or favoring by the United States Government, any agency thereof or any of their contractors or subcontractors. The views and opinions expressed herein do not necessarily state or reflect those of the United States Government, any agency thereof or any of their contractors.

Printed in the United States of America. This report has been reproduced directly from the best available copy.

Available to DOE and DOE contractors from  
Office of Scientific and Technical Information  
PO Box 62  
Oak Ridge, TN 37831

Prices available from (615) 576-8401, FTS 626-8401

Available to the public from  
National Technical Information Service  
US Department of Commerce  
5285 Port Royal Rd  
Springfield, VA 22161

NTIS price codes  
Printed copy: A09  
Microfiche copy: A01

**ANALYSIS OF THE FLUID-PRESSURE RESPONSES  
OF THE RUSTLER FORMATION AT H-16  
TO THE CONSTRUCTION OF THE AIR-INTAKE SHAFT  
AT THE WASTE ISOLATION PILOT PLANT (WIPP) SITE\***

John D. Avis and George J. Saulnier, Jr.  
INTERA Inc.  
6850 Austin Center Blvd., Suite 300  
Austin, Texas 78731

ABSTRACT

The construction of the air-intake shaft (AIS) at the Waste Isolation Pilot Plant (WIPP) site in 1987 and 1988 initiated fluid-pressure responses which were used to estimate the hydrologic properties of the Culebra Dolomite, Magenta Dolomite, and Forty-niner Members of the Rustler Formation. Fluid-pressure responses were monitored with downhole transducers at observation-well H-16, about 17 meters (m) northwest of the AIS, and water-level responses were observed and measured in observation wells H-1, ERDA-9, and WIPP-21, the closest observation wells to the AIS.

The AIS pilot hole, with a 0.25-m diameter, was drilled to a depth of 650 m and reamed to a diameter of 0.37 m. The pilot hole remained open and draining to the underground facility for about three months. The pilot hole was then upreamed (raise bored) to a 6.17-m diameter shaft from the underground facility to land surface. The pilot hole was drilled and reamed using a bentonite-mud-based brine as a drilling fluid. During the construction period, the fluid-pressure responses of the the Culebra dolomite were also affected by grouting and sealing of the Rustler Formation in the waste-handling shaft (WHS), by a multipad/tracer test at the H-11 hydropad in the southern WIPP site, and by water-quality sampling at WIPP-19 and H-15.

The well-test simulator GTFM was used to analyze the fluid-pressure responses of the Culebra and Magenta dolomites and the Forty-niner claystone. The AIS was modeled as a test well with a zero-wellbore-pressure boundary condition. H-16 was modeled as an observation well. The pilot-hole drilling/reaming period was modeled as a wellbore-history period and was simulated separately for each unit whose fluid-pressure responses

\* The work described in this report was done for Sandia National Laboratories under Contract No. 32-1025.

were analyzed. A cement-invasion skin was used in simulating the Culebra dolomite's drilling/reaming period. A mud-filter-cake skin was used to create reduced wellbore pressures in simulating the pilot-hole drilling/reaming periods of the Magenta dolomite and Forty-niner claystone.

The estimated Culebra transmissivity ranged from  $1.3 \times 10^{-7}$  to  $6.6 \times 10^{-7} \text{ m}^2/\text{s}$ . The most representative transmissivity of the Culebra between H-16 and the AIS was estimated to be  $6.6 \times 10^{-7} \text{ m}^2/\text{s}$ . This estimate was obtained by calibrating the simulation of the Culebra's H-16 fluid-pressure response to a measurement of the flow rate from the Culebra to the AIS made 133 days after the upreaming of the Culebra. The transmissivity of the Culebra between the AIS and observation-wells H-1, ERDA-9, and WIPP-21 was estimated to range from  $1 \times 10^{-6} \text{ m}^2/\text{s}$  to  $1 \times 10^{-7} \text{ m}^2/\text{s}$ .

Radial formation-heterogeneity boundaries were employed to simulate the H-16 fluid-pressure responses in the Magenta dolomite and the Forty-niner claystone. The formation-heterogeneity boundary for the Magenta dolomite was estimated to be 40 m from the AIS with a near-field transmissivity of  $8.0 \times 10^{-8} \text{ m}^2/\text{s}$  and a far-field transmissivity of  $3.5 \times 10^{-8} \text{ m}^2/\text{s}$ . The formation-heterogeneity boundary for the Forty-niner claystone was also estimated to be 40 m from the AIS with a near-field transmissivity of  $9.0 \times 10^{-9} \text{ m}^2/\text{s}$  and a far-field transmissivity of  $1.3 \times 10^{-9} \text{ m}^2/\text{s}$ .

GTFM was used to simulate the flow rates of ground water draining from the Culebra dolomite, the Magenta dolomite, and the Forty-niner claystone to the open AIS. The simulated Culebra flow rate on the day of the water-ring measurement in the AIS was 0.058 L/s and is in excellent agreement with the measured rate of 0.056 L/s indicating an acceptable model calibration. One hundred days after upreaming, the simulated Culebra flow-rate was 0.06 L/s, the simulated Magenta flow rate was 0.007 L/s, and the simulated Forty-niner flow rate was 0.0004 L/s. The simulated Forty-niner flow-rate curve indicated a transition to the less-permeable, far-field system after 15 days.

## CONTENTS

1.0 INTRODUCTION .....	1-1
1.1 Background .....	1-1
1.2 Objectives .....	1-2
2.0 MONITORING SYSTEMS .....	2-1
2.1 H-16 Multipacker Monitoring System .....	2-2
2.2 Observation Wells .....	2-3
3.0 AIR-INTAKE SHAFT CONSTRUCTION HISTORY .....	3-1
3.1 Pilot Hole .....	3-1
3.1.1 Drilling .....	3-2
3.1.2 Reaming .....	3-3
3.2 Upreaming of the Air-Intake Shaft .....	3-4
4.0 OTHER HYDROLOGIC ACTIVITIES AFFECTING HYDROLOGIC RESPONSES .....	4-1
4.1 Aquifer Testing .....	4-1
4.2 Water-Quality Sampling .....	4-2
4.3 Grouting in the Waste-Handling Shaft .....	4-2
5.0 INTERPRETATION METHODOLOGY .....	5-1
5.1 GTFM Well-Test Simulator .....	5-1
5.2 Drilling-Period Wellbore Boundary Conditions .....	5-5
5.2.1 Mud-Related Uncertainties .....	5-8
5.2.2 Flow Reduction .....	5-8
5.2.3 Filter-Cake Skin .....	5-10
5.3 Wellbore Boundary Conditions After Penetration of the Underground Facility .....	5-12
5.4 Formation Heterogeneities .....	5-12
5.4.1 Cement-Invasion Skin .....	5-12
5.4.2 Radial Heterogeneity Boundaries .....	5-13
5.5 Diffusivity Relationship .....	5-14

CONTENTS (cont.)

6.0 ESTIMATION OF TRANSMISSIVITIES .....	6-1
6.1 Culebra Dolomite .....	6-2
6.1.1 Simulation Results .....	6-5
6.1.2 Discussion of Simulation Results .....	6-8
6.2 Magenta Dolomite .....	6-10
6.2.1 Simulation Results .....	6-11
6.2.2 Discussion of Simulation Results .....	6-15
6.3 Forty-Niner Claystone .....	6-16
6.3.1 Simulation Results .....	6-19
6.3.2 Discussion of Simulation Results .....	6-22
7.0 POTENTIAL LEAKAGE INTO THE AIR-INTAKE SHAFT .....	7-1
8.0 SUMMARY AND CONCLUSIONS .....	8-1
8.1 General .....	8-1
8.2 Summary of Transmissivities .....	8-4
8.2.1 Culebra Dolomite.....	8-4
8.2.2 Magenta Dolomite.....	8-5
8.2.3 Forty-Niner Claystone .....	8-6
8.3 Conclusions .....	8-7
9.0 REFERENCES .....	9-1
APPENDIX A: Specified and Simulated Wellbore Pressures and Simulated and Observed Formation Fluid Pressures for the Drilling/Reaming Periods of the Simulations of the H-16 Fluid-Pressure Responses of the Culebra Dolomite, the Magenta Dolomite, and the Forty- Niner Claystone .....	A-1

## FIGURES

Figure 1.1	Locations of the Air-Intake Shaft and Other Underground- Access Shafts Relative to the WIPP-Site Observation-Well Network .....	1-3
Figure 1.2	Schematic Illustration of the WIPP-Site Underground-Access Shafts and the Underground Facility.....	1-4
Figure 1.3	Generalized Stratigraphy of the Formations Encountered by the Shafts at the WIPP Site .....	1-5
Figure 2.1	Schematic Illustration of the Multipacker Completion Tool Installed in Observation-Well H-16 .....	2-4
Figure 3.1	Schematic Illustration of the Time Sequence of the Various Phases of the Construction History of the AIS .....	3-5
Figure 3.2	Schematic Illustration of the Different Segments of the Drilling/Reaming History of the AIS Pilot Hole .....	3-6
Figure 5.1	Fluid-Pressure Response for the Forty-Niner Claystone at H-16 During the Drilling/Reaming Period .....	5-16
Figure 5.2	Fluid-Pressure Response for the Magenta Dolomite at H-16 During the Drilling/Reaming Period .....	5-17
Figure 5.3	Fluid-Pressure Response for the Culebra Dolomite at H-16 During the Drilling/Reaming Period .....	5-18
Figure 5.4	Filter-Cake-Skin Simulation Pressure at the Skin/Formation Interface .....	5-19
Figure 5.5	Filter-Cake-Skin Simulation Pressure at Radius of Observation-Well H-16 .....	5-20
Figure 6.1	Observed Fluid-Pressure Responses of the Five Members of the Rustler Formation at Observation-Well H-16 During the Construction of the AIS .....	6-23

FIGURES (cont.)

Figure 6.2 Fluid-Pressure Response of the Culebra Dolomite Observed at Observation-Well H-16 During the Construction of the AIS ..... 6-24

Figure 6.3 Fluid-Pressure Responses of the Culebra Dolomite Measured at Observation-Wells H-1, ERDA-9, and WIPP-21 During the Construction of the AIS ..... 6-25

Figure 6.4 Fluid-Pressure Response of the Culebra Dolomite Observed at Observation-Well H-16 During the Drilling/Reaming Period of the Construction of the AIS ..... 6-26

Figure 6.5 Simulated and Observed Fluid-Pressure Responses for the Culebra Dolomite at H-16 Without Using a Cement-Invasion Skin ..... 6-27

Figure 6.6 Simulated and Observed Fluid-Pressure Responses for the Culebra Dolomite at H-1, ERDA-9, and WIPP-21 Using the H-16 Best-Match Simulation Without Using a Cement-Invasion Skin ..... 6-29

Figure 6.7 Simulated and Observed Fluid-Pressure Responses for the Culebra Dolomite at H-16 Using a Cement-Invasion Skin ..... 6-30

Figure 6.8 Simulated and Observed Fluid-Pressure Responses for the Culebra Dolomite at H-1, ERDA-9, and WIPP-21 Using the H-16 Best-Match Simulation Using a Cement-Invasion Skin ..... 6-31

Figure 6.9 Simulated and Observed Fluid-Pressure Responses for the Culebra Dolomite at H-16 Matching the Culebra-to-AIS Flow Rate Using a Cement-Invasion Skin ..... 6-32

Figure 6.10 Simulated and Observed Fluid-Pressure Responses for the Culebra Dolomite at H-1, ERDA-9, and WIPP-21 Using the H-16 Best-Match Simulation Matching the Culebra-to-AIS Flow Rate Using a Cement-Invasion Skin ..... 6-33

Figure 6.11 Simulated and Observed Fluid-Pressure Responses for the Culebra Dolomite at H-16 Matching the H-1 Fluid-Pressure Response Using a Cement-Invasion Skin ..... 6-34

FIGURES (cont.)

Figure 6.12 Simulated and Observed Fluid-Pressure Responses for the Culebra Dolomite at H-1, ERDA-9, and WIPP-21 Matching the H-1 Fluid-Pressure Response Using a Cement-Invasion Skin ..... 6-35

Figure 6.13 Simulated and Observed Fluid-Pressure Responses for the Culebra Dolomite at H-16 Showing Sensitivity to the Use of a Cement-Invasion Skin ..... 6-36

Figure 6.14 Post-Upreaming Simulated and Observed Flow Rates from the Culebra Dolomite to the AIS Using Four Values of Transmissivity ..... 6-37

Figure 6.15 Fluid-Pressure Response of the Magenta Dolomite Observed at Observation-Well H-16 During the Construction of the AIS ..... 6-38

Figure 6.16 Fluid-Pressure Response of the Magenta Dolomite Observed at Observation-Well H-16 During the Drilling/Reaming Period of the Construction of the AIS ..... 6-39

Figure 6.17 Simulation of the Magenta Dolomite Fluid-Pressure Response at H-16 During the Construction of the AIS Using a Homogeneous-Formation Characterization ..... 6-40

Figure 6.18 Simulation of the Magenta Dolomite Fluid-Pressure Response at H-16 During the Construction of the AIS Using a Formation-Heterogeneity Boundary ..... 6-41

Figure 6.19 Simulation of the Magenta Dolomite Fluid-Pressure Response at H-16 During the Construction of the AIS Using a Formation-Heterogeneity Boundary and Showing Sensitivity to  $T_i$  ..... 6-42

Figure 6.20 Simulation of the Magenta Dolomite Fluid-Pressure Response at H-16 During the Construction of the AIS Using a Formation-Heterogeneity Boundary and Showing Sensitivity to  $T_o$  ..... 6-43

Figure 6.21 Simulation of the Magenta Dolomite Fluid-Pressure Response at H-16 During the Construction of the AIS Using a Formation-Heterogeneity Boundary and Showing Sensitivity to  $r_b$  ..... 6-44

Figure 6.22 Semi-log Plot of the Fluid-Pressure Response of the Magenta Dolomite at H-16 Showing Sensitivity to  $T_i$ ,  $T_o$ , and  $r_b$  During the Post-Reaming Draining Period ..... 6-45

**FIGURES (cont.)**

Figure 6.23 Simulation of the Magenta Dolomite Fluid-Pressure Response at H-16 Using a Homogeneous-Formation Characterization and Showing Sensitivity of  $T_f$  to  $T_i$  and  $T_o$  of the Best-Match Heterogeneous Characterization ..... 6-46

Figure 6.24 Fluid-Pressure Response of the Forty-Niner Claystone Observed at Observation-Well H-16 During the Construction of the AIS ..... 6-47

Figure 6.25 Fluid-Pressure Response of the Forty-Niner Claystone Observed at Observation-Well H-16 During the Drilling/Reaming Period of the Construction of the AIS ..... 6-48

Figure 6.26 Simulation of the Forty-Niner Claystone Fluid-Pressure Response at H-16 During the Construction of the AIS Using a Homogeneous-Formation Characterization ..... 6-49

Figure 6.27 Simulation of the Forty-Niner Claystone Fluid-Pressure Response at H-16 During the Construction of the AIS Using a Formation-Heterogeneity Boundary ..... 6-50

Figure 6.28 Simulation of the Forty-Niner Claystone Fluid-Pressure Response at H-16 During the Construction of the AIS Using a Formation-Heterogeneity Boundary and Showing Sensitivity to  $T_i$  ..... 6-51

Figure 6.29 Simulation of the Forty-Niner Claystone Fluid-Pressure Response at H-16 During the Construction of the AIS Using a Formation-Heterogeneity Boundary and Showing Sensitivity to  $T_o$  ..... 6-52

Figure 6.30 Simulation of the Forty-Niner Claystone Fluid-Pressure Response at H-16 During the Construction of the AIS Using a Formation-Heterogeneity Boundary and Showing Sensitivity to  $r_b$  ..... 6-53

Figure 6.31 Semi-log Plot of the Fluid-Pressure Response of the Forty-Niner Claystone at H-16 Showing Sensitivity to  $T_i$ ,  $T_o$ , and  $r_b$  During the Post-Reaming Draining Period ..... 6-55

FIGURES (cont.)

Figure 6.32 Simulation of the Forty-Niner Claystone Fluid-Pressure Response at H-16 Using a Homogeneous-Formation Characterization and Showing Sensitivity of  $T_f$  to  $T_i$  and  $T_o$  of the Best-Match Heterogeneous Characterization ..... 6-56

Figure 7.1 Calculated Flow Rate to the AIS Versus Time Since Upreaming for the Culebra and Magenta Dolomites and the Forty-Niner Claystone ..... 7-3

Figure A.1 Specified and Simulated Wellbore Pressures and Simulated and Observed Formation Fluid Pressures for the Culebra Dolomite Drilling/Reaming Period Without a Cement-Invasion Skin and Matching H-16 Fluid-Pressure Response ..... A-3

Figure A.2 Specified and Simulated Wellbore Pressures and Simulated and Observed Formation Fluid Pressures for the Culebra Dolomite Drilling/Reaming Period Using a Cement-Invasion Skin ..... A-4

Figure A.3 Specified and Simulated Wellbore Pressures and Simulated and Observed Formation Fluid Pressures for the Culebra Dolomite Drilling/Reaming Period With a Cement-Invasion Skin and Matching the Culebra-to-AIS Flow Rate ..... A-5

Figure A.4 Specified and Simulated Wellbore Pressures and Simulated and Observed Formation Fluid Pressures for the Culebra Dolomite Drilling/Reaming Period with a Cement-Invasion Skin and Matching the Observation-Well Responses ..... A-6

Figure A.5 Specified and Simulated Wellbore Pressures and Simulated and Observed Formation Fluid Pressures for the Culebra Dolomite Drilling/Reaming Period Without a Cement-Invasion Skin and Using a  $T_f = 1.3 \times 10^{-7} \text{ m}^2/\text{s}$  ..... A-7

Figure A.6 Specified and Simulated Wellbore Pressures and Simulated and Observed Formation Fluid Pressures for the Culebra Dolomite Drilling/Reaming Period Without a Cement-Invasion Skin and Using a  $T_f = 6.6 \times 10^{-7} \text{ m}^2/\text{s}$  ..... A-8

FIGURES (cont.)

Figure A.7 Specified and Simulated Wellbore Pressures and Simulated and Observed Formation Fluid Pressures for the Magenta Dolomite Drilling/Reaming Period Using a Homogeneous-Formation Characterization ..... A-9

Figure A.8 Specified and Simulated Wellbore Pressures and Simulated and Observed Formation Fluid Pressures for the Magenta Dolomite Drilling/Reaming Period Using a Formation-Heterogeneity Boundary ..... A-10

Figure A.9 Specified and Simulated Wellbore Pressures and Simulated and Observed Formation Fluid Pressures for the Magenta Dolomite Drilling/Reaming Period Using a Formation-Heterogeneity Boundary and  $T_i = 2.5 \times 10^{-8} \text{ m}^2/\text{s}$  ..... A-11

Figure A.10 Specified and Simulated Wellbore Pressures and Simulated and Observed Formation Fluid Pressures for the Magenta Dolomite Drilling/Reaming Period Using a Formation-Heterogeneity Boundary and  $T_i = 2.5 \times 10^{-7} \text{ m}^2/\text{s}$  ..... A-12

Figure A.11 Specified and Simulated Wellbore Pressures and Simulated and Observed Formation Fluid Pressures for the Magenta Dolomite Drilling/Reaming Period Using a Formation-Heterogeneity Boundary and  $T_o = 1.3 \times 10^{-8} \text{ m}^2/\text{s}$  ..... A-13

Figure A.12 Specified and Simulated Wellbore Pressures and Simulated and Observed Formation Fluid Pressures for the Magenta Dolomite Drilling/Reaming Period Using a Formation-Heterogeneity Boundary and  $T_o = 1.3 \times 10^{-7} \text{ m}^2/\text{s}$  ..... A-14

Figure A.13 Specified and Simulated Wellbore Pressures and Simulated and Observed Formation Fluid Pressures for the Magenta Dolomite Drilling/Reaming Period Using a Formation-Heterogeneity Boundary and  $r_b = 20 \text{ m}$  ..... A-15

Figure A.14 Specified and Simulated Wellbore Pressures and Simulated and Observed Formation Fluid Pressures for the Magenta Dolomite Drilling/Reaming Period Using a Formation-Heterogeneity Boundary and  $r_b = 80 \text{ m}$  ..... A-16

FIGURES (cont.)

Figure A.15 Specified and Simulated Wellbore Pressures and Simulated and Observed Formation Fluid Pressures for the Magenta Dolomite Drilling/Reaming Period Without a Formation-Heterogeneity Boundary and  $T_f = 8.0 \times 10^{-8} \text{ m}^2/\text{s}$  ..... A-17

Figure A.16 Specified and Simulated Wellbore Pressures and Simulated and Observed Formation Fluid Pressures for the Magenta Dolomite Drilling/Reaming Period Without a Formation-Heterogeneity Boundary and  $T_f = 4.0 \times 10^{-8} \text{ m}^2/\text{s}$  ..... A-18

Figure A.17 Specified and Simulated Wellbore Pressures and Simulated and Observed Formation Fluid Pressures for the Forty-Niner Claystone Drilling/Reaming Period Using a Homogeneous-Formation Characterization ..... A-19

Figure A.18 Specified and Simulated Wellbore Pressures and Simulated and Observed Formation Fluid Pressures for the Forty-Niner Claystone Drilling/Reaming Period Using a Formation-Heterogeneity Boundary ..... A-20

Figure A.19 Specified and Simulated Wellbore Pressures and Simulated and Observed Formation Fluid Pressures for the Forty-Niner Claystone Drilling/Reaming Period Using a Formation-Heterogeneity Boundary and  $T_i = 3.0 \times 10^{-9} \text{ m}^2/\text{s}$  ..... A-21

Figure A.20 Specified and Simulated Wellbore Pressures and Simulated and Observed Formation Fluid Pressures for the Forty-Niner Claystone Drilling/Reaming Period Using a Formation-Heterogeneity Boundary and  $T_i = 3.0 \times 10^{-8} \text{ m}^2/\text{s}$  ..... A-22

Figure A.21 Specified and Simulated Wellbore Pressures and Simulated and Observed Formation Fluid Pressures for the Forty-Niner Claystone Drilling/Reaming Period Using a Formation-Heterogeneity Boundary and  $T_o = 5.0 \times 10^{-10} \text{ m}^2/\text{s}$  ..... A-23

Figure A.22 Specified and Simulated Wellbore Pressures and Simulated and Observed Formation Fluid Pressures for the Forty-Niner Claystone Drilling/Reaming Period Using a Formation-Heterogeneity Boundary and  $T_o = 5.0 \times 10^{-9} \text{ m}^2/\text{s}$  ..... A-24

FIGURES (cont.)

- Figure A.23 Specified and Simulated Wellbore Pressures and Simulated and Observed Formation Fluid Pressures for the Forty-Niner Claystone Drilling/Reaming Period Using a Formation-Heterogeneity Boundary and  $r_b = 20$  m ..... A-25
- Figure A.24 Specified and Simulated Wellbore Pressures and Simulated and Observed Formation Fluid Pressures for the Forty-Niner Claystone Drilling/Reaming Period Using a Formation-Heterogeneity Boundary and  $r_b = 80$  m ..... A-26
- Figure A.25 Specified and Simulated Wellbore Pressures and Simulated and Observed Formation Fluid Pressures for the Forty-Niner Claystone Drilling/Reaming Period Without a Formation-Heterogeneity Boundary and  $T_f = 9.0 \times 10^{-9}$  m<sup>2</sup>/s ..... A-27
- Figure A.26 Specified and Simulated Wellbore Pressures and Simulated and Observed Formation Fluid Pressures for the Forty-Niner Claystone Drilling/Reaming Period Without a Formation-Heterogeneity Boundary and  $T_f = 1.5 \times 10^{-9}$  m<sup>2</sup>/s ..... A-28

## TABLES

Table 1.1	Nomenclature and Abbreviations for Parameters and Terms Used in the Text and on Figures and Tables .....	1-6
Table 5.1	Depths and Thicknesses of the Rustler Units Analyzed at H-16 .....	5-21
Table 5.2	Calculated Rustler-Unit Mud Overpressures for Simulation of the Drilling Periods of the AIS Pilot Hole .....	5-22
Table 5.3	Parameters for Simulations Including Filter-Cake Skin .....	5-23
Table 6.1	Values and Durations of Wellbore Pressures Used for Fixed- Pressure Wellbore Boundary Conditions During Simulation of the Culebra Dolomite Drilling/Reaming Period .....	6-57
Table 6.2	Values and Durations of Wellbore Pressures Used for Fixed- Pressure Wellbore Boundary Conditions During Simulation of the Magenta Dolomite Drilling/Reaming Period .....	6-58
Table 6.3	Values and Durations of Wellbore Pressures Used for Fixed- Pressure Wellbore Boundary Conditions During Simulation of the Forty-Niner Claystone Drilling/Reaming Period .....	6-60
Table 7.1	Calculated Flow Rates from the Units of the Rustler Formation to the AIS on 1987 Calendar Day 667 .....	7-4
Table 8.1	Summary of the Transmissivities Determined from the Analysis of the Fluid-Pressure Responses of the Culebra Dolomite, Magenta Dolomite, and the Forty-Niner Claystone .....	8-8
Table 8.2	Calculated Transmissivities for a Range of Storativities Using the Diffusivities from the Results of the Analyses Presented in this Report .....	8-9

## 1.0 INTRODUCTION

### 1.1 Background

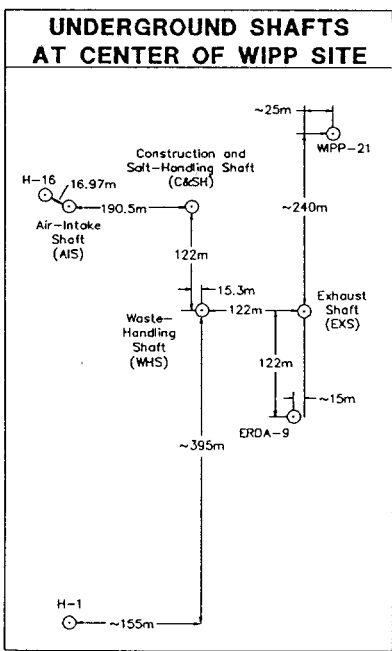
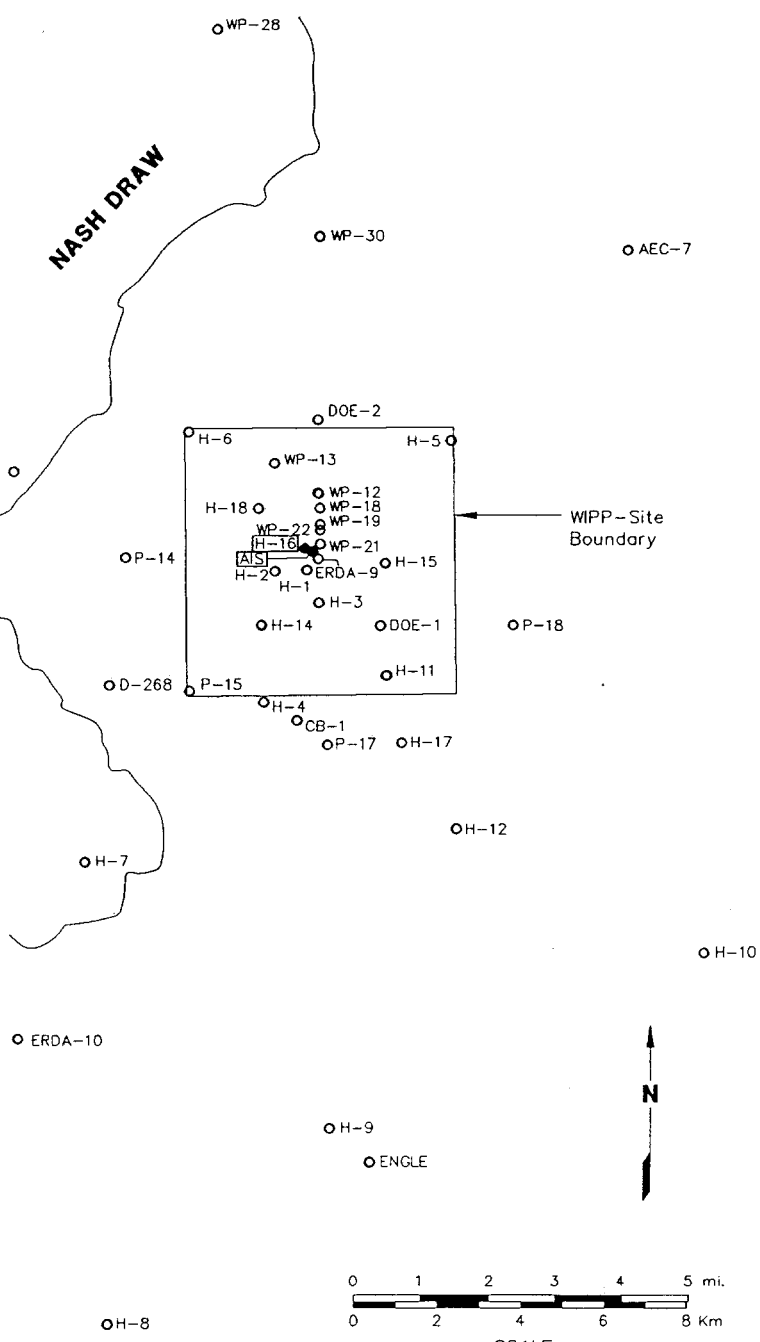
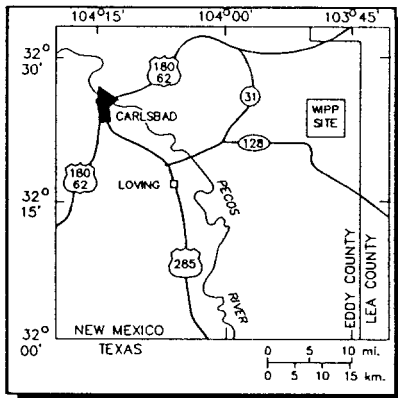
The decision to construct a fourth underground-access shaft, the air-intake shaft (AIS), at the Waste Isolation Pilot Plant (WIPP) site (Figures 1.1 and 1.2) provided a unique opportunity to observe closely the effect of a large point-discharge feature on the hydrology of the five members of the Rustler Formation near the center of the WIPP site. Figure 1.3 shows the generalized stratigraphy of the geologic units encountered by the AIS and the other WIPP-site shafts. The hydrogeologic influences of the other three shafts at the center of the WIPP site, the waste-handling shaft (WHS), the construction and salt-handling shaft (C&SH), and the exhaust shaft (EXS), have been analyzed in earlier reports (Stevens and Beyeler, 1985; Haug and others, 1987; and LaVenue and others, 1988). However, because of the limited data base available for those reports the Rustler's hydrologic properties were determined with a moderate degree of uncertainty. Observation-well H-16 (Figure 1.1) was drilled four months before the AIS pilot hole and is located 16.97 meters (m) northwest of the AIS. H-16 was equipped with a multipacker completion tool with downhole pressure transducers to monitor the formation-pressure changes in the five members of the Rustler Formation during the drilling and upreaming (raise boring) of the AIS. The combination of detailed fluid-pressure data from H-16, water-level measurements at 3 of the Culebra dolomite observation wells near the center of the WIPP site, and the construction history of the AIS and its pilot hole provided an ideal setting to obtain estimates of the transmissivity and formation pressure of the members of the Rustler Formation.

## 1.2 Objectives

The fluid-pressure and water-level responses to construction of the AIS were analyzed with the well-test simulator GTFM (Pickens and others, 1987). Because the source of the pressure changes, the AIS pilot hole and shaft, was an uncontrolled hydrologic drain on the affected units, the observation wells' responses were simulated using a fixed-pressure boundary condition at the AIS. The drilling period was essentially a series of constant-pressure injections to the Rustler and the draining periods were atmospheric-pressure discharge periods with no control on the quantity of discharge and no means of measuring the discharge during most of the open period. The fixed-pressure boundary condition at the point of discharge meant that the simulation of the effects of the shaft's construction was governed by the diffusivity relationship in which transmissivity and storativity are interrelated, as discussed in detail in Section 5.0, thus preventing completely independent estimates of these hydrologic parameters. Table 1.1 presents the nomenclature and abbreviations used throughout this report and on figures and tables.

The objectives of the analysis of the effects of the construction of the AIS on the fluid pressure of the Rustler Formation were to:

- o estimate the transmissivity of the members of the Rustler Formation from H-16 and observation-well responses to the construction of the AIS; and
- o estimate the potential leakage rate of ground water into the AIS under the observed open-hole conditions.

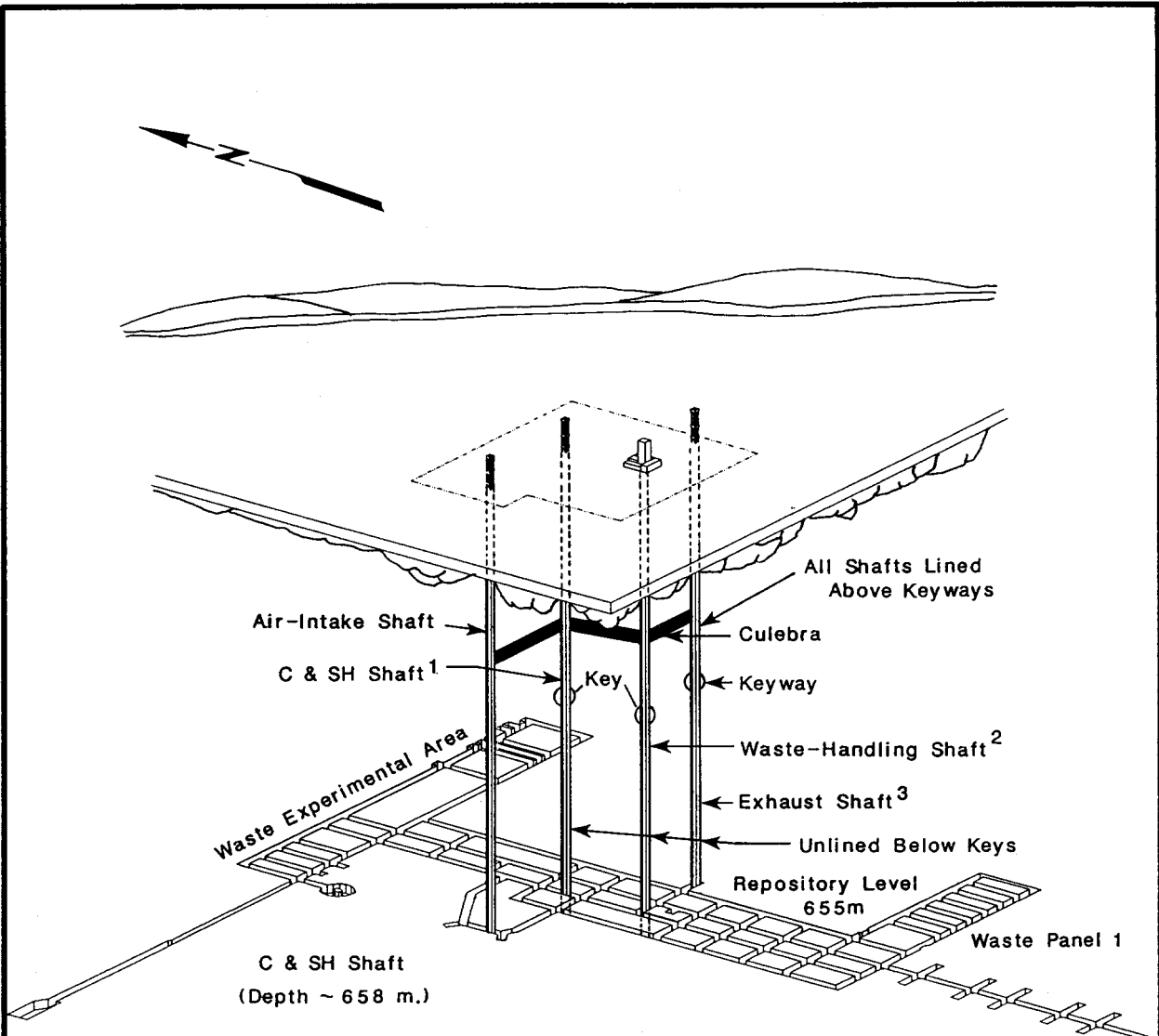


Drawn by	ABW	Date	1/15/90
Checked by	G.S.	Date	1/15/90
Revisions		Date	
H09700R876		1/15/90	

**Locations of the Air-Intake Shaft and Other  
Underground-Access Shafts Relative to the  
WIPP-Site Observation-Well Network**

**INTERA Technologies**

Figure 1.1



NOT TO SCALE

- NOTES:
- 1. Previously known as exploratory shaft.
  - 2. Previously known as ventilation shaft.
  - 3. Exhaust shaft not part of SPDV.

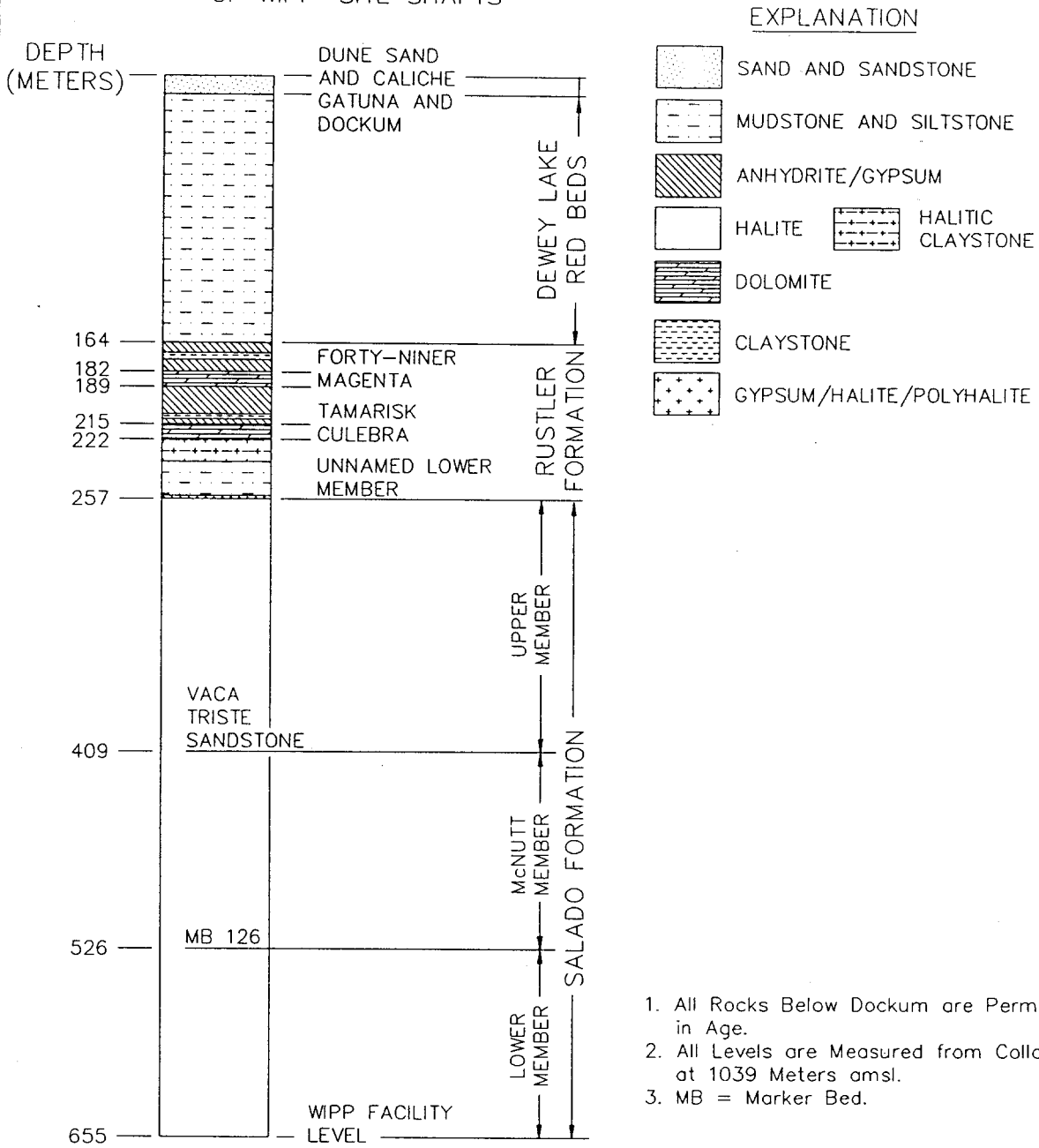
Drawn by ABW	Date 1/12/89
Checked by G.S.	Date 1/12/89
Revisions G.S.	Date 6/6/89
H09700R876	1/4/89

Schematic Illustration of the WIPP-Site  
Underground-Access Shafts and the  
Underground Facility

**INTERA** Technologies

Figure 1.2

## GENERALIZED STRATIGRAPHY OF WIPP-SITE SHAFTS



1. All Rocks Below Dockum are Permian in Age.
2. All Levels are Measured from Collar at 1039 Meters amsl.
3. MB = Marker Bed.

Modified from Bechtel National, Inc. (1985)

Drawn by	ABW	Date	1/24/89
Checked by	G.S.	Date	1/25/89
Revisions	G.S.	Date	6/6/89
H09700R876			1/25/89

### Generalized Stratigraphy of the Formations Encountered by the Shafts at the WIPP Site

**INTERA Technologies**

Figure 1.3

- AIS - Air-Intake Shaft
- C&SH - Construction and Salt-Handling Shaft
- EXS - Exhaust Shaft
- WHS - Waste-Handling Shaft
- D - Diffusivity
- ft - Foot
- Ks - Skin Hydraulic Conductivity
- L - Liter
- m - Meter
- MPa - Megapascal
- Ps - Reduced Wellbore Pressure
- psi - Pounds per square inch
- r<sub>b</sub> - Radius to Formation Boundary
- S - Storativity
- s - Second
- T - Transmissivity
- T<sub>f</sub> - Formation Transmissivity
- T<sub>i</sub> - Formation Transmissivity Inside Radial Heterogeneity Boundary
- T<sub>o</sub> - Formation Transmissivity Outside Radial Heterogeneity Boundary
- X - Observed Data

Drawn by	Date	Nomenclature and Abbreviations for Parameters and Terms Used in the Text and on Figures
Checked by	Date	
Revisions	Date	
		Table 1.1

## 2.0 MONITORING SYSTEMS

The drilling of the AIS pilot hole and the upreaming of the AIS caused fluid-pressure changes in the members of the Rustler Formation. The most important observation well was H-16 which was drilled specifically to observe and monitor the effects of the construction of the AIS on the permeable members of the Rustler.

Water-level responses were also observed in other Culebra dolomite observation wells around the center of the WIPP site. The closest Magenta dolomite observation wells, at H-1 and at the H-2 hydropad, did not appear to respond to the AIS construction, apparently because of the lower permeability of the Magenta relative to the Culebra.

Pressure transducers in the other shafts at the WIPP site were potentially capable of monitoring the AIS construction. However, the transducers in the WHS and the C&SH shaft were out of service during this period due to the extensive grouting operations in the WHS and due to a complete overhaul of the instrumentation in the C&SH shaft because of salt corrosion and haulage damage. The transducers in the EXS were potentially able to monitor the AIS construction. However, because the WHS lies between the AIS and the EXS, the EXS fluid-pressure responses during the important early period of the AIS construction were dominated by the grouting activity in the WHS. Fluid-pressure data from the EXS were therefore not analyzed.

The following sections describe the H-16 monitoring system and the observation wells. Note that in this discussion and throughout this report, especially on plots and tables, time will be referenced by the date of occurrence and by the 1987 Calendar Day or the number of days counted consecutively from January 1, 1987.

## 2.1 H-16 Multipacker Monitoring System

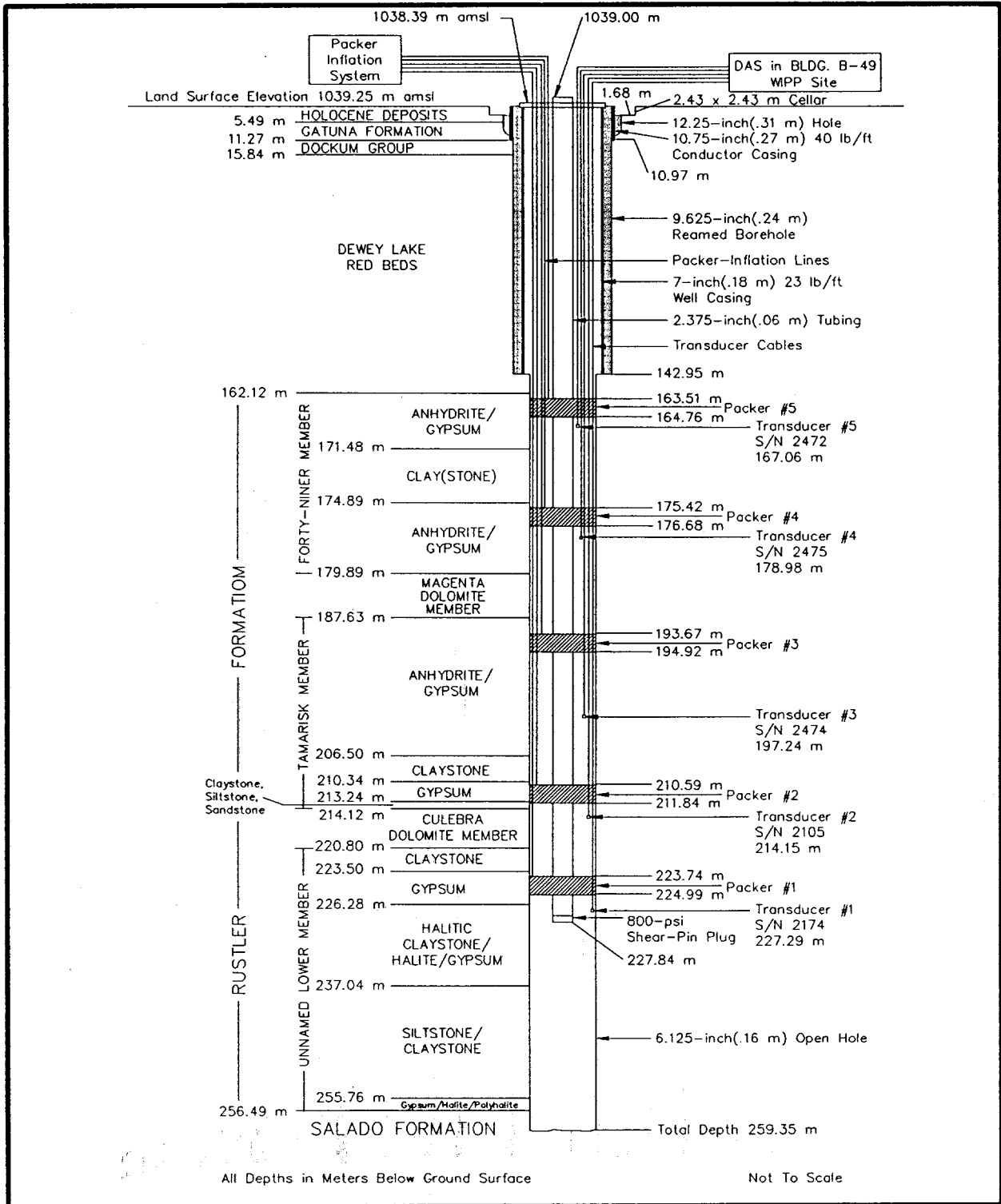
Borehole H-16 was drilled in July and August 1987. The center of the borehole was located 16.97 m northwest of the center of the AIS and was installed to monitor the fluid pressures in the five members of the Rustler Formation during the construction of the AIS. As described in Stensrud and others (1988a), H-16 was drilled and cased to the lower Dewey Lake Red Beds at a depth of 142.95 m below ground surface (BGS), then extended open hole to a depth of 259.35 m BGS, about 2.74 m into the upper Salado Formation. Each of the five members of the Rustler was hydraulically tested during the drilling of H-16. The data collected during the testing at H-16 are presented in Stensrud and others (1988a) and interpretations of those tests are found in Beauheim (1987a).

In late August 1987, well H-16 was equipped with a multipacker completion tool manufactured by Baker Service Tools (BST), Houston, Texas (Figure 2.1). The device includes 5 fluid-inflatable packers which isolate the 5 members of the Rustler Formation, and 5 downhole pressure transducers (see Stensrud and others, 1988a) which monitor the fluid pressures in those isolated intervals. The data collected by the transducers are transmitted by a data-link cable to a surface recorder and stored on magnetic tape. The original data are recorded in pounds per square inch (psi) and are adjusted to the temperature at the depths of the transducers using correction curves supplied by the manufacturer. The data and the correction curves are periodically published in hydrologic data reports (Stensrud and others, 1988a, 1988b, 1989). Note that the transducers do not share a common reference elevation datum.

## 2.2 Observation Wells

Hydrologic responses to the construction of the AIS were observed in observation wells near the center of the WIPP site. The data and data-collection methods for these and other WIPP-site observation wells are presented in Stensrud and others (1988a, 1988b, 1989). The data show that only the Culebra observation wells within 1.25 km of the AIS, H-1, H-2a, H-2b2, ERDA-9, WIPP-18, WIPP-19, WIPP-21, and WIPP-22, showed significant water-level responses to the presence of the AIS. Because other hydrologically significant activities were concurrent with the construction of the AIS, as described in Section 4.0, data from some of these observation wells could not be analyzed.

Observation wells H-1, ERDA-9, and WIPP-21 were sufficiently isolated from other hydrologic influences to provide data which could be used to analyze the effect of the AIS on the Culebra dolomite. However, the early-time responses in these wells could not be used because they were affected by grouting operations in the WHS and only the post-drilling/reaming and post-upreaming periods were used for analysis. The data collected at H-1, ERDA-9, and WIPP-21 are water levels measured with electric water-level sounders. These data were converted to pressure in MPa at the center of the Culebra intervals using the best available data for borehole-fluid density in these wells as presented in Cauffman and others (1990, Appendix F).



Drawn by S.C.	Date 1/4/89
Checked by G.S.	Date 1/11/89
Revisions ABW	Date 6/23/89
H09700R876	1/4/89

**Schematic Illustration of the Multipacker Completion Tool Installed in Observation-Well H-16 (after Beauheim, 1987a)**



Figure 2.1

### 3.0 AIR-INTAKE SHAFT CONSTRUCTION HISTORY

Construction of the AIS consisted of drilling and reaming a pilot hole and upreaming the shaft. The 0.25-m pilot hole was drilled using a bentonite-mud-based brine drilling fluid through the Dewey Lake Red Beds and the Rustler and Salado Formations to a depth of 635 m, immediately above the WIPP-site underground facility. With the pilot hole remaining full of drilling fluid, the initial pilot hole was reamed to a 0.37-m diameter to the same depth. The reamed 0.37-m pilot hole was then extended into the underground facility, a depth of 655 m, and drained of drilling fluid. The pilot hole provided a guide for the introduction of 0.35-m drill pipe which controlled and raised a 6.17-m diameter upreaming bit which raise bored the AIS from the underground facility to ground surface. No drilling fluid was used during upreaming. Following geologic mapping, the shaft was finished with a concrete liner to a final inside diameter of 5.9 m.

The following sections present descriptions of each of the phases of the AIS construction history, highlighting activities of hydrologic interest which affected the fluid-pressure responses of the members of the Rustler Formation analyzed in Section 6.0 (Figure 3.1). Construction information was developed from the daily drilling reports (DDR) of CAP-STAR Drilling, Inc. (the drilling contractor), discussions with Dana Downes of Frontier-Kemper, Inc. (the supervisor of construction operations), and Table 1.4, Part D of Stensrud and others (1988b).

#### 3.1 Pilot Hole

The following subsections describe the principal events of the drilling/reaming history of the AIS pilot hole with particular attention to events affecting the formation fluid pressures of the members of the Rustler Formation. Figure 3.2 schematically illustrates the events of the drilling/reaming period.

### 3.1.1 Drilling

The drilling of the 0.25-m pilot hole began on December 5, 1987 (Calendar Day 339) using conventional rotary drilling methods and a bentonite-based brine drilling mud as a circulating medium. The actual mud weight was not recorded in the DDR on a daily basis. However, on January 13, 1988 (Calendar Day 378) the DDR indicated that the drilling fluid weighed 9.8 pounds per gallon (1174.44 kilograms/cubic meter [ $\text{kg}/\text{m}^3$ ]) with a viscosity of 28 centipoises and a pH of 8. Subsequent discussions with Frontier-Kemper and CAP-STAR have not uncovered any additional information concerning the drilling fluid's parameters. Therefore, the January 13, 1988, mud parameters were assumed to be in effect throughout the drilling period.

Drilling of the initial stages of the pilot hole proceeded slowly due to administrative delays concerning the safety of the drilling location and technical delays caused by caving in the Gatuña Formation. Drilling penetrated the Forty-niner and Magenta Members of the Rustler on December 11 and 12, 1987 (Calendar Days 345 and 346). On December 12 (Calendar Day 346), after finding the borehole was slightly deviated, CAP-STAR began reaming the upper part of the borehole to a 0.37-m diameter in an attempt to correct the deviation. From December 12 to 20 (Calendar Day 354) the pilot hole was reamed to a depth of 92.97 m BGS. Operations were halted until December 26 (Calendar Day 360) when the borehole was cemented from 190 to 130 m BGS in a further attempt to correct borehole deviation. The borehole was flushed and cleaned of drill cuttings and the drilling fluid was circulated until preparations for cementing were completed.

The pilot hole was reentered on December 27 (Calendar Day 361) and the cement and formations below 130 m BGS were redrilled in conformance with deviation standards to a 0.25-m diameter. The Forty-niner and Magenta Members were redrilled on December 29 and 30 (Calendar Days 363 and 364), respectively. The Culebra dolomite was penetrated on January 1, 1988 (Calendar Day 366). Drilling continued to 262 m BGS to the upper part of the Salado Formation on January 3 (Calendar Day 368), when excessive borehole deviation was again detected. The borehole was cemented from 262 to 195 m BGS on January 6 (Calendar Day 371). On January 7 (Calendar Day 372), the cemented interval was redrilled at a 0.25-m diameter to try to correct the deviation. The Culebra was redrilled on January 8 and 9 (Calendar Days 373 and 374), and drilling continued through the remainder of the Rustler and into the Salado. Drilling to the total depth of the 0.25-m pilot hole at 635 m BGS continued until January 30 (Calendar Day 395) with a short interruption on January 16 and 17 (Calendar Days 381 and 382) when the Salado Formation was cemented from 367 to 305 m BGS to correct excessive borehole deviation.

### 3.1.2 Reaming

The 0.25-m borehole was reamed to a 0.37-m diameter from 91.5 to 655 m BGS from January 31 to February 7, 1988 (Calendar Days 396 to 403) with a full column of brine-based drilling mud. The pilot hole penetrated the WIPP underground facility on Calendar Day 403. The Forty-niner and Magenta were reamed on February 1 (Calendar Day 397) and the Culebra dolomite was reamed on February 2 (Calendar Day 398). The drilling fluid was pumped from the pilot hole just before penetration of the underground facility. The pilot hole remained open and the Culebra and Magenta were draining to the pilot hole and later to the upreamed shaft from 2330 hours on February 7 (Calendar Day 403) until the time of this report.

### 3.2 Upreaming of the Air-Intake Shaft

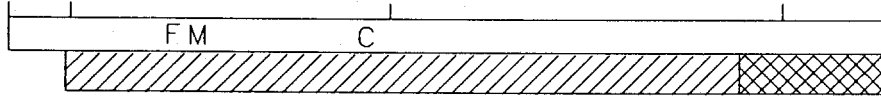
Upreaming of the AIS began on May 1, 1988 (Calendar Day 487) after 2-1/2 months of preparatory work on the foundation for the AIS collar and installation of the drill pipe for the 6.17-m diameter upreaming tool. Before installing the drill pipe, a 13-7/8-inch (0.35 m) drill bit was used to clear hole obstructions at 80 m and 226 m BGS. The obstruction at the 226-m depth, 5.2 m below the Culebra, was cleared on April 7, 1988 (Calendar Day 463) using compressed air as a circulation medium. The cleaning operation caused a slight offset in the H-16 fluid-pressure data for the Culebra but did not disturb the overall pressure trend.

The members of the Rustler Formation isolated in H-16 were encountered by the upreaming tool from June 16 to 28 (Calendar Days 533 to 545). Specifically, the Culebra was upreamed on June 17 (Calendar Day 534), the Magenta on June 23 (Calendar Day 540), and the Forty-niner claystone on June 26 (Calendar Day 543). After upreaming of the Rustler, upreaming slowed considerably in the Dewey Lake Red Beds. Due to construction delays, the AIS upreaming was not completed until August 24, 1988 (Calendar Day 602). Throughout and after the upreaming period, the Rustler members remained open and draining to the AIS.

**DRILLING / REAMING PERIOD**

Penetration of WIPP-Site Underground  
Facility 649 meters Below Ground  
Surface

Dec. 1, 1987   Dec. 5, 1987   Jan. 1, 1988   Feb. 1, 1988   Feb. 7, 1988



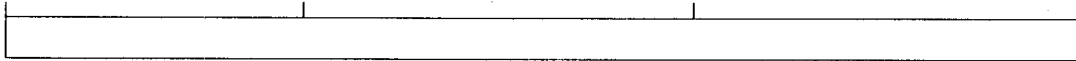
Drilling 0.25-m-diameter Pilot Hole  
to 628.5 m from Ground Surface

Hole reamed  
to 0.37-m-diameter

- First { F, Forty-Niner Penetration 12/11/87  
M, Magenta Penetration 12/12/87  
C, Culebra Penetration 12/31/87

**OPEN-BOREHOLE PERIOD**

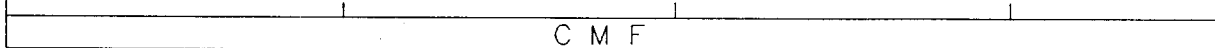
Feb. 8, 1988   Mar. 1, 1988   April 1, 1988   May 1, 1988



Construction of Foundation for Upreaming Rig

**UPREAMING PERIOD**

May 1, 1988   June 1, 1988   July 1, 1988   August 1, 1988   August 23, 1988



Upreaming Pilot Hole to 6.17-m Diameter  
from Underground Facility to Ground Surface

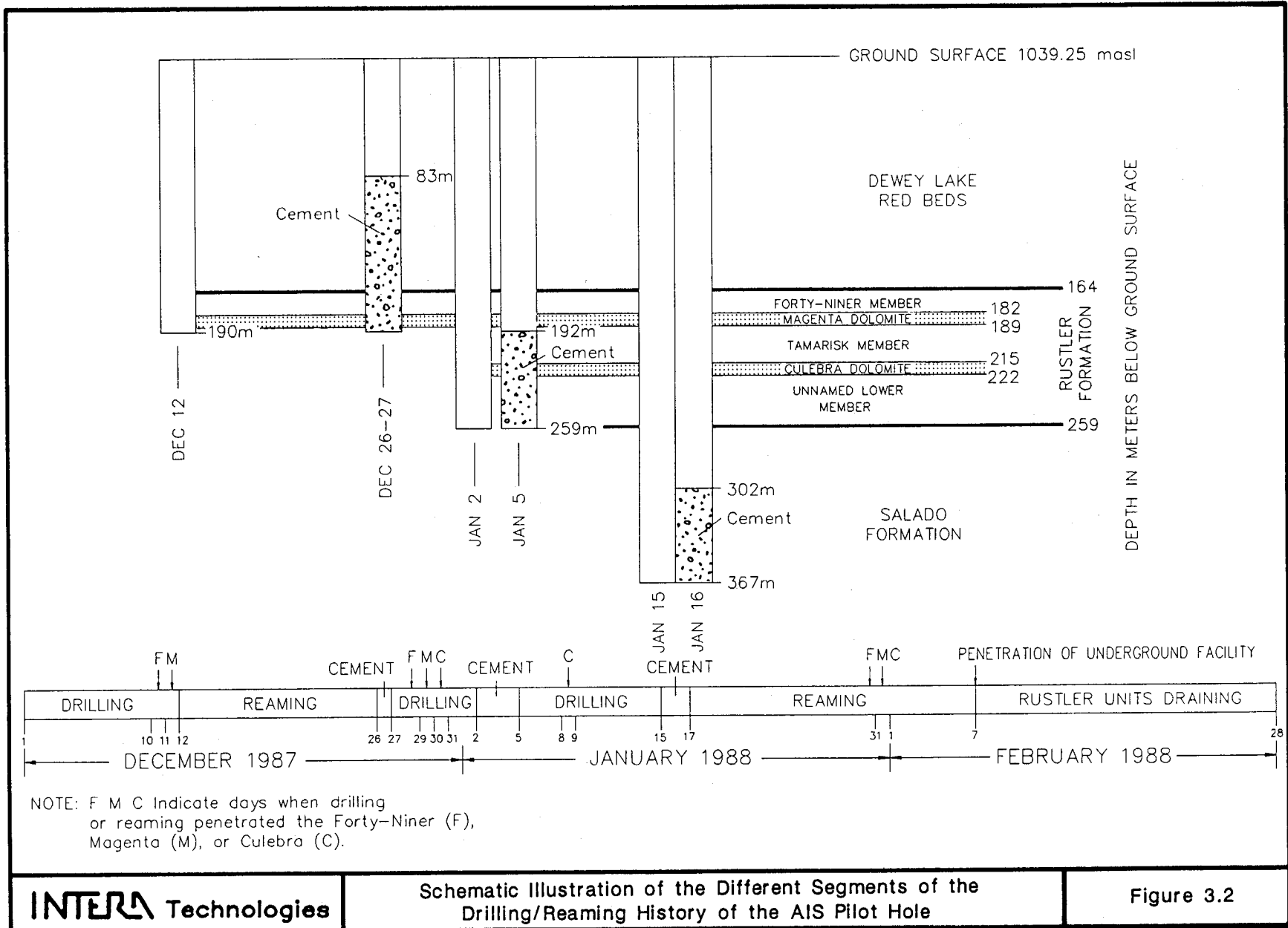
- C, Upreaming Culebra June 16, 1988  
M, Upreaming Magenta June 21, 1988  
F, Upreaming Forty-Niner June 25, 1988

Drawn by ABW	Date 2/9/89
Checked by G.S.	Date 2/9/89
Revisions	Date
H09700R876	2/9/89

**Schematic Illustration of the Time Sequence of the  
Various Phases of the Construction History  
of the AIS**

**INTERA Technologies**

Figure 3.1



**INTERA Technologies**

Schematic Illustration of the Different Segments of the Drilling/Reaming History of the AIS Pilot Hole

Figure 3.2

#### 4.0 OTHER HYDROLOGIC ACTIVITIES AFFECTING HYDROLOGIC RESPONSES

Water-level and fluid-pressure responses from over 50 observation wells and shafts in the WIPP-site observation-well network were recorded from December 1987 to December 1988. During that time, hydrologically related activities other than the AIS construction affected the members of the Rustler Formation. A compilation of all such activities can be found in Stensrud and others (1988a, 1988b, and 1989). The following sections describe those activities that may have affected the area near the center of the WIPP site during construction of the AIS.

##### 4.1 Aquifer Testing

The major aquifer test conducted during the construction of the AIS was the H-11 multipad/tracer test (Stensrud and others, 1989). During this test, well H-11b1 was pumped at a relatively constant rate of 0.38 liters per second (L/s) from May 5 to July 7, 1988 (Calendar Days 491 to 554). Water-level responses to the H-11 multipad/tracer test were recorded at 10 observation wells in addition to the fluid-pressure responses recorded at H-11b2, H-11b3, and H-11b4 at the H-11 hydropad. H-1, ERDA-9, and wells at the H-2 hydropad potentially could have responded to the H-11 multipad/tracer test, but the presence of the AIS dominated water-level responses at these locations during the test.

Well development and a 3-day pumping test of the Culebra dolomite were performed at H-18, located about 1.5 km northwest of the AIS, from February 26 to March 14, 1988 (Calendar Days 422 to 439). The H-18 pumping test was followed by three weeks of pumping for water-quality sampling as described in Section 4.2. The pumping at H-18 was observed at DOE-2, WIPP-13, P-14, and the H-6 hydropad. No evidence of the H-18 pumping was detected at H-2, H-1, ERDA-9, and WIPP-21.

#### 4.2 Water-Quality Sampling

Water-quality sampling of the Culebra dolomite as part of the WIPP site's Water Quality Sampling Program (Colton and Morse, 1985) was conducted at WIPP-19, H-18, H-14, H-15, and DOE-2 during the period analyzed for this report. The wells were pumped with an air-lift pump at pumping rates of 0.003 to 0.03 L/s. Responses to these pumping episodes were measured in some nearby wells, but the influence of these exercises was limited.

The water-quality pumping at WIPP-19 from January 26 to February 12, 1988 (Calendar Days 391 to 408) was observed distinctly at WIPP-18 and WIPP-22, but its effects could not be distinguished from drawdown induced by AIS construction at other nearby wells such as WIPP-21 (Stensrud and others, 1988b).

Water-quality sampling at H-15 was performed on January 7 to 13 and October 25 to November 7, 1988. The January sampling was not observed at nearby wells due to the dominating influence of activities in the AIS. However, the August sampling exercise appears to have affected water levels in ERDA-9 and H-1 (see Section 6.0).

#### 4.3 Grouting in the Waste-Handling Shaft

Grouting in the WIPP-site shafts affected the fluid pressure of the Culebra dolomite as noted during pressure grouting in the exhaust shaft from July through December 1986. Examination of grouting reports indicated that drilling the grout-injection boreholes, which included opening the shaft-instrumentation sleeves (Bechtel, 1985; Saulnier, 1987a) to prevent their being sealed by the grout, caused fluid-pressure decreases in the more permeable members of the Rustler such as the Culebra. These pressure decreases were observed at nearby observation well WIPP-21 and in the EXS (Stensrud and others, 1987; Saulnier and others, 1987).

The WHS was constructed as a 5.79-m-diameter shaft between November 1983 and August 1984 (Bechtel, 1985). Special grouting methods were employed to seal the Culebra and Magenta dolomites. However, continued seepage was observed from the Culebra as well as from the other Rustler units (Saulnier, 1987a; Deshler and McKinney, 1988). In October 1987, an extensive grouting and sealing program was initiated to stop leakage from all members of the Rustler Formation in the WHS. The grouting procedures involved drilling annular rings of 16 boreholes, 0.05 m in diameter, through the WHS liner from 1.5 to 3 m apart vertically, and 0.6 m into the formations in contact with the liner. Class C cement followed by a chemical grout was then injected through these boreholes at pressures as high as 4.8 MPa to seal the liner-to-formation contact, any shrinkage cracks that may have developed in the liner itself, and to seal any incompletely sealed construction joints (Deshler and McKinney, 1988). Drilling and grouting of the Magenta, Culebra, and Forty-niner Members of the Rustler Formation occurred according to the following schedule:

UNIT	DRILLING DATE (Calendar Day)	GROUTING DATE (Calendar Day)	GROUT
Culebra	12/15/87(349)		
		12/18/87(352)	Cement
	12/19/87(353)		
		02/07/88(403)	Chemical
Magenta	02/13/88(409)		
		02/14/88(410)	Chemical
	12/29/87(363)		
	01/09/88(374)		
	01/21/88(386)		
		01/22/88(387)	Cement
		01/24/88(389)	Cement
	01/26/88(391)		
	01/27/88(392)	Chemical	
	01/28/88(393)	Chemical	
	02/14/88(410)	Chemical	

UNIT	DRILLING DATE (Calendar Day)	GROUTING DATE (Calendar Day)	GROUT
Forty-niner	01/21/88(386)	01/21/88(386)	Cement
		01/22/88(387)	Cement
		01/26/88(391)	
		01/28/88(393)	Chemical
	02/13/88(409)		
		02/14/88(410)	Chemical

The decline in the Culebra fluid pressure in H-16 from December 19, 1987 to January 1, 1988 (Calendar Days 353 to 366) appears to have been caused by the drilling of the chemical-grout holes in the Culebra interval of the WHS liner. (Plots of the Culebra's fluid-pressure response during this time period are included in Section 6.0 of this report.) These grout holes remained open and draining until they were sealed on February 7, 1988 (Calendar Day 403). Similar fluid-pressure decreases were not noted for the Magenta or the Forty-niner because their grout holes were drilled and sealed on successive or near-successive days after the start of the drilling of the AIS pilot hole, apparently allowing insufficient time for any pressure decrease to be transmitted to the observation wells.

## 5.0 INTERPRETATION METHODOLOGY

A consistent interpretation methodology was applied to the analysis of the fluid-pressure-response data from the Forty-niner claystone, Magenta dolomite, and Culebra dolomite in H-16. A well-test simulator was used to simulate the response of each individual unit to stresses induced by the events occurring during drilling of the pilot hole and upreaming of the AIS. Simulation results for different formation parameters were compared graphically to pressures measured in observation wells. Parameters providing the best simulation of observed pressures in H-16 and water-level responses from other observation wells were assumed to be representative of the unit being analyzed. The Culebra simulations were also compared to a single measurement of the flow rate from the Culebra to the AIS.

### 5.1 GTFM Well-Test Simulator

The GTFM well-test simulator (Pickens and others, 1987) was used for all interpretations. GTFM is a numeric simulator which models the response of a radial-flow regime to boundary conditions applied at a well located at the center of the flow system. Simulation results consist of calculated fluid-pressure responses at radial distances from the well corresponding to the locations of the observation wells, and of calculated fluid pressure, flow rate, and production volume in the well itself. A description of GTFM can be found in Pickens and others (1987). Application of GTFM to the simulation of pulse testing in low-permeability formations is described in Saulnier and Avis (1988). Assumptions inherent in the formulation of GTFM and capabilities of the model relevant to the AIS simulations are described below.

GTFM assumes that the hydrogeologic unit subject to analysis is horizontal, of constant thickness, and bounded above and below by impermeable layers. For the AIS simulations, formation thicknesses and formation depth were assumed identical to those described for H-16 in Beauheim (1987a) and are given in Table 5.1. Although both formation thicknesses and elevations vary over the WIPP site and surrounding area, variability in the immediate vicinity of the AIS is assumed to be minimal. Therefore, given the proximity of H-16 to the AIS, interval thickness values derived from H-16 are considered to be representative. Differences in formation thickness and elevation at the more distant monitoring locations, ERDA-9, WIPP-21, and H-1, will introduce uncertainty as to the accuracy of simulation results at the corresponding radii. All intervals of concern are bounded above and below by low-permeability anhydrite beds with little or no production potential (Beauheim, 1987a). Mapping in the WHS and EXS did not indicate any leakage from these anhydrite units (Holt and Powers, 1984, 1986) and these units were assumed to have had little impact on the observed fluid-pressure responses.

GTFM simulates a formation of finite radial extent centered on a finite-radius well. The well is assumed to be the only source of hydraulic stress applied to the unit being analyzed. For the AIS simulations, the well consisted initially of the pilot hole, and after upreaming, the AIS. The radial extent of the formation was set at 10,000 m, large enough to preclude external boundary conditions from having any effects on the simulation results. The single-hydraulic-stress assumption is obviously not representative of the entire modeled area. For example, drilling and grouting operations in the WHS and hydraulic tests on other wells in the monitoring system appear to have affected water levels and observed pressures in the observation wells, including H-16. However, the AIS was the closest and most significant stress on the portion of the formation which includes the H-16 monitoring well. Within this area, the effects of any other stress events were assumed to have only minimal impact on

the H-16 pressure response. Water-level responses at observation-wells H-1, ERDA-9, and WIPP-21 were apparently more significantly affected by non-AIS hydraulic stresses, particularly those due to drilling and grouting operations in the WHS.

Boundary conditions at the external boundary can be either fixed pressure or zero flow. The potential effects of external boundary conditions were minimized by using a large formation radius. Fixed-pressure boundary conditions were used in all simulations. Fluid pressures (corrected to the center of the water-bearing interval under consideration) measured at H-16 before the pilot-hole drilling intercepted the intervals (and applied stress to the units) were used as initial formation pressures.

GTFM assumes that formation-fluid properties are constant. The only formation-fluid property required for the AIS simulations was fluid density. A value of  $1020 \text{ kg/m}^3$  (see Cauffman and others, 1990) was assumed to be representative of formation-fluid density for all three units of interest within the modeled area.

GTFM allows the interval being analyzed to contain a single radially centered heterogeneity. The boundary of the heterogeneity is specified at some distance from the wellbore, thus allowing the tested formation to be represented by two zones with different hydraulic properties; an inner zone comprising the portion of the formation between the wellbore and the heterogeneity boundary, and an outer zone which includes the portion of the formation between the heterogeneity boundary and the external boundary of the modeled system. Formation properties such as transmissivity and storativity are assumed to be constant in each radial zone, but may be different between zones. Heterogeneities are most frequently used to model skin zones where, due to the effects of drilling, properties in the formation immediately surrounding the well are assumed to differ from those of the remainder of the formation.

However, heterogeneities may be placed at much larger radii, allowing simulation of the effects of larger-scale differences in formation properties. Both of these approaches were used in the AIS simulations. A skin zone was applied to portions of the Culebra simulations in order to simulate the effects of cement invasion, while larger-scale heterogeneities were used to simulate the fluid-pressure responses of the Forty-niner and Magenta units.

As a numeric model, GTFM can simulate well tests with complex wellbore boundary conditions. Testing periods are subdivided into a number of discrete time intervals, known as sequences, which are distinguished by differing wellbore boundary conditions, due to either the type or value of the boundary conditions. Wellbore boundary conditions used in the AIS simulations consisted primarily of specified pressure corresponding to calculated mud overpressure during the pilot-hole drilling, and zero pressure after penetration of the underground facility by the pilot hole. A limited number of short-duration, specified-flow boundary conditions were also applied during the drilling period to simulate: a) the interval's fluid-pressure responses when the pilot hole was cemented to aid in reorienting the hole; and b) the apparent reduction in flow from the units caused by settling of drilling mud in the borehole which may have blocked the formations. Wellbore boundary conditions are discussed in greater detail in Sections 5.2 and 5.3.

GTFM simulations are usually conducted with a constant wellbore radius. However, three wellbore radii were used for the AIS simulations. The intervals whose responses were analyzed in this report were initially penetrated by a 9-7/8-inch (0.25 m) diameter drilling bit. Shortly before penetration of the underground facility, the pilot hole was reamed to a diameter of 0.37 m. Subsequently, the intervals were upreamed to a 6.17-m diameter. The effects of the different wellbore radii were simulated by subdividing the entire period of interest into three different sub-simulations corresponding to the times of the different

wellbore radii. For each sub-simulation performed, the pressure distributions over the radial extent of the modeled flow regime were adjusted to reflect the geometry of the subsequent sub-simulation. These adjusted pressure distributions were then used as initial conditions for the next sub-simulation.

## 5.2 Drilling-Period WellBore Boundary Conditions

As described in the following paragraphs, the actual wellbore boundary conditions in effect during the simulation periods corresponding to the drilling phase of the AIS construction were not known exactly. The principal areas of uncertainty were: 1) the degree to which the formation overpressure from the column of drilling fluid above the formation was reduced by mud-filter-cake skin; and 2) the lengths of time the formations were exposed to full-borehole mud pressure; i.e., before the effects of filter-cake skin affected the formations overpressured condition. Therefore, the approach used in the AIS simulations was to vary the reduced formation overpressures due to filter-cake skin arbitrarily, and to vary the durations of time periods with full-borehole-mud pressure (Section 5.2.2). These parameters were varied until a satisfactory match to the H-16 fluid-pressure responses was achieved. This approach was taken to increase the reliability of the simulations for the period following penetration of the pilot hole into the repository horizon, when the post-penetration wellbore boundary conditions under open and draining conditions were known with much greater certainty.

During the period from the initial interception of the intervals of interest by the pilot hole until penetration of the underground facility, wellbore boundary conditions show considerable complexity. The basic sequence of events common to all intervals was as follows:

- 1) initial interception - the time when the 9-7/8-inch (0.25-m) drill bit used for drilling the pilot hole intersected the centers of the intervals.
- 2) cementing - two cementing operations were performed to allow correction of excessive deviation of the pilot hole. The first occurred on December 26, 1987 (Calendar Day 360), when the hole was cemented from 190 to 93 m, affecting only the Forty-niner and Magenta units. The second cementation occurred January 6, 1988 (Calendar Day 371) when the hole was cemented from 259 to 195 m BGS, which affected only the Culebra.
- 3) second unit interception - the time, after the cementation events, when the pilot hole intercepted the centers of the intervals for the second time.
- 4) reaming - the time at which the 14-3/4-inch (0.37-m) reaming bit intersected the center of the intervals.
- 5) final penetration - the penetration of the pilot hole into the WIPP-site underground facility on February 7, 1988 (Calendar Day 403).

Unit interception times for events 1, 3, and 4 were calculated based on hole-penetration data given in the pilot-hole DDR. Ideally, the wellbore boundary conditions for the periods between subsequent events would be described as follows:

Sequence 1, drilling - a fixed pressure corresponding to the calculated pressure at formation center due to an annulus filled with drilling mud. The pressure at formation center due to the mud filled annulus was in excess of actual formation pressure (see for example Stensrud, 1988a, 1988b) and is referred to as mud overpressure. Mud-overpressure values were calculated using a mud density of  $1174 \text{ kg/m}^3$ , as noted in the DDR for January 13, 1988 (Calendar Day 378), and a depth equivalent to the center of the interval. Calculated mud overpressures for each of the three intervals analyzed are given in Table 5.2.

Sequence 2, cementation - specified flow at a flow rate of zero. Well diameter of 0.25 m.

Sequence 3, drilling - same conditions as Sequence 1.

Sequence 4, reaming - fixed pressure using the same parameters as Sequence 1 and a well diameter of 0.37 m.

The actual types and values of the boundary conditions used in the simulations of the intervals' responses were affected by the true mud weight and height of the column of drilling fluid, by the amount of decrease in flow from the borehole to the formation due to settling of drilling mud in the borehole during periods when circulation was interrupted, and by the thickness and character of the build-up of mud filter cake on the face of the wellbore. The following subsections describe the techniques used to compensate for the effects of these factors.

### 5.2.1 Mud-Related Uncertainties

The pilot hole was assumed to be constantly full of mud during drilling periods. This assumption is somewhat unrealistic considering that installing and removing the drill string during bit changes and other operations probably affected the mud level. In addition, this assumption postulated that no mud was lost to the formations during periods when drilling operations were suspended. Variations in mud levels could have caused changes in mud overpressure at the intervals, which in turn would have affected the fluid-pressure responses at the observation wells.

A second mud-related uncertainty is the actual density of the drilling fluid used during drilling. Changes in drilling-fluid density due to variations in the amount and/or quality of makeup water and loss or gain of formation fluid can affect the fluid-pressure response of the formation. The DDR for the AIS pilot hole includes very few notations about the properties of the drilling fluid.

### 5.2.2 Flow Reduction

The measured formation-fluid pressures for the Forty-niner and Magenta intervals at H-16 (Figures 5.1 and 5.2) show periods where the fluid-pressure responses appear to have been affected by events consistent with an apparent loss of flow from the borehole to these intervals. The timing of the onset of these events is coincident with periods when pilot-hole drilling operations were suspended. Mud solids may have settled in the borehole when drilling-fluid circulation stopped. The settled solids may have partially occluded the formation causing reduced flow from the borehole to the intervals, thus allowing the interval fluid pressure to decrease toward formation pressure.

For the Magenta interval, flow reduction appears to have occurred over a nine-day period starting on December 13, 1987 (Calendar Day 347). During this period, drilling operations were suspended for safety reasons from December 13 until December 16 (Calendar Days 347 to 350). Drilling operations resumed with the reaming of the upper portion of the pilot hole to a depth of 93 m on December 20 (Calendar Day 354). Drilling of the 0.25-m pilot hole resumed on December 22 (Calendar Day 356) and mud circulation was restored over the entire depth of the pilot hole.

The H-16 fluid-pressure data indicate that flow to the Magenta was not restored to the interval during the first abbreviated reaming operation. The lack of circulation affecting the Magenta probably occurred because this reaming took place only in the upper portion of the pilot hole.

The H-16 fluid-pressure data for the Forty-niner interval (Figure 5.1) indicate a flow reduction similar to that observed for the Magenta. However, complete loss of flow to the Forty-niner apparently did not occur until some time after the resumption of reaming on December 16 (Calendar Day 347). The delay in developing reduced flow was probably because the Forty-niner claystone lies 5 m above the Magenta and the fillup of drilling solids may have taken longer to reach this interval.

The actual reduced flow rates for the Magenta or Forty-niner intervals could not be determined. Therefore, the reduced-flow-rate periods were assumed to result in complete flow loss and were simulated as specified-flow boundary conditions with a zero flow rate.

### 5.2.3 Filter-Cake Skin

The H-16 fluid-pressure responses for all three units analyzed indicates the probable development of filter-cake skins, or the buildup of a layer of mud solids on the intervals' borehole faces, which created a flow impedance at the wellbore. The relatively flat fluid-pressure responses for the H-16 Magenta and Culebra (Figures 5.2 and 5.3) intervals over the period from January 6 until February 1, 1988 (Calendar Days 371 to 397) can be interpreted as the result of some mechanism substantially impeding flow into the intervals from the wellbore. Similarly, the almost linear rate of fluid-pressure increase in the Forty-niner interval over the same period (Figure 5.1) can be attributed to less severe flow impedance.

Filter-cake-skin development is well understood qualitatively. One of the reasons for using clay-based muds is to promote formation of such skins, and thus prevent loss of drilling fluids to permeable formations. However, quantifying filter-cake skin parameters such as thickness and permeability, and estimating the rate of accumulation of the filter cake are difficult because of their dependence on drilling procedures and mud and formation properties (Krueger, 1986; Holditch and others, 1983). There are few quantitative data available on the actual dimensions of these filter-cake skins, primarily because the impact of filter-cake skins is not severe in conventional hydraulic testing where pretest well-development procedures are used to remove or ameliorate the effects of the filter-cake skins.

The simulation of the proposed filter-cake skins was difficult primarily because of the lack of justifiable parameters for specifying the skins. Also, because GTFM can only simulate a single heterogeneity, simulating the filter-cake skin as a heterogeneity would have precluded the simulation of other, and potentially more significant, formation heterogeneities. As an alternative approach,

the reduced formation-to-wellbore permeability of the filter-cake skins was assumed to cause a constant pressure drop across the skins making them appear to the formation as a fixed-pressure boundary condition with wellbore pressure significantly less than the mud overpressure but greater than the formation pressure.

The reduced-wellbore-pressure approach was validated by performing a number of scoping simulations with GTFM. The results of these simulations are shown in Figures 5.4 and 5.5. The formation and well-geometry parameters used for the scoping simulations are given in Table 5.3. Figure 5.4 illustrates the simulated fluid-pressure response at the skin/formation interface to an applied wellbore pressure of 2.498 MPa, 1.618 MPa above the assumed formation pressure of 0.88 MPa, for a range of skin hydraulic conductivities. Figure 5.4 shows that the wellbore pressure transmitted to the formation is relatively constant. Figure 5.5 illustrates the differences in fluid-pressure responses, at a radial distance equivalent to the distance between the pilot hole and observation-well H-16, between simulations performed using a skin heterogeneity and those performed using reduced wellbore pressures. The reduced pressures selected for the comparison simulations were based on the skin/formation interface pressures from Figure 5.4 at a time equal to 1 day. Figure 5.5 demonstrates that reduced mud overpressures can produce reliable and defensible results when simulating the impact of filter-cake skins.

Most periods when the formations of interest were exposed to mud overpressures were simulated using two or more sequences. The initial sequence had a relatively short duration and simulated the period before the build-up of a significant filter-cake skin, when full mud pressure was applied to the formation, as a fixed-pressure wellbore boundary condition. For subsequent sequences, reduced wellbore pressures were applied to simulate the effect of filter-cake skins on formation fluid pressures.

### 5.3 Wellbore Boundary Conditions After Penetration of the Underground Facility

After penetration of the pilot hole into the WIPP-site underground facility, the complete wellbore was exposed to atmospheric pressure. Wellbore boundary conditions for all intervals analyzed during this period used a fixed wellbore pressure of 0 MPa.

Filter-cake skins that developed on the intervals' faces before penetration of the WIPP-site underground facility were assumed to be removed as soon as the formations' flow directions reversed, because the removal of the drilling fluid from the pilot hole allowed the members of the Rustler to drain into the open hole or the AIS after upreaming.

### 5.4 Formation Heterogeneities

#### 5.4.1 Cement-Invasion Skin

Following cementation of the Culebra interval on January 5, 1987 (Calendar Day 370), the fluid-pressure response of the Culebra in H-16, when compared to the fluid-pressure response after upreaming of the shaft, indicates a flow-reduction condition similar to that caused by a damage or skin zone (Figure 5.3). This condition persisted after the pilot hole was reamed and drained of drilling fluid after penetration of the underground facility. To simulate the Culebra's fluid-pressure response after cementation, a radially-oriented cement-invasion skin was added to the Culebra for the post-cementation drilling and reaming periods and for the draining of the Culebra before upreaming intercepted the Culebra. The vuggy and fractured nature of the Culebra dolomite enhances its permeability and probably allowed relatively easy penetration of the cement grout into the formation.

The cement-invasion skin zone was assumed to be a radial zone with a finite thickness having a permanent reduced permeability due to the presence of cement in the formation. The cement was assumed to be responsible for the formation's slower response times and relatively higher pressures during the post-cementation drilling and reaming periods.

The simulations accounted for the cement-invasion skin by specifying a radial zone with an assigned permeability lower than that of the rest of the formation. In contrast to the use of reduced-wellbore-pressure boundary conditions to simulate the effect of filter-cake skins as described in Section 5.2.3, GTFM treated the cement-invasion skin as a formation heterogeneity. The thickness and permeability of the cement-invasion-skin heterogeneity were determined in an iterative manner by varying these parameters until a suitable match of observed and simulated data for the Culebra's drilling and reaming periods was achieved. Detailed descriptions of the use of the cement-invasion skin in the analysis of the Culebra fluid-pressure response to the construction of the AIS accompanies the discussion of the Culebra simulations in Section 6.1

#### 5.4.2 Radial Heterogeneity Boundaries

The H-16 fluid-pressure responses of the Magenta dolomite and the Forty-niner claystone indicated that these units behaved as heterogeneous formations. The formation heterogeneities were assumed to correspond to zones of differing permeability within the formations. The radial-flow model employed by GTFM dictates that formation heterogeneities can only be included as radial boundaries at specified distances from the pumping, injection, or, in the case of the AIS, draining well. The direction to and physical character of the actual boundaries must be derived from hydrogeologic and structural data.

The simulation of the H-16 fluid-pressure responses of the Magenta and Forty-niner included specified formation transmissivities for inner (near-field) and outer (far-field) zones radially oriented about the AIS. The distances to the radial boundaries for both units and the inner and outer transmissivities were determined empirically by varying these parameters until achieving satisfactory matches of observed and simulated data. Detailed descriptions of the use of the radial-heterogeneity boundaries used in the analysis of the Magenta and Forty-niner fluid-pressure responses to the construction of the AIS accompanies the discussions of their simulations in Sections 6.2 and 6.3, respectively.

### 5.5 Diffusivity Relationship

As mentioned previously, with the exception of several short-duration zero-flow boundary conditions, fixed-pressure boundary conditions were applied at the wellbore the majority of the time. As a result of the fixed-pressure boundary condition and the radial flow system simulated by GTFM, unique formation responses at observation wells are a function of the value of formation diffusivity, which is defined as:

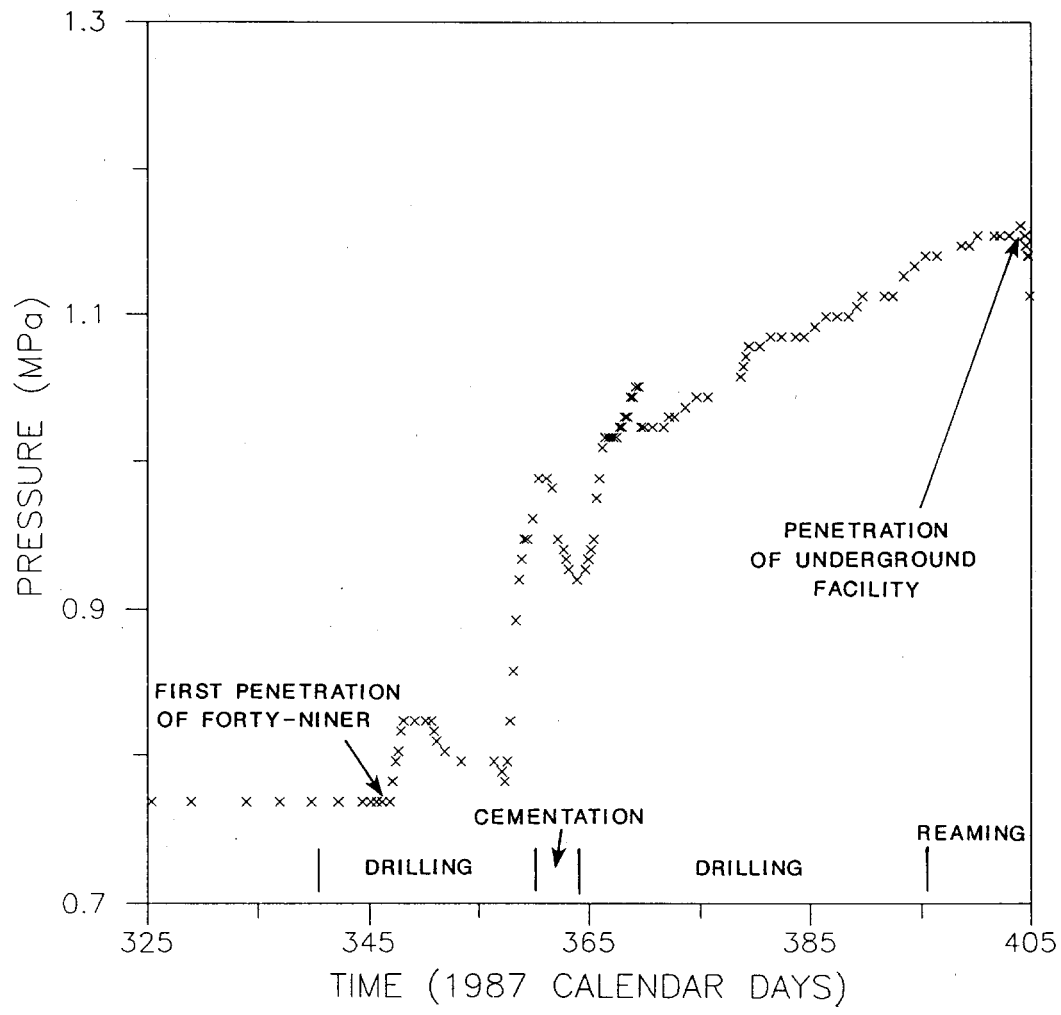
$$D = \frac{T}{S} \tag{5-1}$$

where:     D - diffusivity     [L<sup>2</sup>t<sup>-1</sup>]  
            T - transmissivity [L<sup>2</sup>t<sup>-1</sup>]  
            S - storativity     []

Therefore, simulated interval responses cannot be used to provide completely independent estimates of transmissivity and storativity. Rather, the parameters are lumped, thus providing a single term to characterize the individual intervals.

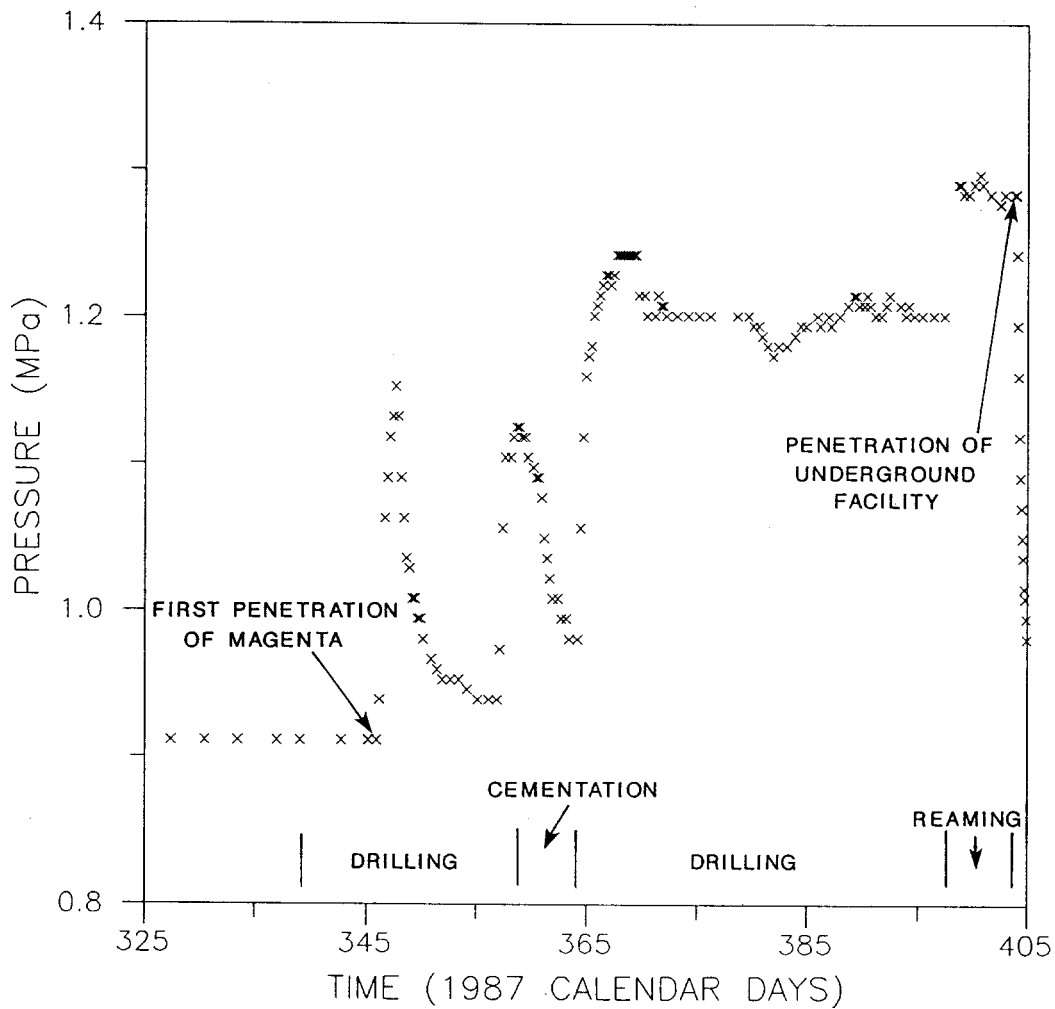
The approach used in the AIS simulations was to fix storativity at a value assumed to be representative of the units analyzed. These data were based on values determined by analyzing the results of previous tests conducted at the WIPP site (Beauheim, 1987a, 1987b; Gonzalez, 1983; Mercer, 1983; and Saulnier, 1987b) and a review of published estimates of the intervals' rock and fluid properties (Touloukian and others, 1981). After fixing the storativity, transmissivity was varied over appropriate ranges until satisfactory simulations were achieved. Simulation of the fluid-pressure responses of the Magenta and Forty-niner used formation-heterogeneity boundaries at various radii. Utilizing these boundaries, those parameters or parameter combinations which produced the closest matches between simulated and observed observation-well fluid-pressure responses were determined to be most characteristic of the intervals being simulated.

Interval transmissivities were calculated for the selected fixed storativities and the upper and lower limits of storativity assumed to be representative of the intervals whose fluid-pressure responses were analyzed (see Section 8.1). Upper- and lower-transmissivity limits were calculated from equation 5-1 and were not independently simulated.



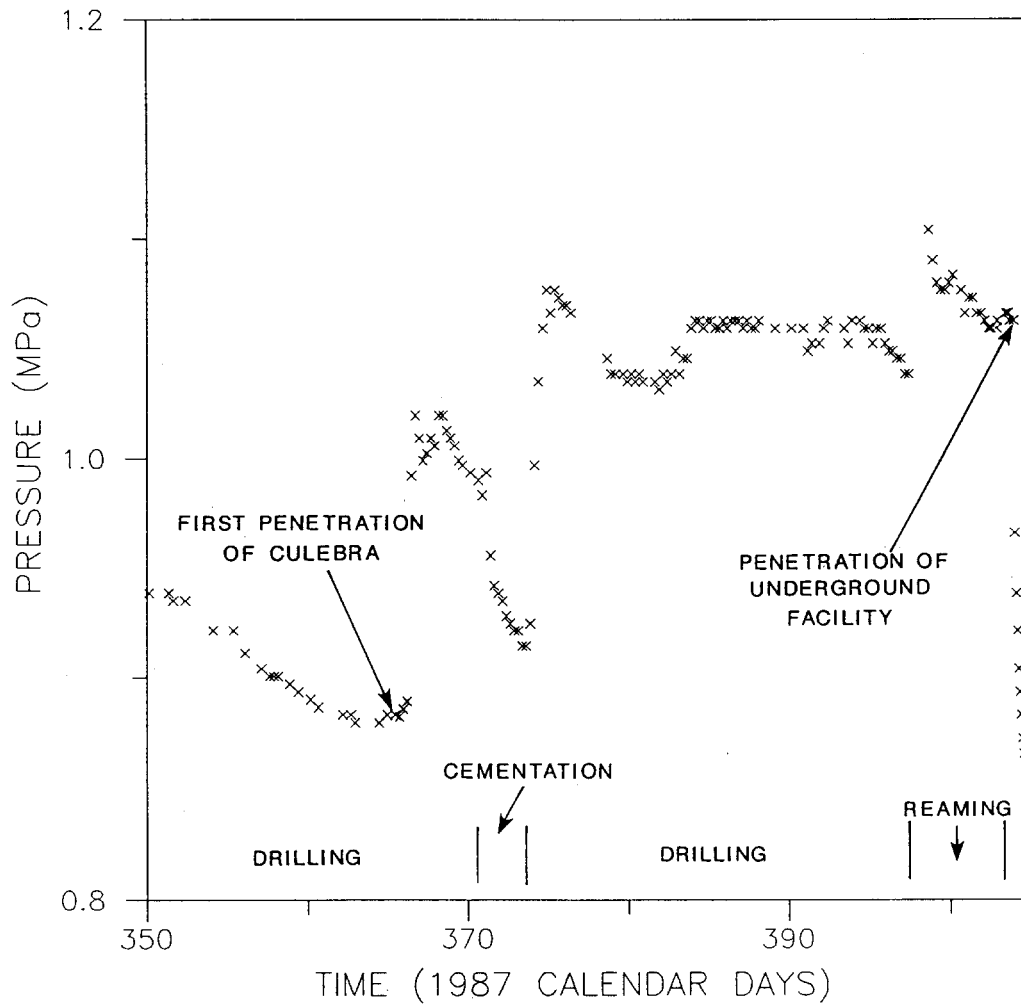
Drawn by J.D.A.	Date 1/16/89	FLUID-PRESSURE RESPONSE FOR THE FORTY-NINER CLAYSTONE AT H-16 DURING THE DRILLING/REAMING PERIOD
Checked by G.S.	Date 1/17/89	
Revisions	Date	
H09700R876	1/19/89	

<b>INTERA Technologies</b>	Figure 5.1
----------------------------	------------



Drawn by J.D.A.	Date 1/16/89
Checked by G.S.	Date 1/17/89
Revisions	Date
H09700R876	1/19/89

FLUID-PRESSURE RESPONSE FOR THE MAGENTA DOLOMITE AT H-16 DURING THE DRILLING/REAMING PERIOD

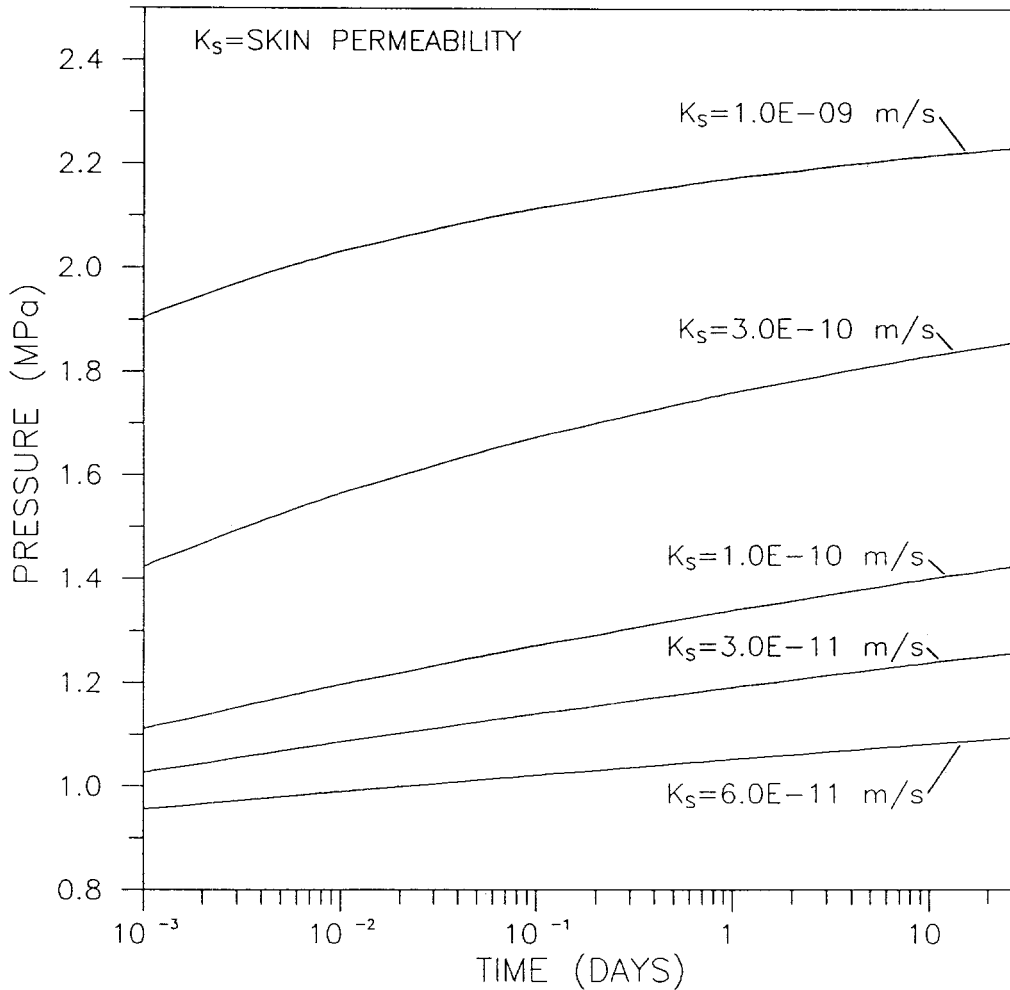


Drawn by J.D. A.	Date 1/16/89
Checked by G.S.	Date 1/17/89
Revisions	Date
H09700R876	1/19/89

FLUID-PRESSURE RESPONSE FOR THE CULEBRA DOLOMITE AT H-16 DURING THE DRILLING/REAMING PERIOD

**INTERA** Technologies

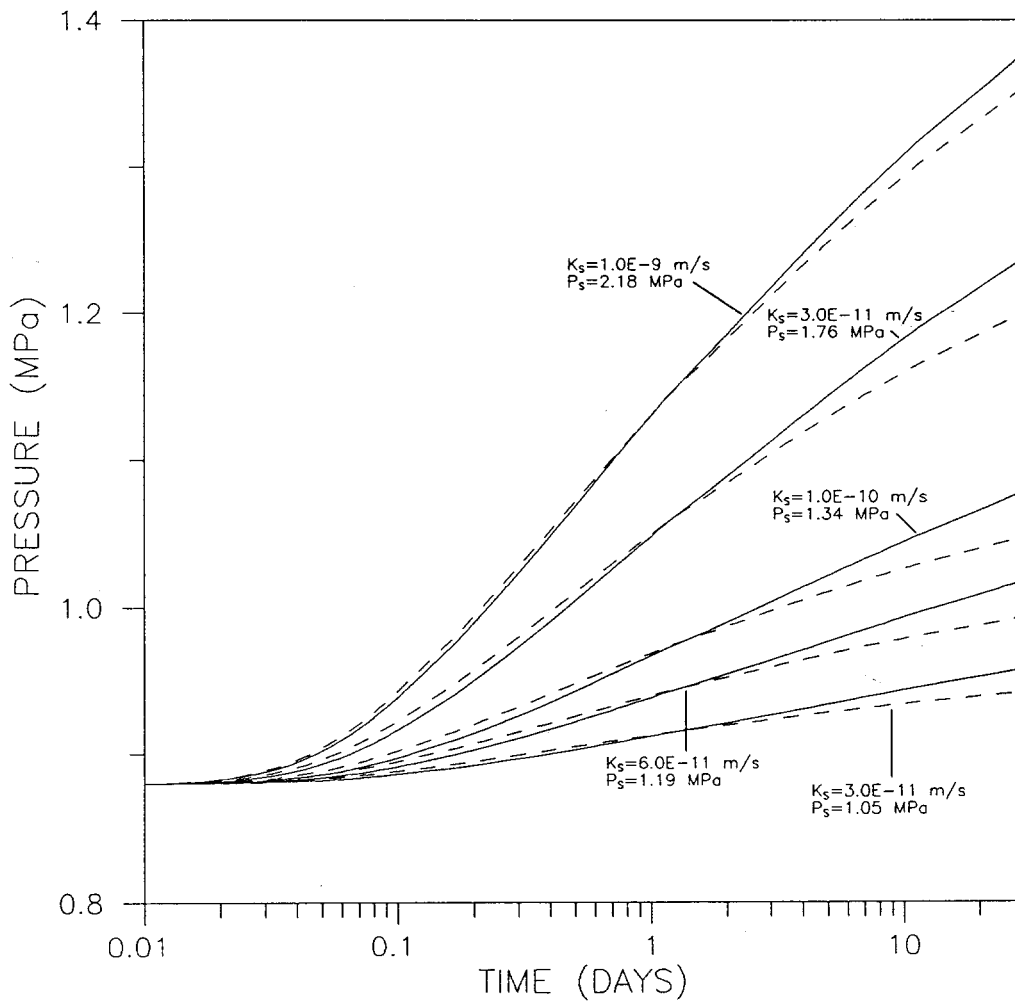
Figure 5.3



THE SIMULATED PRESSURES AT THE SKIN/FORMATION INTERFACE ARE RELATIVELY CONSTANT OVER THE PERIOD OF INTEREST INDICATING THAT A SPECIFIED, REDUCED WELLBORE PRESSURE CAN BE USED TO SIMULATE THE EFFECT OF A FILTER-CAKE SKIN.

Drawn by J.D.A.	Date 1/16/89
Checked by G.S.	Date 1/17/89
Revisions ABW	Date 6/23/89
H09700R876	1/19/89

FILTER-CAKE-SKIN SIMULATION PRESSURE AT THE SKIN/FORMATION INTERFACE



—  $K_S$  = SKIN PERMEABILITY  
 ---  $P_S$  = REDUCED WELLBORE PRESSURE TO SIMULATE THE PRESENCE OF A MUD-FILTER-CAKE SKIN

Drawn by J.D.A.	Date 1/16/89
Checked by G.S.	Date 1/17/89
Revisions ABW	Date 6/23/89
H09700R876	1/19/89

FILTER-CAKE-SKIN SIMULATION PRESSURE AT RADIUS OF OBSERVATION—WELL H-16

	INTERVAL		
	Forty-Niner Claystone	Magenta Dolomite	Culebra Dolomite
Depth [meters]			
Top	171.480	179.893	214.122
Bottom	174.894	187.635	220.797
Center	173.187	183.764	217.460
Thickness [meters]	3.414	7.742	6.675

Drawn by	Date	Depths and Thicknesses of the Rustler Units Analyzed at H-16
Checked by	Date	
Revisions	Date	
<b>INTERA Technologies</b>		Table 5.1

Depth to Interval  
Center  
[meters]

Mud Overpressure  
[MPa]

Interval

Forty-Niner	173.187	1.9895
Magenta	183.764	2.1110
Culebra	217.460	2.4980

Drawn by	Date
Checked by	Date
Revisions	Date

Calculated Rustler-Unit Mud Overpressures for  
Simulation of the Drilling Periods of the AIS-  
Pilot-Hole

**INTERA** Technologies

Table 5.2

**FILTER-CAKE SKIN SIMULATION PARAMETERS**

**Formation Parameters**

Formation transmissivity	1.30003E-07	[m <sup>2</sup> /s]
Formation storativity	9.99998E-06	[ ]

**Skin Parameters**

Radial thickness of skin	10.0	[mm]
Skin-zone storativity	9.99998E-06	[ ]
Skin hydraulic conductivity		
Value #1	1.00000E-09	[m/s]
Value #2	3.00000E-10	[m/s]
Value #3	1.00000E-10	[m/s]
Value #4	6.00000E-11	[m/s]
Value #5	3.00000E-11	[m/s]

**Other Parameters**

Test-interval length	6.675	[m]
Test-interval radius	125	[mm]
Wellbore pressure	2.4980	[MPa]
Static formation pressure	0.8800	[MPa]
Fluid density	1020.00	[kg/m <sup>3</sup> ]

**Calculated Skin Factor**

	$K_S$ [m/sec]	Skin Factor [ ]
Case #1	1.00000E-09	1.421909E+00
Case #2	3.00000E-10	4.919273E+00
Case #3	1.00000E-10	1.491174E+01
Case #4	6.00000E-11	2.490421E+01
Case #5	3.00000E-11	4.988538E+01

Drawn by	Date	Parameters for Simulations Including Filter-Cake Skin
Checked by	Date	
Revisions	Date	
<b>INTERA Technologies</b>		Table 5.3

## 6.0 ESTIMATION OF TRANSMISSIVITIES

The transmissivities of members of the Rustler Formation were estimated by comparing simulation results from the GTFM well-test simulator to: the observed fluid-pressure responses of those members in H-16; water-level responses in observation wells H-1, WIPP-21, and ERDA-9 completed to the Culebra dolomite near the AIS; and a single flow-rate measurement from the Culebra dolomite to the AIS after upreaming the AIS.

The drilling of the AIS pilot hole included periods of drilling, cementation, and reaming which provided a rather complex drilling history (see Sections 3.0 and 5.2). Transmissivities were estimated with GTFM after including the most important elements of the drilling history as they were reflected in the fluid-pressure responses at H-16. Figure 6.1 shows the H-16 fluid-pressure responses for all members of the Rustler isolated in the H-16 borehole during the drilling/reaming of the pilot hole and the upreaming of the AIS. These responses were used to develop the GTFM test sequences used to simulate the responses of the Culebra dolomite, the Magenta dolomite, and the Forty-niner claystone. The simulations were performed for a range of transmissivity values indicating the order of magnitude and variability of formation transmissivity.

Figure 6.1 also shows that the fluid-pressure responses of the Tamarisk and unnamed lower members of the Rustler were not suitable for analysis to estimate their transmissivities. The unnamed lower member fluid pressure did not appear to respond to the construction of the AIS. The large and sudden pressure decrease shown on Figure 6.1 on Calendar Day 650 was due to a slug-withdrawal test of the unnamed lower member designed to establish whether or not its pressure transducer was operating properly. The fluid-pressure data from the Tamarisk Member show continued adjustment with no identified trend during the pre-AIS period. Because the data did not appear to approach a stable pre-AIS formation pressure, they could not be used with confidence to estimate the Tamarisk's hydraulic parameters.

The following sections will describe the GTFM simulation and analysis of the fluid-pressure responses of the Culebra dolomite, the Magenta dolomite, and the Forty-niner claystone. The simulations will be compared to their H-16 fluid-pressure responses and the responses of other observation wells near the WIPP site. As discussed in Section 5.5, the boundary conditions applicable to the simulations resulted in the treatment of transmissivity and storativity parameters as the combined parameter diffusivity. Published estimates of formation hydraulic properties for the WIPP site show that there is much less variability in storativity than in transmissivity. Therefore, to determine representative values of transmissivity, a fixed storativity value of  $1 \times 10^{-5}$ , consistent with the published literature on testing at the WIPP site (Gonzalez, 1983; Mercer, 1983; Beauheim, 1987b; LaVenue and others, 1988), was used for all simulations. In the summary of results presented in Section 8.0, the transmissivities are calculated for a range of storativities assumed to be representative of the intervals studied. Refer to Table 1.1 for the nomenclature used for the simulation parameters in the text and on the figures and tables.

### 6.1 Culebra Dolomite

The Culebra dolomite's fluid-pressure response to the construction of the AIS was simulated using the methodology described in Section 5.2. The analysis was based on the fluid-pressure response of the Culebra as measured in H-16 (Figure 6.2). Because of the complex history of the drilling and reaming of the pilot hole, more weight was given to the fluid-pressure data observed after the pilot hole penetrated the underground facility. The GTFM simulations of the Culebra dolomite's fluid-pressure response were compared to the observed fluid-pressure response at H-16, water levels measured at observation wells H-1, ERDA-9, and WIPP-21 (Figure 6.3), and a single flow-rate measurement of 0.056 L/s from the Culebra to the AIS measured on October 28, 1988 (Calendar Day 667) (R. Deshler, IT Corporation, written communication, December

1988). The flow-rate measurement may be somewhat uncertain because some of the following factors may have affected the measurement: evaporation in the AIS was not taken into consideration; the water ring may not have captured all the flow from the Culebra; and small amounts of water from grouting operations higher in the AIS and from a leaking water connection on the AIS conveyance system may have contributed to the measured flow rate. In spite of the potential inaccuracies, the estimate of 0.056 L/s is considered good and was corroborated by an informal INTERA estimate of 0.063 L/s made during an AIS inspection on October 26, 1988 (Calendar Day 665) (Saulnier, INTERA Inc. internal memorandum, October 28, 1988).

Six simulations were used to analyze the Culebra dolomite's fluid-pressure response. The simulations are distinguished by differences in the simulation's formation transmissivity and by the inclusion or non-inclusion of a cement-invasion skin immediately surrounding the pilot hole as described in Section 5.4. The simulations indicate the range of variability in transmissivity and sensitivity to use of the cement-invasion-skin heterogeneity.

As discussed in Section 5.2, the actual wellbore boundary conditions during the pilot-hole drilling and reaming phases were uncertain. Simulation of this period required assumed wellbore pressures and flow rates to account for the events which occurred during the drilling/reaming period and to approximate the effect of filter-cake skin at the wellbore-formation interface. Using an iterative approach, the boundary conditions which provided the best simulation of the H-16 fluid-pressure data observed during this period were assumed to be representative of the formation's hydrologic conditions.

The simulation period for the Culebra was divided into six discrete time segments (Figure 6.2), the first four of which cover the drilling/reaming phase (Figures A.1 to A.6, Appendix A). The observed H-16 formation fluid pressures for the drilling/reaming phase are shown in Figure 6.4. Segments 1, 3, and 4 were simulated with fixed- wellbore-pressure boundary conditions. As discussed in Section 5.2.3, the effect of a filter-cake skin was simulated, when necessary, by subdividing the drilling and reaming periods and applying reduced pressures to simulate the effects of the assumed filter-cake skin. The period durations and reduced pressures applied for each segment of the Culebra dolomite simulation are given in Table 6.1. Figures A.1 through A.6, Appendix A, show the prescribed and simulated wellbore pressures during the drilling/reaming period for each of the Culebra simulations. (Note that for the period after cementation when the Culebra was isolated from the pilot hole, the formation's fluid-pressure response was simulated using a specified-flow boundary condition with a flow rate of 0.0 L/s to simulate the effects of flow loss due to cementation.)

After the drilling period, the period when the Culebra was open and draining through the pilot hole and/or the AIS to the underground facility was simulated using fixed-pressure wellbore boundary conditions with a value of 0.0 MPa, corresponding to atmospheric pressure. The well diameters used in the simulations were 0.25 m for the pilot hole, 0.37 m for the reaming period, and 6.17 m for the post-upreaming period 6.

All Culebra simulations assumed a static formation pressure of 0.88 MPa before the start of the simulations. This value was based on the Culebra fluid pressure in H-16 (Figure 6.4) immediately before the initial interception of the interval by the pilot hole.

### 6.1.1 Simulation Results

The Culebra simulations are described as follows:

#### **Simulation 1 - Matching The H-16 Fluid-Pressure Response, No Cement-Invasion-Skin Zone**

Because of the complex borehole history before penetration of the underground facility, the first Culebra simulation was intended to provide an initial transmissivity estimate by matching the H-16 fluid-pressure data during the period between penetration of the underground facility and interception of the Culebra by the upreaming of the AIS. The simulation was conducted using homogeneous formation properties with a formation transmissivity of  $2.6 \times 10^{-8} \text{ m}^2/\text{s}$ . The simulated formation pressures at the radii of H-16 and the other observation wells are shown in Figures 6.5 and 6.6, respectively. The simulated flow rate for Calendar Day 667 was 0.0031 L/s. Figure 6.5 shows that the simulated fluid-pressure response during the period before upreaming agrees with the observed H-16 response, but that the simulated response after upreaming does not agree. Figure 6.6 shows that the simulations of the observation-well responses are poor.

#### **Simulation 2 - Matching The H-16 Fluid-Pressure Response With A Cement-Invasion-Skin Zone**

The first simulation indicated a need for increased formation transmissivity. However, an increase in transmissivity, while maintaining homogeneous formation parameters, adversely affected the match to the H-16 data during the post-penetration/pre-upreaming period. To account for this apparent difference in formation transmissivity, a heterogeneity in the form of a reduced-permeability skin zone surrounding the pilot hole caused by cement invasion after cementation of the Culebra interval (see Section 3.1.1) was added to

the post-penetration/pre-upreaming period to restrict the formation's fluid-pressure response. The DDR for January 8, 1988 reports "cement and sand" in the cuttings during the period when the Culebra unit was redrilled following cementation, indicating that the Culebra was probably in contact with, and may have been invaded by, cement.

The second simulation included a cement-invasion-skin heterogeneity during the period from redrilling following cementation until Culebra interception by the AIS upreaming. The skin zone was a radial heterogeneity with a radius of 0.24 m from the borehole center and a transmissivity of  $3.0 \times 10^{-9} \text{ m}^2/\text{s}$ . The formation transmissivity used in the simulation was  $1.3 \times 10^{-7} \text{ m}^2/\text{s}$ , almost 2 orders of magnitude higher. This combination of parameters yielded a calculated skin factor of 3.64 during the drilling phase and 1.44 during the period between pilot hole reaming and AIS upreaming. The skin factor quantifies the pressure difference between the borehole and the formation across a thin skin zone at the borehole-formation interface. The skin factor indicates the degree of damage (positive skin factor) or improvement (negative skin factor) at the borehole-formation interface. The choice of skin-zone parameters was based on those parameter combinations that provided the best match to the H-16 fluid-pressure data. Simulation results for formation fluid pressures at the radius of H-16 and the other observation wells are shown in Figures 6.7 and 6.8. Figure 6.7 shows that the simulation results closely match the H-16 fluid-pressure response. However, although the simulated responses at the observation wells was improved compared to the first simulation (Figure 6.6), Figure 6.8 indicates that a further increase in formation transmissivity was required to match data from those wells adequately.

The simulated flow rate for Calendar Day 667 was 0.013 L/s, significantly less than the measured flow rate of 0.056 L/s, a further indication that an increase in formation transmissivity was needed.

### Simulation 3 - Matching the Culebra-to-AIS Flow Rate Using a Cement-Invasion-Skin Zone

The third simulation attempted to match the flow rate from the Culebra to the AIS of 0.056 L/s measured on Calendar Day 667. A cement-invasion-heterogeneity was included in the simulation to provide an acceptable match to the H-16 fluid-pressure-response data for the post-penetration/pre-upreaming period. The calibrated simulation parameters were a formation transmissivity of  $6.6 \times 10^{-7} \text{ m}^2/\text{s}$ , a skin-zone transmissivity of  $6.0 \times 10^{-9} \text{ m}^2/\text{s}$ , and a skin-zone radius of 0.48 m. The calculated skin factor was 10.26 for the drilling period and 4.05 for the post-reaming period. The simulations are presented in Figures 6.9 and 6.10. Figure 6.10 indicates reasonable agreement with the general character of the observed data for wells ERDA-9 and WIPP-21, but relatively poor agreement with the observed data for H-1. The calculated flow rate at Calendar Day 667 was 0.058 L/s, which compares favorably with the measured value of 0.056 L/s.

### Simulation 4 - Matching Observation-Well Data Using a Cement-Invasion-Skin Zone

The fourth simulation included a cement-invasion skin, and used a formation transmissivity midway between those used for simulations 2 and 3. This simulation was intended to provide a more reasonable match to the water-level response in H-1 and to provide additional sensitivity to the range of formation transmissivities needed to match the WIPP-21 and ERDA-9 data. The simulation used a formation transmissivity of  $2.6 \times 10^{-7} \text{ m}^2/\text{s}$  and assumed a cement-invasion-skin zone with a radius of 0.48 m and a transmissivity of  $3.5 \times 10^{-9} \text{ m}^2/\text{s}$ . The calculated skin factors were 6.72 and 2.65 for the drilling period and the period following pilot-hole reaming, respectively. Simulated and observed fluid-pressure and water-level responses for these simulations are presented in Figures 6.11 and 6.12. The Culebra flow rate to the AIS for this simulation was 0.025 L/s for Calendar Day 667, a little more than half that calculated for simulation 3.

## Simulations 5 and 6 - Sensitivity of H-16 Fluid-Pressure Response to Cement-Invasion-Skin Zone

Figure 6.13 shows the results of two simulations using the formation transmissivities from simulations 2 and 3 ( $1.3 \times 10^{-7} \text{ m}^2/\text{s}$  and  $6.6 \times 10^{-7} \text{ m}^2/\text{s}$ , respectively) without including a cement-invasion-skin zone. The simulations show the sensitivity of the simulated fluid-pressure response of the Culebra in H-16 to the use of a cement-invasion-skin zone. The cement-invasion-skin zone has relatively little impact on the simulated results for the period after upreaming. The primary effect of adding the cement-invasion-skin zone was to retard the formation response during the period when the Culebra was draining to the pilot hole and improve the overall match to the observed fluid-pressure response.

### 6.1.2 Discussion of Simulation Results

Assuming a storativity of  $1 \times 10^{-5}$ , the estimated Culebra transmissivities and the principal assumptions for the simulations presented above can be summarized as follows:

ESTIMATED CULEBRA TRANSMISSIVITY	SIMULATION ASSUMPTIONS
$2.6 \times 10^{-8} \text{ m}^2/\text{s}$	Match to H-16 Fluid-Pressure Response Homogeneous Properties, No Cement-Invasion-Skin Zone
$1.3 \times 10^{-7} \text{ m}^2/\text{s}$	Match to H-16 Fluid-Pressure Response, Cement-Invasion-Skin Zone
$6.6 \times 10^{-7} \text{ m}^2/\text{s}$	Match to the Culebra to AIS Flow Rate Cement-Invasion-Skin Zone
$2.6 \times 10^{-7} \text{ m}^2/\text{s}$	Match to H-1 Water-Level Response Cement-Invasion-Skin Zone

The estimated values of formation transmissivities from the four calibration simulations range from  $2.6 \times 10^{-8} \text{ m}^2/\text{s}$  to  $6.6 \times 10^{-7} \text{ m}^2/\text{s}$ . The lower value determined from the first simulation is considered unrepresentative due to the inadequate match of the simulation results to the post-upreaming fluid-pressure data from H-16, the water-level responses at the observation wells, and the underestimate of flow to the AIS. A revised range of estimated transmissivities for the Culebra is therefore  $1.3 \times 10^{-7} \text{ m}^2/\text{s}$  to  $6.6 \times 10^{-7} \text{ m}^2/\text{s}$ . The value of  $6.6 \times 10^{-7} \text{ m}^2/\text{s}$  appears to be the most representative of the Culebra between the AIS and H-16, between the AIS and ERDA-9, and between the AIS and WIPP-21. Simulation 3, which used this value, has the best match to the H-16 and observation-well data, and Simulation 3 provided the best estimate of the flow rate from the Culebra to the AIS. A transmissivity value of  $2.6 \times 10^{-7} \text{ m}^2/\text{s}$  for the Culebra appears to provide the best approximation of the H-1 response. It should be noted, however, that the simulations of the observation-well responses are less certain because other hydrologically-related influences (see Section 4.0) affecting the observation-well water-level responses, such as the WHS grouting, water-quality sampling, and the H-11 multipad/tracer test, were not included in this analysis.

Figure 6.14 shows simulated flow rates from the Culebra to the AIS for the four principal simulations for the period after upreaming. The shapes of the flow-rate curves are similar, with the differences in the magnitudes of the rates being relative to the differences in simulated formation transmissivities.

## 6.2 Magenta Dolomite

The analysis of the fluid-pressure response of the Magenta dolomite in H-16 (Figure 6.15) was performed using a methodology similar to that described in Section 6.1.1 for the Culebra dolomite. The H-16 fluid-pressure response (Figure 6.15) was the only observed data with which to compare the simulated results. No measurements of the flow from the Magenta to the AIS were available to use for simulation calibration. Personnel mapping the geology in the AIS reported one 0.9-m and one 1.5-m "damp" zone in the Magenta interval (R. Holt and R. Williams, International Technologies, personal communication, October 26, 1988). As was noted in the analysis of the Culebra dolomite (Section 6.1), the complexity of the drilling/reaming period meant that the simulation results were best judged by comparing the simulated fluid-pressure response, at a radius equivalent to the distance between the AIS and H-16, to the observed fluid-pressure data from H-16 after the pilot hole penetrated the underground facility because borehole conditions were known with the most certainty during this period.

Wellbore boundary conditions for the Magenta dolomite simulations were specified in a similar manner as discussed for the Culebra dolomite. The simulation period for the Magenta was divided into eight discrete time segments (Figure 6.15), the first six of which covered the drilling/reaming phase (Figures A.7 to A.16, Appendix A). Segments 1, 3, 5, and 6 were simulated with fixed-wellbore-pressure boundary conditions. Where required, the effects of a filter-cake skin (see Section 5.2.3) were simulated by subdividing the segments into two or more periods and, where necessary, reduced pressures were applied to simulate the effects of the assumed filter-cake skin. The period durations and reduced pressures applied for segments 1, 3, 5, and 6 of each simulation are given in Table 6.2. Table 6.2 shows that the assumed filter-cake skin was not required for some segments of some of the sensitivity simulations. For these segments, the H-16 pressure response during the drilling/reaming phase was either reproduced satisfactorily with full mud

pressure or could not be reproduced. Specified flow boundary conditions, with a flow rate of 0.0 L/s were applied for segments 2 and 4 to simulate the effects of flow loss due to mud settling and cementation, respectively.

The observed H-16 fluid pressures for the Magenta during the drilling/reaming phase are shown in Figure 6.16. Figures A.7 through A.16, Appendix A, show the prescribed (segments 1, 3, 5, and 6) and simulated (segments 2 and 4) wellbore pressures for the drilling/reaming period for each of the Magenta simulations and the simulated formation fluid pressure at H-16 for the drilling/reaming period.

A static formation pressure of 0.928 MPa was used as the initial condition for the Magenta dolomite simulations. This value was based on the Magenta's fluid pressure in H-16 before the initial interception of the interval by the pilot hole. The pressure measured at H-16 before drilling the pilot hole is constant, indicating that the selected formation pressure is representative of the interval.

#### 6.2.1 Simulation Results

Ten simulations of the Magenta's fluid-pressure response in H-16 were conducted. Two simulations, with and without formation-heterogeneity boundaries, compare the simulated data to the Magenta's observed H-16 fluid-pressure response. Eight simulations were performed to show the simulations' sensitivity to formation heterogeneity.

The Magenta simulations are described as follows:

**Simulation 1 - Match to the H-16 Fluid-Pressure Response,  
Homogeneous Formation**

The first simulation (Figure 6.17) shows the best match to the H-16 fluid-pressure response using homogeneous formation properties and a formation transmissivity of  $2.5 \times 10^{-6} \text{ m}^2/\text{s}$ . Although the match appears adequate for the late portion of the post-reaming/pre-upreaming period and only slightly underestimates the post-upreaming period, the match was unacceptable for the early and middle portions of the post-reaming and post-upreaming periods when the pilot hole or the AIS was open and the Magenta was draining. Additionally, the simulated flow rate from the Magenta to the AIS on Calendar Day 667 was 0.21 L/s, four times higher than the 0.056-L/s flow rate measured for the Culebra interval (see Section 6.1). This simulated flow rate is inconsistent with the geologist's report of only "damp" zones in the Magenta in the AIS (R. Holt and R. Williams, International Technologies, personal communication, October 26, 1988) an indication that the transmissivity of the Magenta interval is probably considerably lower than that of the Culebra.

The H-16 fluid-pressure response of the Magenta, unlike that of the Culebra interval, did not appear as if a cement-invasion skin was affecting the Magenta's H-16 response because of the simulation's good late-time matches to both the pilot-hole and AIS draining periods. Moreover, the shape of the H-16 fluid-pressure-response curve for the post-drilling/reaming period was consistent with that expected for a heterogeneous formation, indicating the need to simulate the Magenta's response as the result of a heterogeneous formation with a hydrologic boundary at some distance from the AIS.

**Simulation 2 - Match to the H-16 Fluid-Pressure Response,  
Heterogeneous Formation**

For the second simulation, the Magenta was divided into two radial zones with different transmissivities separated by a hydrologic boundary. The inner zone included the portion of the formation between the wellbore and the heterogeneity boundary. The outer zone consisted of the portion of the formation between the heterogeneity boundary and the external boundary of the modeled system. The three parameters which define the heterogeneity are:  $T_i$ , the inner-zone transmissivity;  $T_o$ , the outer-zone transmissivity; and  $r_b$ , the radius to the boundary between the two zones.

The Magenta's fluid-pressure response was simulated with a  $T_i$  of  $8.0 \times 10^{-8} \text{ m}^2/\text{s}$ , a  $T_o$  of  $4.0 \times 10^{-8} \text{ m}^2/\text{s}$ , and an  $r_b$  of 40 m. Figure 6.18 shows that the match to the H-16 fluid-pressure response is very good over the entire duration of the pilot-hole draining period and the early-time period after the Magenta was intersected by upreaming, and acceptable over the mid- and late-time portions of the post-upreaming period. Furthermore, the simulated flow rate of 0.0063 L/s for Calendar Day 667 is more consistent with the reported "damp" zones in the Magenta.

After achieving a reasonable match to the Magenta's fluid-pressure response using a formation-heterogeneity boundary, sensitivity simulations were performed to provide an indication of the ranges of  $T_i$ ,  $T_o$ , and  $r_b$ . Following is a discussion of these simulations, numbers 3 through 10.

### Simulations 3 through 8 - Sensitivity of the Heterogeneity Parameters of the Simulation of the Magenta's H-16 Fluid-Pressure Response

Six simulations were performed to assess the sensitivity of the Magenta simulation using a formation-heterogeneity boundary. For each simulation, one of the three heterogeneity parameters was changed while the remaining two parameters were the same as the values used in simulation 2. For  $T_0$  and  $T_i$ , values approximately  $\pm$  one half an order of magnitude of the calibration values were used for sensitivity, while  $r_b$  was increased and decreased by a factor of two. Simulations 3 and 4 used  $T_i$ 's of  $2.5 \times 10^{-8} \text{ m}^2/\text{s}$  and  $2.5 \times 10^{-7} \text{ m}^2/\text{s}$ , respectively; simulations 5 and 6 used  $T_0$ 's of  $1.3 \times 10^{-8} \text{ m}^2/\text{s}$  and  $1.3 \times 10^{-7} \text{ m}^2/\text{s}$ , respectively; and simulations 7 and 8 used  $r_b$ 's of 20 and 80 m, respectively. The results of the sensitivity simulations are presented in Figures 6.19 through 6.22. Figures 6.19, 6.20, and 6.21 show the simulated results for simulations 3 and 4, 5 and 6, and 7 and 8, respectively, for the entire simulation period. Figure 6.22 shows semi-log plots which compare the results of the sensitivity simulations with the best-match simulation for the period between penetration of the underground facility and Magenta interception by upreaming. Figure 6.22 illustrates explicitly the two-transmissivity nature of the heterogeneous formation response. The early-time magnitude of the simulated fluid-pressure response at H-16 is largely dependent on the inner-zone transmissivity (Figure 6.22a). Although there are differences in the magnitude of the simulation's late-time fluid-pressure response, Figure 6.22a shows that the shape of the late-time curve is similar for all values of  $T_i$ . In contrast, Figure 6.22b illustrates that the value of  $T_0$  primarily affects the simulation of the late-time fluid-pressure response while having very little impact on the early-time behavior. Figure 6.22c shows that changing the radius of the heterogeneity boundary primarily affects the time of the transition between inner- and outer-zone-dominated fluid-pressure responses.

### Simulations 9 and 10 - Homogeneous-Formation Characterization Showing Sensitivity to $T_i$ and $T_o$ of the Best-Match Heterogeneous Characterization

Simulations 9 and 10 show the Magenta's simulated fluid-pressure response using a homogeneous-formation characterization with formation transmissivities equal to the inner- and outer-zone transmissivities of the best-match heterogeneous simulation. Figure 6.23 shows the simulated fluid-pressure responses at H-16 for a homogeneous formation with transmissivities equal to  $8.0 \times 10^{-8} \text{ m}^2/\text{s}$  and  $4.0 \times 10^{-8} \text{ m}^2/\text{s}$ .

#### 6.2.2 Discussion of Simulation Results

Simulation 1 indicated that the portion of the Magenta dolomite responding to the influence of the pilot hole/AIS does not exhibit behavior consistent with homogeneous formation properties. Therefore, heterogeneous-formation parameters were used in simulation 2 in an attempt to describe the assumed heterogeneity. However, the description is probably not unique, and simulation of the pilot hole drilling/AIS upreaming using models with other geometries, such as a two-dimensional cartesian flow regime, could result in different descriptions of the formation properties. Indeed, this is likely the case as the formation heterogeneities simulated in the heterogeneous simulations assume radial symmetry. The likelihood of radial symmetry in formation transmissivity is remote. Furthermore, the abrupt spatial change in properties used in the GTFM simulations, where the transmissivity decreases by a factor of two at a discrete boundary, is also unlikely.

The physical basis for a formation-heterogeneity boundary in the Magenta is not immediately evident. Only a limited number of test wells are completed to the Magenta and extensive aquifer testing of this unit has not been performed (Mercer, 1983). While core samples from the Magenta indicate a rather uniform geologic character to this formation, Snyder (1985) describes patterns of halite dissolution in the Rustler Formation which may have led to fracturing of the Magenta. Areal differences in fracturing of the formation, such as could develop in response to halite dissolution, could result in heterogeneity in the areal distribution of the formation's hydrogeologic properties. This heterogeneity could affect its fluid-pressure response to major hydraulic stresses.

Notwithstanding the preceding discussion, the high sensitivity of simulated formation response to changes in the heterogeneity properties indicates that formation transmissivities used in the heterogeneous-formation-characterization simulations give a reasonable approximation of effective formation properties for the Magenta dolomite near the AIS. Therefore, the inner- and outer-zone transmissivities of  $8.0 \times 10^{-8} \text{ m}^2/\text{s}$  and  $4.0 \times 10^{-8} \text{ m}^2/\text{s}$  are considered representative of the effective transmissivities for the Magenta dolomite in that area.

### 6.3 Forty-Niner Claystone

The analysis of the H-16 fluid-pressure response of the Forty-niner Member of the Rustler Formation in H-16 was performed with the same procedures used to analyze the Magenta dolomite's response (see Section 6.2). Although the entire Forty-niner was monitored in H-16, the fluid-pressure response was assumed to be derived from the Forty-niner claystone unit (see Beauheim, 1987a for Forty-niner drill-stem-test results). The basic methodology for all simulations is described in Section 5.2 with certain modifications as described in the following paragraphs.

The H-16 fluid-pressure response (Figure 6.24) was the only observed data with which to compare the simulated results. No flow-rate measurements were made from the Forty-niner at the AIS. Geologic mapping of the Forty-niner interval in the AIS indicated only that the unit was "moist" (R. Holt and R. Williams, International Technologies, personal communication, October 26, 1988). As was the case for the Culebra and Magenta dolomites, because of the complex drilling/reaming-period history, the Forty-niner's simulated fluid-pressure response at a radius equivalent to the distance between the AIS and H-16 was compared to the observed fluid-pressure response in H-16 primarily for the period after penetration of the underground facility by the pilot hole.

Unlike that of the more permeable Culebra and Magenta dolomites, the Forty-niner claystone's H-16 fluid-pressure response to events in the AIS was often delayed by periods of a day or more. For example, according to the DDR, the Forty-niner interval was penetrated on December 11, 1987 (Calendar Day 345) while the observed H-16 formation fluid pressure did not definitively deviate from the constant pre-drilling pressure until Calendar Day 347. Consequently, a direct connection between an event described in the DDR and the Forty-niner's resulting H-16 fluid-pressure response was sometimes difficult to establish. Therefore, the DDR was used to determine segment durations and the Forty-niner's H-16 fluid-pressure response was used only to corroborate the timing of events.

Preliminary simulations indicated that the Forty-niner interval exhibited similar but more extreme heterogeneous behavior than that previously described for the Magenta dolomite. Consequently, the simulation approach for the Forty-niner claystone was identical to that performed for the Magenta dolomite. Wellbore boundary conditions for the Forty-niner claystone simulations were specified in a similar manner as discussed for the Culebra dolomite in Section 6.1.1. Like the Magenta

dolomite, the simulation period for the Forty-niner claystone was divided into eight discrete time segments (Figure 6.24), the first six of which covered the drilling/reaming phase (Figures A.17 to A.26, Appendix A). The observed H-16 fluid-pressure response for the drilling/reaming period covered the first six segments as shown on Figure 6.25. Segments 1, 3, 5, and 6 of the drilling/reaming period were simulated with fixed-wellbore-pressure boundary conditions. As discussed in Section 6.2.1 for the Magenta simulations, some of the simulations did not require the use of filter-cake skin to reproduce the H-16 pressure response. The period durations and reduced pressures applied for segments 1, 3, 5, and 6 of each simulation of the drilling/reaming period are given in Table 6.3. Specified-flow boundary conditions with a flow rate of 0.0 L/s were applied for segments 2 and 4 to simulate the effects of flow loss due to mud settling and cementation, respectively. Figures A.17 through A.26 display the prescribed (segments 1, 3, 5, and 6) and simulated (segments 2 and 4) wellbore pressures for each of the Forty-niner claystone simulations and the simulated formation fluid pressure at H-16 for the drilling/reaming period. (Note that when the Forty-niner was isolated from the borehole during cementation, the formation's fluid-pressure response was simulated with a specified 0.0 L/s boundary condition simulating flow loss from the lower pressured borehole.)

The Forty-niner's formation fluid pressure observed at H-16 before the start of the drilling of the pilot hole was 0.796 Mpa (Figure 6.25). This pressure was used as the static formation pressure for the Forty-niner claystone simulations. This pressure was observed during the pre-construction period, indicating that the selected formation pressure was representative of the interval.

### 6.3.1 Simulation Results

Ten simulations of the Forty-niner claystone's fluid-pressure response in H-16 were conducted. Two simulations evaluated the need for a formation-heterogeneity boundary and eight simulations evaluated the sensitivity of the results to the formation-heterogeneity parameters.

The Forty-niner claystone simulations are described as follows.

#### **Simulation 1 - Match to the H-16 Fluid-Pressure Response, Homogeneous Formation**

The goal of the first simulation was to match the Forty-niner's H-16 fluid-pressure response using homogeneous formation properties. A simulated transmissivity of  $4.0 \times 10^{-7} \text{ m}^2/\text{s}$  resulted in the best match as shown in Figure 6.26. The match offers a very poor fit to all portions of the observed H-16 fluid-pressure response except for the very late-time portion of the post-interception/pre-upreaming period. The simulated flow rate from the Forty-niner to the AIS on Calendar Day 667 was 0.033 L/s, just slightly lower than the measured flow rate for the Culebra interval, and inconsistent with the geologist's report that the Forty-niner interval was only "moist".

Like the first simulation of the Magenta dolomite's fluid-pressure response in H-16 (Section 6.2.1), the results of the Forty-niner simulation indicated that the Forty-niner claystone interval was exhibiting a fluid-pressure response characteristic of a strongly heterogeneous formation.

## **Simulation 2 - Match to the H-16 Fluid-Pressure Response, Heterogeneous Formation**

The second Forty-niner simulation assumed a formation-heterogeneity boundary and the Forty-niner was modeled with two radial zones having different transmissivities. The inner zone included the portion of the formation between the wellbore and the heterogeneity boundary. The outer zone consisted of the portion of the formation between the heterogeneity boundary and the external boundary of the modeled system.

The heterogeneous-formation simulation was performed with a  $T_i$  of  $9.0 \times 10^{-9}$  m<sup>2</sup>/s, a  $T_o$  of  $1.5 \times 10^{-9}$  m<sup>2</sup>/s, and an  $r_b$  of 40 m. Results of the simulation are shown in Figure 6.27. The match to the H-16 fluid-pressure response is very good over the entire duration of the pilot-hole draining period and is acceptable for the period after intersection of the interval by upreaming. The simulated flow rate of  $5.5 \times 10^{-4}$  L/s for Calendar Day 667 is consistent with the "moist" interval noted during geologic mapping.

After achieving a reasonable match to the Forty-niner claystone's fluid-pressure response using a formation-heterogeneity boundary, sensitivity simulations were performed to provide an indication of the ranges of  $T_i$ ,  $T_o$ , and  $r_b$ . Following is a discussion of these simulations, numbers 3 through 10.

## **Simulations 3 through 8 - Sensitivity of the Heterogeneity Parameters of the Simulation of the Forty-Niner's H-16 Fluid-Pressure Response**

Six simulations were performed to assess the sensitivity of the Forty-niner simulation using a formation-heterogeneity boundary. For each simulation, one of the three heterogeneity parameters was changed while the remaining two parameters were the same as the values used in simulation 2. The following parameter values were used for the

respective simulations: simulation 3,  $T_i = 3.0 \times 10^{-9} \text{ m}^2/\text{s}$ ; simulation 4,  $T_i = 3.0 \times 10^{-8} \text{ m}^2/\text{s}$ ; simulation 5,  $T_o = 5.0 \times 10^{-10} \text{ m}^2/\text{s}$ ; simulation 6,  $T_o = 5.0 \times 10^{-9} \text{ m}^2/\text{s}$ ; simulation 7,  $r_b = 20 \text{ m}$ ; and simulation 8,  $r_b = 80 \text{ m}$ . Simulation results are shown on Figures 6.28 through 6.31. Figures 6.28, 6.29, and 6.30 show the simulated results for simulations 3 and 4, 5 and 6, and 7 and 8, respectively, for the entire simulation period. Figure 6.31 contains semi-log plots comparing the results of the sensitivity simulations with the best-match simulation for the period between penetration of the underground facility and the interception of the Forty-niner interval during upreaming. In general, the heterogeneous sensitivity simulations for the Forty-niner interval show results similar to those of the corresponding Magenta dolomite simulations. For simulations 3, 6, and 8, the H-16 fluid-pressure response during the drilling/reaming period could not be matched, and therefore the results for the period after penetration of the underground facility are not directly comparable. However, the shape of the simulated fluid-pressure-response curve yields results similar to the Magenta dolomite simulations. Due to the more extreme permeability contrast between the inner and outer zones, the Forty-niner heterogeneous best-match simulation shows more sensitivity to the heterogeneity parameters than did the Magenta best-match simulation.

#### **Simulations 9 and 10 - Homogeneous-Formation Characterization Showing Sensitivity to $T_i$ and $T_o$ of the Best-Match Heterogeneous Characterization**

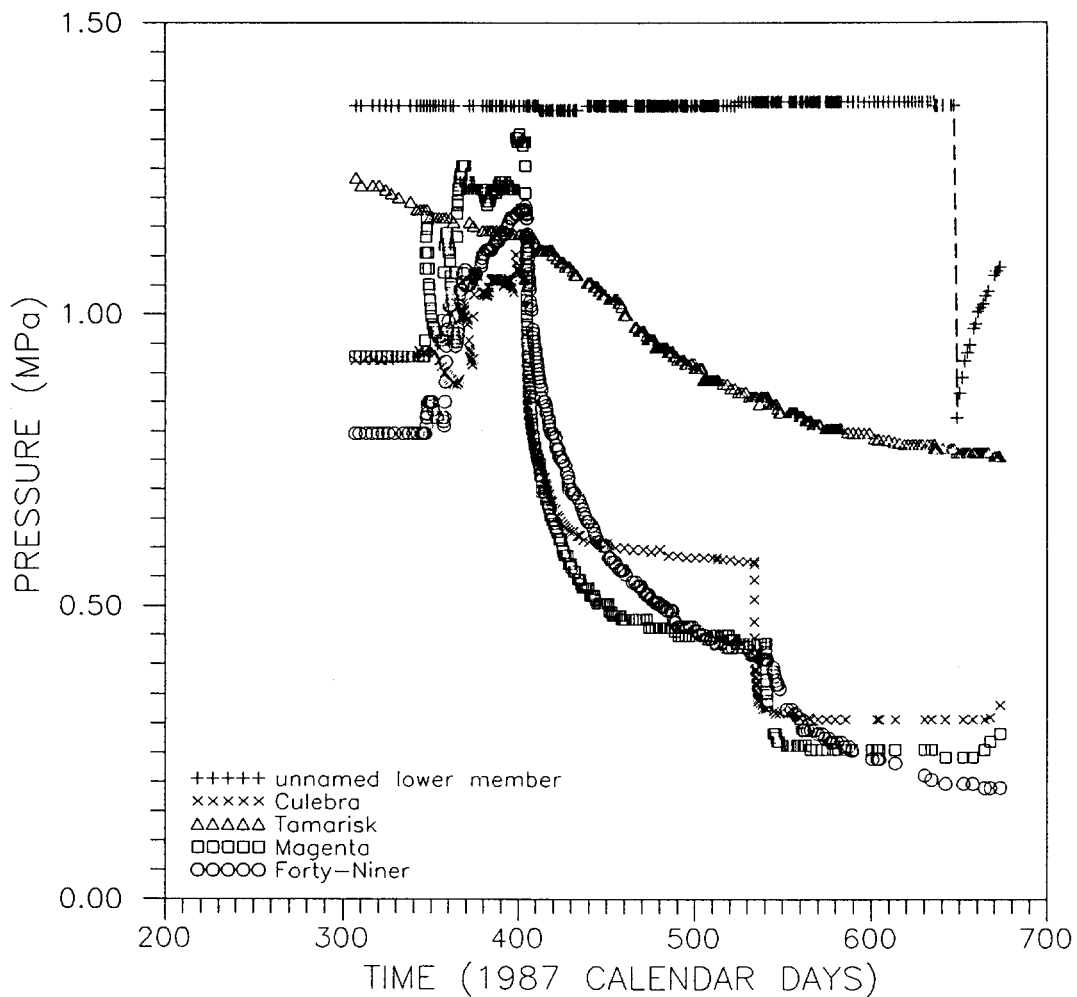
Simulations 9 and 10 illustrate the Forty-niner's fluid-pressure response using a homogeneous-formation characterization with formation transmissivities of  $9.0 \times 10^{-9} \text{ m}^2/\text{s}$  and  $1.5 \times 10^{-9} \text{ m}^2/\text{s}$ , the inner-zone and outer-zone transmissivities of the best-match heterogeneous

characterization, respectively. Results of these simulations are shown on Figure 6.32. Even though full-borehole mud pressure was applied for the entire duration of each fixed-pressure segment of the drilling/reaming period, the observed formation-fluid pressure at H-16 could not be matched. This provides further indication of the heterogeneous nature of the Forty-niner interval.

### 6.3.2 Discussion of Simulation Results

The poor matches of all simulations using a homogeneous-formation characterization, and the sensitivity of the simulation results to variance in the parameters defining the heterogeneities, provide conclusive evidence of heterogeneous behavior of the Forty-niner claystone. The accuracy of the assumed heterogeneity geometry is subject to the same uncertainties discussed in Section 6.2.2 for the Magenta dolomite. However, as for the Magenta dolomite simulations, the formation transmissivities used in the heterogeneous-formation-characterization simulations probably provide a reasonable approximation of effective formation properties for the Forty-niner claystone. The inner-zone and outer-zone transmissivities of  $9.0 \times 10^{-9} \text{ m}^2/\text{s}$  and  $1.5 \times 10^{-9} \text{ m}^2/\text{s}$ , respectively, can therefore be considered representative of effective transmissivities of the Forty-niner claystone in the area near the AIS.

As discussed in Section 6.2.2, the physical basis for the existence of a radial formation-heterogeneity boundary in the Forty-niner is not readily apparent. The fluid-pressure response of the Forty-niner suggests that a type of heterogeneity may exist in the Forty-niner. The heterogeneity could be the result of areal differences in the sedimentary fabric of the Forty-niner claystone.



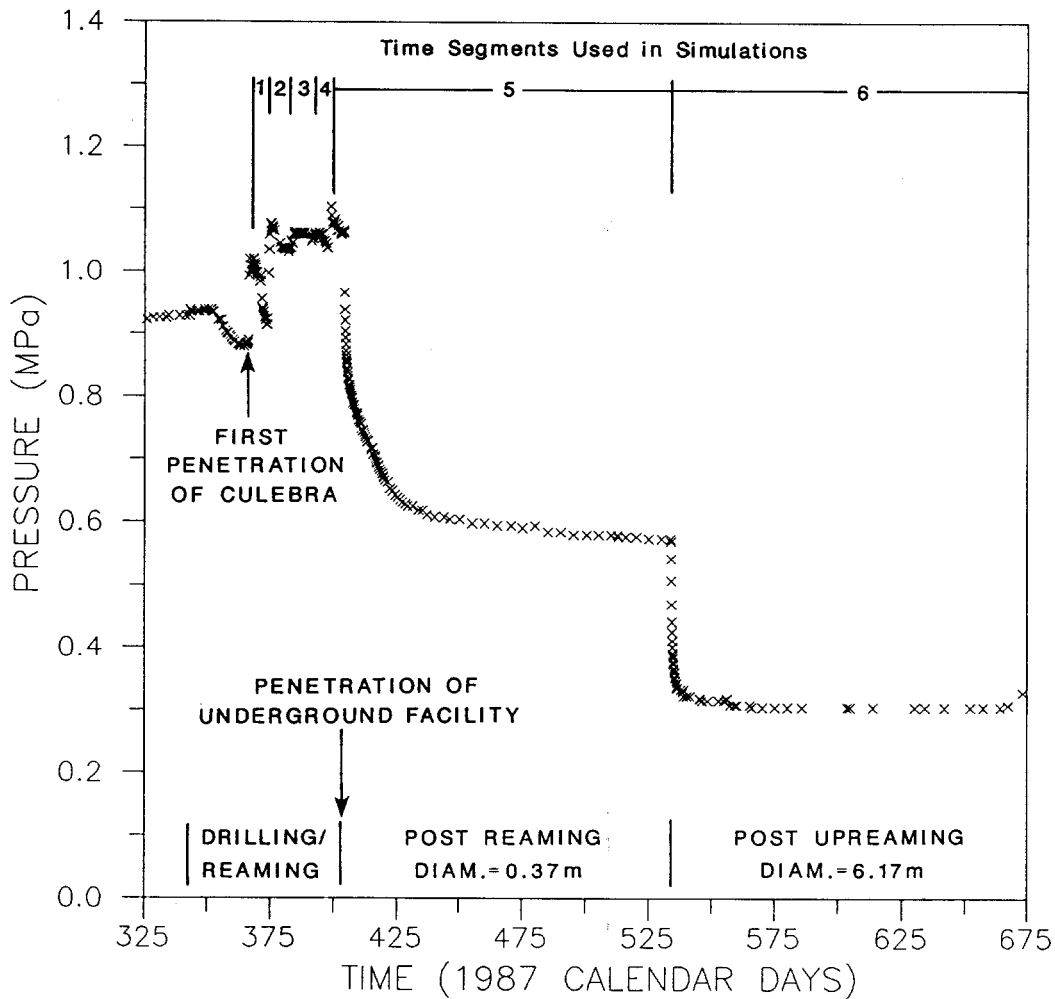
TIME 0 = JANUARY 1, 1987

Drawn by J.D.A.	Date 2/27/89
Checked by G.S.	Date 2/27/89
Revisions	Date
H09700R876	2/27/89

OBSERVED FLUID-PRESSURE RESPONSES OF THE FIVE MEMBERS OF THE RUSTLER FORMATION AT OBSERVATION-WELL H-16 DURING THE CONSTRUCTION OF THE AIS

**INTERA** Technologies

Figure 6.1



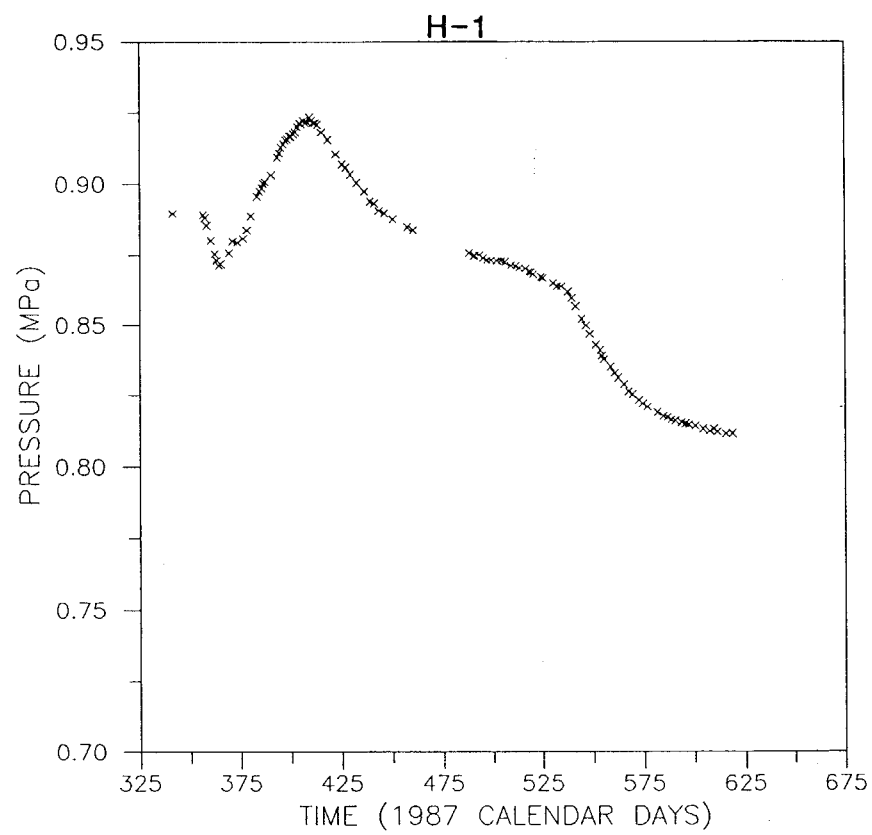
TIME 0 = JANUARY 1, 1987

Drawn by J.D.A.	Date 2/27/89
Checked by G.S.	Date 2/27/89
Revisions ABW	Date 6/23/89
H09700R876	2/27/89

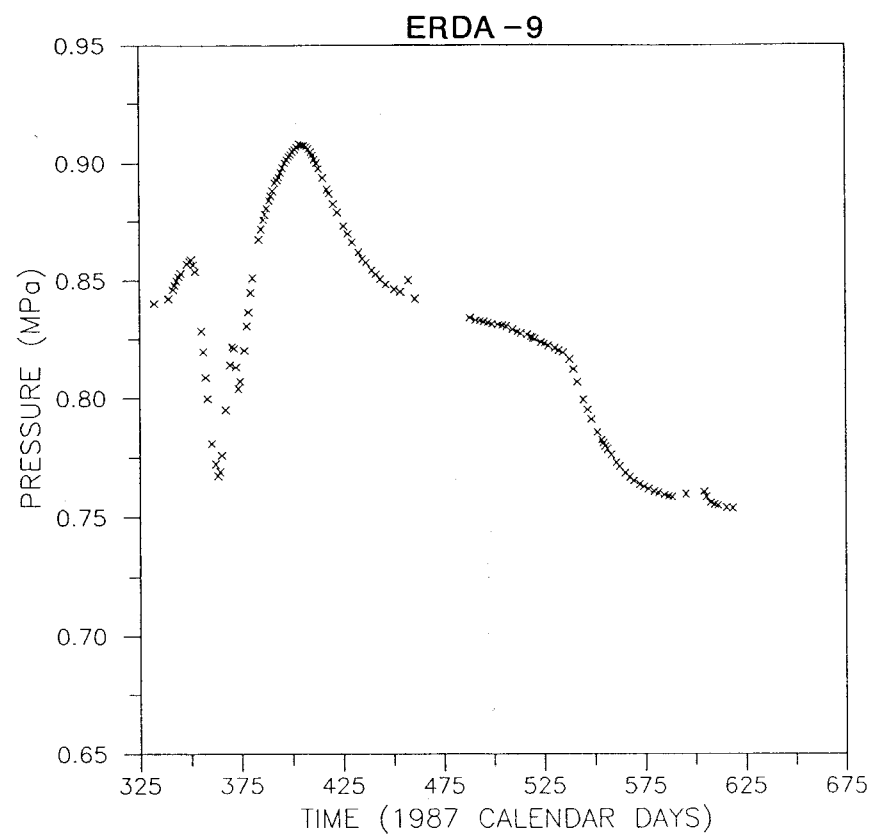
FLUID-PRESSURE RESPONSE OF THE CULEBRA DOLOMITE OBSERVED AT OBSERVATION-WELL H-16 DURING THE CONSTRUCTION OF THE AIS

**INTERA** Technologies

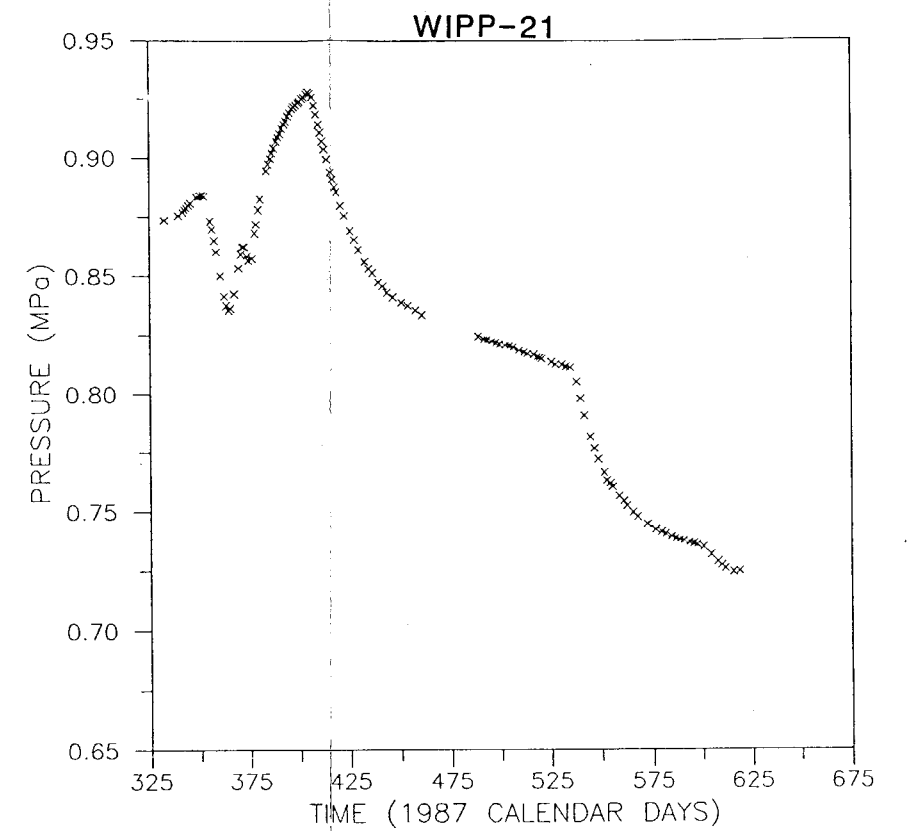
Figure 6.2



TIME 0 = JANUARY 1, 1987



TIME 0 = JANUARY 1, 1987



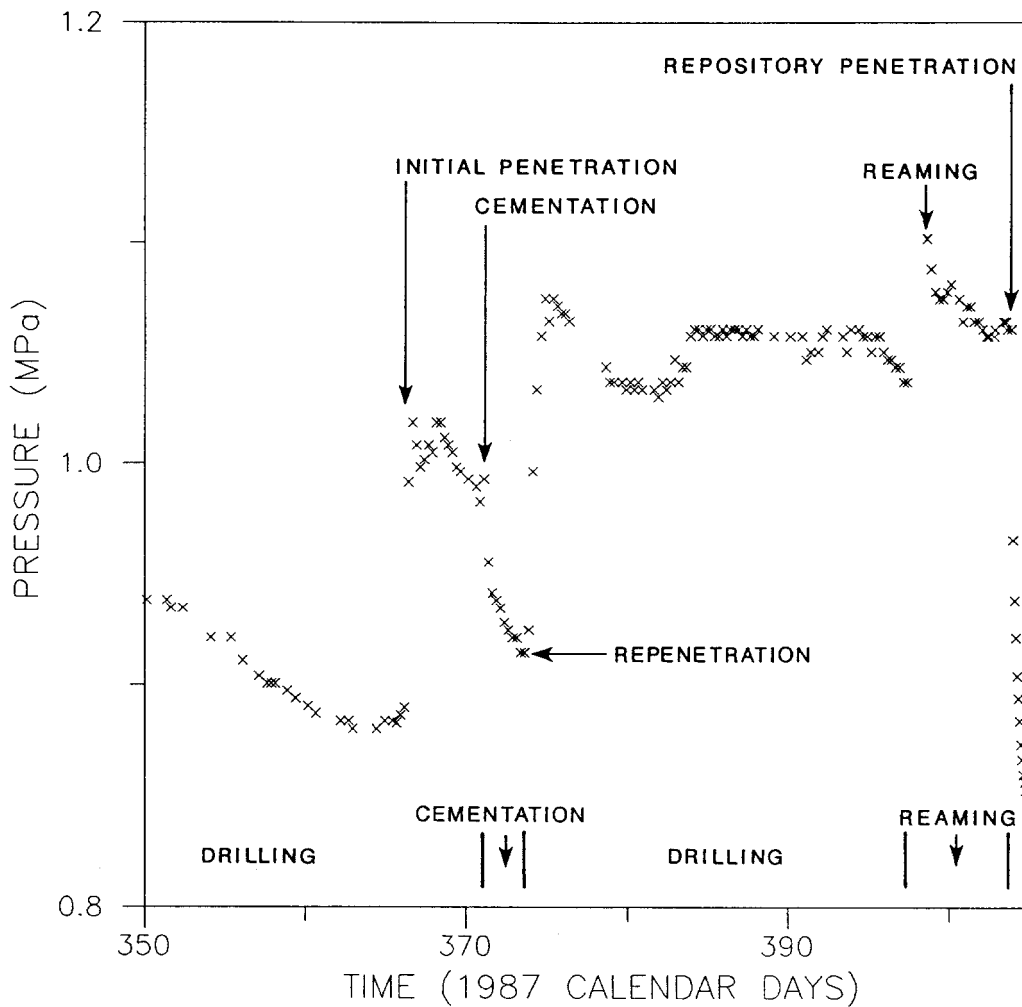
TIME 0 = JANUARY 1, 1987

Drawn by J.D.A.	Date 2/27/89
Checked by G.S.	Date 2/27/89
Revisions G.S.	Date 6/6/89
H09700R876	2/27/89

FLUID-PRESSURE RESPONSES OF THE CULEBRA DOLOMITE MEASURED AT OBSERVATION-WELLS H-1, ERDA-9, AND WIPP-21 DURING THE CONSTRUCTION OF THE AIS

**INTERA** Technologies

Figure 6.3



TIME 0 = JANUARY 1, 1987

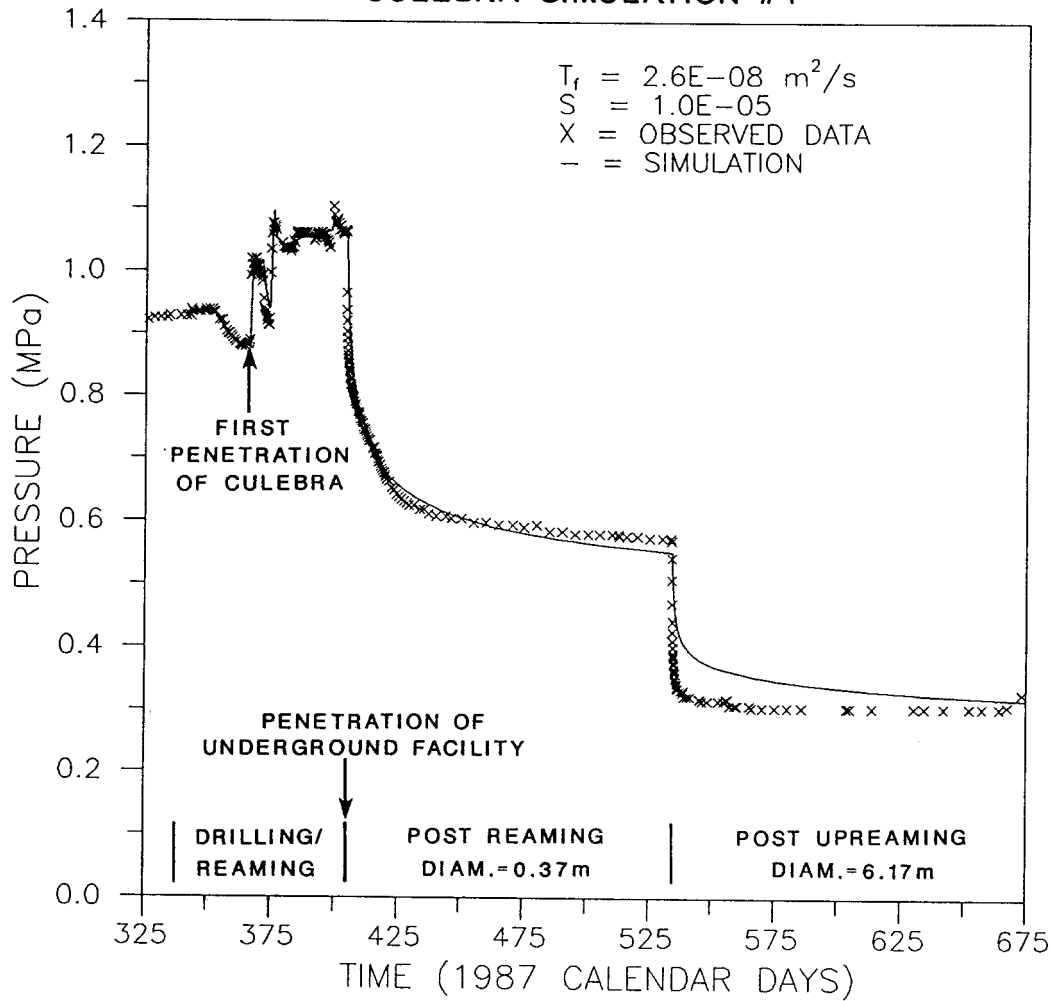
Drawn by J.D.A.	Date 2/27/89
Checked by G.S.	Date 2/27/89
Revisions	Date
H09700R876	2/27/89

FLUID-PRESSURE RESPONSE OF THE CULEBRA DOLOMITE OBSERVED AT OBSERVATION-WELL H-16 DURING THE DRILLING/REAMING PERIOD OF THE CONSTRUCTION OF THE AIS

**INTERA** Technologies

Figure 6.4

### CULEBRA SIMULATION #1



TIME 0 = JANUARY 1, 1987

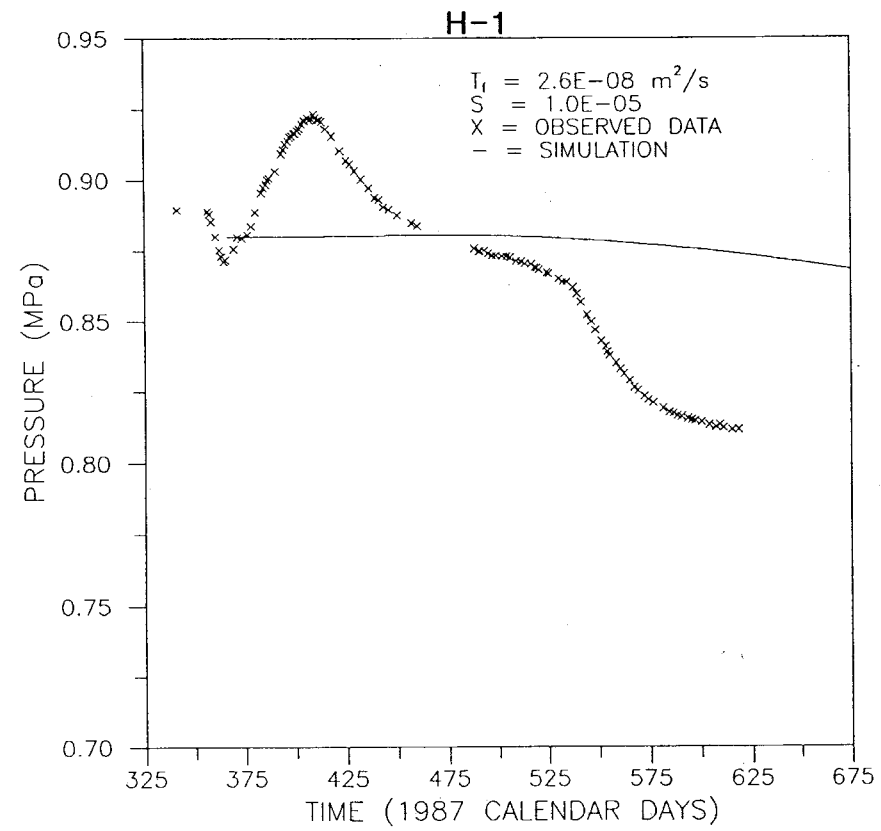
Drawn by J.D.A.	Date 2/27/89
Checked by G.S.	Date 2/27/89
Revisions	Date
H09700R876	2/27/89

SIMULATED AND OBSERVED FLUID-PRESSURE RESPONSES FOR THE CULEBRA DOLOMITE AT H-16 WITHOUT USING A CEMENT-INVASION SKIN

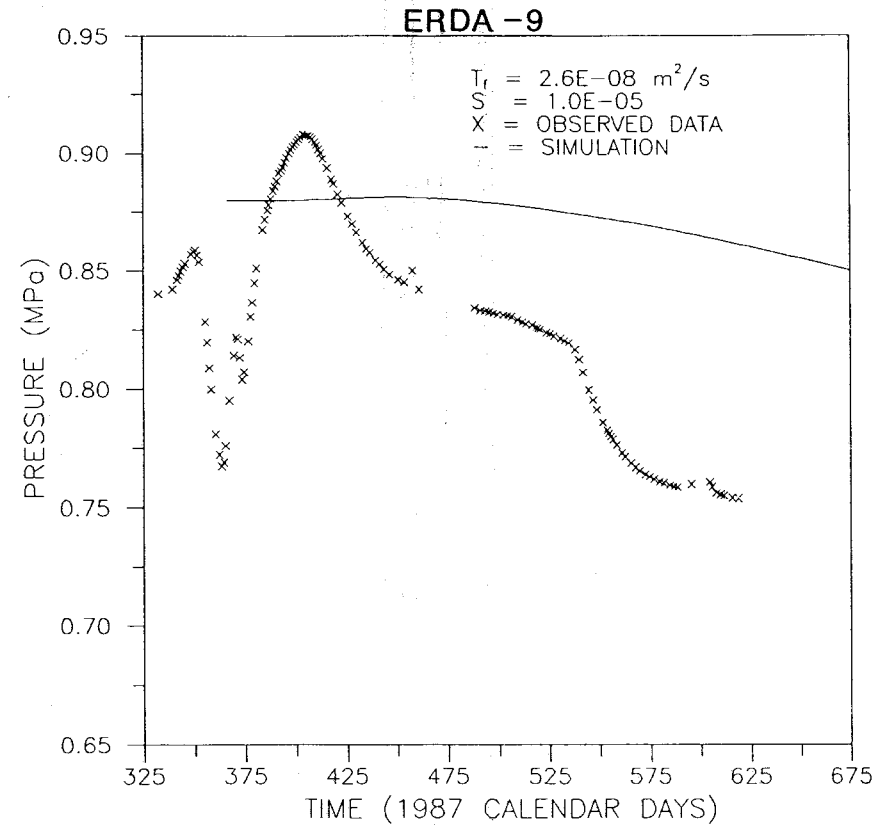
**INTERA** Technologies

Figure 6.5

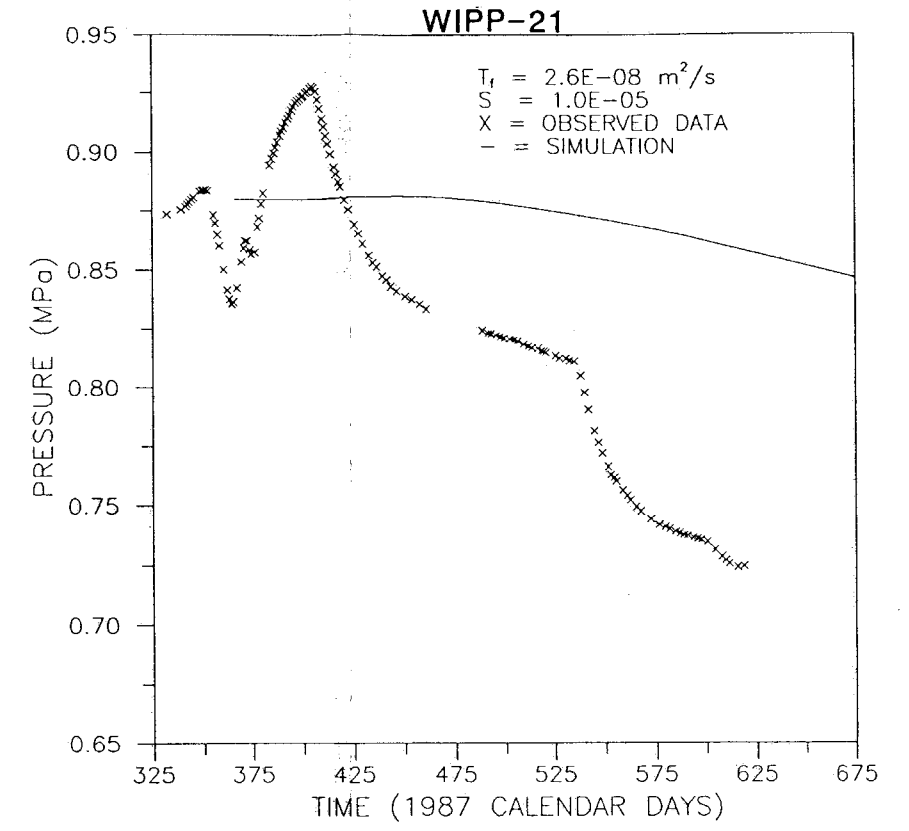
CULEBRA SIMULATION #1



TIME 0 = JANUARY 1, 1987



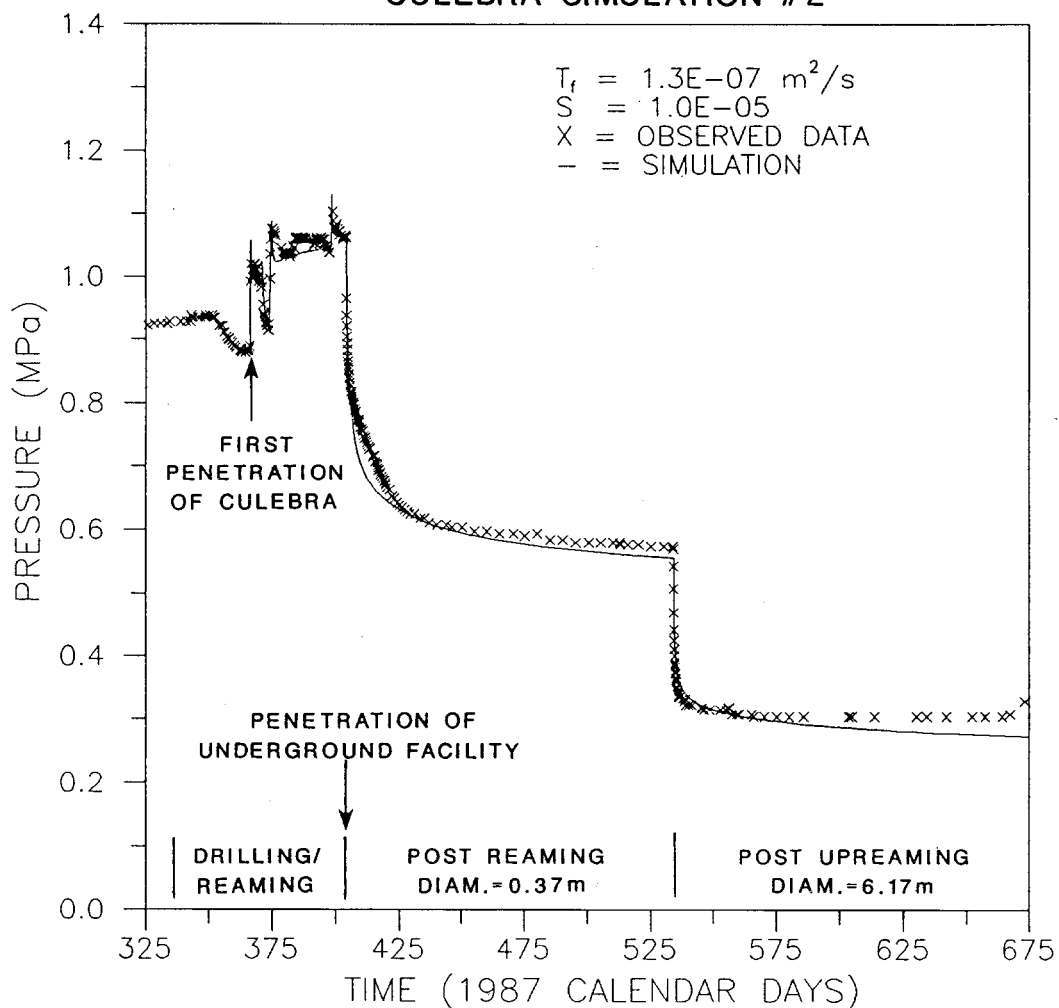
TIME 0 = JANUARY 1, 1987



TIME 0 = JANUARY 1, 1987

Drawn by J.D.A.	Date 2/27/89	SIMULATED AND OBSERVED FLUID-PRESSURE RESPONSES FOR THE CULEBRA DOLOMITE AT H-1, ERDA-9, AND WIPP-21 USING THE H-16 BEST-MATCH SIMULATION WITHOUT USING A CEMENT-INVASION SKIN
Checked by G.S.	Date 2/27/89	
Revisions G.S.	Date 6/16/89	
H09700R876	2/27/89	
<b>INTERA Technologies</b>		<b>Figure 6.6</b>

### CULEBRA SIMULATION #2



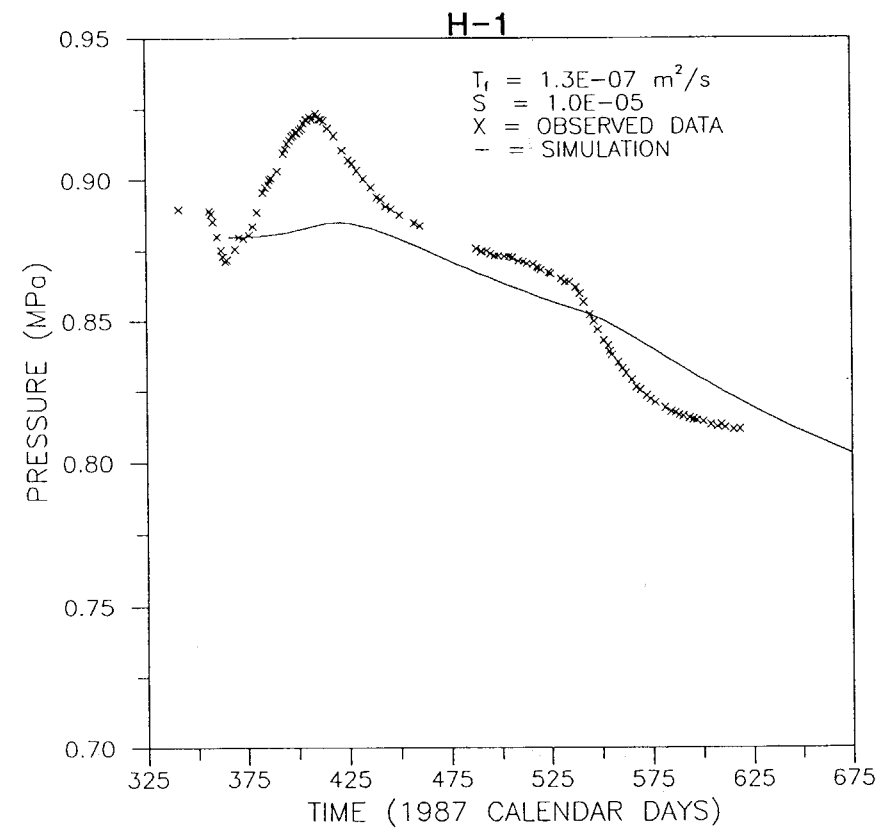
TIME 0 = JANUARY 1, 1987

Drawn by J.D.A.	Date 2/27/89
Checked by G.S.	Date 2/27/89
Revisions	Date
H09700R876	2/27/89

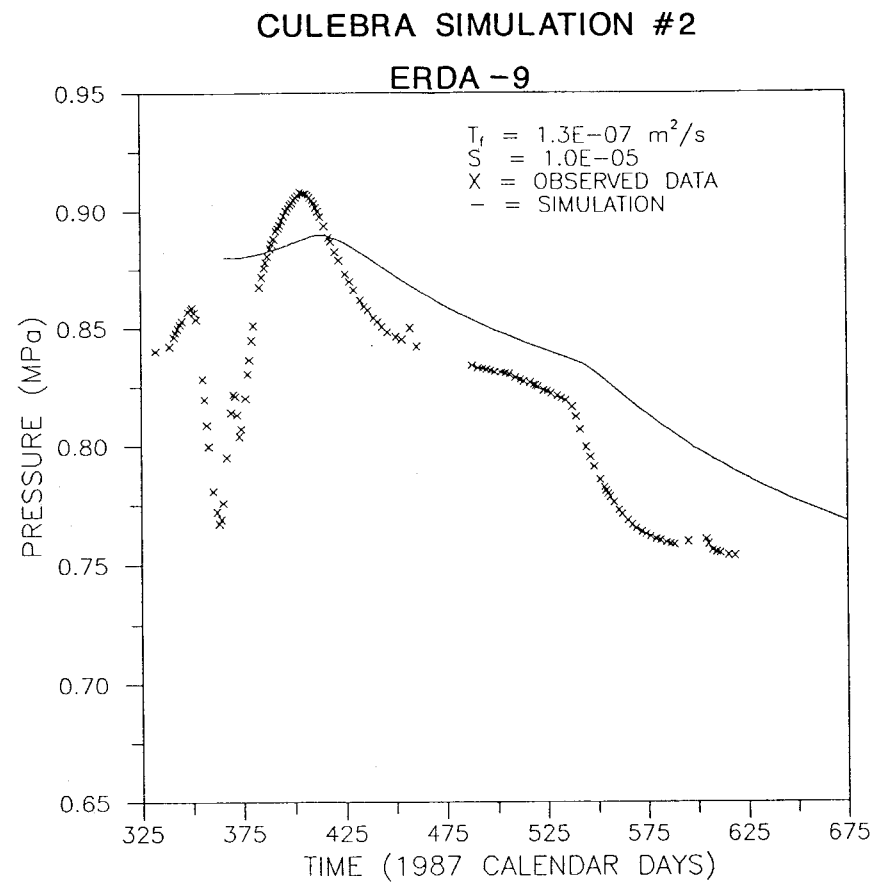
SIMULATED AND OBSERVED FLUID-PRESSURE RESPONSES FOR THE CULEBRA DOLOMITE AT H-16 USING A CEMENT-INVASION SKIN

**INTERA** Technologies

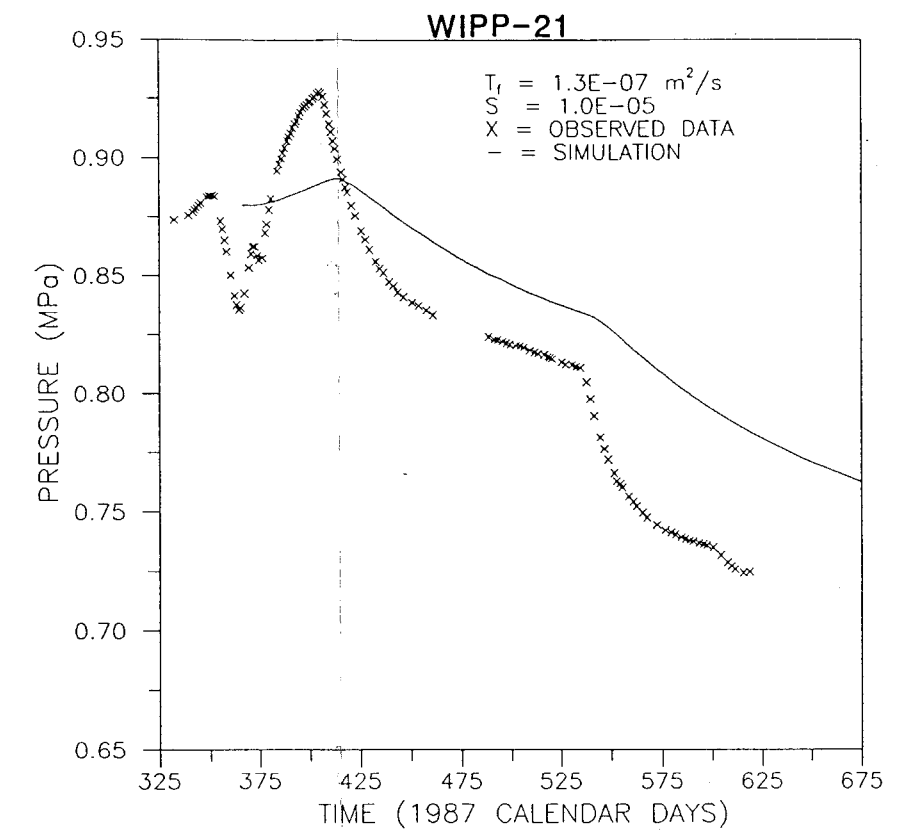
Figure 6.7



TIME 0 = JANUARY 1, 1987



TIME 0 = JANUARY 1, 1987



TIME 0 = JANUARY 1, 1987

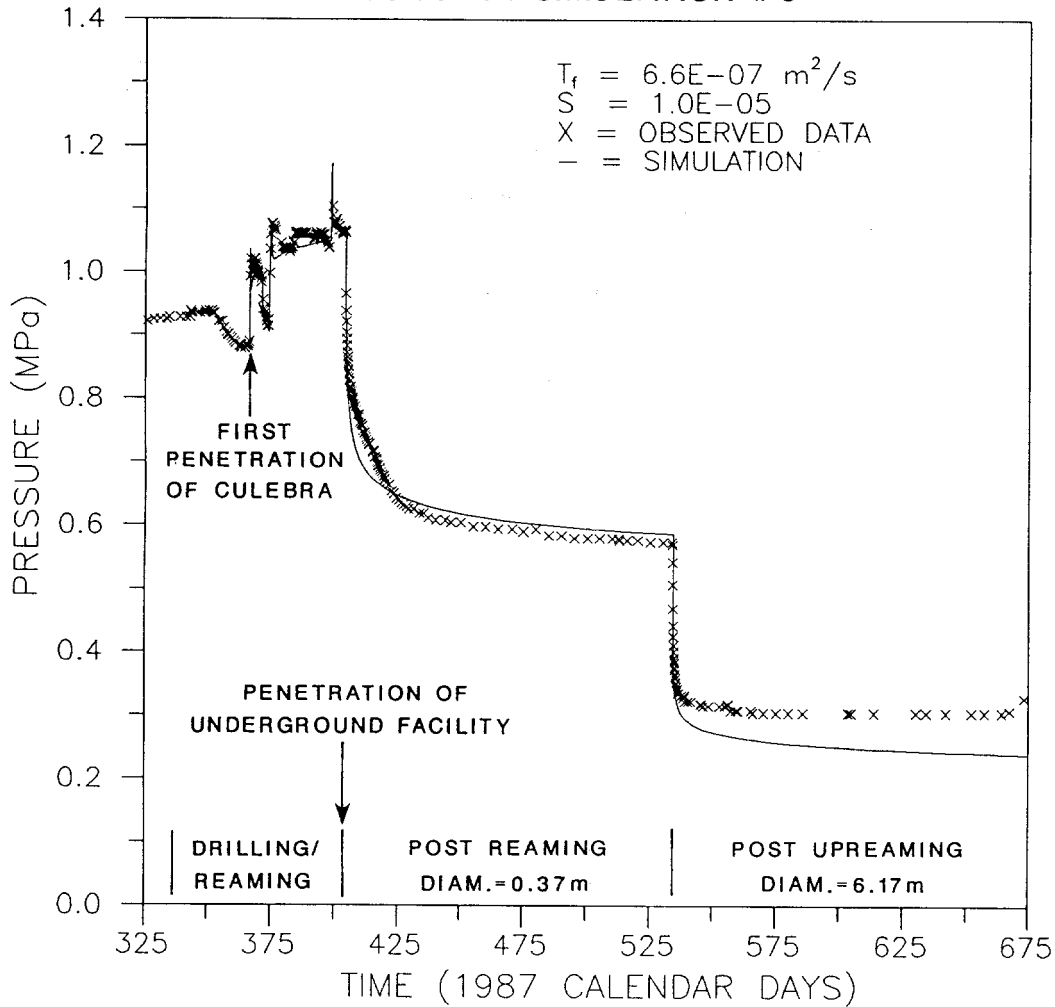
Drawn by	J.D.A.	Date	2/27/89
Checked by	G.S.	Date	2/27/89
Revisions	G.S.	Date	6/6/89
H09700R876		2/27/89	

SIMULATED AND OBSERVED FLUID-PRESSURE RESPONSES FOR THE CULEBRA DOLOMITE AT H-1, ERDA-9, AND WIPP-21 USING THE H-16 BEST-MATCH SIMULATION USING A CEMENT-INVASION SKIN

**INTERA** Technologies

Figure 6.8

### CULEBRA SIMULATION #3



TIME 0 = JANUARY 1, 1987

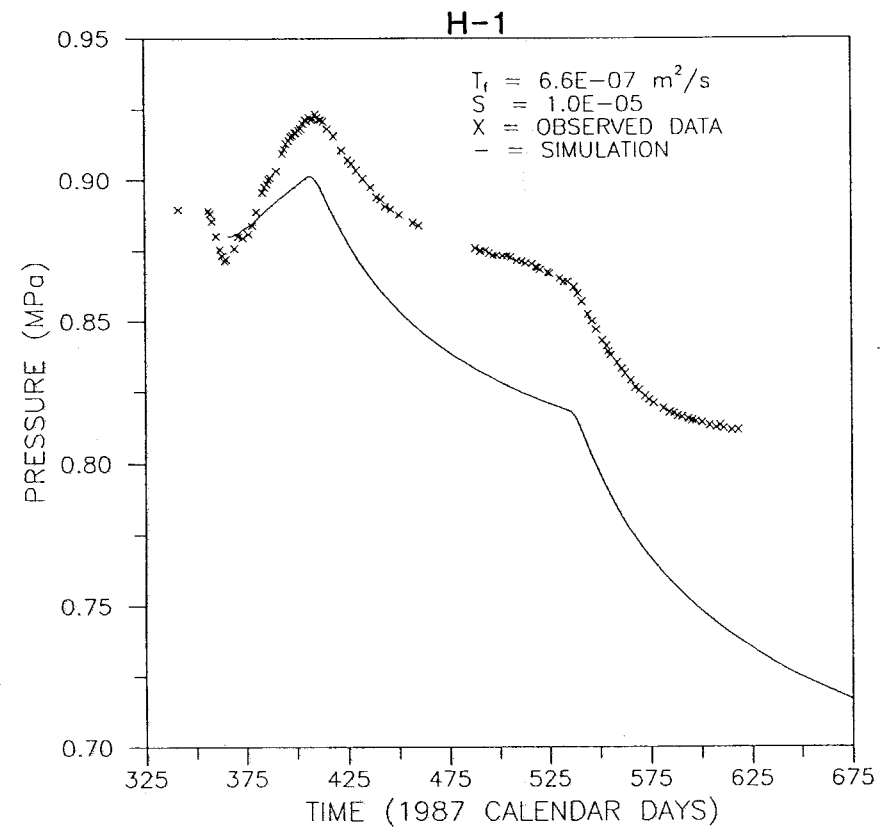
Drawn by J.D.A.	Date 2/27/89
Checked by G.S.	Date 2/27/89
Revisions	Date
H09700R876	2/27/89

SIMULATED AND OBSERVED FLUID-PRESSURE RESPONSES FOR THE CULEBRA DOLOMITE AT H-16 MATCHING THE CULEBRA-TO-AIS FLOW RATE USING A CEMENT-INVASION SKIN

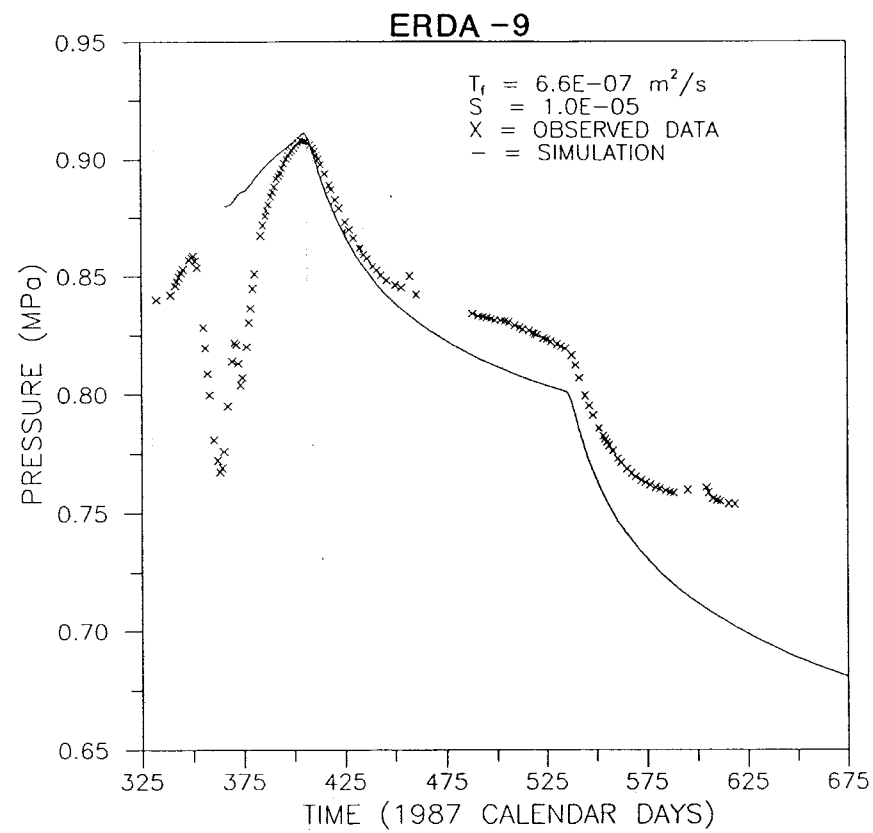
**INTERA** Technologies

Figure 6.9

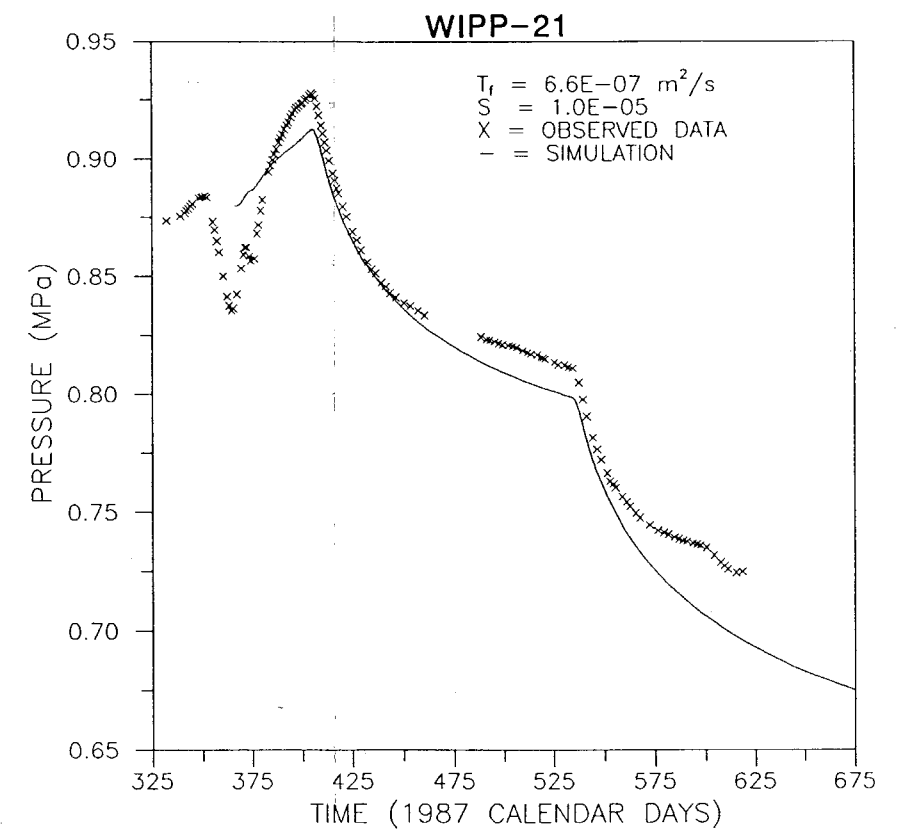
CULEBRA SIMULATION #3



TIME 0 = JANUARY 1, 1987



TIME 0 = JANUARY 1, 1987



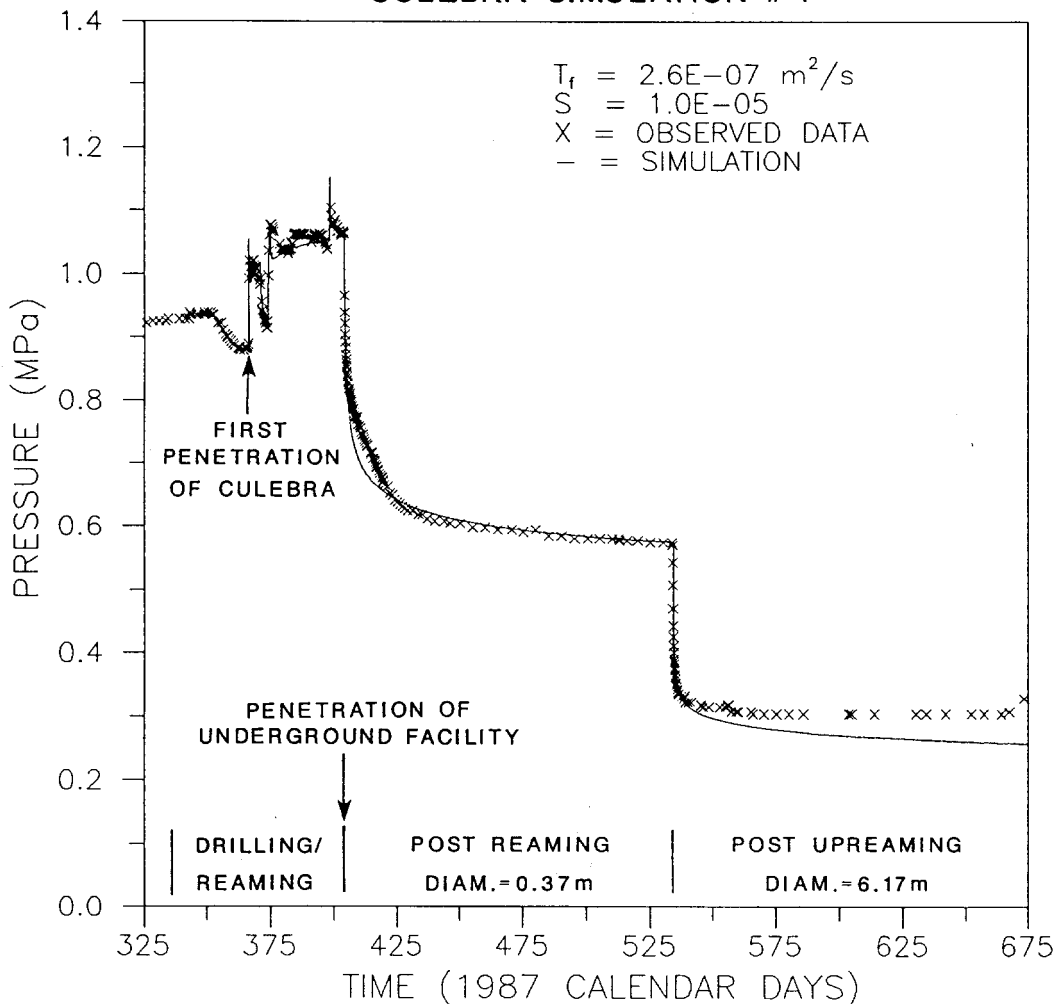
TIME 0 = JANUARY 1, 1987

Drawn by J.D.A.	Date 2/27/89	SIMULATED AND OBSERVED FLUID-PRESSURE RESPONSES FOR THE CULEBRA DOLOMITE AT H-1, ERDA-9, AND WIPP-21 USING THE H-16 BEST-MATCH SIMULATION MATCHING THE CULEBRA-TO-AIS FLOW RATE USING A CEMENT-INVASION SKIN
Checked by G.S.	Date 2/27/89	
Revisions G.S.	Date 6/6/89	
H09700R876	2/27/89	

**INTERA** Technologies

Figure 6.10

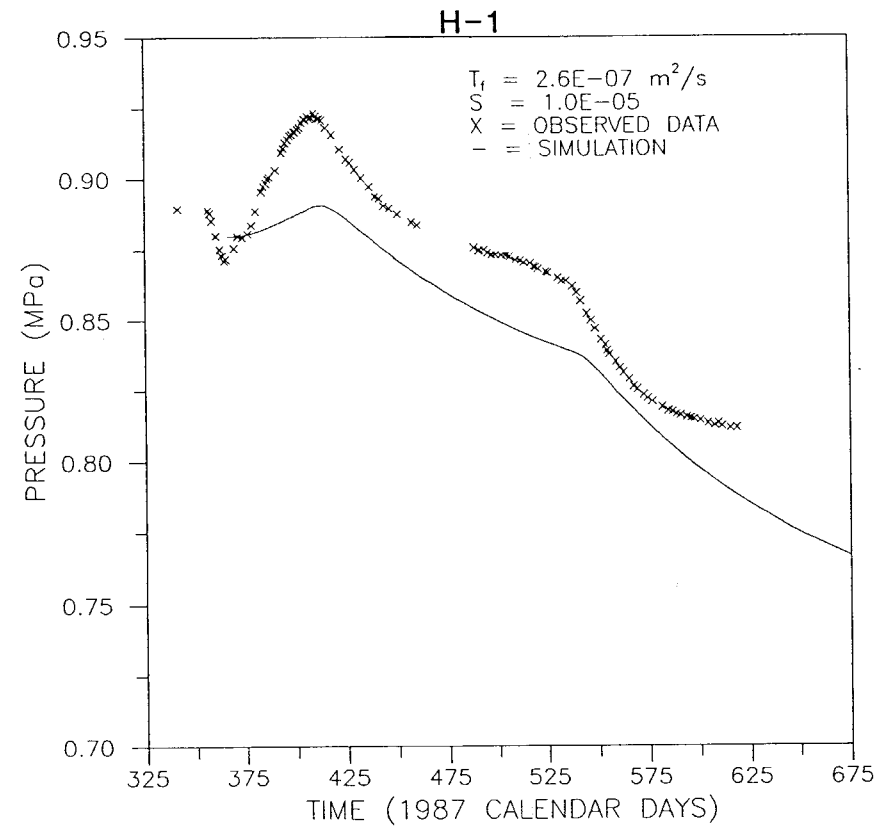
### CULEBRA SIMULATION #4



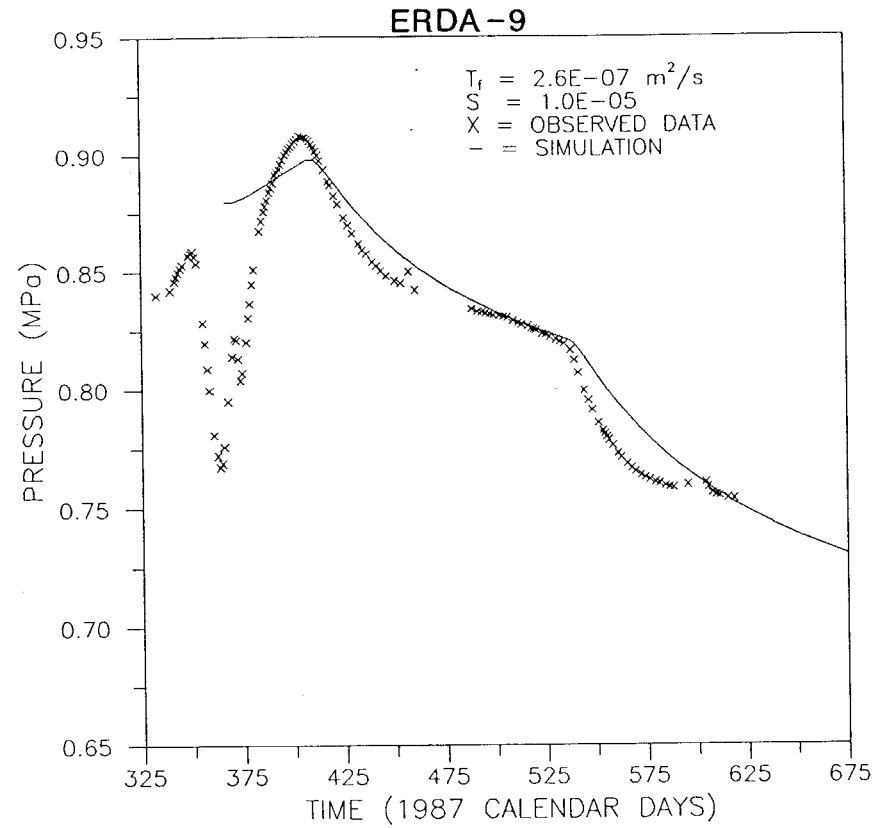
TIME 0 = JANUARY 1, 1987

Drawn by J.D.A.	Date 2/27/89	SIMULATED AND OBSERVED FLUID-PRESSURE RESPONSES FOR THE CULEBRA DOLOMITE AT H-16 MATCHING THE H-1 FLUID-PRESSURE RESPONSE USING A CEMENT-INVASION SKIN
Checked by G.S.	Date 2/27/89	
Revisions	Date	
H09700R876	2/27/89	
<b>INTERA Technologies</b>		Figure 6.11

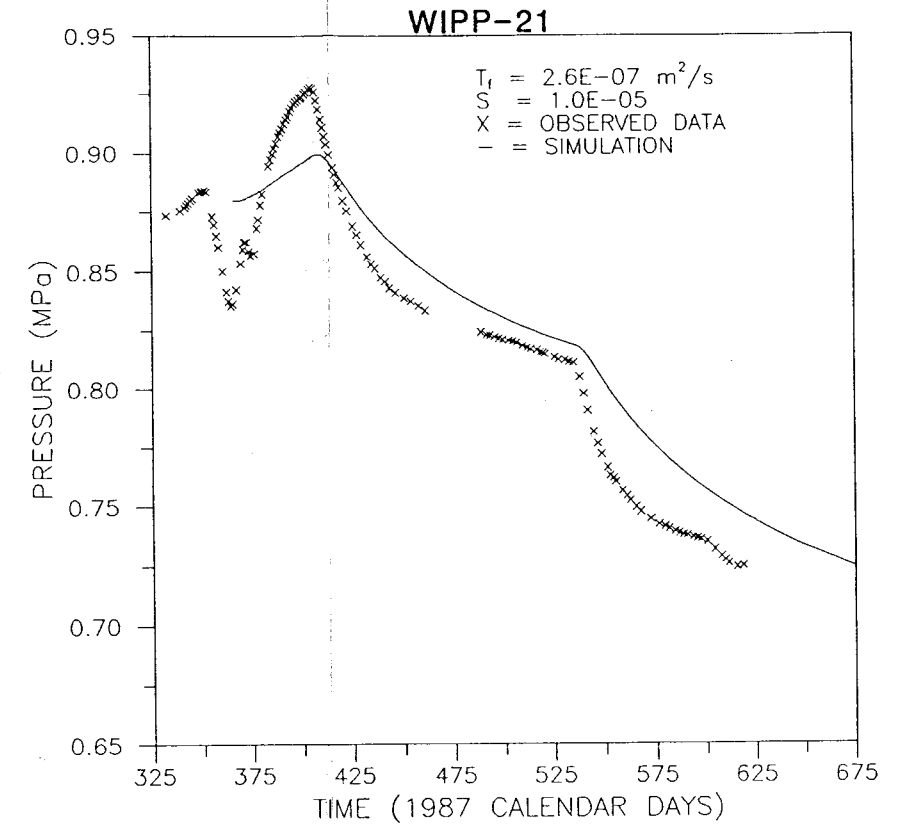
CULEBRA SIMULATION #4



TIME 0 = JANUARY 1, 1987



TIME 0 = JANUARY 1, 1987



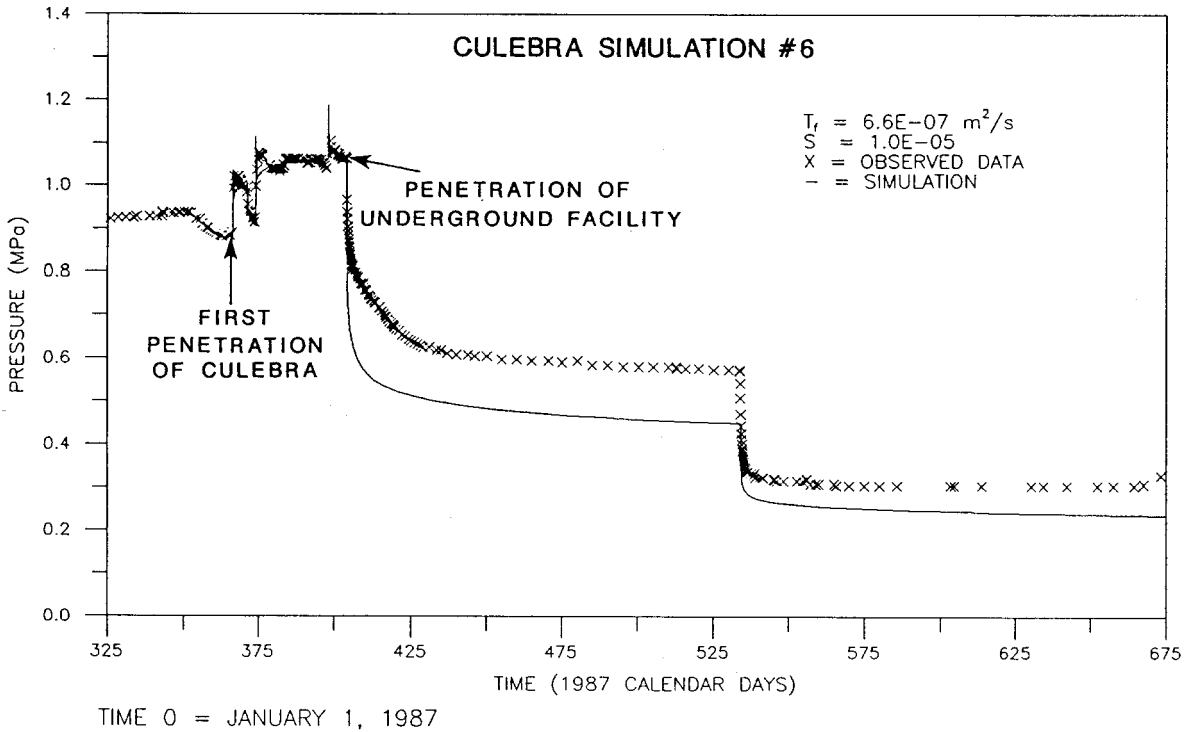
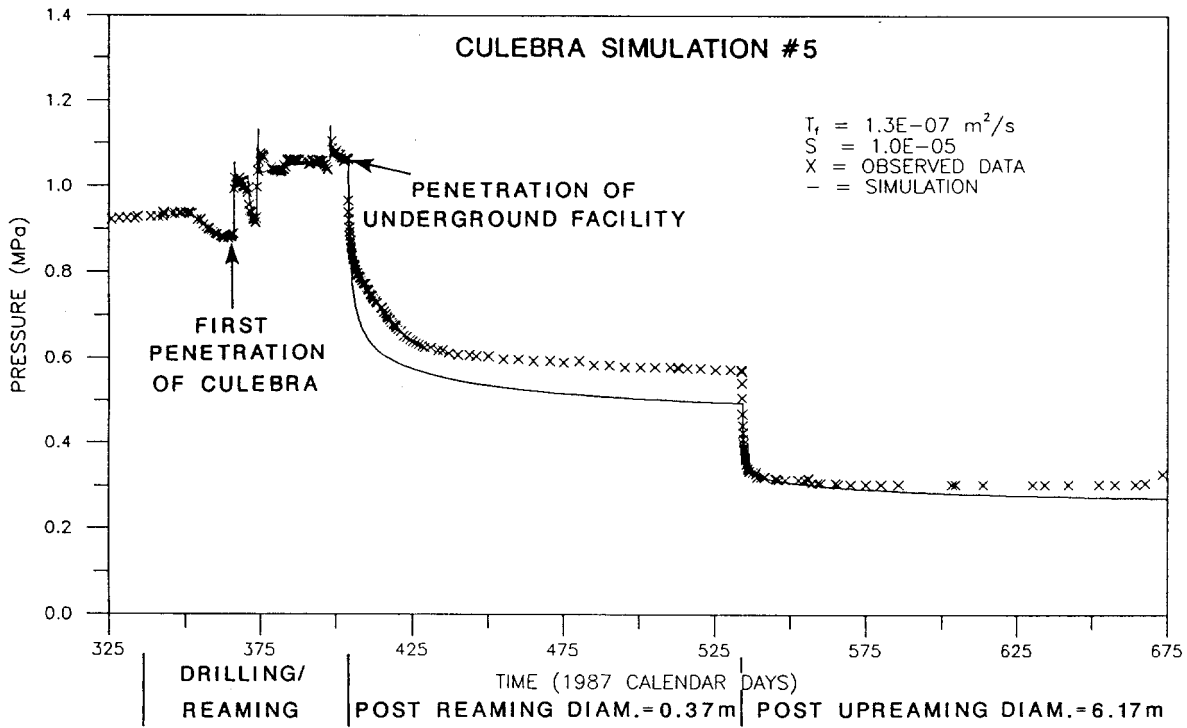
TIME 0 = JANUARY 1, 1987

Drawn by J.D.A.	Date 2/27/89
Checked by G.S.	Date 2/27/89
Revisions G.S.	Date 6/6/89
H09700R876	2/27/89

SIMULATED AND OBSERVED FLUID-PRESSURE RESPONSES FOR THE CULEBRA DOLOMITE AT H-1, ERDA-9, AND WIPP-21 MATCHING THE H-1 FLUID-PRESSURE RESPONSE USING A CEMENT-INVASION SKIN

**INTERA** Technologies

Figure 6.12

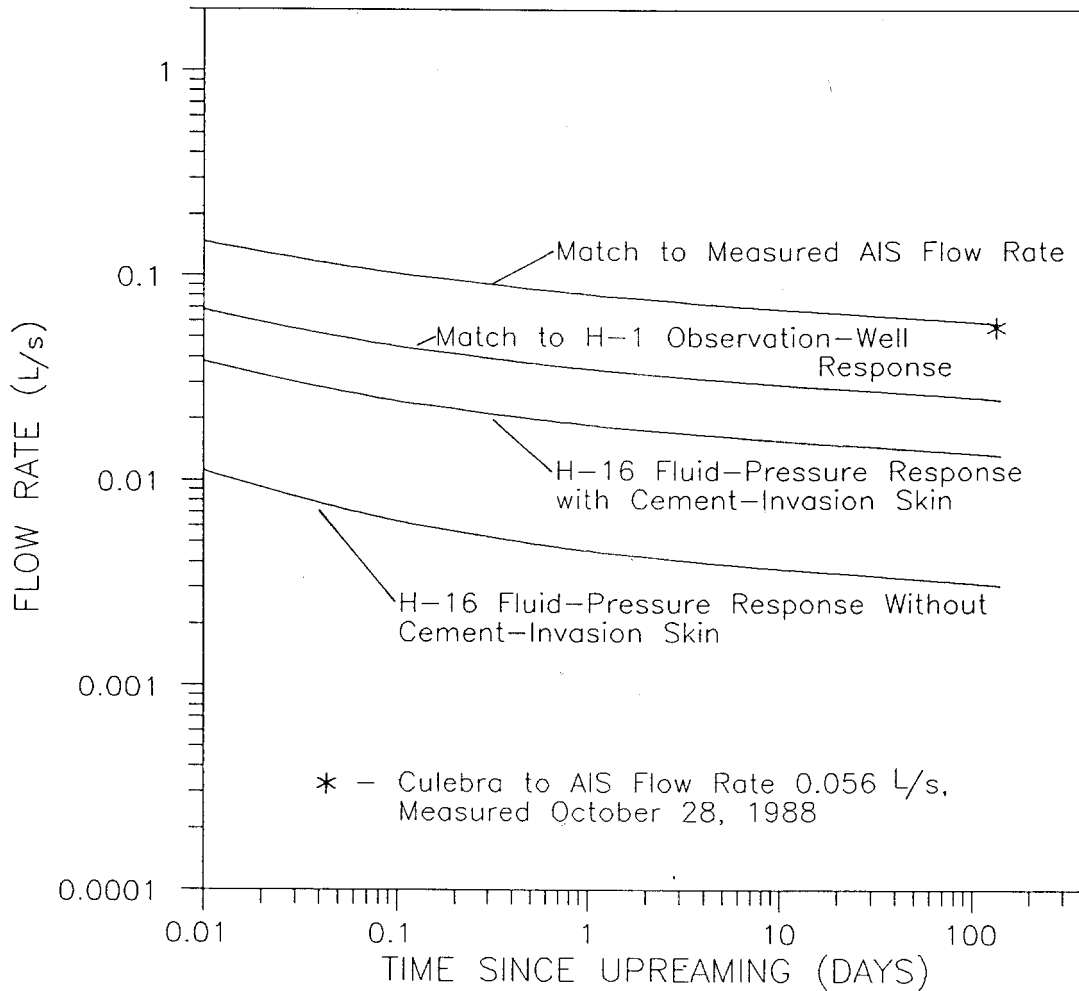


Drawn by J.D.A.	Date 2/27/89
Checked by G.S.	Date 2/27/89
Revisions	Date
H09700R876	2/27/89

SIMULATED AND OBSERVED FLUID-PRESSURE RESPONSES FOR THE CULEBRA DOLOMITE AT H-16 SHOWING SENSITIVITY TO THE USE OF A CEMENT-INVASION SKIN

**INTERA Technologies**

Figure 6.13



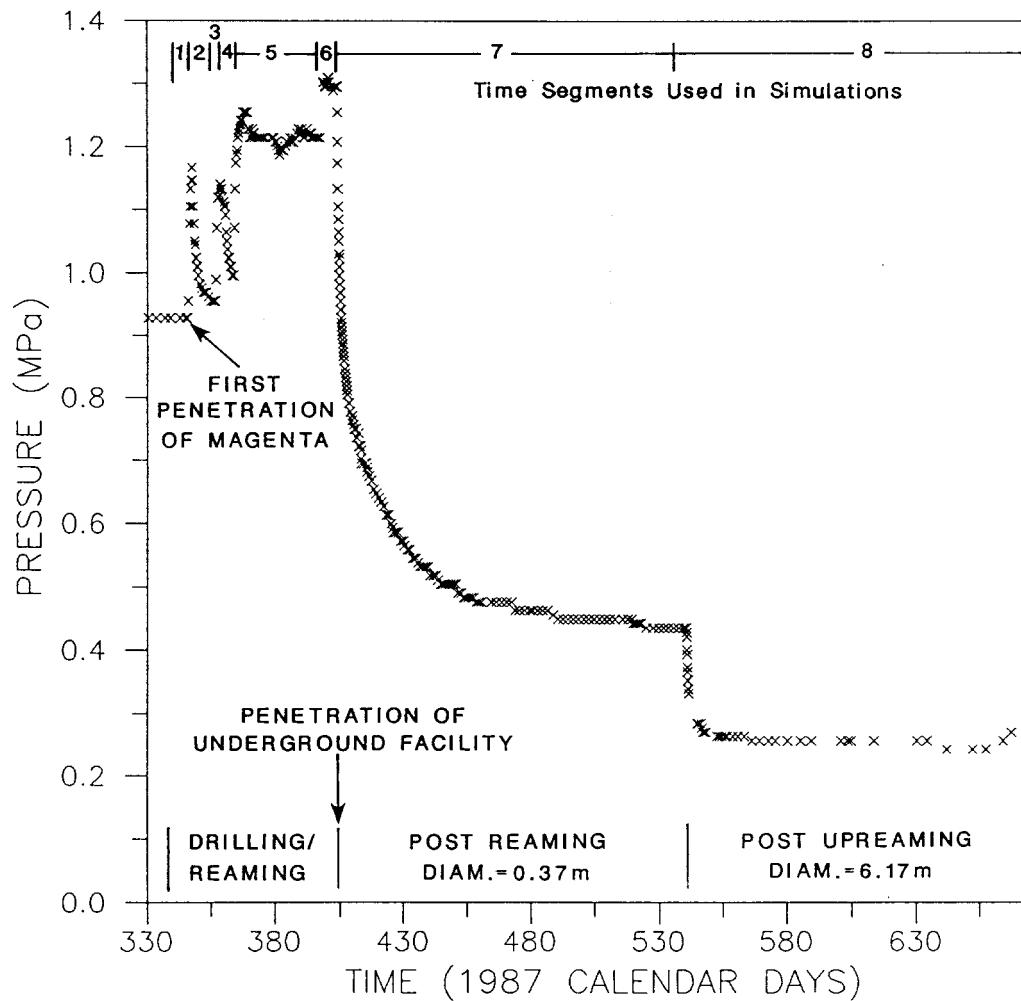
TIME 0 = JANUARY 1, 1987

Drawn by J.D.A.	Date 2/27/89
Checked by G.S.	Date 2/27/89
Revisions	Date
H09700R876	2/27/89

POST-UPREAMING SIMULATED AND OBSERVED FLOW RATES FROM THE CULEBRA DOLOMITE TO THE AIS USING FOUR VALUES OF TRANSMISSIVITY

**INTERA** Technologies

Figure 6.14



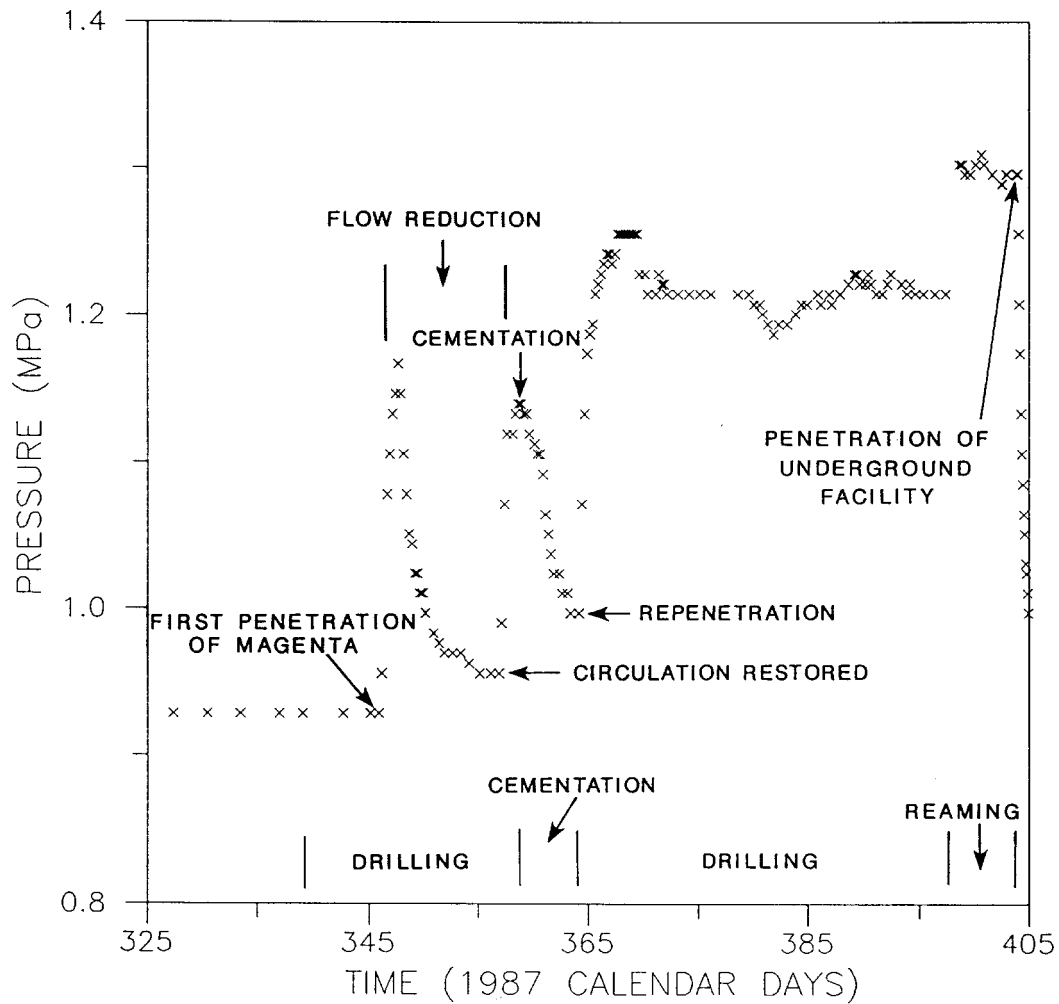
TIME 0 = JANUARY 1, 1987

Drawn by J.D.A.	Date 2/27/89
Checked by G.S.	Date 2/27/89
Revisions ABW	Date 6/23/89
H09700R876	2/27/89

FLUID-PRESSURE RESPONSE OF THE MAGENTA DOLOMITE OBSERVED AT OBSERVATION-WELL H-16 DURING THE CONSTRUCTION OF THE AIS

**INTERA** Technologies

Figure 6.15



TIME 0 = JANUARY 1, 1987

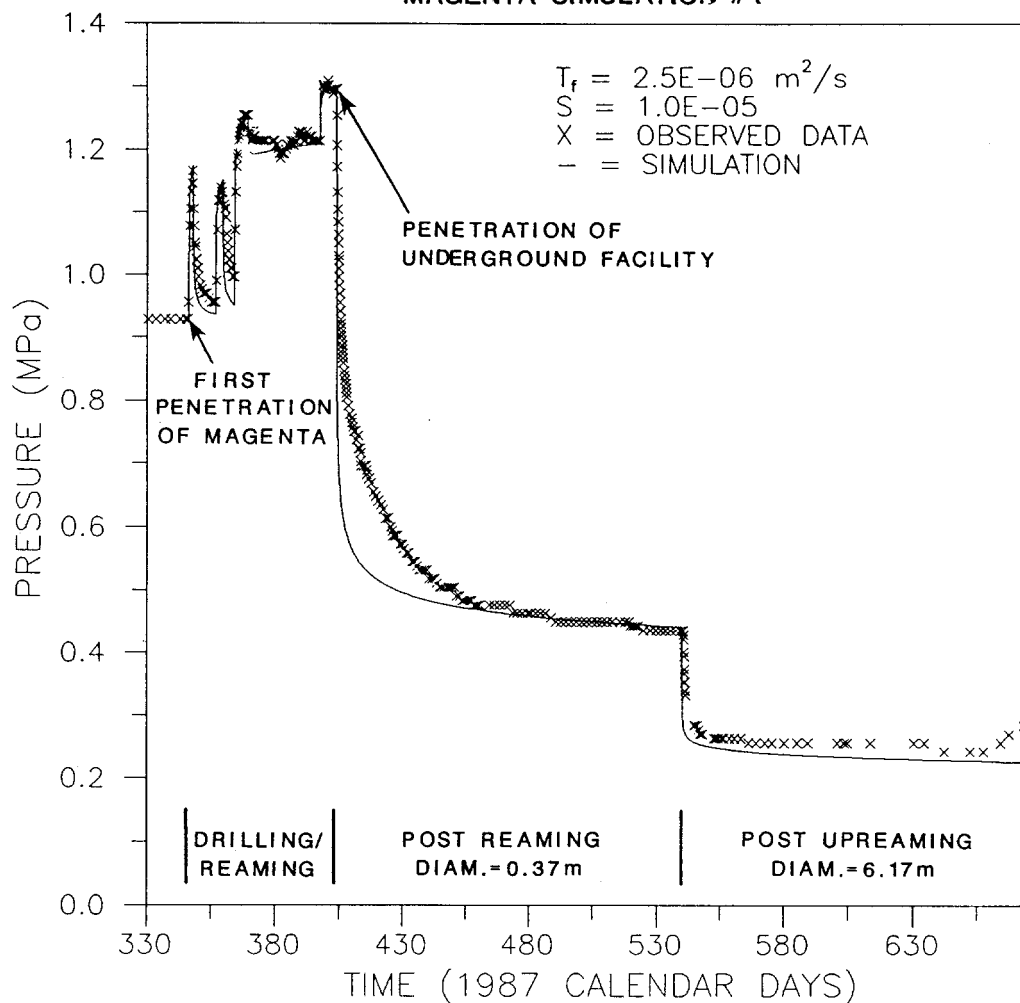
Drawn by J.D.A.	Date 2/27/89
Checked by G.S.	Date 2/27/89
Revisions	Date
H09700R876	2/27/89

FLUID-PRESSURE RESPONSE OF THE MAGENTA DOLOMITE OBSERVED AT OBSERVATION-WELL H-16 DURING THE DRILLING/REAMING PERIOD OF THE CONSTRUCTION OF THE AIS

**INTERA Technologies**

Figure 6.16

MAGENTA SIMULATION #1



TIME 0 = JANUARY 1, 1987

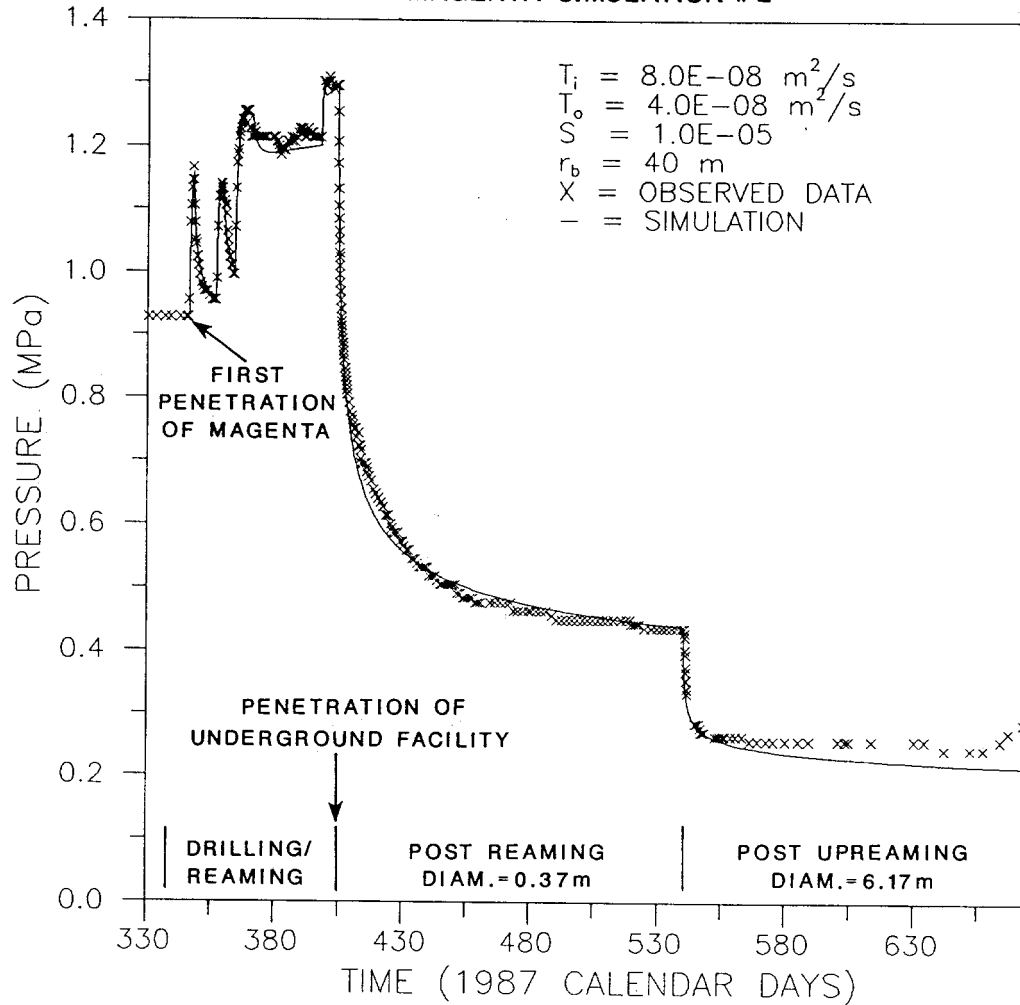
Drawn by J.D.A.	Date 2/27/89
Checked by G.S.	Date 2/27/89
Revisions	Date
H09700R876	2/27/89

SIMULATION OF THE MAGENTA DOLOMITE FLUID-PRESSURE RESPONSE AT H-16 DURING THE CONSTRUCTION OF THE AIS USING A HOMOGENEOUS-FORMATION CHARACTERIZATION

**INTERA** Technologies

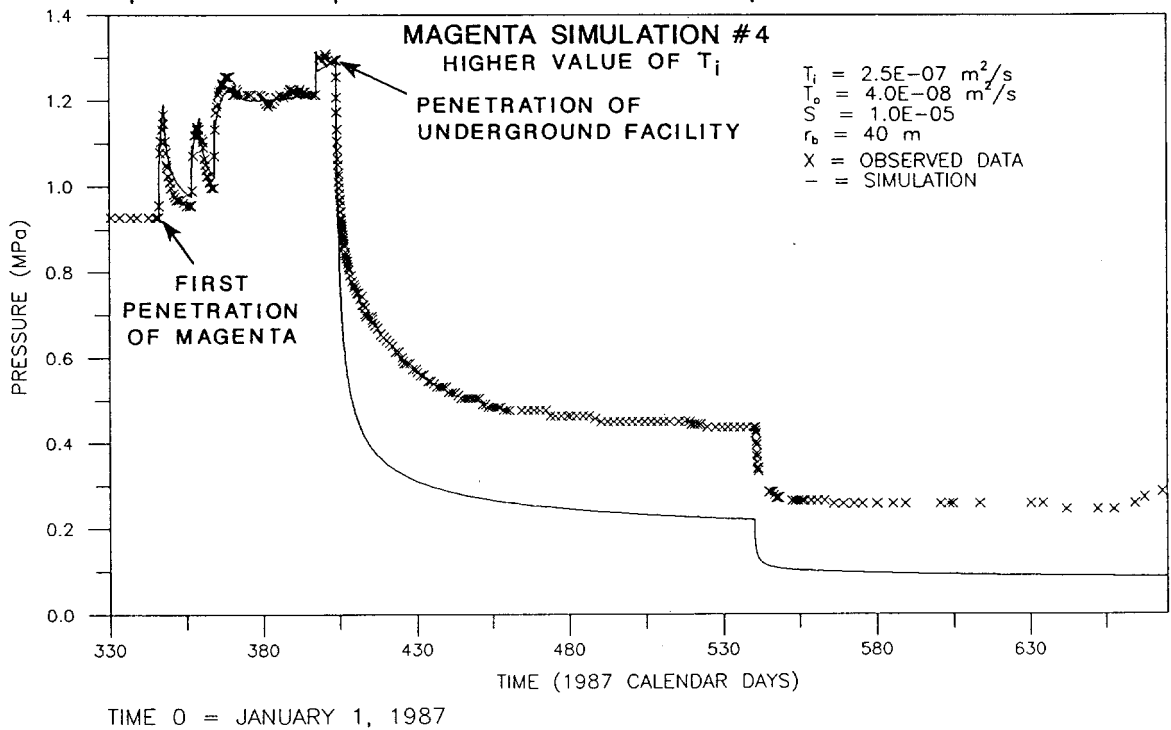
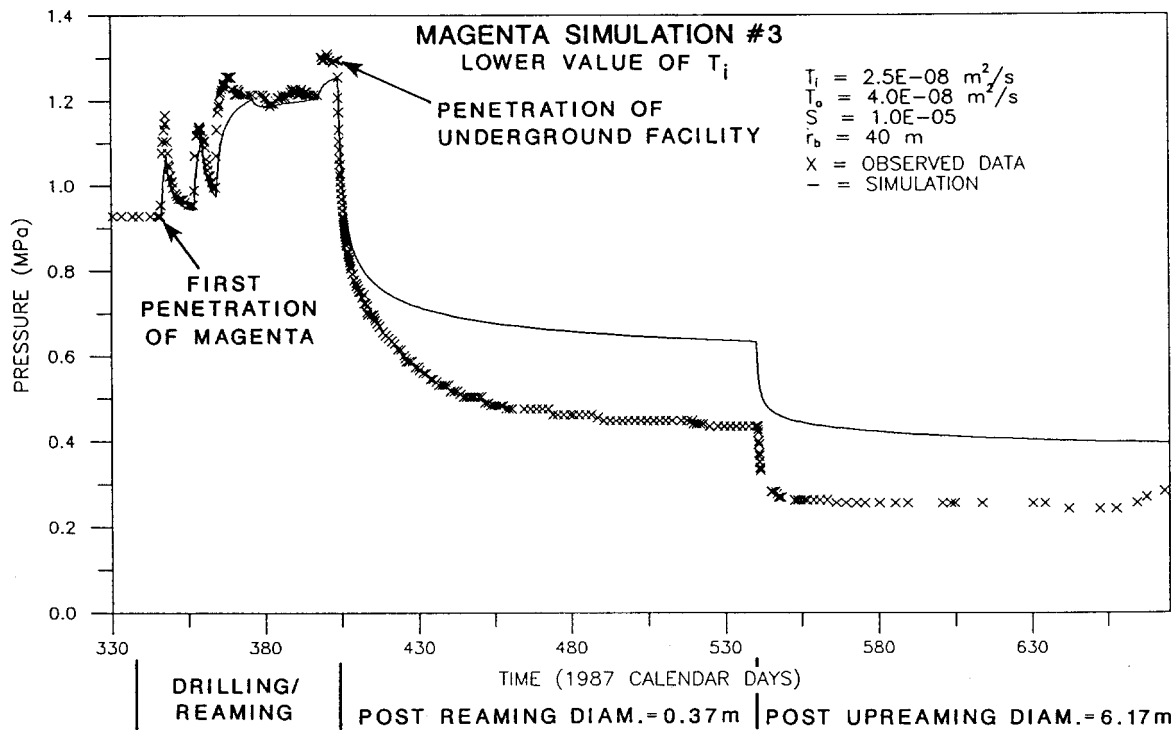
Figure 6.17

MAGENTA SIMULATION #2



TIME 0 = JANUARY 1, 1987

Drawn by J.D.A.	Date 2/27/89	SIMULATION OF THE MAGENTA DOLOMITE FLUID-PRESSURE RESPONSE AT H-16 DURING THE CONSTRUCTION OF THE AIS USING A FORMATION-HETEROGENEITY BOUNDARY
Checked by G.S.	Date 2/27/89	
Revisions	Date	
H09700R876	2/27/89	
<b>INTERA Technologies</b>		Figure 6.18

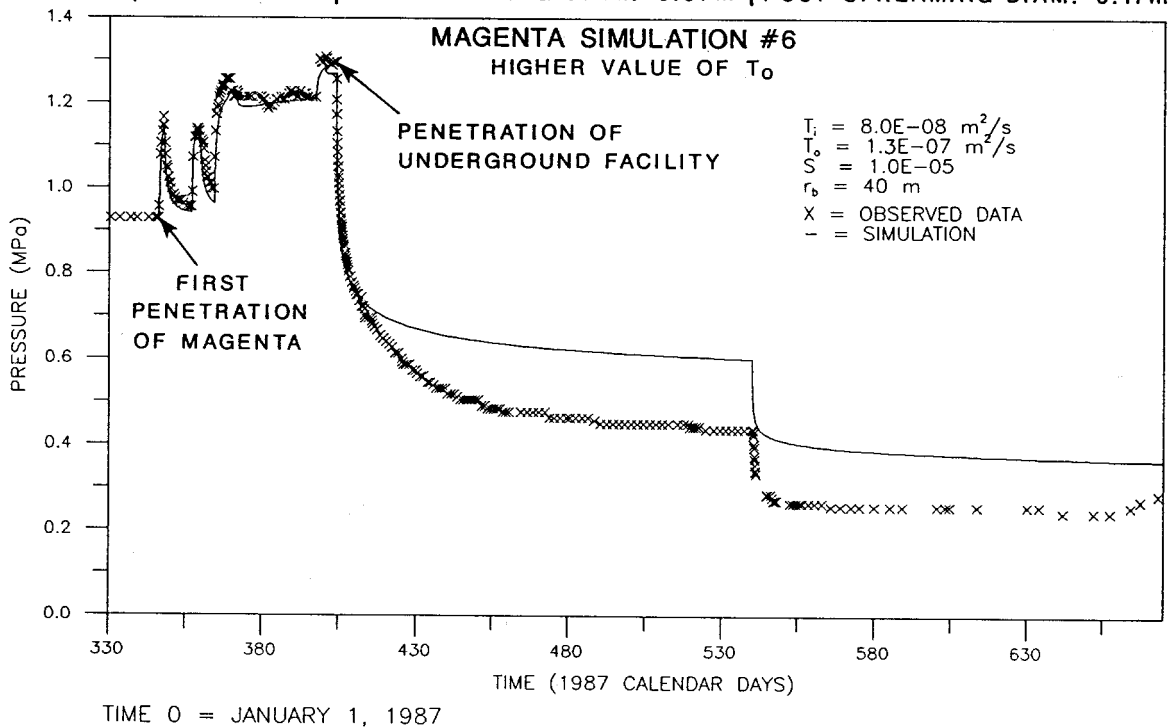
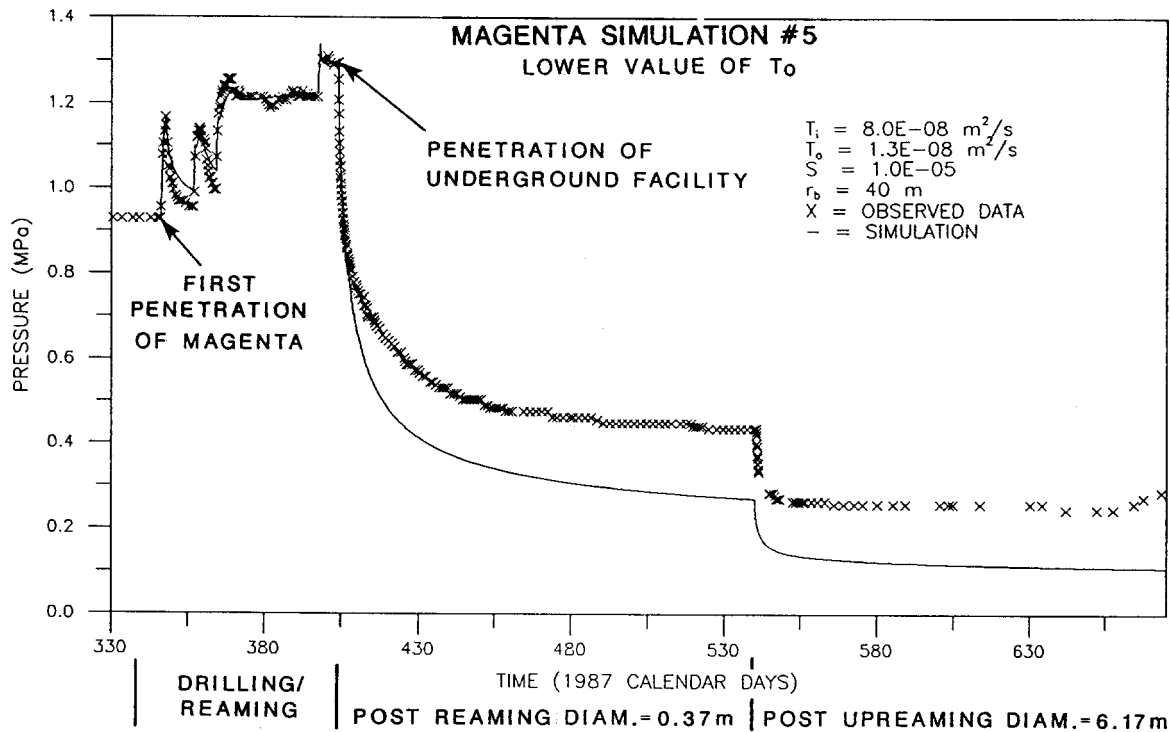


Drawn by J.D.A.	Date 2/27/89
Checked by G.S.	Date 2/27/89
Revisions	Date
H09700R876	2/27/89

SIMULATION OF THE MAGENTA DOLOMITE FLUID-PRESSURE RESPONSE AT H-16 DURING THE CONSTRUCTION OF THE AIS USING A FORMATION-HETEROGENEITY BOUNDARY AND SHOWING SENSITIVITY TO  $T_i$

**INTERA Technologies**

Figure 6.19

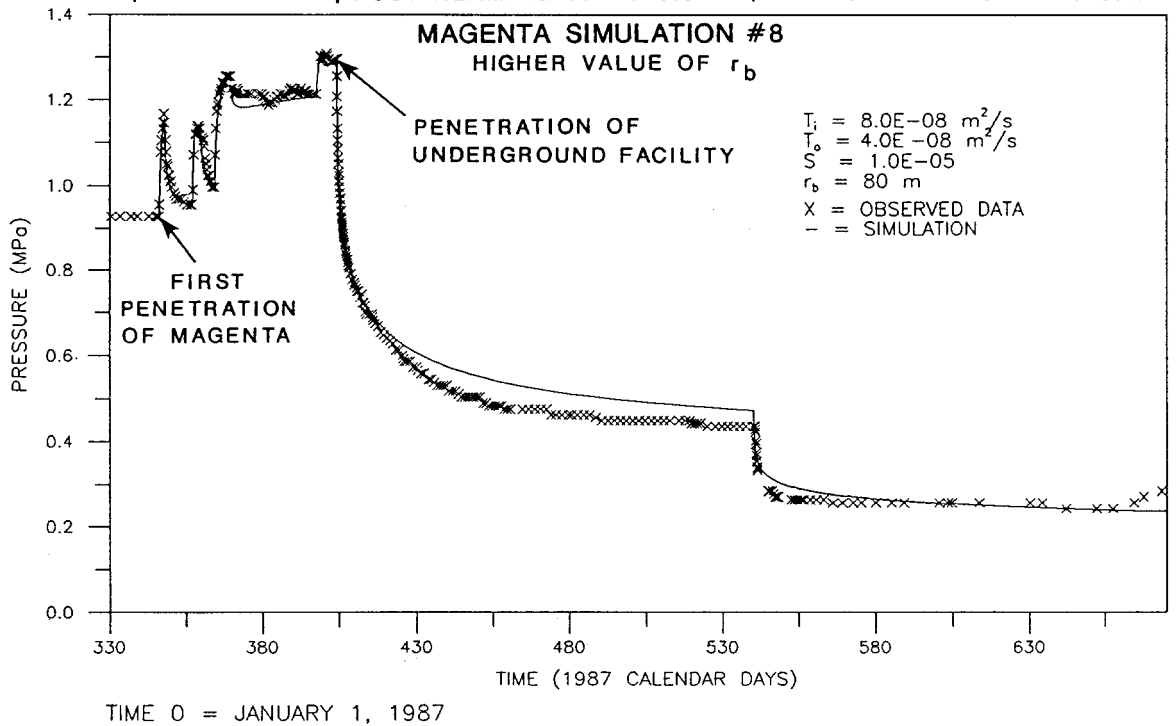
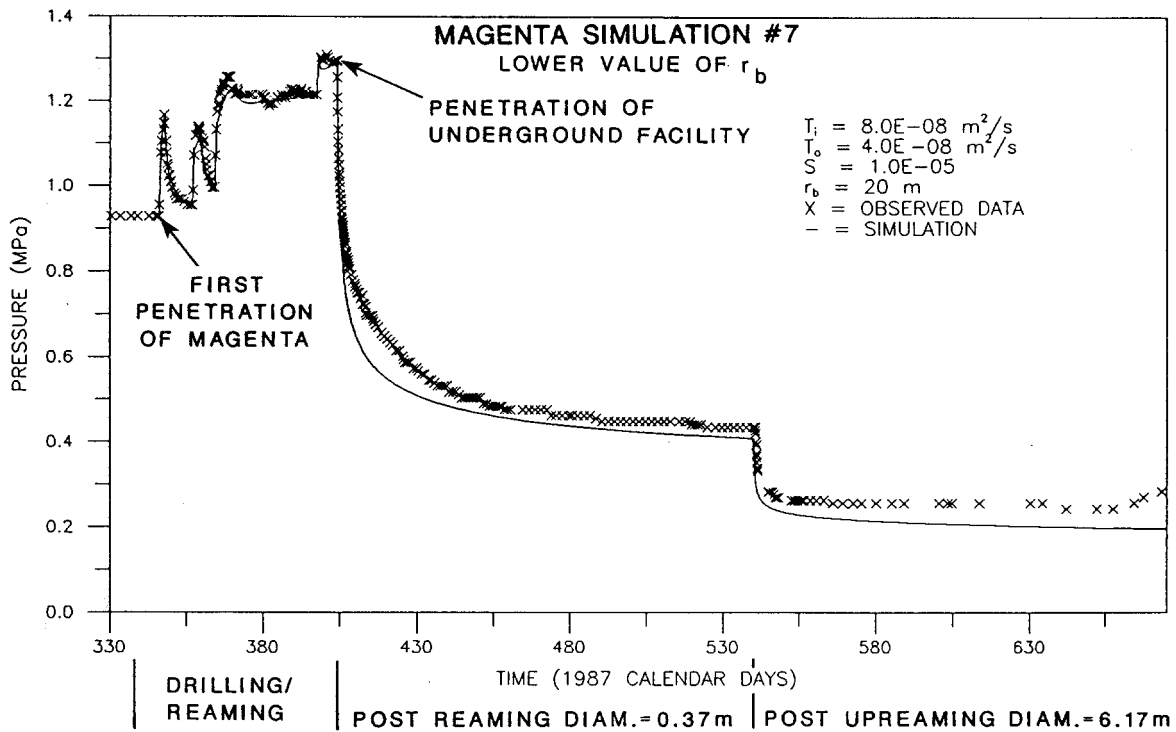


Drawn by J.D.A.	Date 2/27/89
Checked by G.S.	Date 2/27/89
Revisions	Date
H09700R876	2/27/89

SIMULATION OF THE MAGENTA DOLOMITE FLUID-PRESSURE RESPONSE AT H-16 DURING THE CONSTRUCTION OF THE AIS USING A FORMATION-HETEROGENEITY BOUNDARY AND SHOWING SENSITIVITY TO  $T_0$ .

**INTERA Technologies**

Figure 6.20

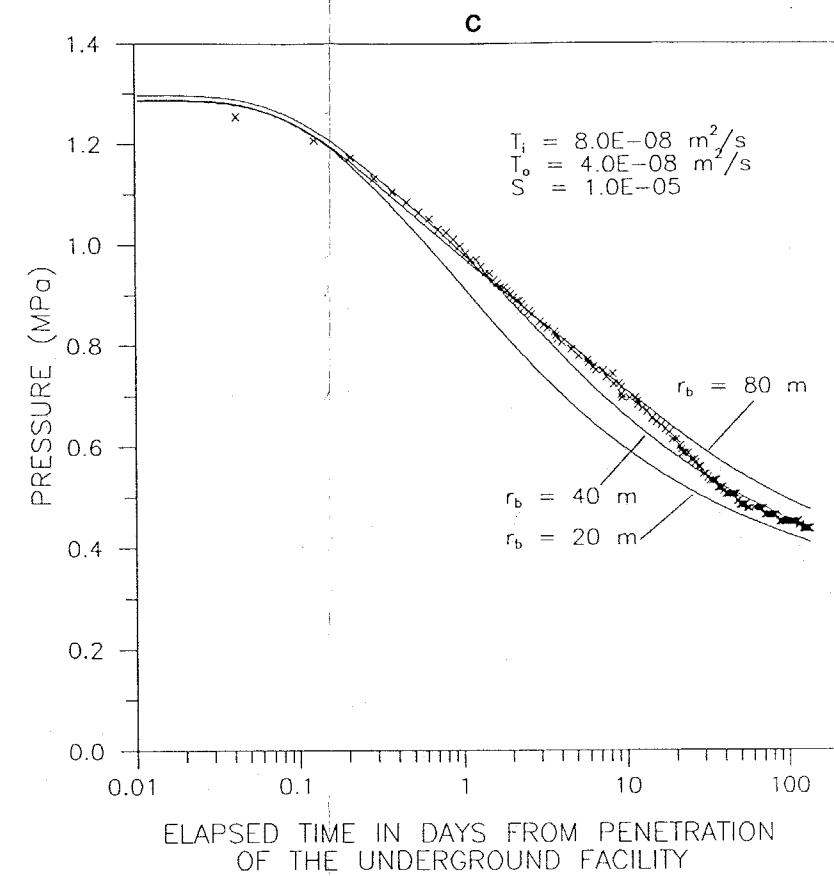
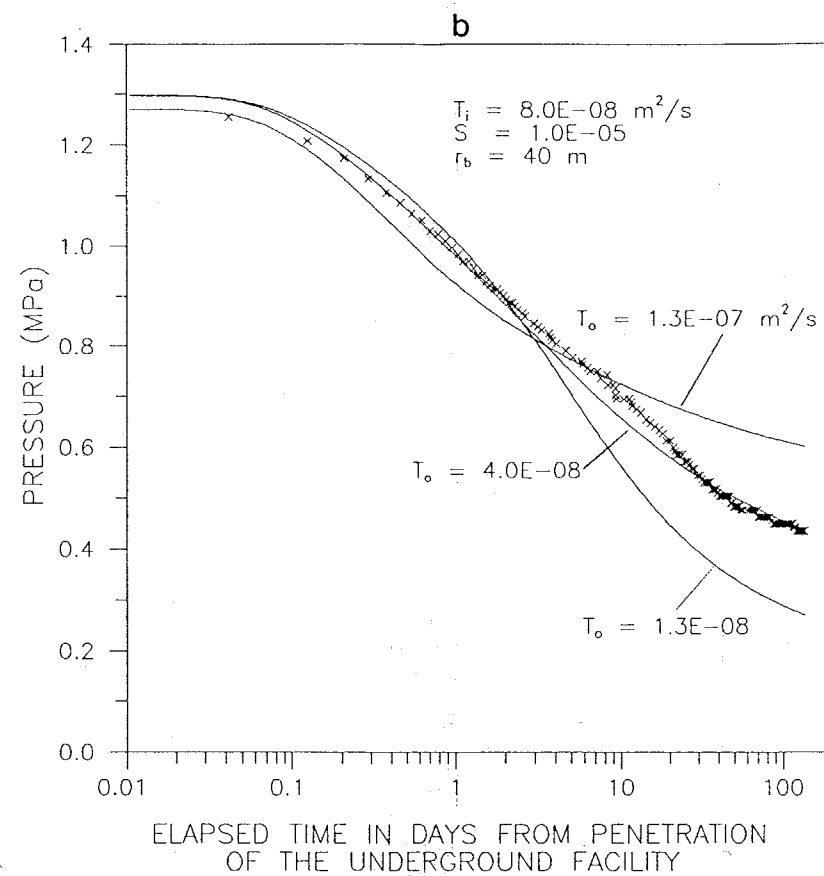
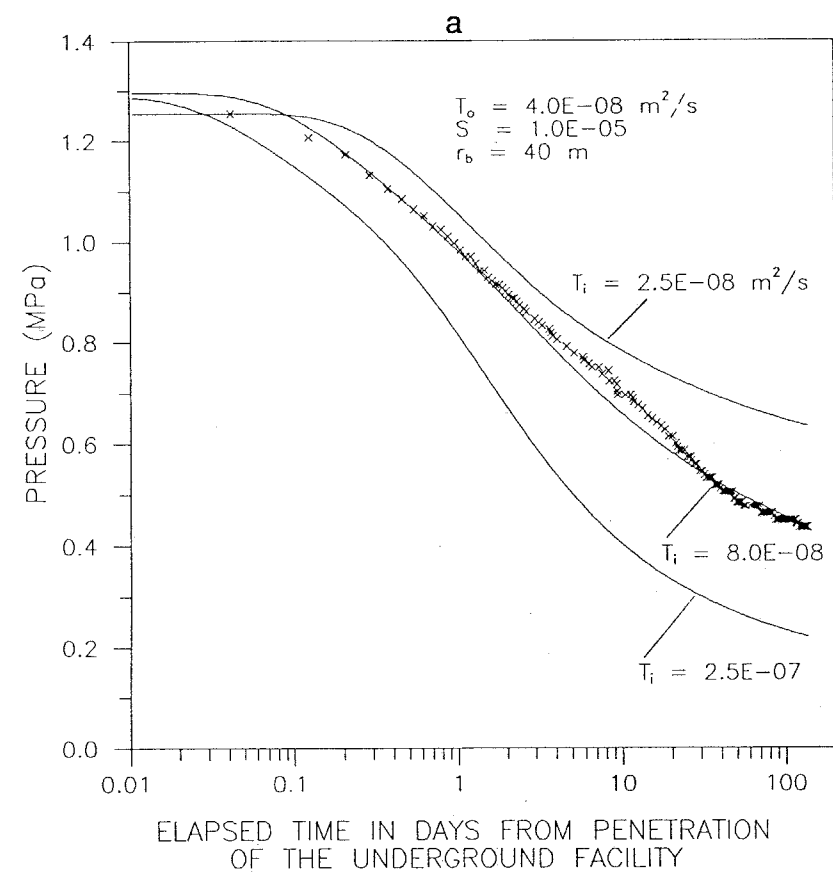


Drawn by J.D.A.	Date 2/27/89
Checked by G.S.	Date 2/27/89
Revisions	Date
H09700R876	2/27/89

SIMULATION OF THE MAGENTA DOLOMITE FLUID-PRESSURE RESPONSE AT H-16 DURING THE CONSTRUCTION OF THE AIS USING A FORMATION-HETEROGENEITY BOUNDARY AND SHOWING SENSITIVITY TO  $r_b$

**INTERA Technologies**

Figure 6.21

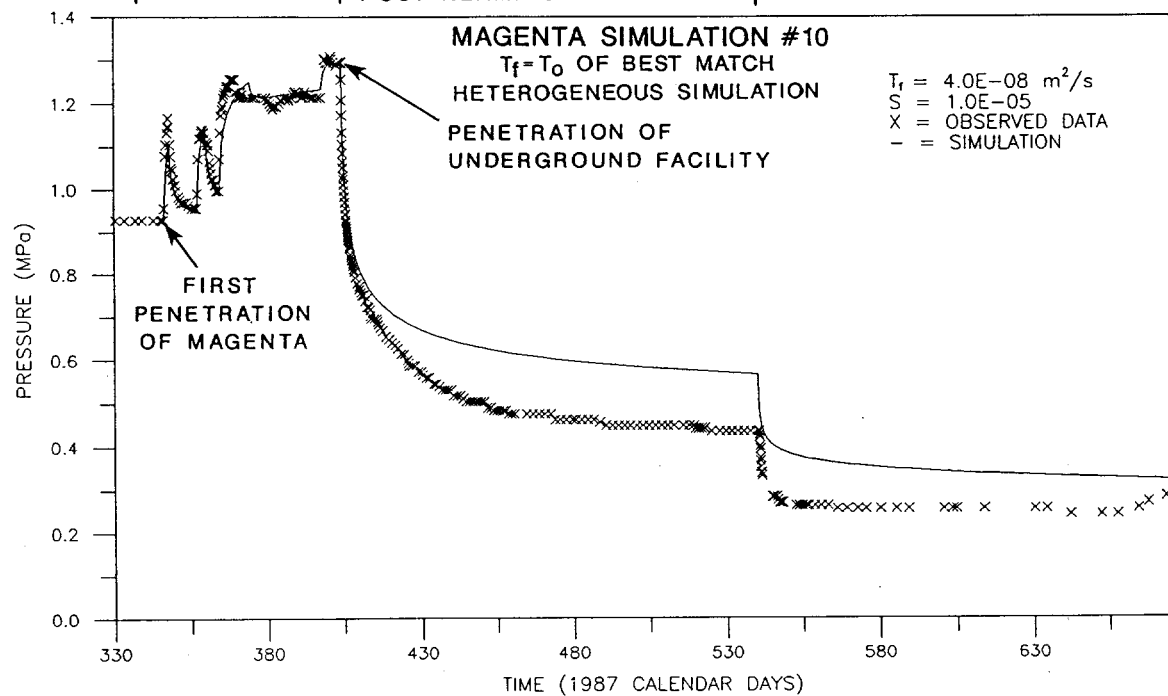
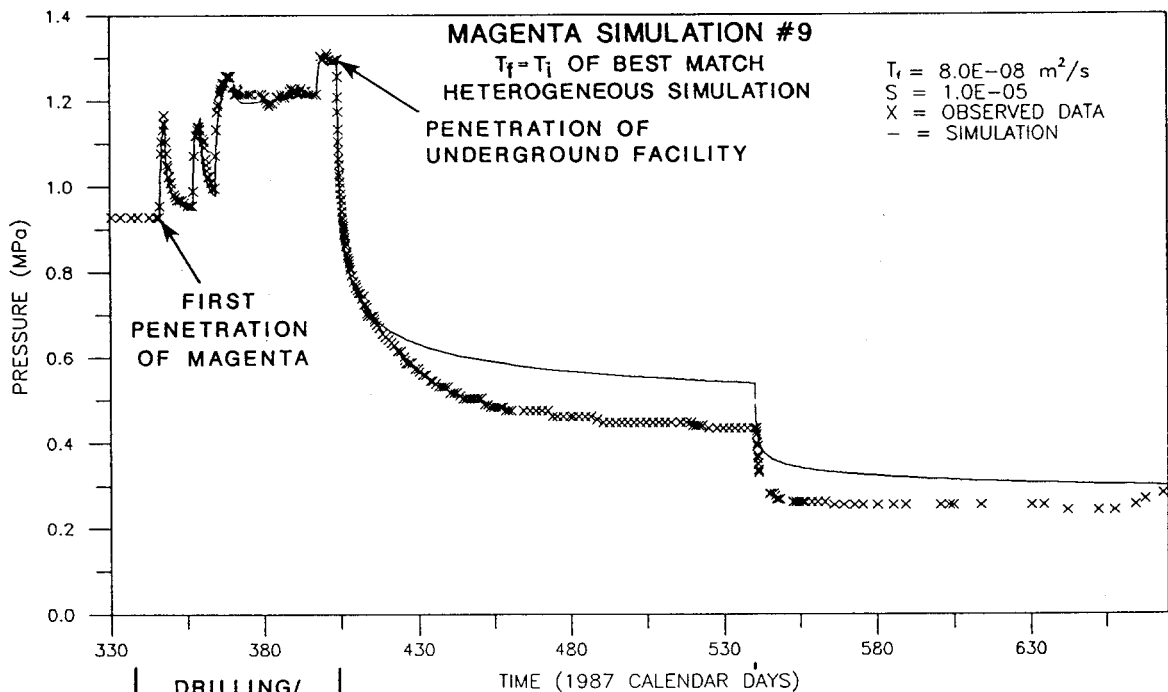


Drawn by J.D.A.	Date 2/27/89
Checked by G.S.	Date 2/27/89
Revisions	Date
H09700R876	2/27/89

SEMI-LOG PLOT OF THE FLUID-PRESSURE RESPONSE OF THE MAGENTA DOLOMITE AT H-16 SHOWING SENSITIVITY TO  $T_i$ ,  $T_o$ , AND  $r_b$  DURING THE POST-REAMING DRAINING PERIOD

**INTERA** Technologies

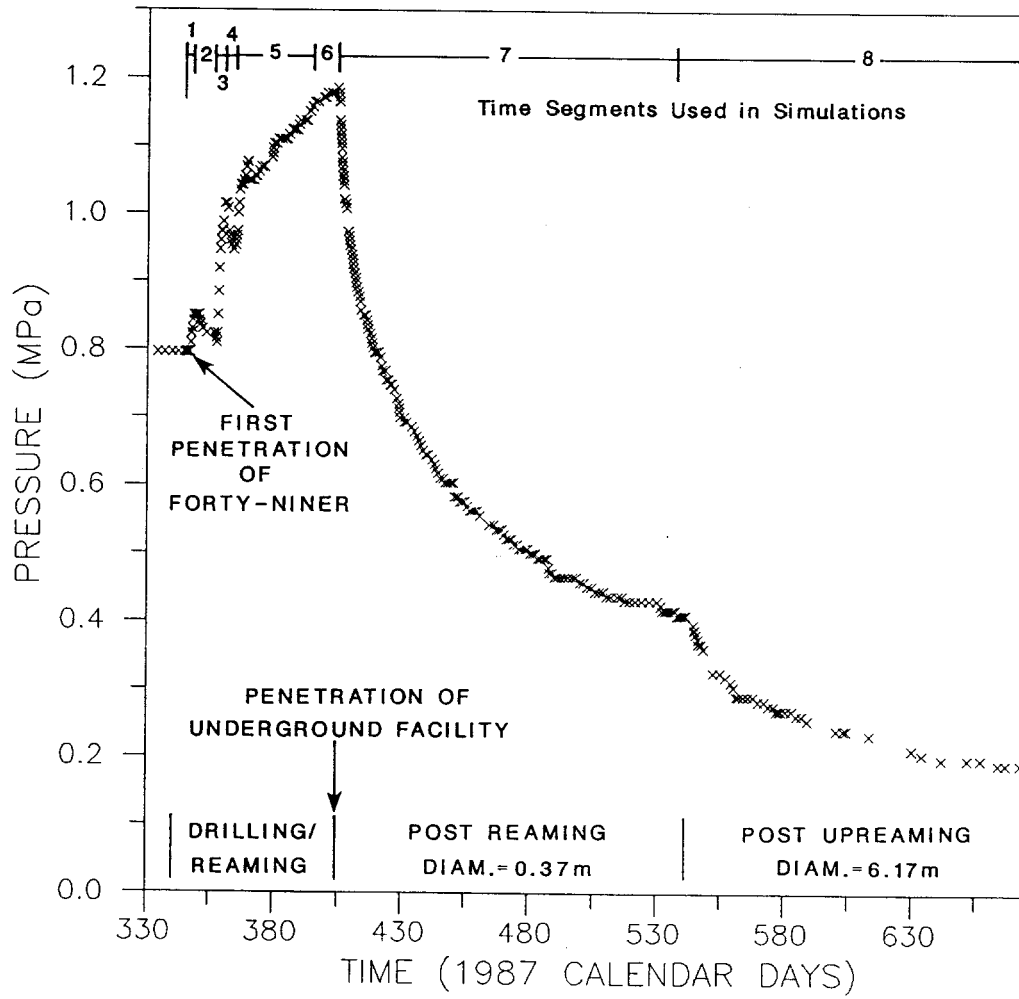
Figure 6.22



TIME 0 = JANUARY 1, 1987

Drawn by	J.D.A.	Date	2/27/89
Checked by	G.S.	Date	2/27/89
Revisions		Date	
H09700R876		2/27/89	

SIMULATION OF THE MAGENTA DOLOMITE FLUID-PRESSURE RESPONSE AT H-16 USING A HOMOGENEOUS-FORMATION CHARACTERIZATION AND SHOWING SENSITIVITY OF  $T_r$  TO  $T_i$  AND  $T_o$  OF THE BEST-MATCH HETEROGENEOUS CHARACTERIZATION



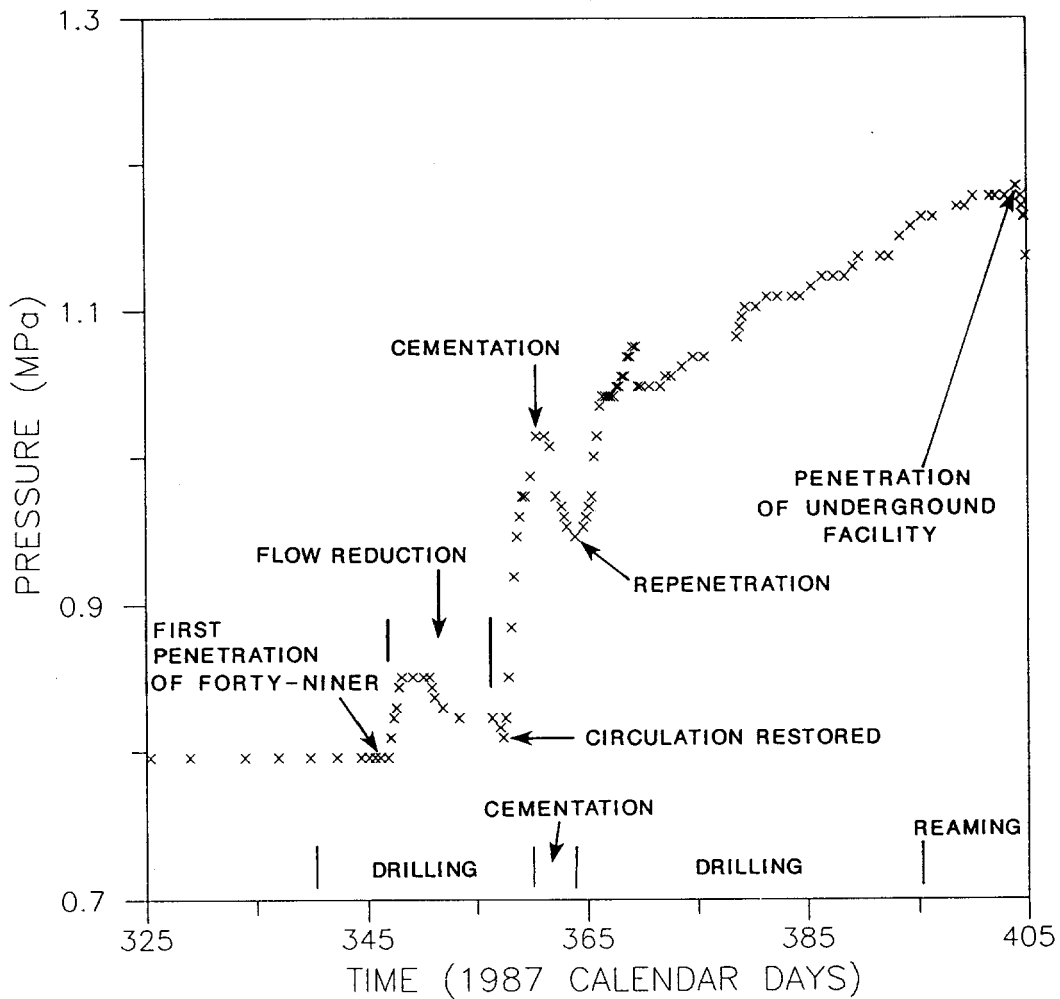
TIME 0 = JANUARY 1, 1987

Drawn by J.D.A.	Date 2/27/89
Checked by G.S.	Date 2/27/89
Revisions ABW	Date 6/23/89
H09700R876	2/27/89

FLUID-PRESSURE RESPONSE OF THE FORTY-NINER CLAYSTONE OBSERVED AT OBSERVATION-WELL H-16 DURING THE CONSTRUCTION OF THE AIS

**INTERA** Technologies

Figure 6.24



TIME 0 = JANUARY 1, 1987

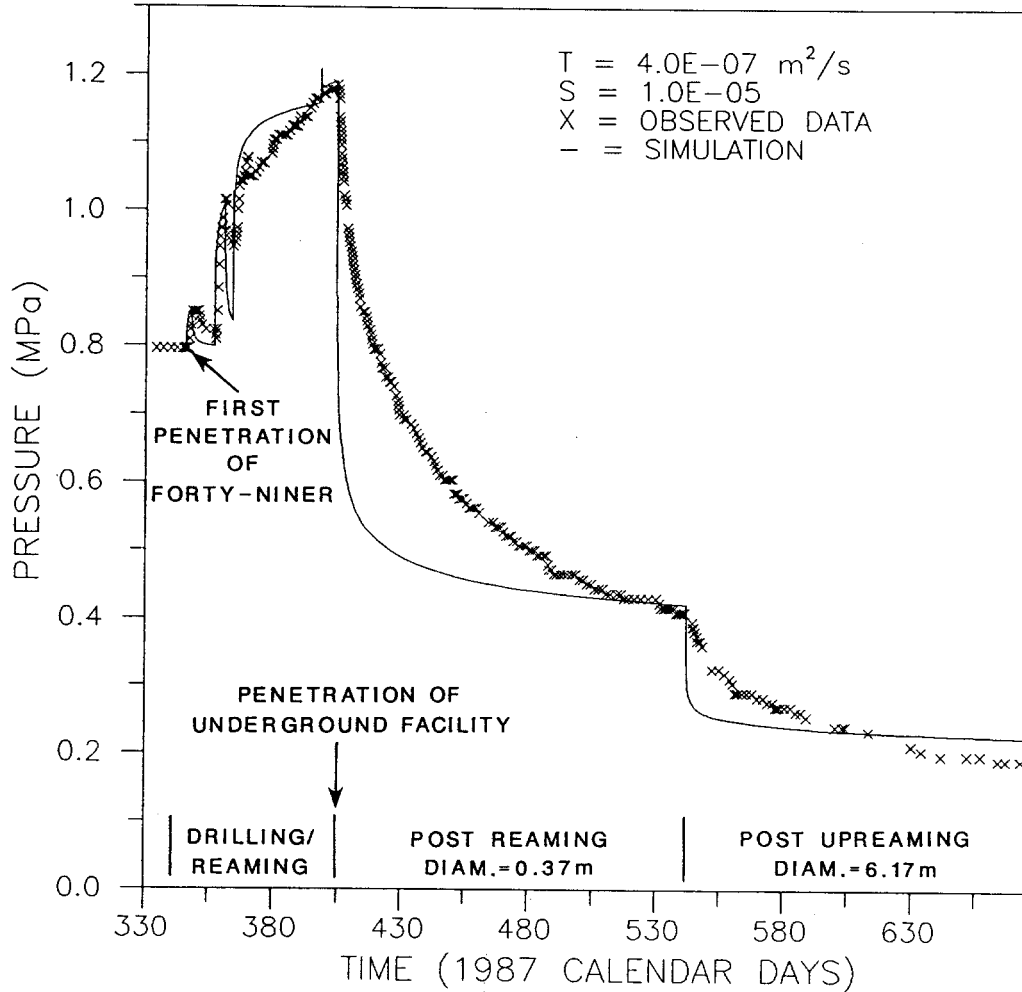
Drawn by J.D.A.	Date 2/27/89
Checked by G.S.	Date 2/27/89
Revisions	Date
H09700R876	2/27/89

FLUID-PRESSURE RESPONSE OF THE FORTY-NINER CLAYSTONE OBSERVED AT OBSERVATION-WELL H-16 DURING THE DRILLING/REAMING PERIOD OF THE CONSTRUCTION OF THE AIS

**INTERA** Technologies

Figure 6.25

FORTY-NINER SIMULATION #1



TIME 0 = JANUARY 1, 1987

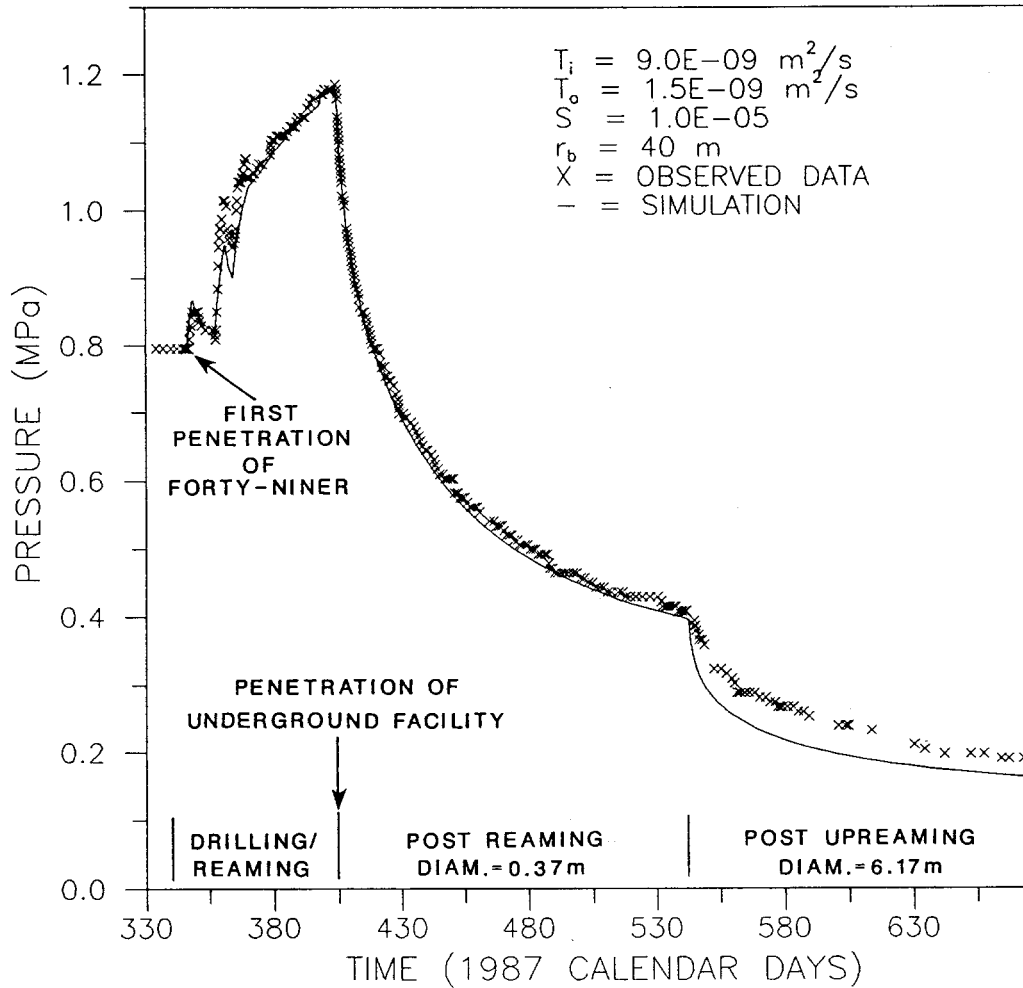
Drawn by J.D.A.	Date 2/27/89
Checked by G.S.	Date 2/27/89
Revisions	Date
H09700R876	2/27/89

SIMULATION OF THE FORTY-NINER CLAYSTONE FLUID-PRESSURE RESPONSE AT H-16 DURING THE CONSTRUCTION OF THE AIS USING A HOMOGENEOUS-FORMATION CHARACTERIZATION

**INTERA** Technologies

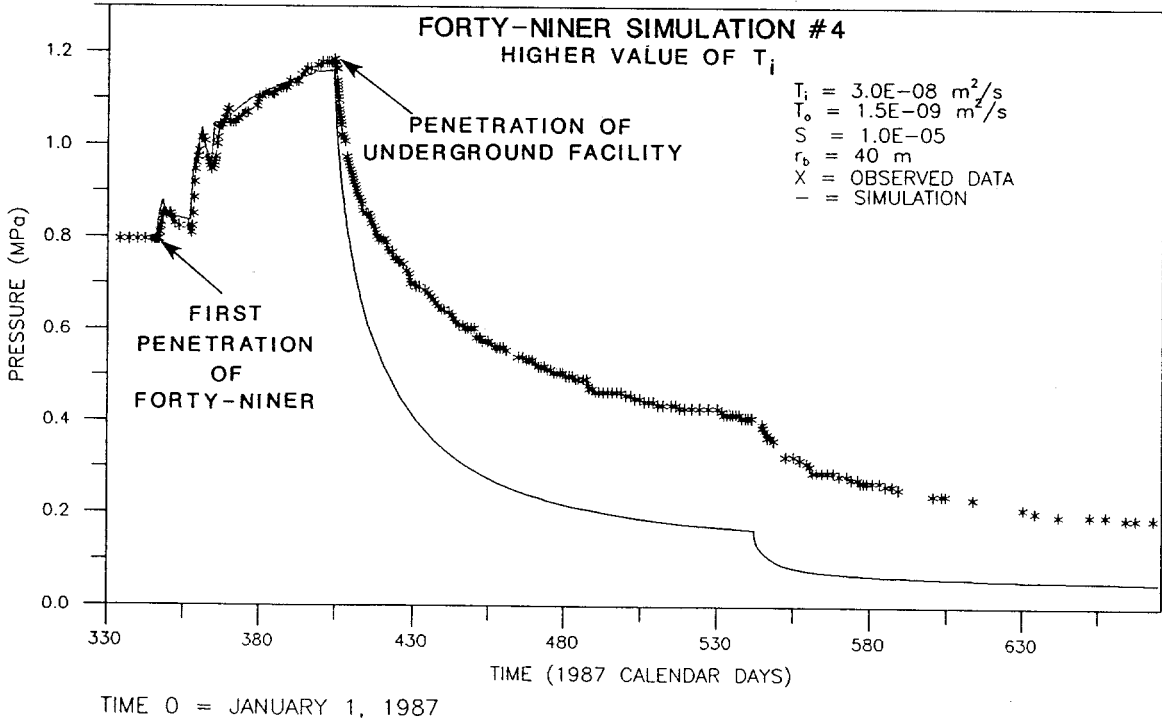
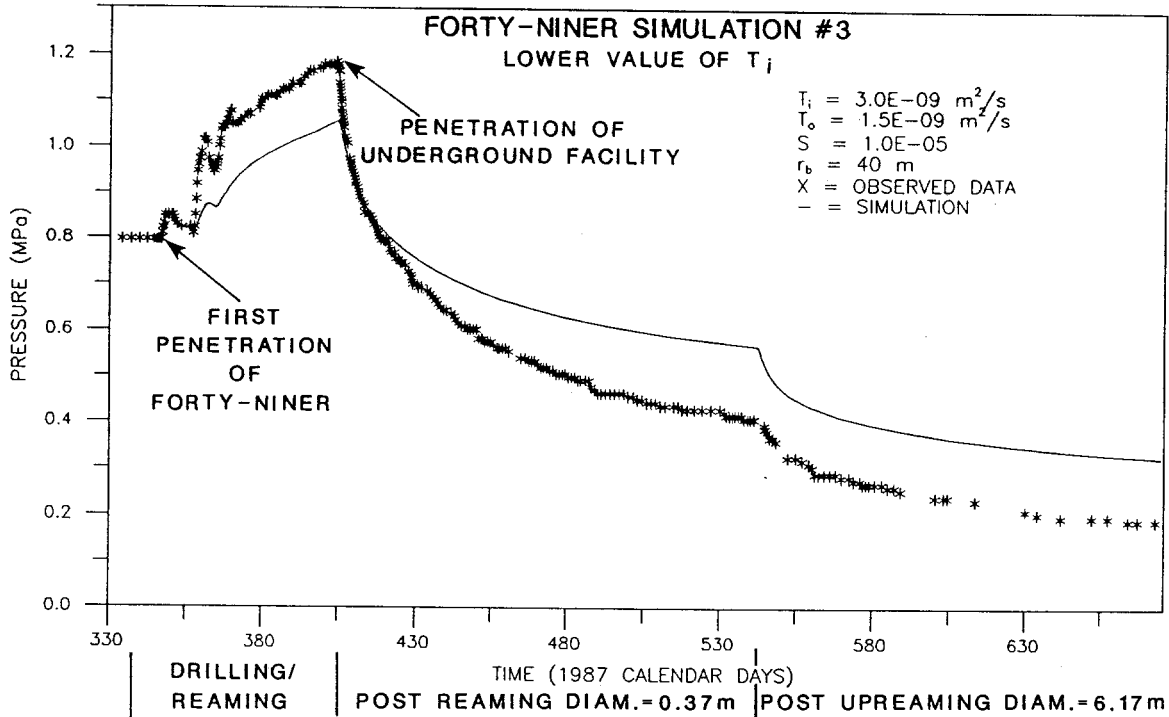
Figure 6.26

FORTY-NINER SIMULATION #2



TIME 0 = JANUARY 1, 1987

Drawn by J.D.A.	Date 2/27/89	SIMULATION OF THE FORTY-NINER CLAYSTONE FLUID-PRESSURE RESPONSE AT H-16 DURING THE CONSTRUCTION OF THE AIS USING A FORMATION-HETEROGENEITY BOUNDARY
Checked by G.S.	Date 2/27/89	
Revisions	Date	
H09700R876	2/27/89	
<b>INTERA Technologies</b>		Figure 6.27

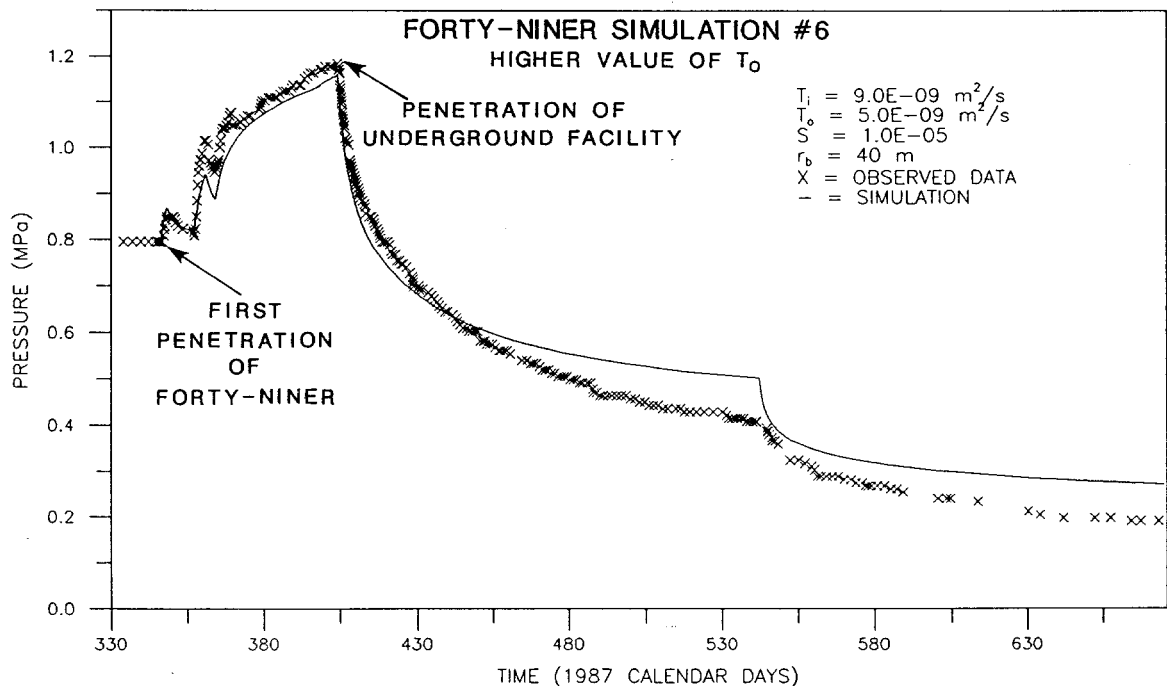
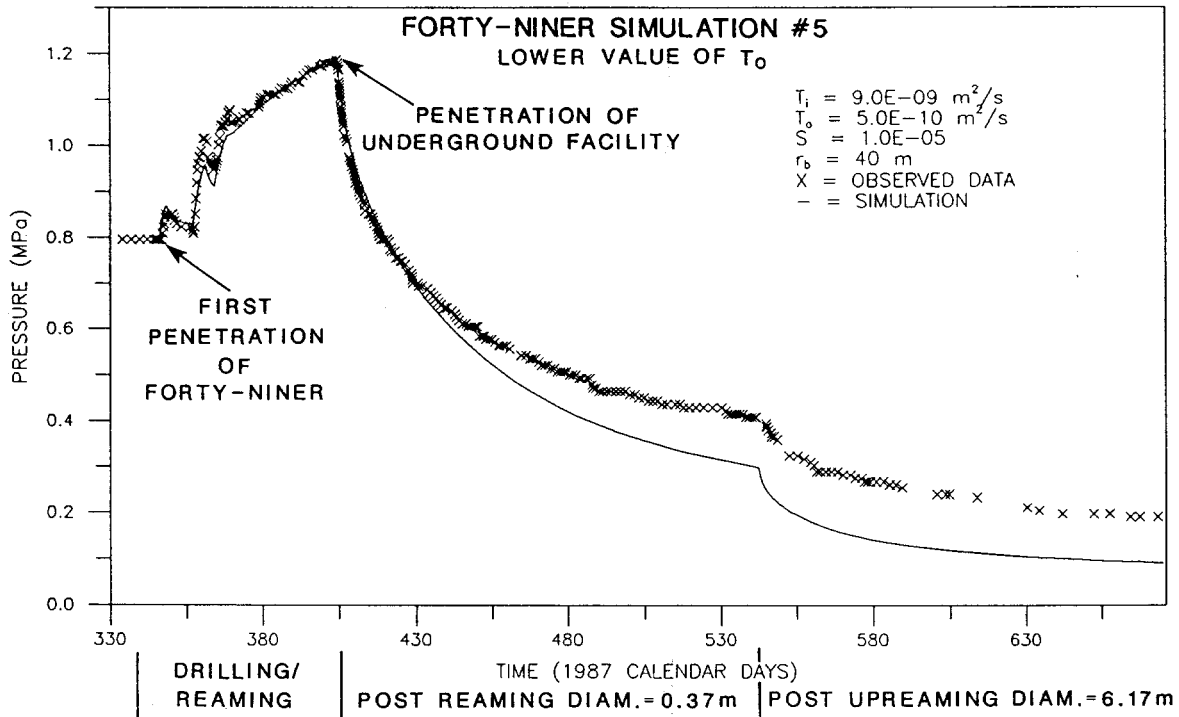


Drawn by J.D.A.	Date 2/27/89
Checked by G.S.	Date 2/27/89
Revisions	Date
H09700R876	2/27/89

SIMULATION OF THE FORTY-NINER CLAYSTONE FLUID-PRESSURE RESPONSE AT H-16 DURING THE CONSTRUCTION OF THE AIS USING A FORMATION-HETEROGENEITY BOUNDARY AND SHOWING SENSITIVITY TO  $T_i$

**INTERA Technologies**

Figure 6.28



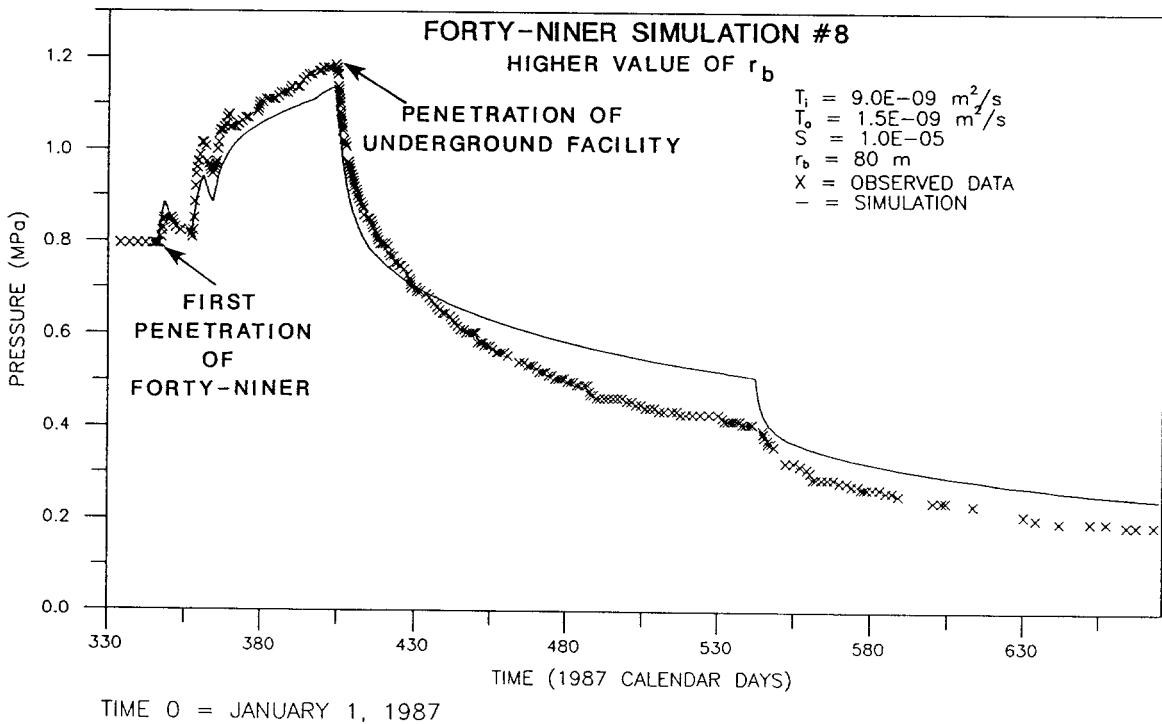
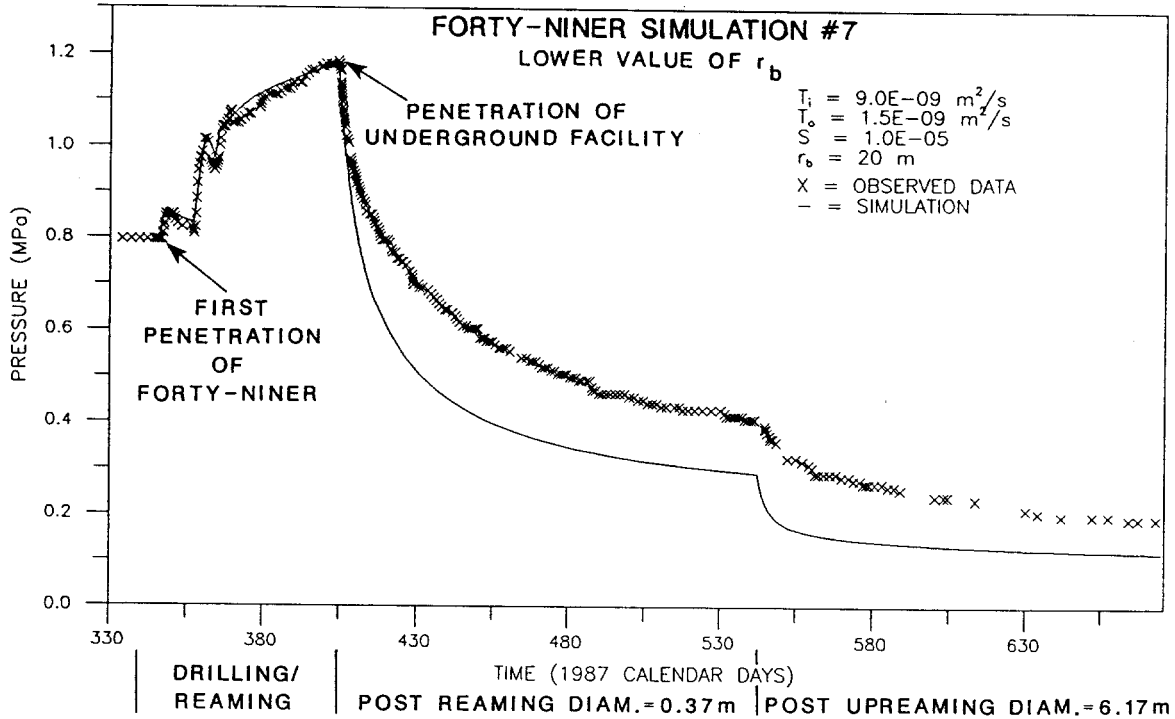
TIME 0 = JANUARY 1, 1987

Drawn by J.D.A.	Date 2/27/89
Checked by G.S.	Date 2/27/89
Revisions	Date
H09700R876	2/27/89

SIMULATION OF THE FORTY-NINER CLAYSTONE FLUID-PRESSURE RESPONSE AT H-16 DURING THE CONSTRUCTION OF THE AIS USING A FORMATION-HETEROGENEITY BOUNDARY AND SHOWING SENSITIVITY TO  $T_o$ .

**INTERA Technologies**

Figure 6.29

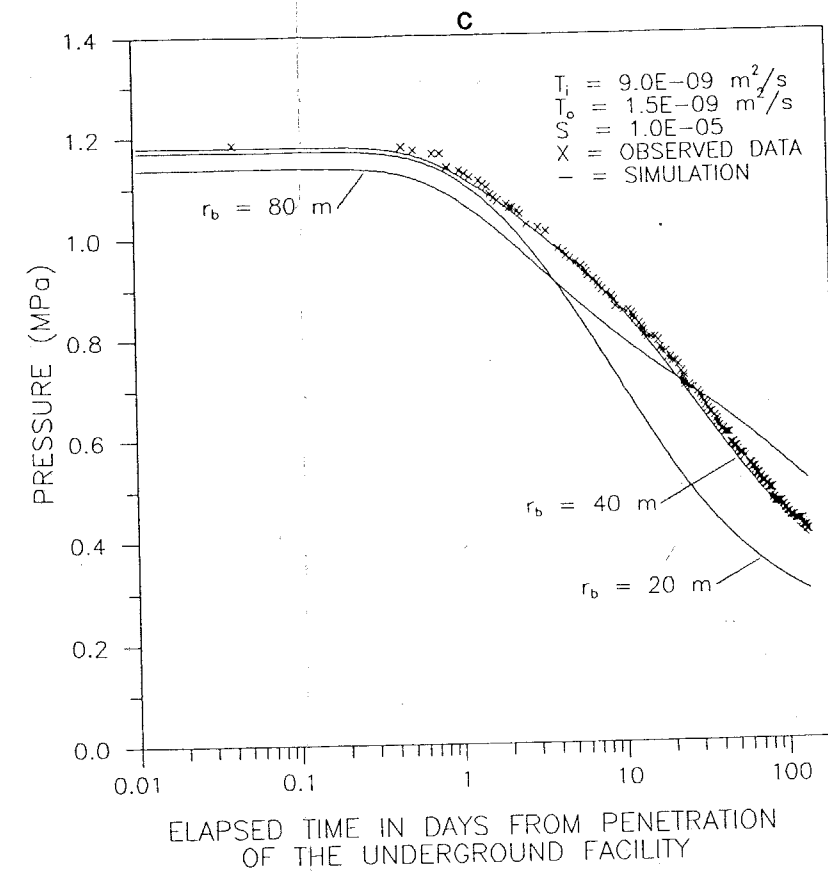
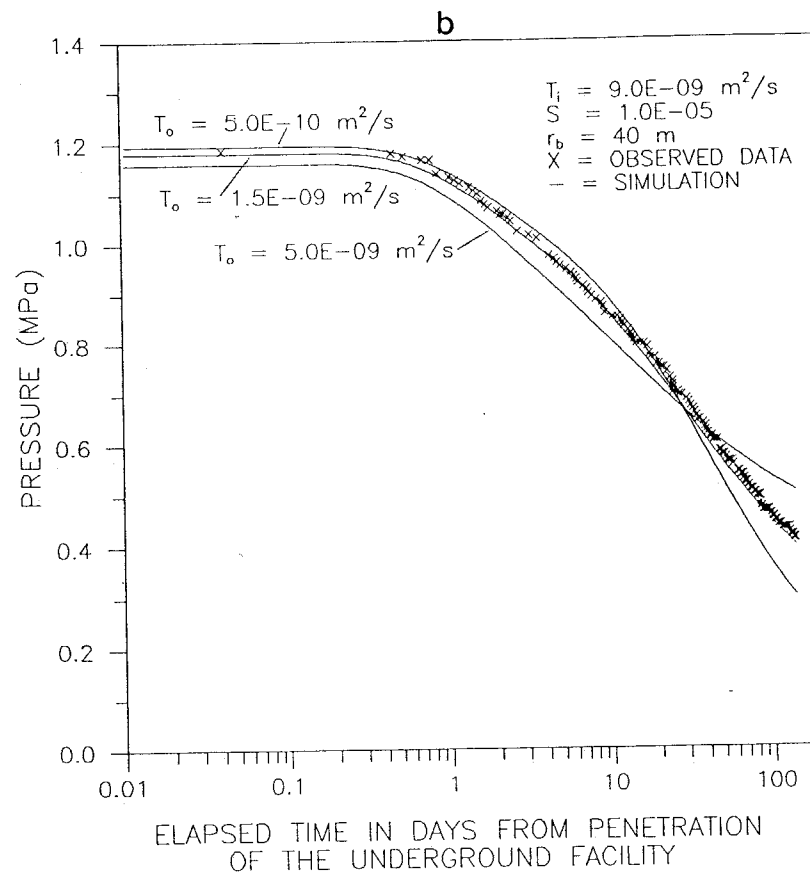
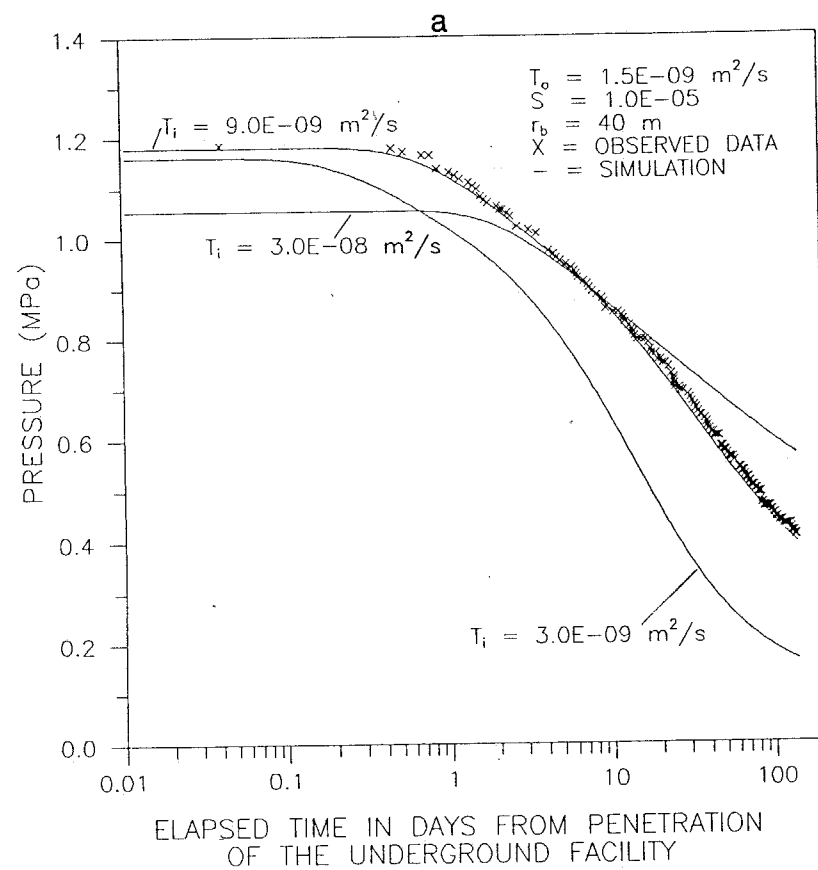


Drawn by	J.D.A.	Date	2/27/89
Checked by	G.S.	Date	2/27/89
Revisions		Date	
H09700R876		2/27/89	

SIMULATION OF THE FORTY-NINER CLAYSTONE FLUID-PRESSURE RESPONSE AT H-16 DURING THE CONSTRUCTION OF THE AIS USING A FORMATION-HETEROGENEITY BOUNDARY AND SHOWING SENSITIVITY TO  $r_b$

**INTERA** Technologies

Figure 6.30

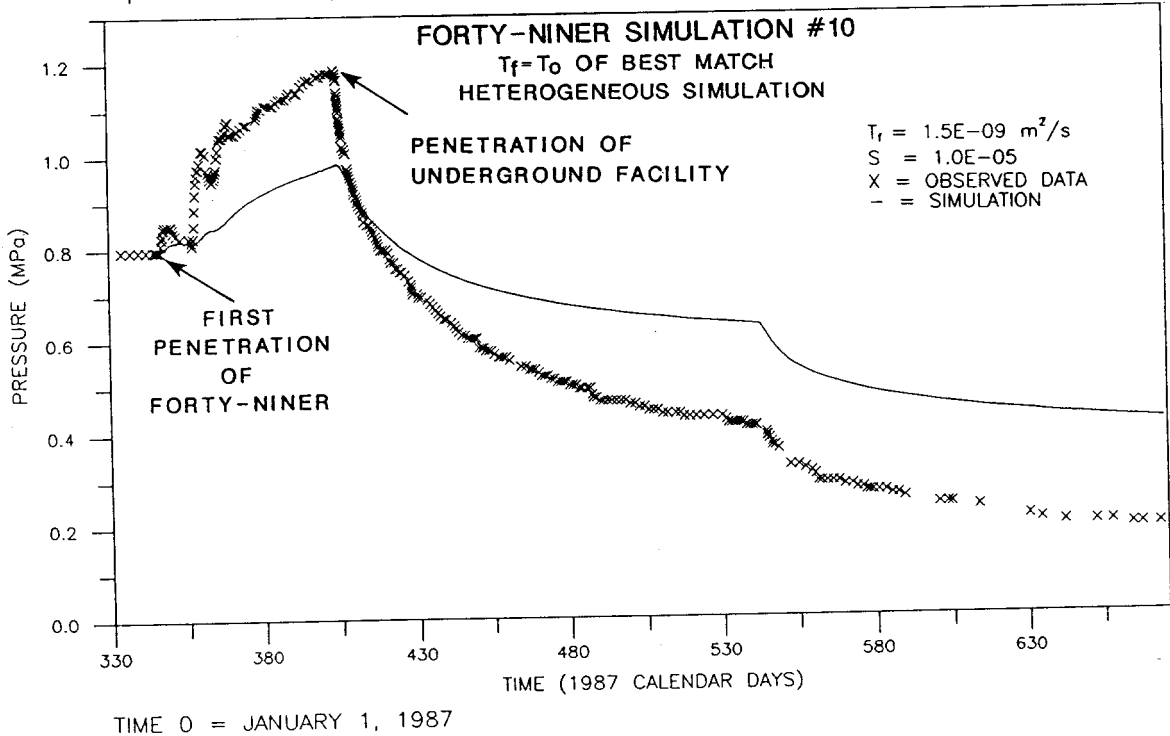
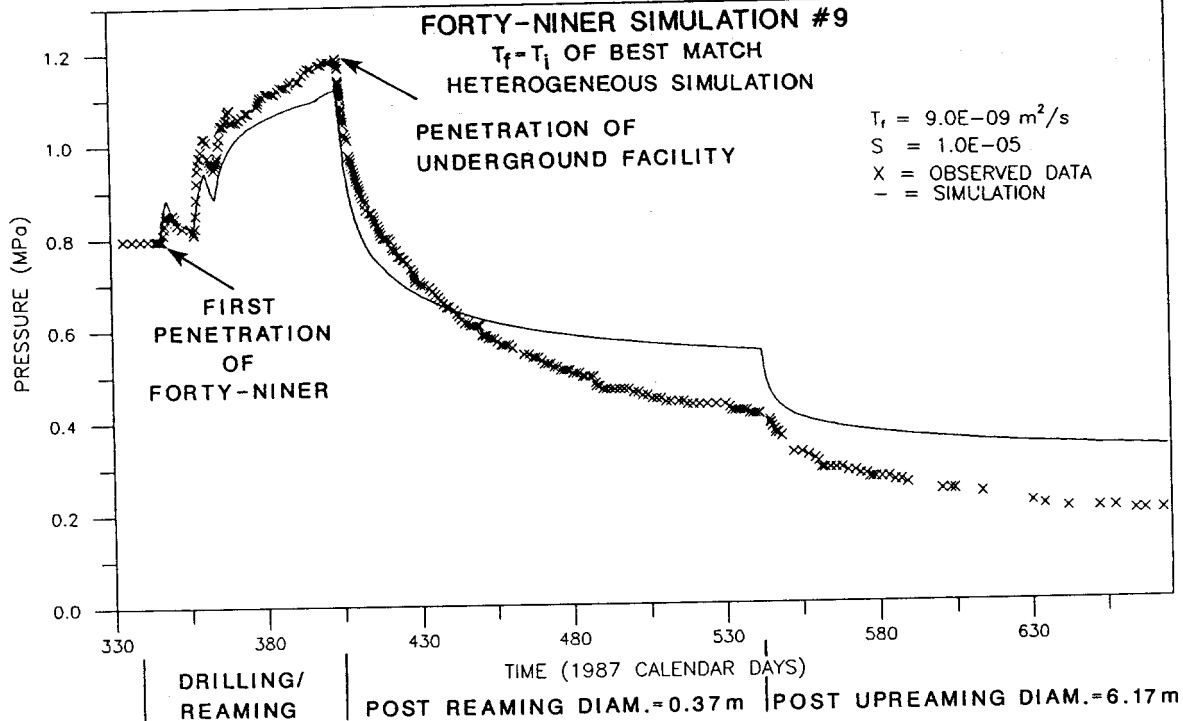


Drawn by J.D.A.	Date 2/27/89
Checked by G.S.	Date 2/27/89
Revisions	Date
H09700R876	2/27/89

SEMI-LOG PLOT OF THE FLUID-PRESSURE RESPONSE OF THE FORTY-NINER CLAYSTONE AT H-16 SHOWING SENSITIVITY TO  $T_i$ ,  $T_o$ , AND  $r_b$  DURING THE POST-REAMING DRAINING PERIOD

INTERA Technologies

Figure 6.31



Drawn by J.D.A.	Date 2/27/89
Checked by G.S.	Date 2/27/89
Revisions ABW	Date 6/23/89
H09700R876	2/27/89

SIMULATION OF THE FORTY-NINER CLAYSTONE FLUID-PRESSURE RESPONSE AT H-16 USING A HOMOGENEOUS-FORMATION CHARACTERIZATION AND SHOWING SENSITIVITY OF  $T_r$  TO  $T_i$  AND  $T_o$  OF THE BEST-MATCH HETEROGENEOUS CHARACTERIZATION

**INTERA Technologies**

Figure 6.32

Simulation Number	Transmissivity [m <sup>2</sup> /s]	Time at Full Mud Overpressure [hour]	Time at Reduced Pressure [hour]	Reduced Pressure [MPa]
-------------------	---------------------------------------	---	------------------------------------	---------------------------

**Segment 1 - initial penetration to cementing**

Total duration = 113.448 hours

1)	T <sub>f</sub> = 2.6E-08, no cement skin	16.432	97.016	1.550
2)	T <sub>f</sub> = 1.3E-07, cement skin	6.432	107.016	1.380
3)	T <sub>f</sub> = 6.6E-07, cement skin	3.000	110.448	1.310
4)	T <sub>f</sub> = 2.6E-07, cement skin	1.000	112.448	1.240
5)	T <sub>f</sub> = 1.3E-07, no cement skin	6.432	107.016	1.380
6)	T <sub>f</sub> = 6.6E-07, no cement skin	1.000	112.448	1.240

**Segment 3 - post-cement penetration to reaming**

Total duration = 576.432 hours

1)	T <sub>f</sub> = 2.6E-08, no cement skin	29.776	546.656	1.500
2)	T <sub>f</sub> = 1.3E-07, cement skin	19.776	556.656	1.550
3)	T <sub>f</sub> = 6.6E-07, cement skin	19.776	556.656	1.690
4)	T <sub>f</sub> = 2.6E-07, cement skin	19.776	556.656	1.760
5)	T <sub>f</sub> = 1.3E-07, no cement skin	9.776	566.656	1.370
6)	T <sub>f</sub> = 6.6E-07, no cement skin	1.776	574.656	1.310

**Segment 4 - reaming to underground facility penetration**

Total duration = 141.84 hours

1)	T <sub>f</sub> = 2.6E-08, no cement skin	4.800	137.040	1.450
2)	T <sub>f</sub> = 1.3E-07, cement skin	4.800	137.040	1.450
3)	T <sub>f</sub> = 6.6E-07, cement skin	4.800	137.040	1.510
4)	T <sub>f</sub> = 2.6E-07, cement skin	4.800	137.040	1.520
5)	T <sub>f</sub> = 1.3E-07, no cement skin	1.800	140.040	1.280
6)	T <sub>f</sub> = 6.6E-07, no cement skin	2.800	139.040	1.350

Drawn by	Date	Values and Durations of Wellbore Pressures Used for Fixed-Pressure Wellbore Boundary Conditions During Simulation of the Culebra Dolomite Drilling/Reaming Period
Checked by	Date	
Revisions	Date	

**INTERA Technologies**

Table 6.1

Simulation Number	Time at Full Mud Overpressure [hour]	Time at Reduced Pressure [hour]	Reduced Pressure [MPa]
-------------------	--------------------------------------	---------------------------------	------------------------

**Segment 1 - initial penetration to flow reduction**

Total duration = 40.080 hours

**Formation-Characterization Simulations**

1) Homogeneous	0.080	40.000	1.600
2) Heterogenous	22.000	18.080	2.000

**Heterogeneity-Parameter-Sensitivity Simulations**

3) $T_i = 2.5E-08 \text{ m}^2/\text{s}$	40.080	0.000	n/a
4) $T_i = 2.5E-07 \text{ m}^2/\text{s}$	5.000	35.080	1.600
5) $T_o = 1.3E-08 \text{ m}^2/\text{s}$	22.000	18.080	1.900
6) $T_o = 1.3E-07 \text{ m}^2/\text{s}$	40.080	0.000	n/a
7) $r_b = 20 \text{ m}$	12.000	28.080	1.800
8) $r_b = 80 \text{ m}$	40.080	0.000	n/a

**Homogeneous Characterization Showing Sensitivity to Heterogeneity Simulation Parameters**

9) $T_f = 8.0E-08 \text{ m}^2/\text{s}$	40.080	0.000	n/a
10) $T_f = 4.0E-08 \text{ m}^2/\text{s}$	40.080	0.000	n/a

**Segment 3 - circulation restoration to cementing**

Total duration = 63.000 hours

**Formation-Characterization Simulations**

1) Homogeneous	0.500	62.500	1.500
2) Heterogeneous	18.250	44.750	1.700

**Heterogeneity-Parameter-Sensitivity Simulations**

3) $T_i = 2.5E-08 \text{ m}^2/\text{s}$	63.000	0.000	n/a
4) $T_i = 2.5E-07 \text{ m}^2/\text{s}$	3.000	60.000	1.400
5) $T_o = 1.3E-08 \text{ m}^2/\text{s}$	8.250	54.750	1.500
6) $T_o = 1.3E-07 \text{ m}^2/\text{s}$	18.250	44.750	1.950
7) $r_b = 20 \text{ m}$	8.250	54.750	1.500
8) $r_b = 80 \text{ m}$	18.250	44.750	1.800

**Homogeneous Characterization Showing Sensitivity to Heterogeneity Simulation Parameters**

9) $T_f = 8.0E-08 \text{ m}^2/\text{s}$	23.250	39.750	1.900
10) $T_f = 4.0E-08 \text{ m}^2/\text{s}$	63.000	0.000	n/a

Drawn by	Date	Values and Durations of Wellbore Pressures Used for Fixed-Pressure Wellbore Boundary Conditions During Simulation of the Magenta Dolomite Drilling/Reaming Period
Checked by	Date	
Revisions	Date	
<b>INTERA Technologies</b>		Table 6.2

Simulation Number	Time at Full Mud Overpressure [hour]	Times at Reduced Pressure [hour]	Reduced Pressure [MPa]
-------------------	--------------------------------------	----------------------------------	------------------------

**Segment 5 - re-penetration to reaming interception**

Total duration = 799.536 hours

**Formation-Characterization Simulations**

1) Homogeneous	1.536	124.000 674.000	1.700 1.520
2) Heterogeneous	60.000	104.712 634.824	1.800 1.520

**Heterogeneity-Parameter-Sensitivity Simulations**

3) $T_i = 2.5E-08 \text{ m}^2/\text{s}$	284.712	514.824	1.950
4) $T_i = 2.5E-07 \text{ m}^2/\text{s}$	4.000	160.712 634.824	1.450 1.330
5) $T_o = 1.3E-08 \text{ m}^2/\text{s}$	12.000	116.712 670.824	1.600 1.400
6) $T_o = 1.3E-07 \text{ m}^2/\text{s}$	164.712	634.824	1.850
7) $r_b = 20 \text{ m}$	12.000	152.712 634.824	1.700 1.500
8) $r_b = 80 \text{ m}$	116.712	682.824	1.600

**Homogeneous Characterization Showing Sensitivity to Heterogeneity Simulation Parameters**

9) $T_f = 8.0E-08 \text{ m}^2/\text{s}$	140.712	658.824	1.720
10) $T_f = 4.0E-08 \text{ m}^2/\text{s}$	236.712	562.824	1.850

**Segment 6 - reaming interception to underground facility penetration**

Total duration = 154.656 hours

**Formation Characterization Simulations**

1) Homogeneous	0.656	154.000	1.700
2) Heterogeneous	19.992	134.664	1.750

**Parameter-Sensitivity Simulations**

3) $T_i = 2.5E-08 \text{ m}^2/\text{s}$	154.656	0.000	n/a
4) $T_i = 2.5E-07 \text{ m}^2/\text{s}$	3.992	150.664	1.450
5) $T_o = 1.3E-08 \text{ m}^2/\text{s}$	15.992	138.664	1.520
6) $T_o = 1.3E-07 \text{ m}^2/\text{s}$	67.992	86.664	2.000
7) $r_b = 20 \text{ m}$	10.992	143.664	1.650
8) $r_b = 80 \text{ m}$	31.992	122.664	1.800

**Homogeneous Characterization Showing Sensitivity to Heterogeneity Simulation Parameters**

9) $T_f = 8.0E-08 \text{ m}^2/\text{s}$	43.992	110.664	1.900
10) $T_f = 4.0E-08 \text{ m}^2/\text{s}$	67.992	86.664	2.000

Drawn by	Date	Wellbore Pressures and Durations used for Fixed Pressure Well-bore Boundary Conditions During Simulation of Magenta Dolomite Drilling/Reaming Period
Checked by	Date	
Revisions	Date	
<b>INTERA Technologies</b>		Table 6.2 (cont.)

Simulation Number	Time at Full Mud Overpressure [hour]	Time at Reduced Pressure [hour]	Reduced Pressure [MPa]
-------------------	--------------------------------------	---------------------------------	------------------------

**Segment 1 - initial penetration to flow reduction**

Total duration = 48.000 hour

**Calibration Simulations**

1) Homogeneous	0.250	47.750	1.000
2) Heterogeneous	24.000	24.000	1.600

**Heterogeneity Parameter Sensitivity Simulations**

3) $T_i = 3.0E-09 \text{ m}^2/\text{s}$	48.000	0.000	n/a
4) $T_i = 3.0E-08 \text{ m}^2/\text{s}$	4.000	44.000	1.300
5) $T_o = 5.0E-10 \text{ m}^2/\text{s}$	24.000	24.000	1.600
6) $T_o = 5.0E-09 \text{ m}^2/\text{s}$	24.000	24.000	1.600
7) $r_b = 20 \text{ m}$	10.000	38.000	1.300
8) $r_b = 80 \text{ m}$	48.000	0.000	n/a

**Homogeneous Characterization Showing Sensitivity to Heterogeneity Simulation Parameters**

9) $T_f = 9.0E-09 \text{ m}^2/\text{s}$	48.000	0.000	n/a
10) $T_f = 1.5E-09 \text{ m}^2/\text{s}$	48.000	0.000	n/a

**Segment 3 - circulation restoration to cementing**

Total duration = 90.000 hour

**Calibration Simulations**

1) Homogeneous	2.000	88.000	1.450
2) Heterogeneous	90.000	0.000	n/a

**Heterogeneity Parameter Sensitivity Simulations**

3) $T_i = 3.0E-09 \text{ m}^2/\text{s}$	90.000	0.000	n/a
4) $T_i = 3.0E-08 \text{ m}^2/\text{s}$	20.000	70.000	1.700
5) $T_o = 5.0E-10 \text{ m}^2/\text{s}$	90.000	0.000	n/a
6) $T_o = 5.0E-09 \text{ m}^2/\text{s}$	90.000	0.000	n/a
7) $r_b = 20 \text{ m}$	90.000	0.000	n/a
8) $r_b = 80 \text{ m}$	90.000	0.000	n/a

**Homogeneous Characterization Showing Sensitivity to Heterogeneity Simulation Parameters**

9) $T_f = 9.0E-09 \text{ m}^2/\text{s}$	90.000	0.000	n/a
10) $T_f = 1.5E-09 \text{ m}^2/\text{s}$	90.000	0.000	n/a

Drawn by	Date
Checked by	Date
Revisions	Date

Values and Durations of Wellbore Pressures Used for Fixed-Pressure Wellbore Boundary Conditions During Simulation of the Forty-Niner Claystone Drilling/Reaming Period

**INTERA Technologies**

Table 6.3

Simulation Number	Time at Full Mud Overpressure [hour]	Time at Reduced Pressure [hour]	Reduced Pressure [MPa]
-------------------	--------------------------------------	---------------------------------	------------------------

**Segment 5 - re-penetration to reaming interception**

Total duration = 806.232 hour

**Formation Characterization Simulations**

1) Homogeneous	5.232	801.000	1.670
2) Heterogeneous	156.232	650.000	1.780

**Heterogeneity-Parameter-Sensitivity Simulations**

3) $T_i = 3.0E-09 \text{ m}^2/\text{s}$	806.232	0.000	n/a
4) $T_i = 3.0E-08 \text{ m}^2/\text{s}$	16.232	790.000	1.330
5) $T_o = 5.0E-10 \text{ m}^2/\text{s}$	98.232	708.000	1.650
6) $T_o = 5.0E-09 \text{ m}^2/\text{s}$	806.232	0.000	n/a
7) $r_b = 20 \text{ m}$	26.232	780.000	1.500
8) $r_b = 80 \text{ m}$	806.232	0.000	n/a

**Homogeneous Characterization Showing Sensitivity to Heterogeneity Simulation Parameters**

9) $T_f = 9.0E-09 \text{ m}^2/\text{s}$	806.232	0.000	n/a
10) $T_f = 1.5E-09 \text{ m}^2/\text{s}$	806.232	0.000	n/a

**Segment 6 - reaming interception to underground facility penetration**

Total duration = 157.776 hour

**Formation Characterization Simulations**

1) Homogeneous	2.776	155.000	1.700
2) Heterogeneous	17.776	140.000	1.750

**Heterogeneity-Parameter-Sensitivity Simulations**

3) $T_i = 3.0E-09 \text{ m}^2/\text{s}$	157.776	0.000	n/a
4) $T_i = 3.0E-08 \text{ m}^2/\text{s}$	1.776	156.000	1.300
5) $T_o = 5.0E-10 \text{ m}^2/\text{s}$	17.776	140.000	1.600
6) $T_o = 5.0E-09 \text{ m}^2/\text{s}$	157.776	0.000	n/a
7) $r_b = 20 \text{ m}$	4.776	153.000	1.450
8) $r_b = 80 \text{ m}$	157.776	0.000	n/a

**Homogeneous Characterization Showing Sensitivity to Heterogeneity Simulation Parameters**

9) $T_f = 9.0E-09 \text{ m}^2/\text{s}$	157.776	0.000	n/a
10) $T_f = 1.5E-09 \text{ m}^2/\text{s}$	157.776	0.000	n/a

Drawn by	Date	Values and Durations of Wellbore Pressures Used for Fixed-Pressure Wellbore Boundary Conditions During Simulation of the Forty-Niner Claystone Drilling/Reaming Period
Checked by	Date	
Revisions	Date	

**INTERA Technologies**

Table 6.3 (cont.)

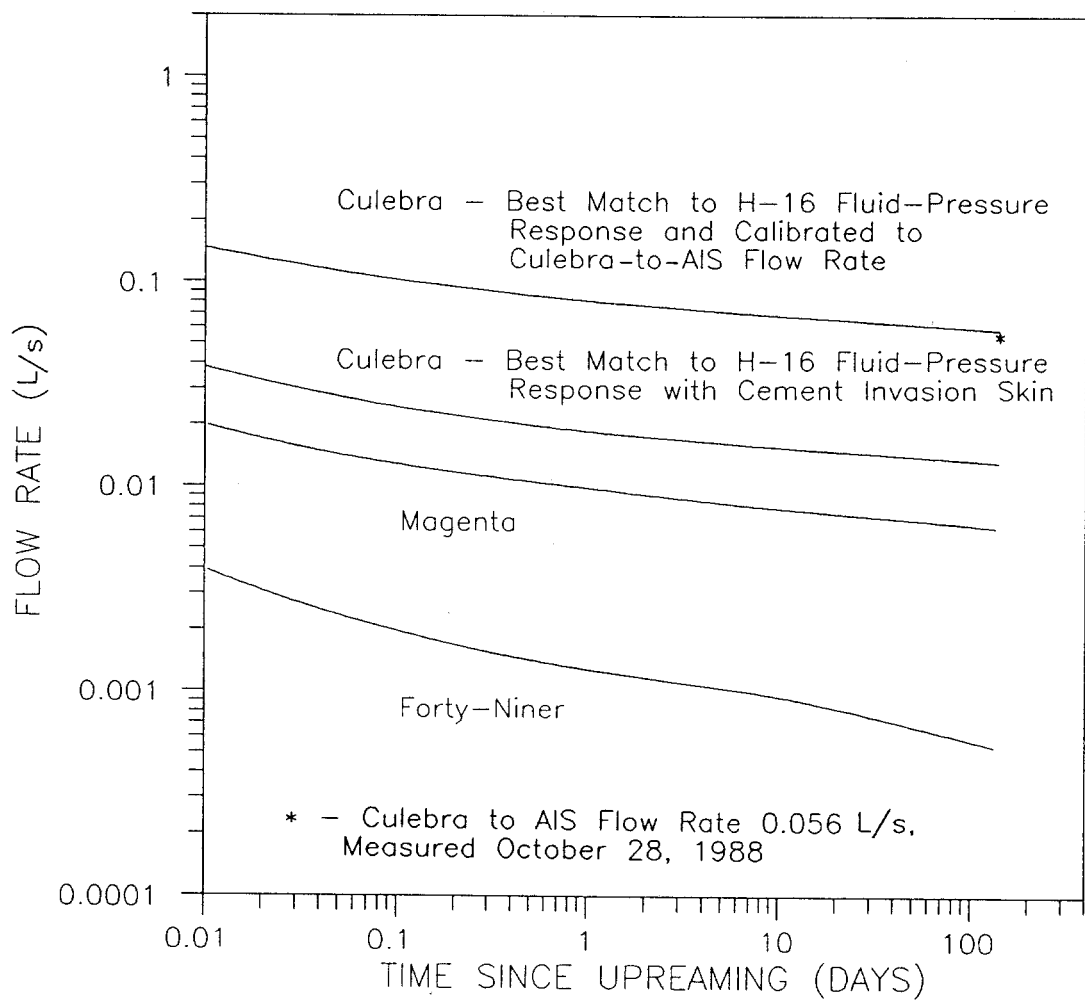
## 7.0 POTENTIAL LEAKAGE INTO THE AIR-INTAKE SHAFT

GTFM was used to calculate the flow rate to the AIS for each of the three members of the Rustler whose fluid-pressure responses were analyzed in this report. Figure 7.1 is a log-log plot of the simulated flow rate from these members to the AIS versus time since the interval was intercepted by the upreaming of the AIS for the following simulations: the flow rate from the Culebra for the best-match simulation with a cement-invasion-skin zone for the period before upreaming; the flow rate from the Culebra for the best-match simulation with a cement-invasion-skin zone and calibrated to the single measured flow rate from the Culebra to the AIS after upreaming; the flow rate from the Magenta for the best-match simulation using a formation-heterogeneity boundary; and the flow rate from the Forty-niner claystone for the best-match simulation using a formation-heterogeneity boundary. Also shown on the figure is the measured flow-rate of 0.056 L/s. Note that the time scale on Figure 7.1 is elapsed time in days since interception by the upreaming of the AIS, which occurred on different days for each of the formations.

Assuming that the transmissivity used for the best-match simulation calibrated to the single measured flow rate is the most representative for the Culebra, then the order-of magnitude differences in flow-rate estimates for all the units, as shown on Figure 7.1, are consistent with the published estimates of transmissivities for these units from observation-well H-16 (Beauheim, 1987a). As an additional comparison, Haug and others (1987) and LaVenue and others (1988) estimated a steady-state water inflow from the Culebra to a single model grid block representing a composite open shaft (comprising the open, unsealed time periods of the WHS, C&SH shaft, and EXS) of 0.085 L/s.

Figure 7.1 also shows that after about 15 days of drainage, the Forty-niner claystone flow rate begins to decrease at a higher rate, indicating transition of the controlling flow regime from the higher permeability inner or near-field zone to the lower permeability outer or far-field zone. This transition is more obvious for the Forty-niner than for the Magenta because the Forty-niner's permeability contrast between the inner and outer zones is greater than that of the Magenta. However, the derivative of the flow rate versus time shows a similar transition for the Magenta.

Table 7.1 provides a summary of simulated flow rates on Calendar Day 667 for the four simulations whose estimated flow rates are plotted on Figure 7.1. Table 7.1 also includes two calculations of total combined inflow to the AIS from all three units analyzed. The first calculation is based on the best-match simulation with a cement-invasion skin, and the second calculation is based on the best-match simulation with a cement-invasion skin and calibrated to the single flow-rate measurement. Using the highest estimated inflow rates for each unit, and considering the consistent flow-rate decline indicated on Figure 7.1, total estimated inflow from the Rustler Formation to the unsealed AIS would be less than 0.065 L/s.



Drawn by J.D.A.	Date 3/15/89	CALCULATED FLOW RATE TO THE AIS VERSUS TIME SINCE UPREAMING FOR THE CULEBRA AND MAGENTA DOLOMITES AND THE FORTY-NINER CLAYSTONE
Checked by G.S.	Date 3/15/89	
Revisions ABW	Date 6/23/89	
H09700R876	3/15/89	
<b>INTERA Technologies</b>		Figure 7.1

Rustler Unit	Simulation	Flow rate [L/s]
Culebra	Best Match to H-16 Fluid-Pressure Response with Cement-Invasion Skin	1.3E-2
Culebra	Best Match to H-16 Fluid-Pressure Response with Cement-Invasion Skin and Calibrated to the Culebra for Culebra to AIS Flow-Rate Measurement	5.8E-2
Magenta	Heterogeneous-Formation Characterization	6.4E-3
Forty-Niner	Heterogeneous-Formation Characterization	5.5E-4
Total Rustler Flow Rate Using the Culebra Best-Match Simulation of the H-16 Fluid-Pressure Response with a Cement-Invasion Skin		1.9E-2
Total Rustler Flow Rate Using the Culebra Best-Match Simulation of the H-16 Fluid-Pressure Response with a Cement-Invasion Skin and Calibrated to the Culebra to AIS Flow-Rate Measurement		6.5E-2

Drawn by	Date	Calculated Flow Rates From the Units of the Rustler Formation to the AIS on Calendar Day 667
Checked by	Date	
Revisions	Date	

**INTERA** Technologies

Table 7.1

## 8.0 SUMMARY AND CONCLUSIONS

### 8.1 General

The effect of the construction of a fourth underground-access shaft, the AIS, at the WIPP site on the hydrology of the Rustler Formation was analyzed using the Rustler's fluid-pressure responses at observation-well H-16, water-level responses at observation wells H-1, ERDA-9, and WIPP-21, and a single measurement of the flow rate from the Culebra dolomite to the AIS. Well H-16 was drilled approximately 17 m northwest of the AIS and is equipped with a multipacker completion tool which monitors the formation fluid pressure of five packer-isolated members of the Rustler Formation using downhole pressure transducers. The formation fluid pressures of the isolated units were recorded before and during the drilling of the 0.25-m pilot hole for the AIS, the reaming of the pilot hole to 0.37-m diameter, and the upreaming (raise boring) of the pilot hole to a 6.17-m diameter. The responses of three of the Rustler members, the Culebra dolomite, the Magenta dolomite, and the Forty-niner, were analyzed to provide estimates of the hydraulic parameters of these units near the center of the WIPP site. Fluid-pressure data from the Tamarisk Member were not analyzed because they did not indicate that the formation had achieved a stable formation pressure or was proceeding on a definable trend before the construction of the AIS. The unnamed lower member did not appear to respond to the construction of the AIS.

Transmissivity estimates for the three Rustler members were obtained primarily by analyzing their H-16 fluid-pressure responses, as well as other available response and flow-rate data using the well-test simulator GTFM. The analysis required separate consideration of the drilling/reaming period when the pilot hole was filled with drilling

fluid and the post-reaming/pre-upreaming period when the pilot hole had penetrated the WIPP-site underground facility and all units were open and draining to the pilot hole and/or shaft and subject to a zero-wellbore-pressure boundary condition.

The fluid-pressure data for the drilling/reaming period were influenced by a complex sequence of drilling operations which were affected by excessive borehole deviation and the use of a bentonite-mud-based-brine drilling fluid. Drilling the 0.25-m-diameter pilot hole included three periods when borehole intervals, including the units analyzed, were cemented and redrilled using directional-drilling techniques. In addition, a drilling-mud-related filter-cake skin appeared to have developed on the borehole walls of the more permeable units encountered by the pilot hole during drilling and reaming. The drilling/reaming periods were analyzed using primarily fixed-pressure wellbore boundary conditions which corresponded to calculated mud overpressures and reduced pressures representing the effect of the apparent filter-cake skins. In addition, specified zero-flow boundary conditions were applied for short periods to simulate the effects of cementation (which affected all units) and apparent flow-reduction due to the settling of the fine particles in the bentonite-mud-based drilling fluid (which affected the Magenta dolomite and Forty-niner claystone only). Zero-wellbore-pressure boundary conditions, corresponding to formation exposure to atmospheric pressure, were applied to the three units analyzed after the pilot hole penetrated the WIPP-site underground facility.

The combination of predominantly fixed-wellbore-pressure boundary conditions and the radial-flow system modeled by GTFM resulted in simulated formation fluid-pressure responses as a function of formation diffusivity or transmissivity divided by the storativity. Based on the available literature on hydrologic tests at the WIPP site (Beauheim,

1987a, 1987b; Gonzalez, 1983; Mercer, 1983; and Saulnier, 1987b), the transmissivity of the units analyzed appears to be more variable than the storativity. Therefore, the approach used for the AIS simulations was to fix storativity at a representative value for the unit analyzed, and to use the simulation results to estimate transmissivity. The transmissivity values which provided the closest match between the observed and simulated fluid-pressure data were assumed to be characteristic of the formations being analyzed. Transmissivity estimates for the three units analyzed are discussed in Section 8.2.

The analysis of the Culebra dolomite's H-16 fluid-pressure response to the construction of the AIS included fluid-pressure-response simulations which indicated the presence of a heterogeneity corresponding to a postulated cement-invasion skin assumed to be caused by cementation operations during the pilot-hole drilling period.

The analysis of the H-16 fluid-pressure responses of the Magenta and Forty-niner provided evidence of heterogeneity in these formations. The heterogeneities were best characterized by considering that the Magenta and Forty-niner contained near-field and far-field permeability zones characterized by different transmissivities. A sensitivity analysis of the simulation results with respect to the parameters characterizing the heterogeneity, the inner-zone (near-field) transmissivity, the outer-zone (far-field) transmissivity, and the radius of the heterogeneity boundary, provided a degree of confidence in the estimated parameter values for the assumed heterogeneity geometry.

The results of the simulations of the H-16 fluid-pressure responses were used to estimate the inflow to the AIS from the Culebra and Magenta dolomites and the Forty-niner claystone. The simulations indicated that the Culebra provided the majority of the inflow to the AIS, a conclusion

corroborated by observations in the AIS during geologic mapping. Inflow from the Magenta dolomite was estimated to be one order of magnitude less than that from the Culebra, and the inflow from the Forty-niner claystone was estimated to be one order of magnitude less than inflow from the Magenta.

## 8.2 Summary of Transmissivities

Table 8.1 summarizes the results of the analyses of the H-16 fluid-pressure responses of the Culebra and Magenta dolomites and the Forty-niner claystone. All transmissivity values were estimated assuming a storativity of  $1 \times 10^{-5}$ .

### 8.2.1 Culebra Dolomite

Figures 6.7 to 6.12 indicate that the best match between observed and simulated data for the Culebra dolomite was achieved using a cement-invasion skin and a formation transmissivity ranging from  $1.3 \times 10^{-7} \text{ m}^2/\text{s}$  ( $0.12 \text{ ft}^2/\text{day}$ ) to  $6.6 \times 10^{-7} \text{ m}^2/\text{s}$  ( $0.62 \text{ ft}^2/\text{day}$ ). However, the estimated transmissivity obtained using the single measurement of the flow rate from the Culebra to the AIS as a calibration point was  $6.6 \times 10^{-7} \text{ m}^2/\text{s}$  ( $0.62 \text{ ft}^2/\text{day}$ ), a value considered to be the most representative of the Culebra's transmissivity between the AIS and H-16, and between the AIS and observation-wells ERDA-9 and WIPP-21. Beauheim (1987a) analyzed the Culebra's fluid-pressure responses to drill-stem and slug tests in H-16 and reports a range of transmissivity of  $9.13 \times 10^{-7} \text{ m}^2/\text{s}$  ( $0.85 \text{ ft}^2/\text{day}$ ) to  $7.42 \times 10^{-7} \text{ m}^2/\text{s}$  ( $0.69 \text{ ft}^2/\text{day}$ ). The transmissivity data from Beauheim (1987a) and the transmissivity values in Table 8.1 indicate that the near-field transmissivity of the Culebra dolomite in the vicinity of the underground-access shafts is probably between  $1 \times 10^{-7}$  and  $1 \times 10^{-6} \text{ m}^2/\text{s}$  ( $0.093$  to  $0.93 \text{ ft}^2/\text{day}$ ). All the simulations overestimated the drawdown (i.e., fluid-pressure response)

for the post-upreaming period during which all the units were open and draining to the AIS. This lack of correspondence may be due to the influences of other activities at the WIPP site, most probably due to pressure recovery from grouting and sealing operations in the WHS, and possible lesser influences from water-quality sampling in nearby wells and recovery from the H-11 multipad/tracer test (see Section 4.0). Table 8.2 shows the Culebra transmissivity ranges for a range of Culebra storativities from  $1 \times 10^{-6}$  to  $1 \times 10^{-4}$  using diffusivities calculated from the results of the analyses presented in this report. These diffusivities are of the same order of magnitude as the diffusivities used by Stevens and Beyeler (1985) ( $4.6 \times 10^{-2}$  to  $9.3 \times 10^{-2} \text{ m}^2/\text{s}$ ) to model the Culebra responses at the H-1 and H-3 hydropads during the construction of the C&SH shaft.

#### 8.2.2 Magenta Dolomite

The results of the analyses and simulation of the Magenta dolomite's H-16 fluid-pressure responses, Figures 6.17 and 6.18, indicate that the Magenta dolomite is a heterogeneous formation. The inner- and outer-zone transmissivities were estimated to be  $8.0 \times 10^{-8} \text{ m}^2/\text{s}$  ( $0.074 \text{ ft}^2/\text{day}$ ) and  $4.0 \times 10^{-8} \text{ m}^2/\text{s}$  ( $0.033 \text{ ft}^2/\text{day}$ ), respectively, and the heterogeneity boundary between the inner and outer zones was located at a radial distance of 40 m from the center of the AIS. The Magenta was not involved in any other testing or sampling activities during the time its fluid-pressure response was analyzed. However, part of the Magenta's response may have been affected by grouting operations in the WHS.

Beauheim (1987a) analyzed drill-stem and slug tests of the Magenta in H-16 and estimated the transmissivity to be  $3.01 \times 10^{-8} \text{ m}^2/\text{s}$  ( $0.028 \text{ ft}^2/\text{day}$ ) and  $2.58 \times 10^{-8} \text{ m}^2/\text{sec}$  ( $0.024 \text{ ft}^2/\text{day}$ ), respectively. Because of the potential non-uniqueness of the assumed heterogeneity geometry, the best-match inner-zone and outer-zone transmissivities provide only estimates of the range of effective formation

transmissivities for the Magenta dolomite. Table 8.2 shows the possible range in estimated Magenta transmissivity for a representative range of storativity of  $1 \times 10^{-6}$  to  $1 \times 10^{-4}$  using diffusivities calculated from the results of the analyses presented in this report. As with the Culebra results, the Magenta diffusivities are of the same order of magnitude as those presented in Stevens and Beyeler (1985) ( $2.8 \times 10^{-3} \text{ m}^2/\text{s}$ ).

### 8.2.3 Forty-Niner Claystone

The results of the analyses and simulation of the Forty-niner claystone's H-16 fluid-pressure responses, Figures 6.26 and 6.27, indicate that the Forty-niner is a strongly heterogeneous formation, with a stronger transmissivity contrast than observed for the Magenta dolomite (see Section 8.2.2). The inner-zone and outer-zone transmissivities were estimated to be  $9.0 \times 10^{-9} \text{ m}^2/\text{s}$  ( $8.4 \times 10^{-3} \text{ ft}^2/\text{day}$ ) and  $1.5 \times 10^{-9} \text{ m}^2/\text{s}$  ( $1.4 \times 10^{-3} \text{ ft}^2/\text{day}$ ), respectively, and the heterogeneity boundary between the inner and outer zones was located at a radial distance of 40 m from the center of the AIS. Beauheim (1987a) analyzed pulse, slug, and drill-stem tests in H-16 and estimated that the transmissivity of the Forty-niner claystone ranges from  $2.4 \times 10^{-10} \text{ m}^2/\text{s}$  ( $2.2 \times 10^{-4} \text{ ft}^2/\text{day}$ ) from the analysis of a pulse test, to  $6.0 \times 10^{-9} \text{ m}^2/\text{s}$  ( $5.6 \times 10^{-3} \text{ ft}^2/\text{day}$ ) from the analysis of a drill-stem test. As noted in Section 8.2.2 for the Magenta dolomite, the potential non-uniqueness of the assumed heterogeneity geometry means that the best-match inner-zone and outer-zone transmissivities for the Forty-niner provide estimates of the range of its effective formation transmissivities. Table 8.2 shows the possible range in estimated Forty-niner transmissivity for a representative range of storativity of  $1 \times 10^{-6}$  to  $1 \times 10^{-4}$ .

### 8.3 Conclusions

The results of the analysis of the H-16 fluid-pressure responses to the construction of the AIS indicate:

- o in the area between the AIS and H-16, the transmissivity of the Culebra dolomite is approximately one order of magnitude greater than the transmissivity of the Magenta dolomite, and the Magenta transmissivity is one order of magnitude greater than the transmissivity of the Forty-niner claystone;
- o the cementing of the AIS pilot hole to correct excessive borehole deviation during the drilling period created a cement-invasion skin in the Culebra dolomite but not in the Magenta dolomite or Forty-niner claystone; cement invasion of the Culebra dolomite was probably facilitated by its higher permeability and the vuggy, fractured character of the dolomite which may have allowed easier penetration of the formation by the cement grout;
- o the water-level responses of Culebra observation wells H-1, ERDA-9, and WIPP-21 were affected by other hydrologic and construction activities at the WIPP site, and the analyses of those responses provided a general indication of the range of formation transmissivity;
- o the analysis of the fluid-pressure responses of the Magenta dolomite and Forty-niner claystone indicated that both units behave as heterogeneous formations in the vicinity of the AIS; and
- o the estimated long-term flow rate from all of the Rustler units to the unsealed AIS is less than 0.065 L/s.

GEOLOGIC UNIT	APPLICABLE AREA	TRANSMISSIVITY		STORATIVITY
		(m <sup>2</sup> /s)	(ft <sup>2</sup> /day)	
CULEBRA DOLOMITE	AIS to H-16	6.6E-7	6.2E-1	1E-5
	AIS to H-1	6.6E-7	6.2E-1	1E-5
	AIS to ERDA-9	2.6E-7	2.4E-1	1E-5
	AIS to WIPP-21	6.6E-7	6.2E-2	1E-5
MAGENTA DOLOMITE	AIS to H-16	8.0E-8	7.4E-2	1E-5
	>40 m from AIS	4.0E-8	3.7E-2	1E-5
FORTY-NINER CLAYSTONE	AIS to H-16	9.0E-9	8.4E-3	1E-5
	>40 m from AIS	1.5E-9	1.4E-3	1E-5

Drawn by	Date	Summary of the Transmissivities Determined From the Analysis of the Fluid-Pressure Responses of the Culebra Dolomite, Magenta Dolomite, and Forty-Niner Claystone
Checked by	Date	
Revisions	Date	
<b>INTERA Technologies</b>		Table 8.1

	DIFFUSIVITY* (T/S) [m <sup>2</sup> /s]	STORATIVITY (S) [ ]	TRANSMISSIVITY (T) [m <sup>2</sup> /s]
CULEBRA	6.6E-02	1.0E-04	6.6E-06
		1.0E-05*	6.6E-07*
		2.0E-05	1.3E-06
		1.0E-06	6.6E-08
	2.6E-02	1.0E-04	2.6E-06
		1.0E-05*	2.6E-07*
		2.0E-05	5.2E-07
		1.0E-06	2.6E-08
	1.3E-02	1.0E-04	1.3E-06
		1.0E-05*	1.3E-07*
		2.0E-05	2.6E-07
		1.0E-06	1.3E-08
MAGENTA	8.0E-03	1.0E-04	8.0E-07
		1.0E-05*	8.0E-08*
		2.0E-05	1.6E-07
		1.0E-06	8.0E-09
	4.0E-03	1.0E-04	4.0E-07
		1.0E-05*	4.0E-08*
		2.0E-05	8.0E-08
		1.0E-06	4.0E-09
FORTY-NINER	9.0E-04	1.0E-04	9.0E-08
		1.0E-05*	9.0E-09*
		2.0E-05	1.8E-08
		1.0E-06	9.0E-10
	1.5E-04	1.0E-04	1.5E-08
		1.0E-05*	1.5E-09*
		2.0E-05	3.0E-09
		1.0E-06	1.5E-10

\* Values Determined From Simulations and Presented on Table 8.1.

Drawn by	Date	Calculated Transmissivities for a Range of Storativities Using the Diffusivities From the Results of the Analyses Presented in this Report
Checked by	Date	
Revisions	Date	
<b>INTERA Technologies</b>		Table 8.2

## 9.0 REFERENCES

- Beauheim, R.L., 1987a. Interpretations of Single-Well Hydraulic Tests Conducted at and near the Waste Isolation Pilot Plant (WIPP) Site, 1983-1987. Sandia National Laboratories, SAND87-0039, 169 pp.
- Beauheim, R.L., 1987b. Analysis of Pumping Tests of the Culebra Dolomite Conducted at the H-3 Hydropad at the Waste Isolation Pilot Plant (WIPP) Site. Sandia National Laboratories, SAND86-2311, 169 pp.
- Bechtel National Inc., 1985. Quarterly Geotechnical Field Data Report. U.S. Department of Energy, Waste Isolation Pilot Plant Office, Carlsbad, New Mexico, DOE-WIPP-218.
- Cauffman, T.L., A.M. LaVenu, and J.P. McCord, 1990. Ground-Water Flow Modeling of the Culebra Dolomite: Volume II - Data Base. Sandia National Laboratories, Contractor Report SAND89-7068/2.
- Colton, I.D. and J. Morse, 1985. Water Quality Sampling Plan. U.S. Department of Energy, WIPP-DOE-215.
- Deshler, R. and R. McKinney, 1988. Construction and Water Inflow Histories for the Shafts at the Waste Isolation Pilot Plant. IT Corporation, February 1988, 14 pp.
- Gonzalez, D.D., 1983. Hydrogeochemical Parameters of Fluid-Bearing Zones in the Rustler and Bell Canyon Formations: Waste Isolation Pilot Plant (WIPP) Southeastern New Mexico (SENM). Sandia National Laboratories, SAND83-0210, 37 pp.

- Haug, A., V.A. Kelley, A.M. LaVenue, and J.F. Pickens, 1987. Modeling of Ground-Water Flow in the Culebra Dolomite at the Waste Isolation Pilot Plant (WIPP) Site: Interim Report. Sandia National Laboratories, Contractor Report SAND86-7167.
- Holditch, S.A., W.J. Lee, D.E. Lancaster, and T.B. Davis, 1983. Effect of Mud Filtrate Invasion on Apparent Productivity in Drillstem Tests in Low-Permeability Gas Formations. Journal of Petroleum Technology, Vol. 35, No. 2, p. 299-305.
- Holt, R.M. and D.W. Powers, 1984. Geotechnical Activities in the Waste Handling Shaft, Waste Isolation Pilot Plant (WIPP) Project, Southeastern New Mexico. U.S. DOE, WTSD-TME-038.
- Holt, R.M. and D.W. Powers, 1986. Geotechnical Activities in the Exhaust Shaft. U.S. Department of Energy, DOE-WIPP-86-008.
- Krueger, R.F., 1986. An Overview of Formation Damage and Well Productivity in Oilfield Operations. Journal of Petroleum Technology, Vol. 38, No. 2, p. 131-152.
- LaVenue, A.M., A. Haug, and V.A. Kelley, 1988. Numerical Simulation of Ground-Water Flow in the Culebra Dolomite at the Waste Isolation Pilot Plant (WIPP) Site: Second Interim Report. Sandia National Laboratories, Contractor Report SAND88-7002.
- Mercer, J.W., 1983. Geohydrology of the Proposed Waste Isolation Pilot Plant Site, Los Medaños Area, Southeastern New Mexico. U.S. Geological Survey Water-Resources Investigation Report 83-4016, 113 pp.

- Pickens, J.F., G.E. Grisak, J.D. Avis, D.W. Belanger, and M. Thury, 1987. Analysis and Interpretation of Borehole Hydraulic Tests in Deep Boreholes: Principles, Model Development, and Applications. Water Resources Research, Vol. 23, No. 7, p. 1341-1375.
- Saulnier, G.J., Jr., 1987a. Appendix F., Review and Chronology of Known Information of Ground-Water Leakage into the Shafts at the WIPP Site in Modeling of Ground-Water Flow in the Culebra Dolomite at the Waste Isolation Pilot Plant (WIPP) Site: Interim Report, By Haug, A. and others, Sandia National Laboratories, Contractor Report SAND86-7167.
- Saulnier, G.J., Jr., 1987b. Analysis of Pumping Tests of the Culebra Dolomite Conducted at the H-11 Hydropad at the Waste Isolation Pilot Plant (WIPP) Site. Sandia National Laboratories, Contractor Report SAND87-7124.
- Saulnier, G.J., Jr., G.A. Freeze, and W.A. Stensrud, 1987. WIPP Hydrology Program Waste Isolation Pilot Plant Southeastern New Mexico. Hydrologic Data Report #4. Sandia National Laboratories, Contractor Report SAND86-7166.
- Saulnier, G.J., Jr., and J.D. Avis, 1988. Interpretation of Hydraulic Tests Conducted in the Waste-Handling Shaft at the Waste Isolation Pilot Plant (WIPP) Site. Sandia National Laboratories, Contractor Report SAND88-7001.
- Snyder, R.P., 1985. Dissolution of Halite and Gypsum, and Hydration of Anhydrite to Gypsum, Rustler Formation in the Vicinity of the Waste-Isolation Pilot Plant, Southeastern New Mexico. U.S. Geological Survey Open-File Report 85-229, 11 p.

Stensrud, W.A., M.A. Bame, K.D. Lantz, A.M. LaVenue, J.B. Palmer, and G.J. Saulnier, Jr., 1987. WIPP Hydrology Program, Waste Isolation Pilot Plant, Southeastern New Mexico, Hydrologic Data Report #5. Sandia National Laboratories, Contractor Report SAND87-7125.

Stensrud, W.A., M.A. Bame, K.D. Lantz, T.L. Cauffman, J.B. Palmer, and G.J. Saulnier, Jr., 1988a. WIPP Hydrology Program, Waste Isolation Pilot Plant Southeastern New Mexico, Hydrologic Data Report #6. Sandia National Laboratories, Contractor Report SAND87-7166.

Stensrud, W.A., M.A. Bame, K.D. Lantz, J.B. Palmer, and G.J. Saulnier, Jr., 1988b. WIPP Hydrology Program, Waste Isolation Pilot Plant Southeastern New Mexico, Hydrologic Data Report #7. Sandia National Laboratories, Contractor Report SAND88-7014.

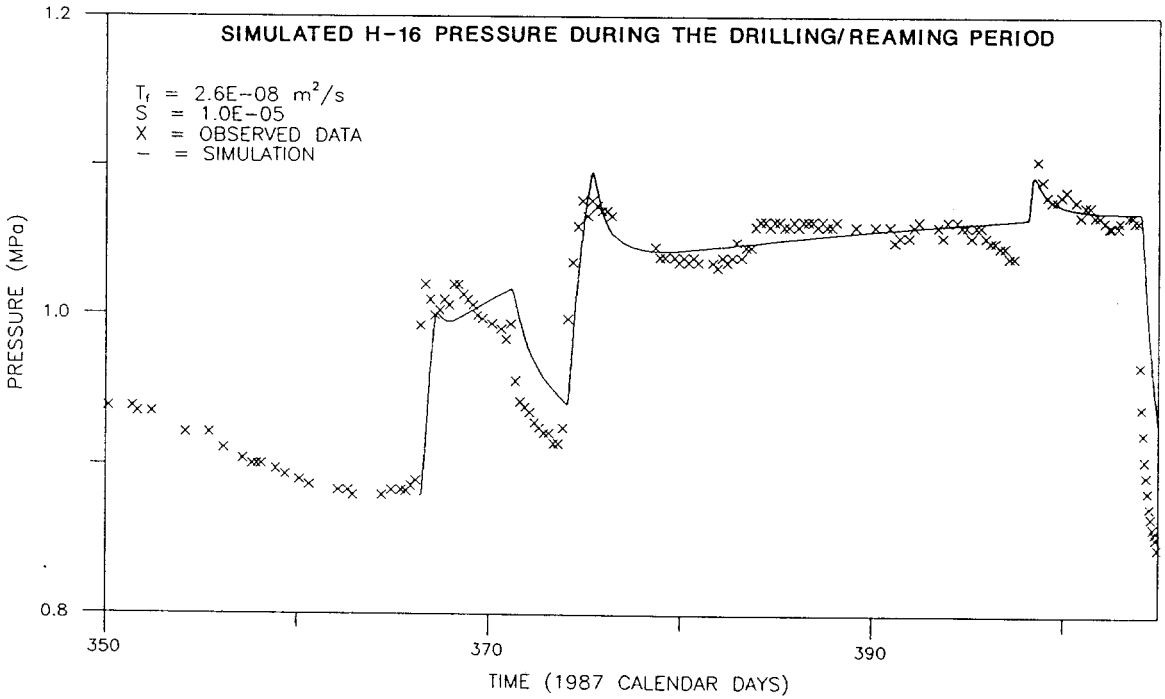
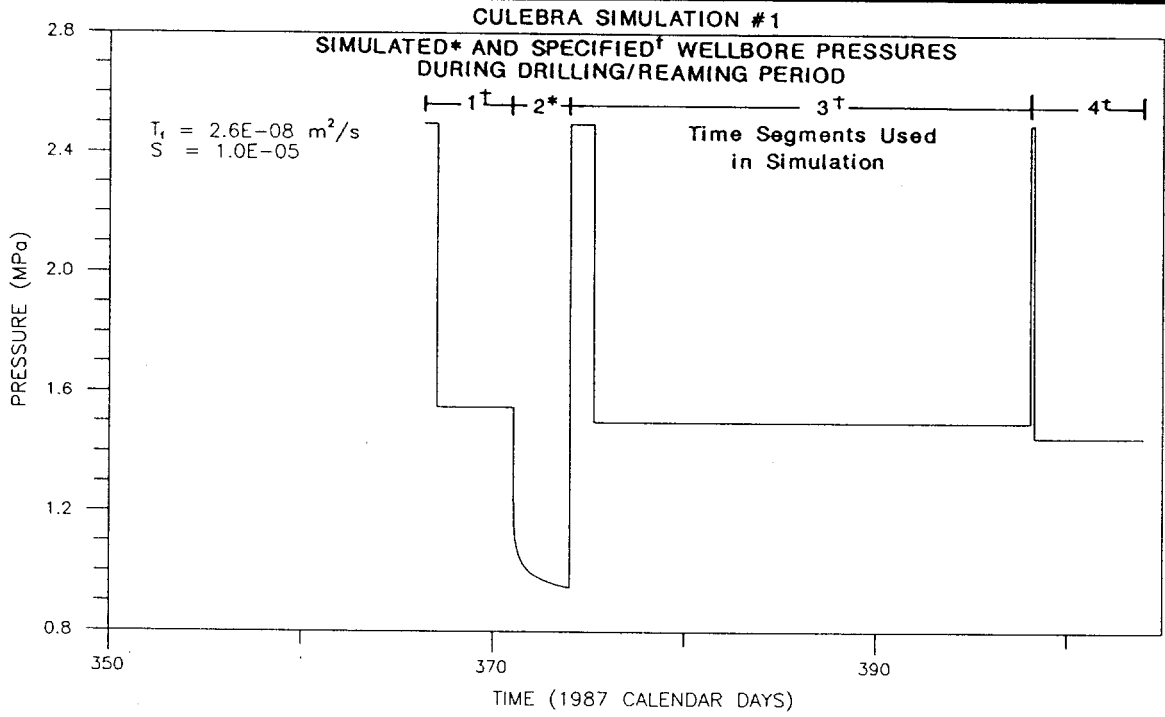
Stensrud, W.A., M.A. Bame, K.D. Lantz, J.B. Palmer, and G.J. Saulnier, Jr., 1990, in preparation. WIPP Hydrology Program, Waste Isolation Pilot Plant Southeastern New Mexico, Hydrologic Data Report #8. Sandia National Laboratories, Contractor Report SAND89-7056.

Stevens, K. and W. Beyeler, 1985. Determination of Diffusivities in the Rustler Formation from Exploratory-Shaft Construction at the Waste Isolation Pilot Plant in Southeastern New Mexico. U.S. Geological Survey Water-Resources Investigations Report 85-4020, 32 pp.

Touloukian, Y.S., W.R. Judd, and R.F. Roy, 1981. Physical Properties of Rocks and Minerals. McGraw-Hill/Cindas Data Series on Material Properties, Y.S. Touloukian and C.Y. Ho, Editors, Volume II-2, 548 p.

**APPENDIX A:**

**SPECIFIED AND SIMULATED WELLBORE PRESSURES AND SIMULATED  
AND OBSERVED FORMATION FLUID PRESSURES FOR THE  
DRILLING/REAMING PERIODS OF THE SIMULATIONS OF THE  
H-16 FLUID-PRESSURE RESPONSES OF THE CULEBRA DOLOMITE,  
THE MAGENTA DOLOMITE, AND THE FORTY-NINER CLAYSTONE**



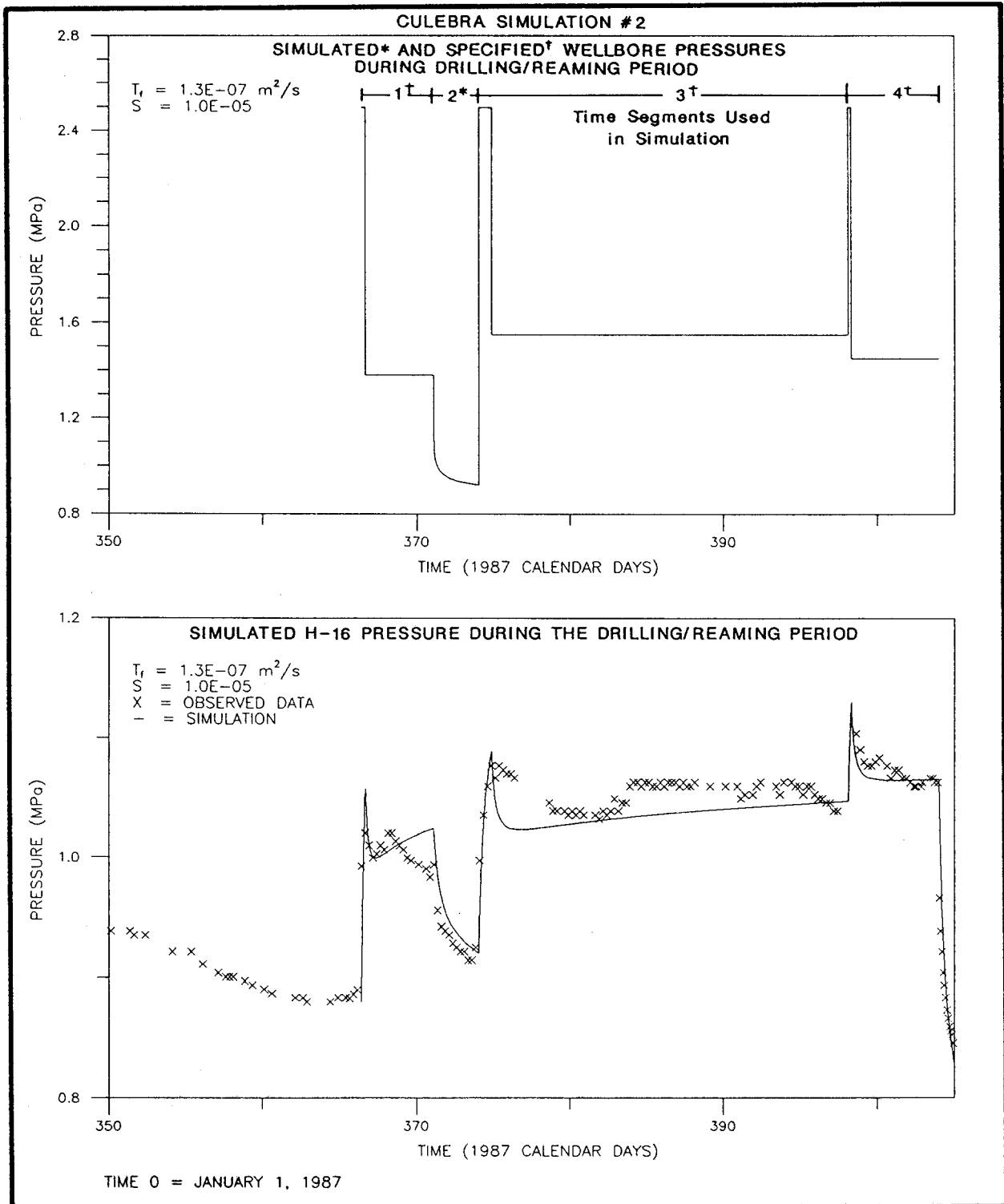
TIME 0 = JANUARY 1, 1987

Drawn by	J.D.A.	Date	2/23/89
Checked by	G.S.	Date	2/23/89
Revisions	ABW	Date	6/23/89
H09700R876			2/23/89

SPECIFIED AND SIMULATED WELLBORE PRESSURES AND SIMULATED AND OBSERVED FORMATION FLUID PRESSURES FOR THE CULEBRA DOLOMITE DRILLING/REAMING PERIOD WITHOUT A CEMENT-INVASION SKIN AND MATCHING H-16 FLUID-PRESSURE RESPONSE

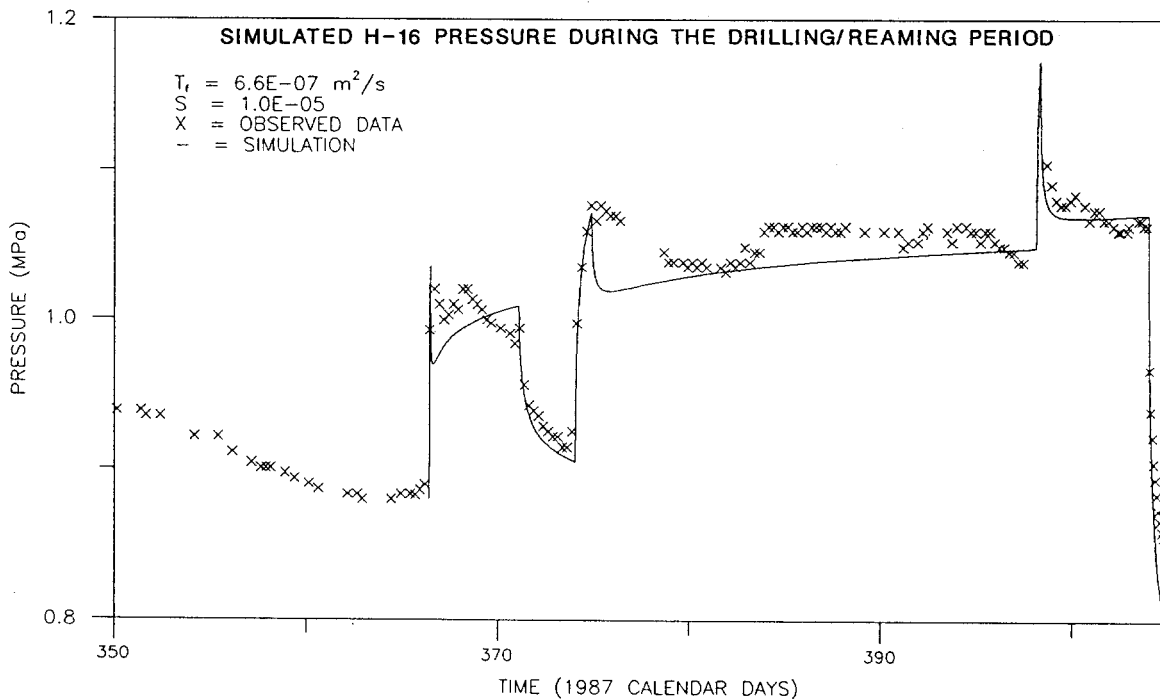
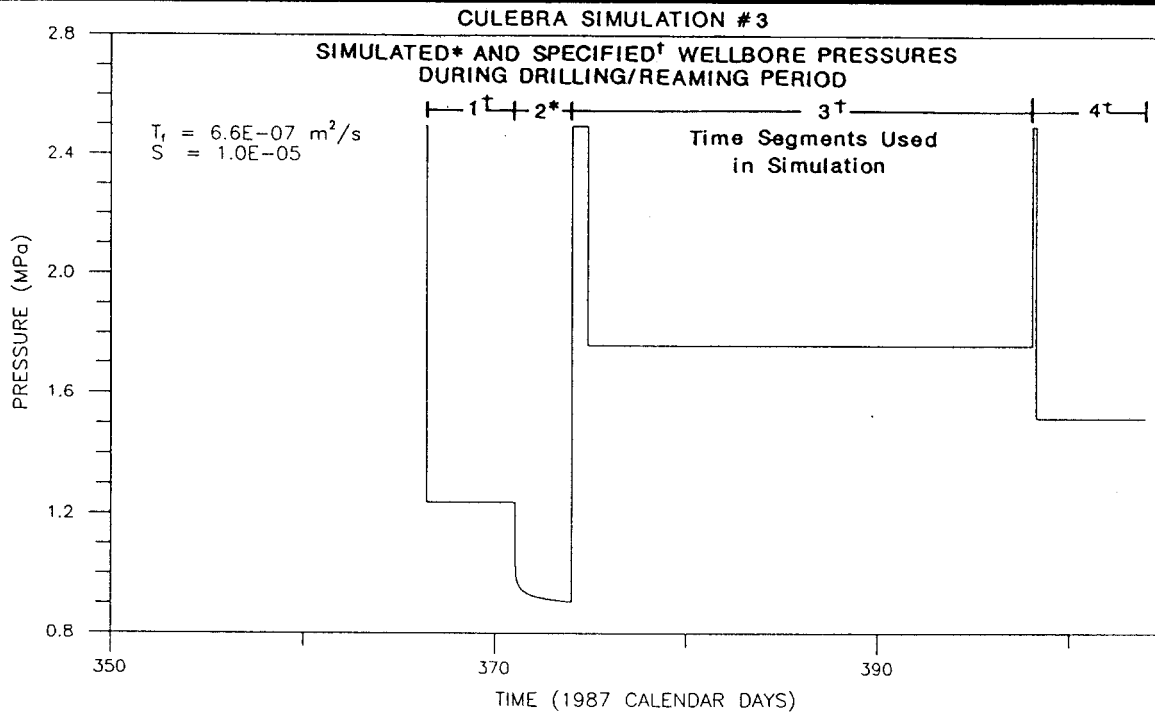
**INTERA Technologies**

Figure A.1



Drawn by J.D.A.	Date 2/23/89
Checked by G.S.	Date 2/23/89
Revisions ABW	Date 6/23/89
H09700R876	2/23/89

SPECIFIED AND SIMULATED WELLBORE PRESSURES AND SIMULATED AND OBSERVED FORMATION FLUID PRESSURES FOR THE CULEBRA DOLOMITE DRILLING/REAMING PERIOD USING A CEMENT-INVASION SKIN



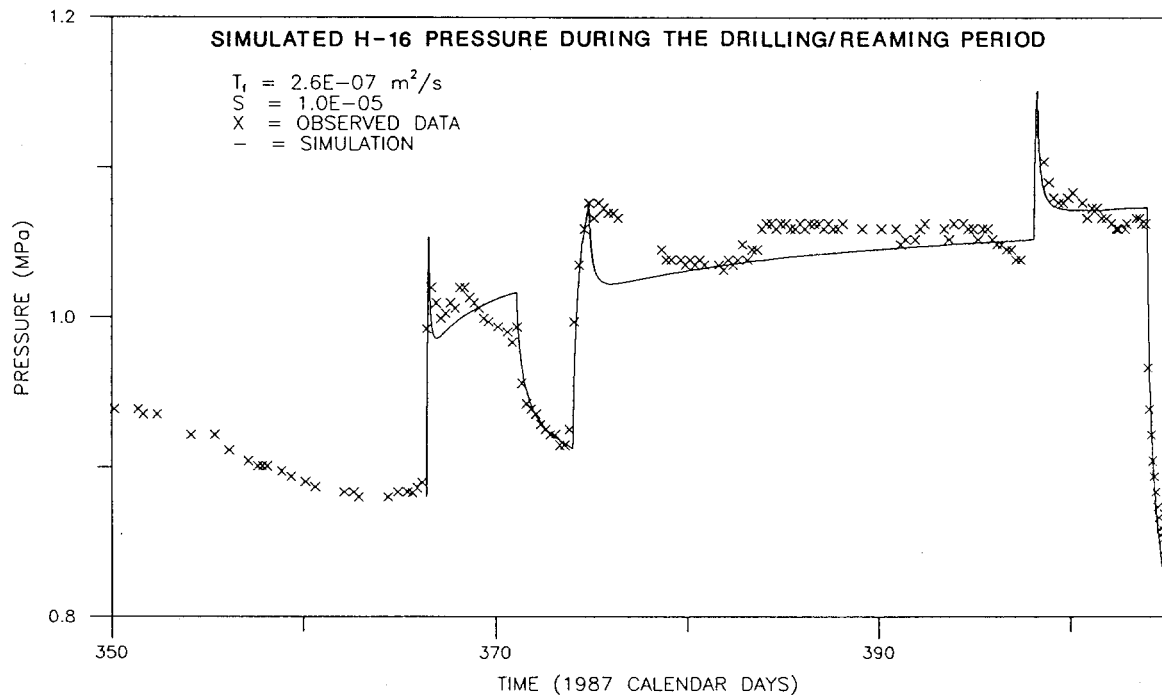
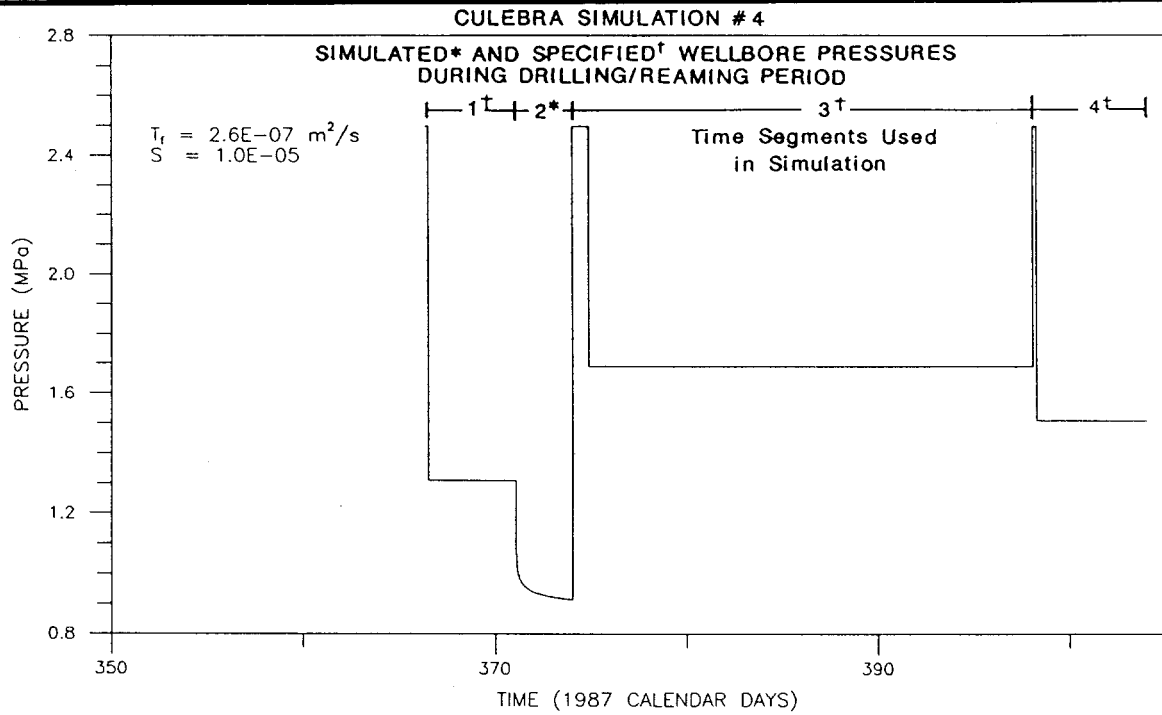
TIME 0 = JANUARY 1, 1987

Drawn by J.D.A.	Date 2/23/89
Checked by G.S.	Date 2/23/89
Revisions ABW	Date 6/23/89
H09700R876	2/23/89

SPECIFIED AND SIMULATED WELLBORE PRESSURES AND SIMULATED AND OBSERVED FORMATION FLUID PRESSURES FOR THE CULEBRA DOLOMITE DRILLING/REAMING PERIOD WITH A CEMENT-INVASION SKIN AND MATCHING THE CULEBRA-TO-AIS FLOW RATE

**INTERA Technologies**

Figure A.3



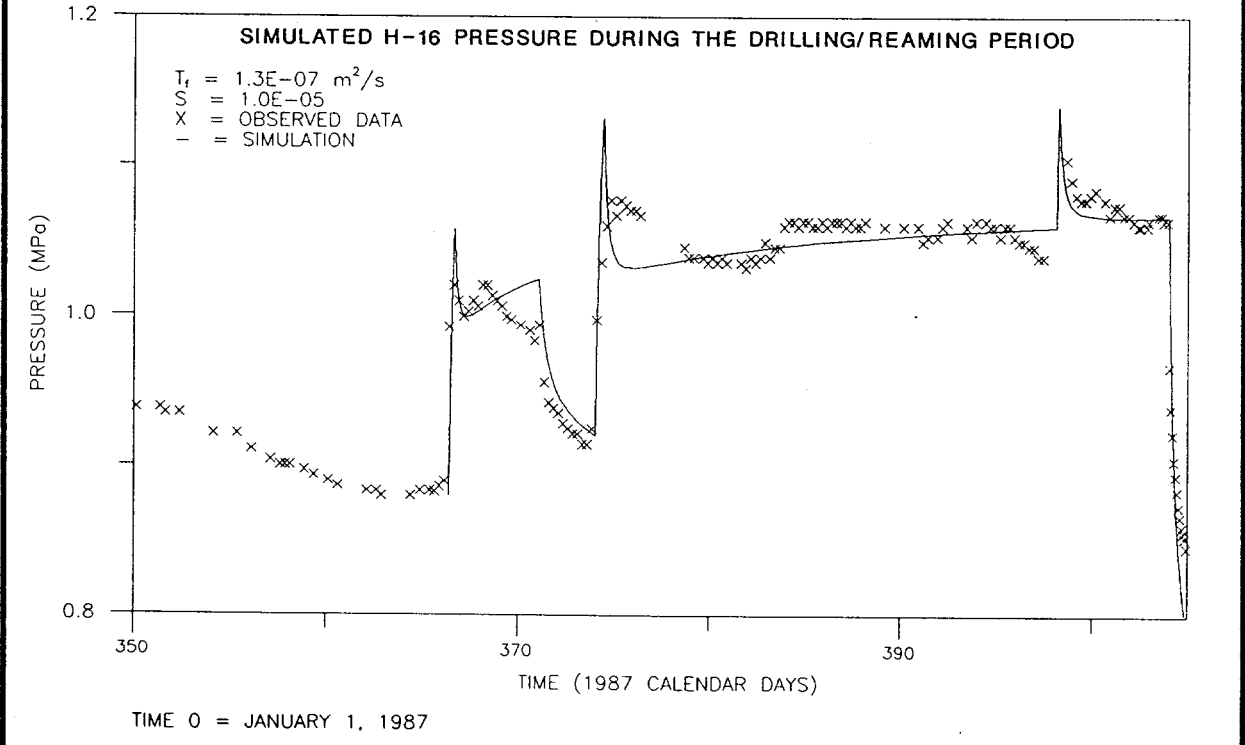
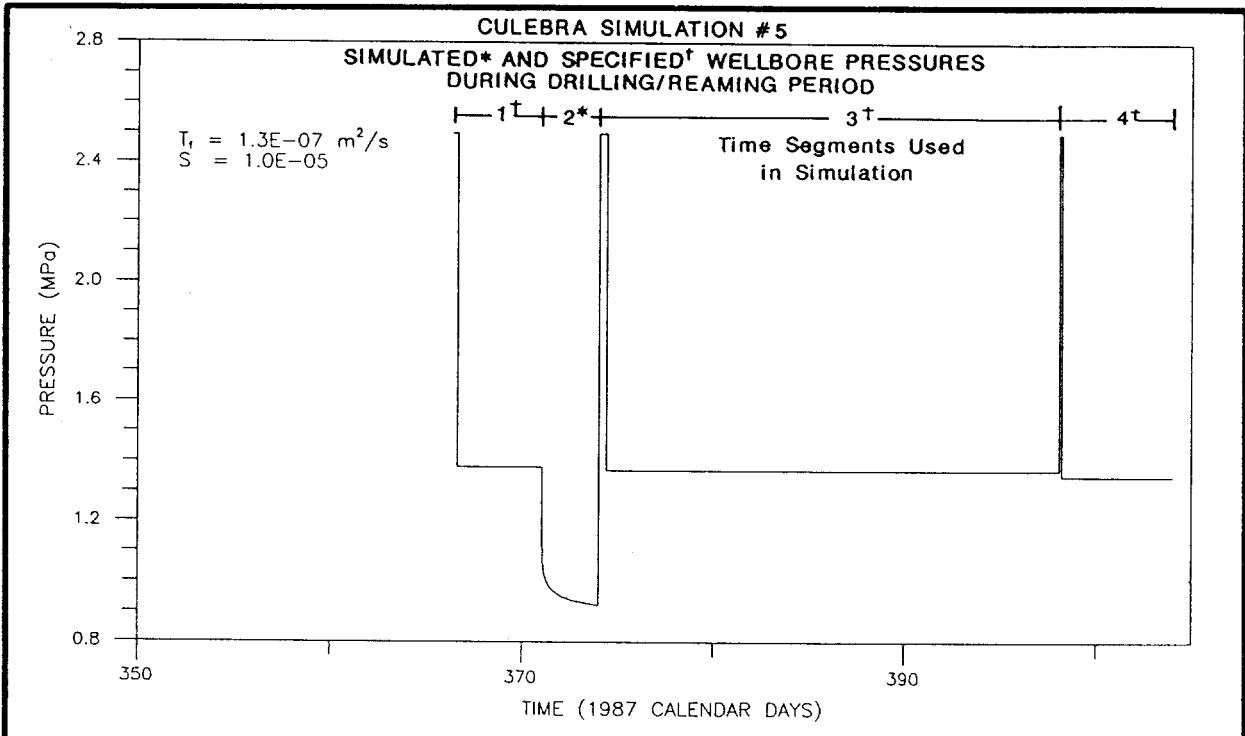
TIME 0 = JANUARY 1, 1987

Drawn by	J.D.A.	Date	2/23/89
Checked by	G.S.	Date	2/23/89
Revisions	ABW	Date	6/23/89
H09700R876			2/23/89

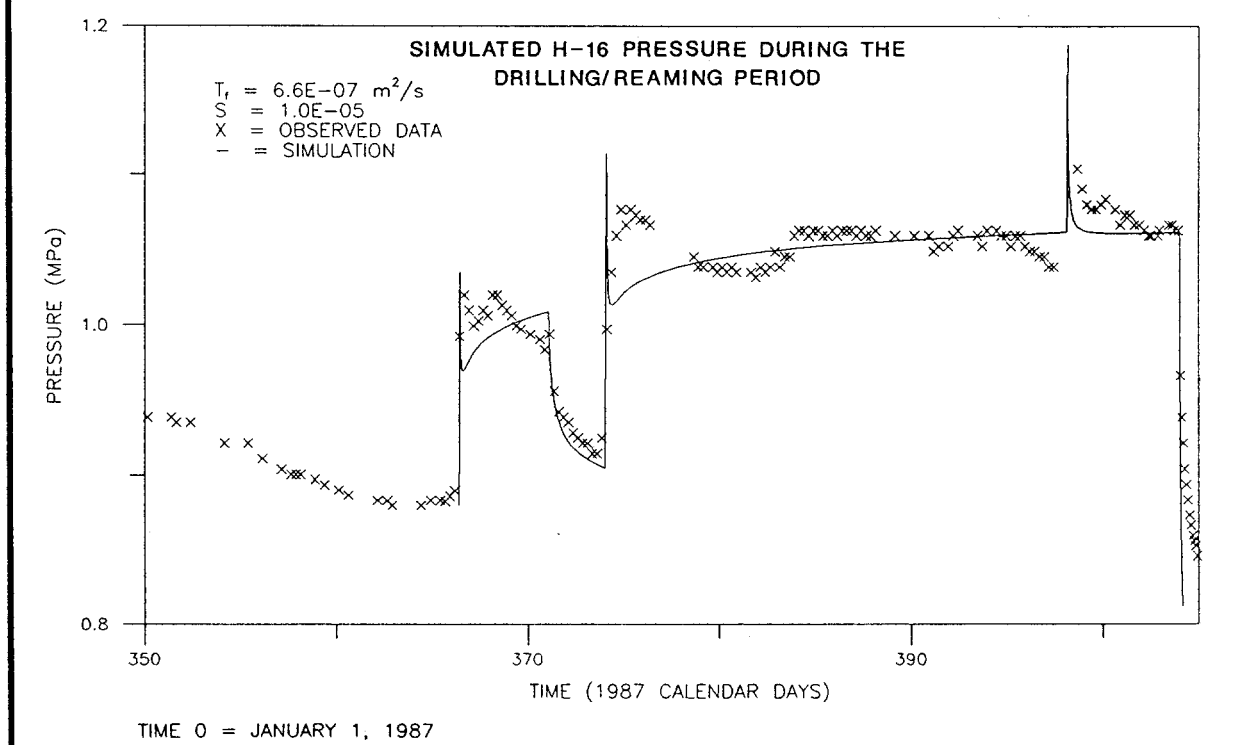
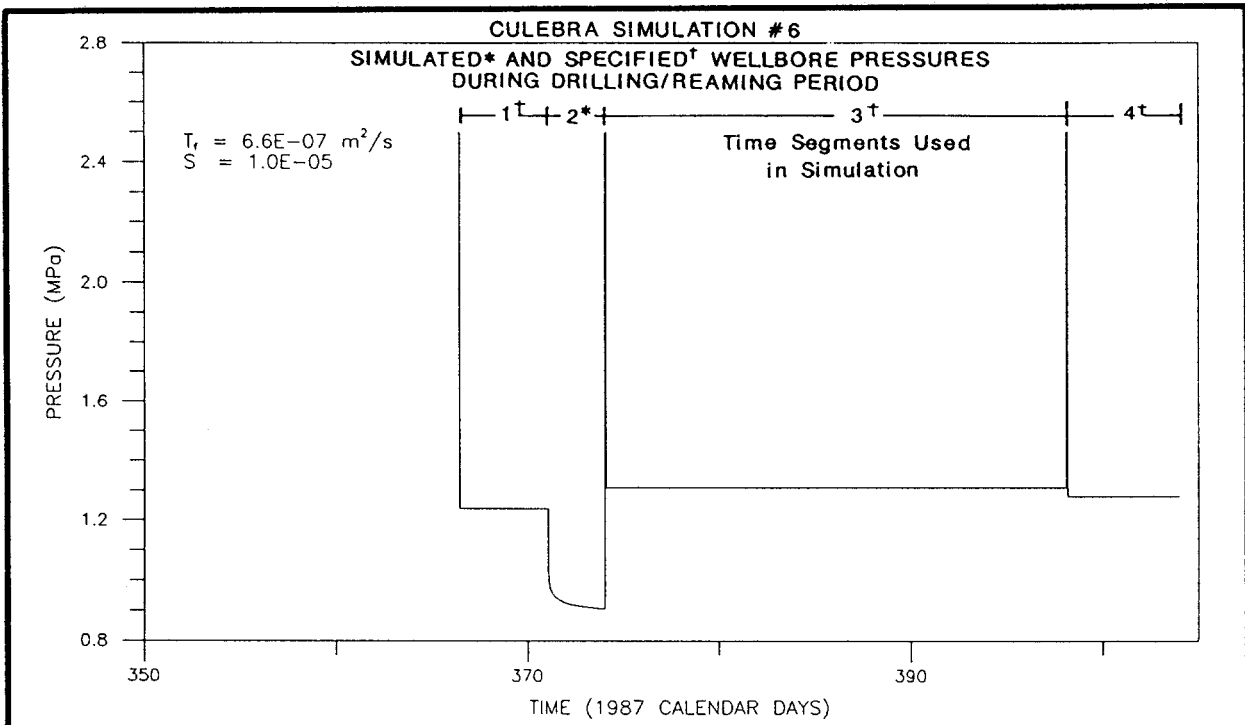
SPECIFIED AND SIMULATED WELLBORE PRESSURES AND SIMULATED AND OBSERVED FORMATION FLUID PRESSURES FOR THE CULEBRA DOLOMITE DRILLING/REAMING PERIOD WITH A CEMENT-INVASION SKIN AND MATCHING THE OBSERVATION-WELL RESPONSES

**INTERA Technologies**

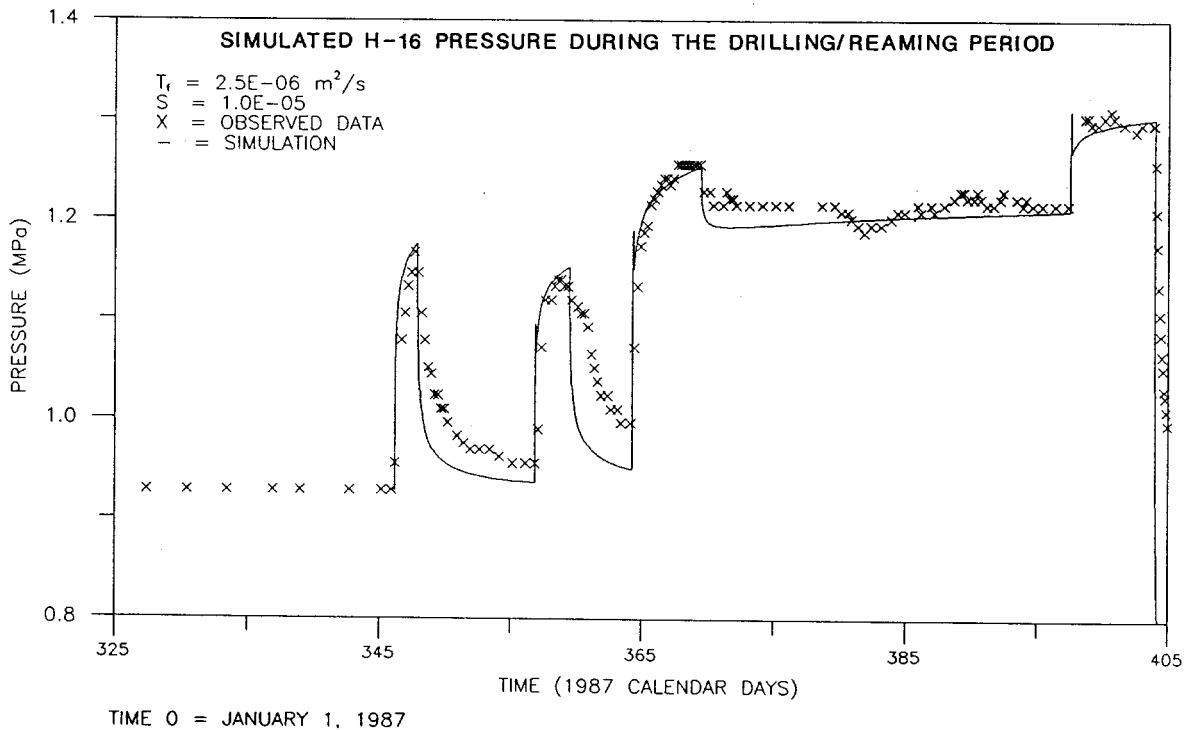
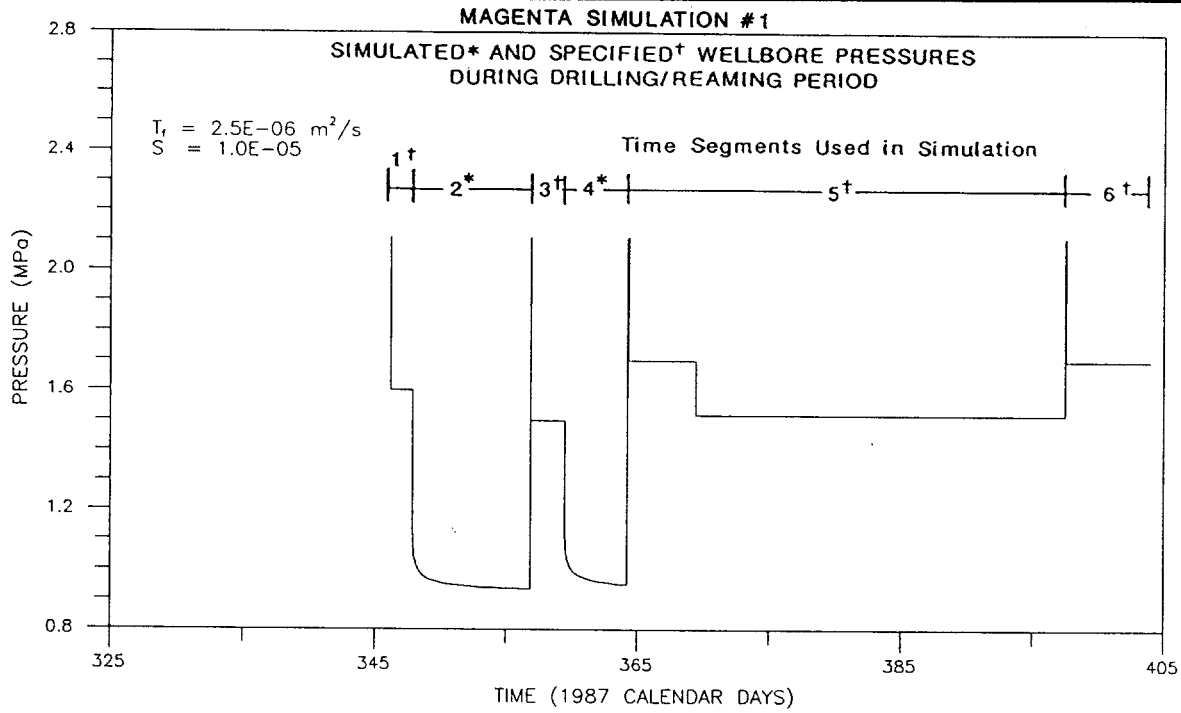
Figure A.4



Drawn by J.D.A.	Date 2/23/89	SPECIFIED AND SIMULATED WELLBORE PRESSURES AND SIMULATED AND OBSERVED FORMATION FLUID PRESSURES FOR THE CULEBRA DOLOMITE DRILLING/REAMING PERIOD WITHOUT A CEMENT-INVASION SKIN AND USING A $T_r = 1.3 \times 10^{-7} \text{ m}^2/\text{s}$
Checked by G.S.	Date 2/23/89	
Revisions ABW	Date 6/23/89	
H09700R876	2/23/89	
<b>INTERA Technologies</b>		Figure A.5



Drawn by	J.D.A.	Date	2/23/89	SPECIFIED AND SIMULATED WELLBORE PRESSURES AND SIMULATED AND OBSERVED FORMATION FLUID PRESSURES FOR THE CULEBRA DOLOMITE DRILLING/REAMING PERIOD WITHOUT A CEMENT-INVASION SKIN AND USING A $T_r = 6.6 \times 10^{-7} \text{ m}^2/\text{s}$
Checked by	G.S.	Date	2/23/89	
Revisions	ABW	Date	6/23/89	
H09700R876			2/23/89	
<b>INTERA Technologies</b>				Figure A.6

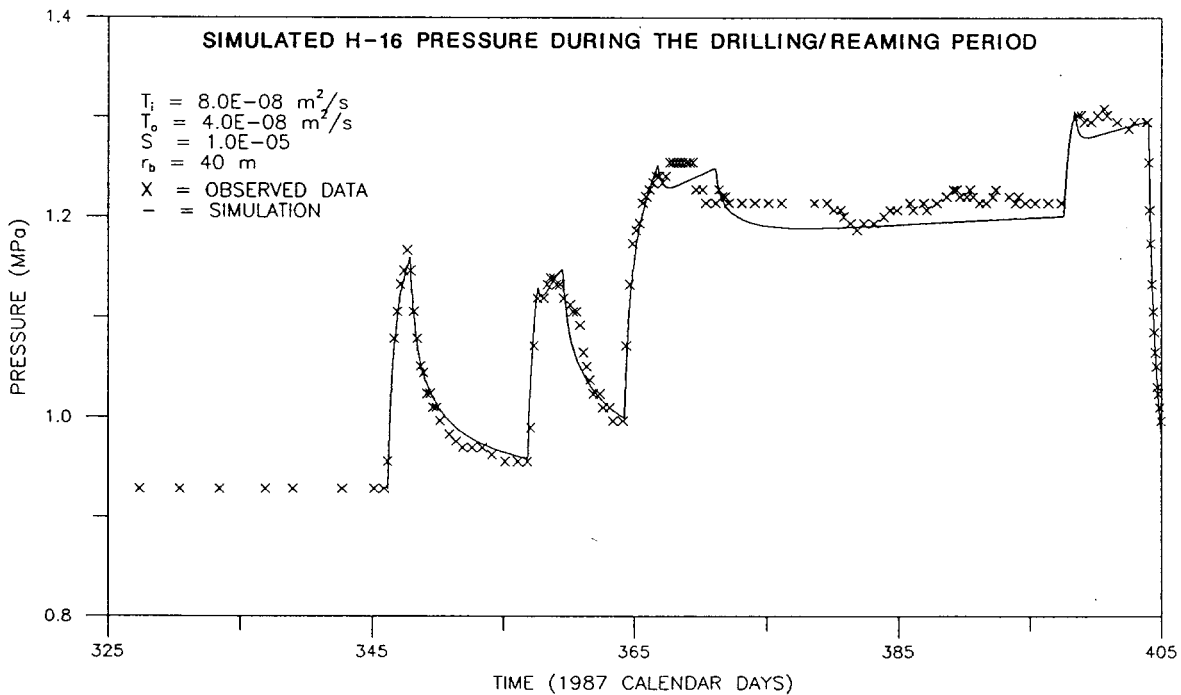
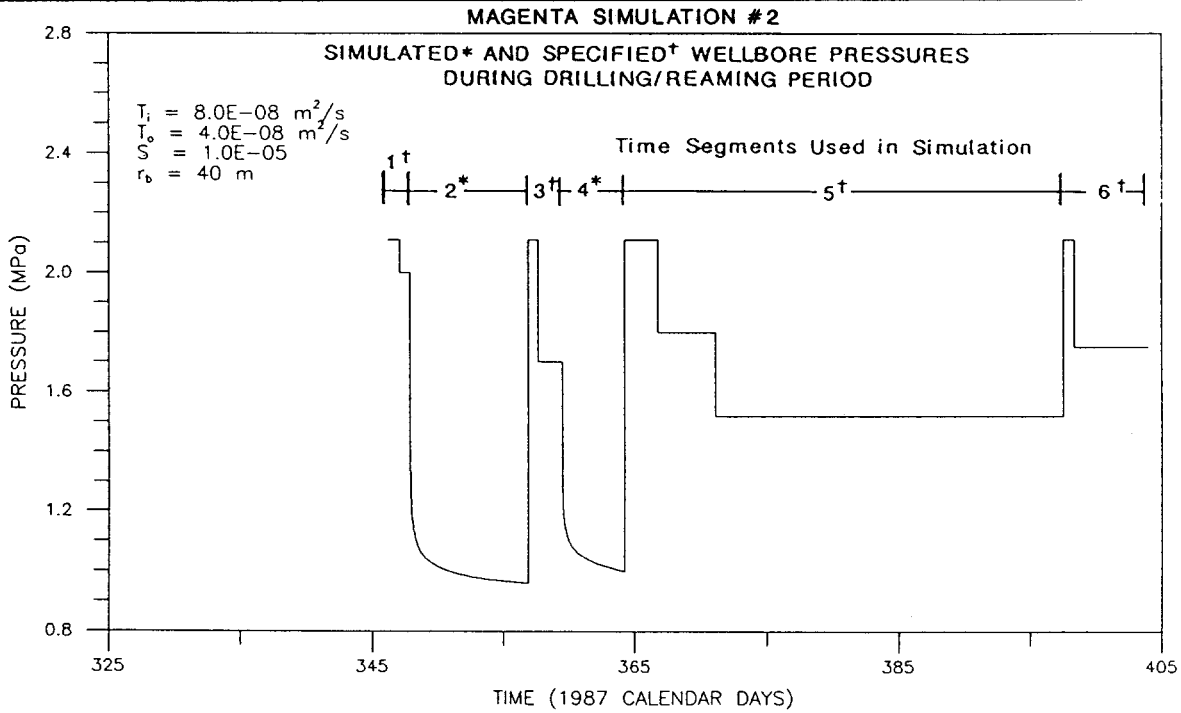


Drawn by J.D.A.	Date 2/23/89
Checked by G.S.	Date 2/23/89
Revisions ABW	Date 6/23/89
H09700R876	2/23/89

SPECIFIED AND SIMULATED WELLBORE PRESSURES AND  
SIMULATED AND OBSERVED FORMATION FLUID PRESSURES  
FOR THE MAGENTA DOLOMITE DRILLING/REAMING PERIOD  
USING A HOMOGENEOUS-FORMATION CHARACTERIZATION

**INTERA Technologies**

Figure A.7



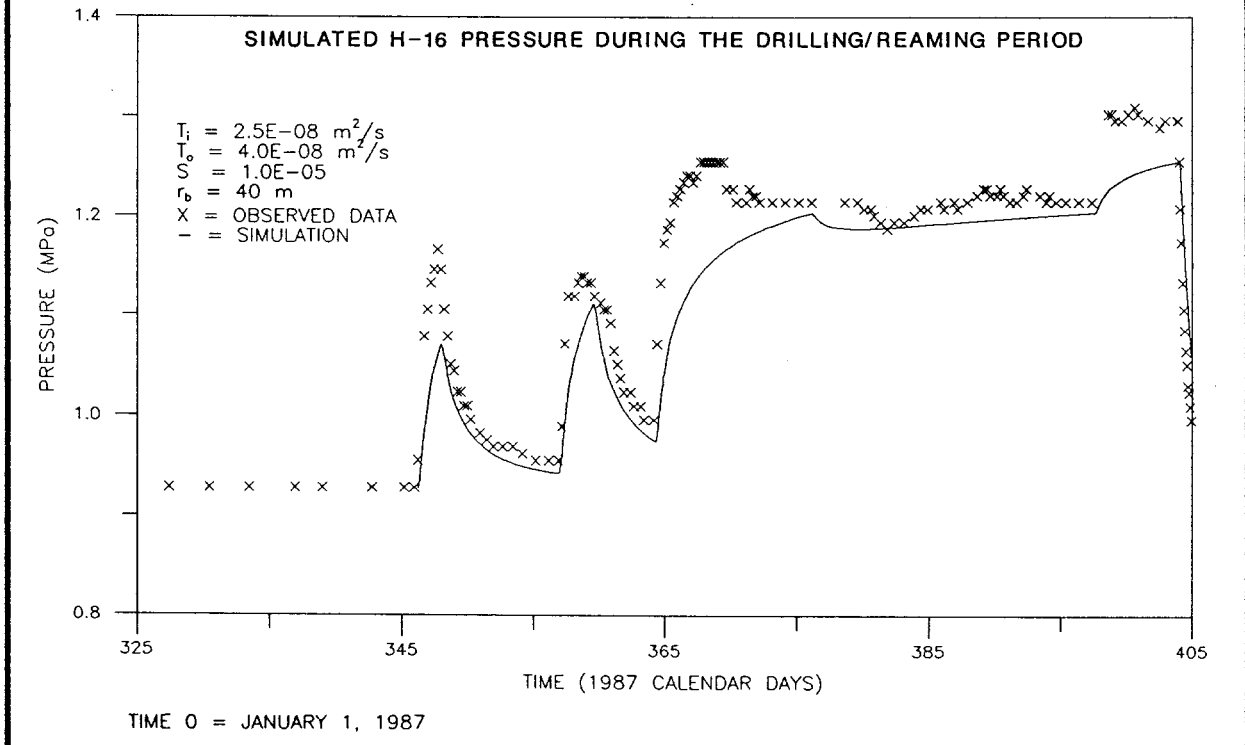
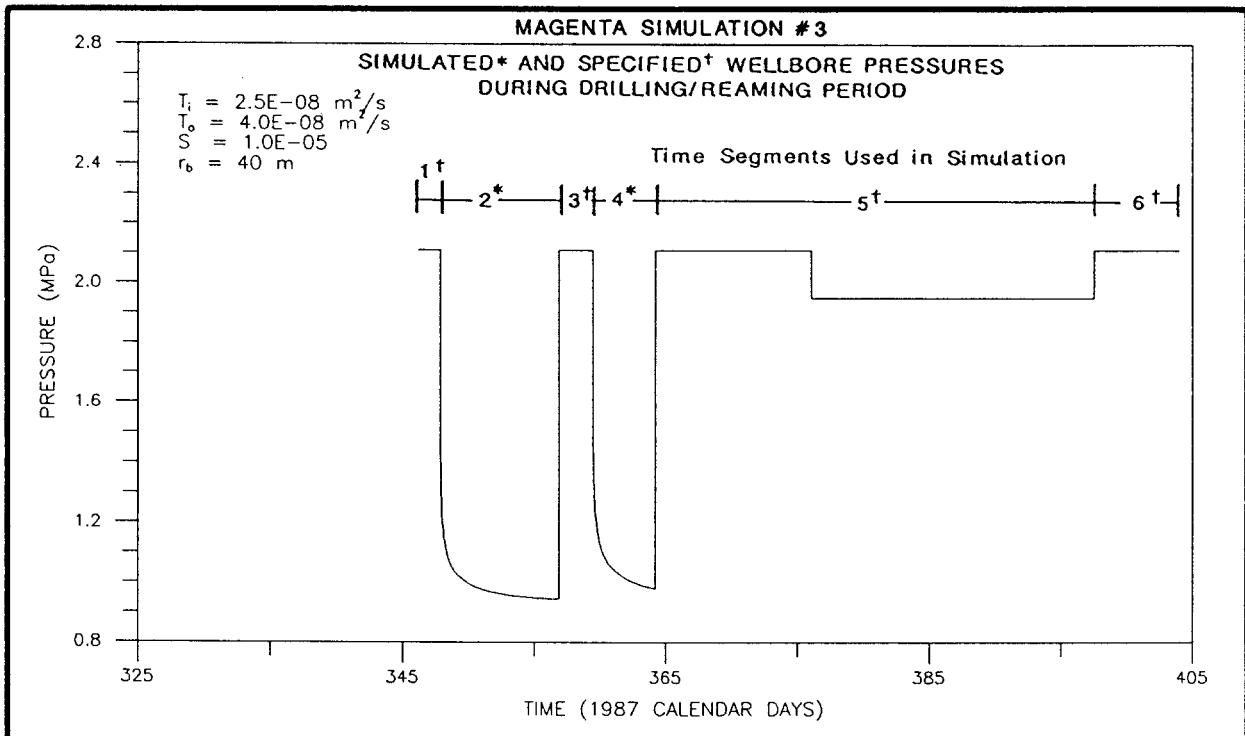
TIME 0 = JANUARY 1, 1987

Drawn by J.D.A.	Date 2/23/89
Checked by G.S.	Date 2/23/89
Revisions ABW	Date 6/23/89
H09700R876	2/23/89

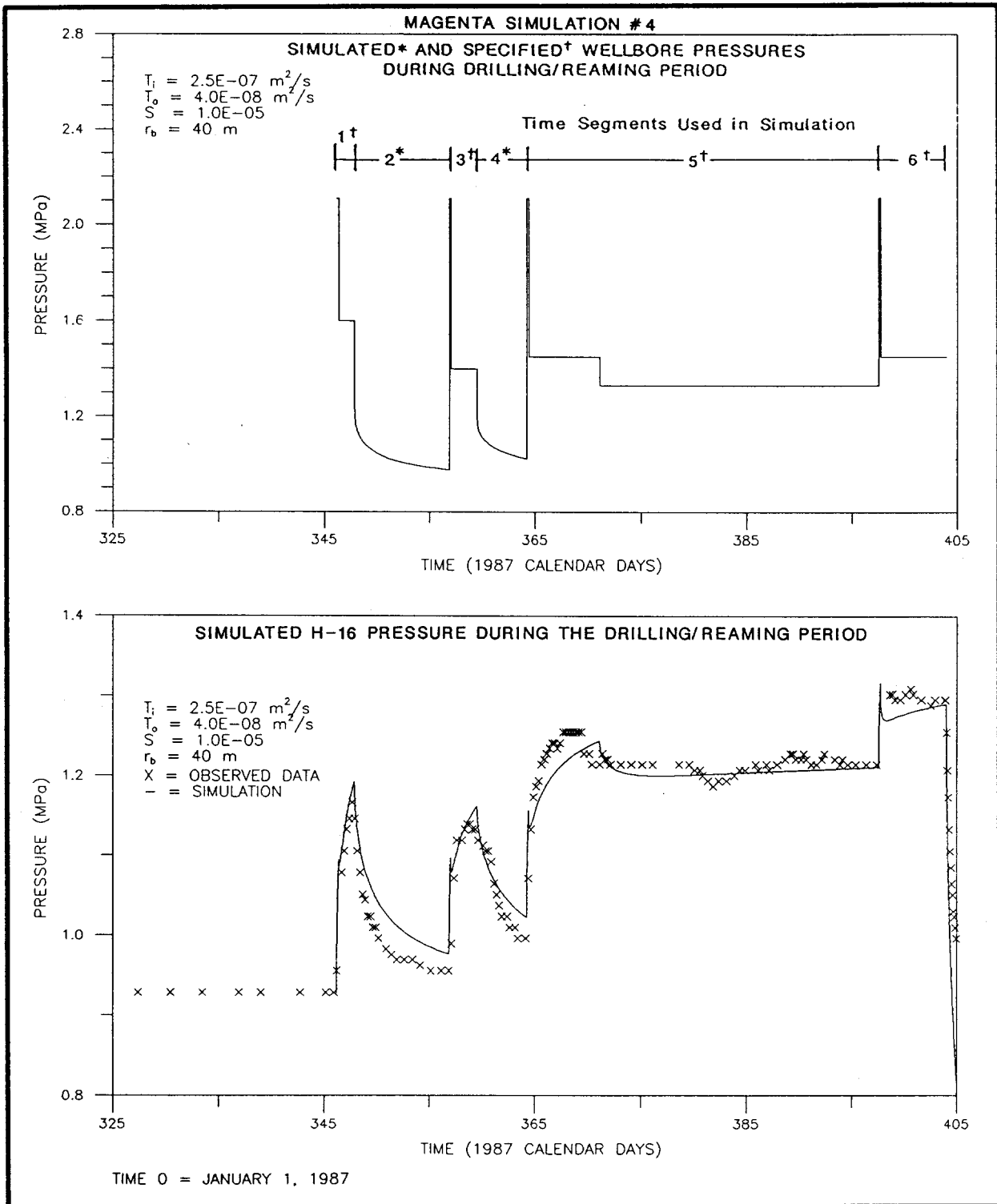
SPECIFIED AND SIMULATED WELLBORE PRESSURES AND SIMULATED AND OBSERVED FORMATION FLUID PRESSURES FOR THE MAGENTA DOLOMITE DRILLING/REAMING PERIOD USING A FORMATION-HETEROGENEITY BOUNDARY

**INTERA Technologies**

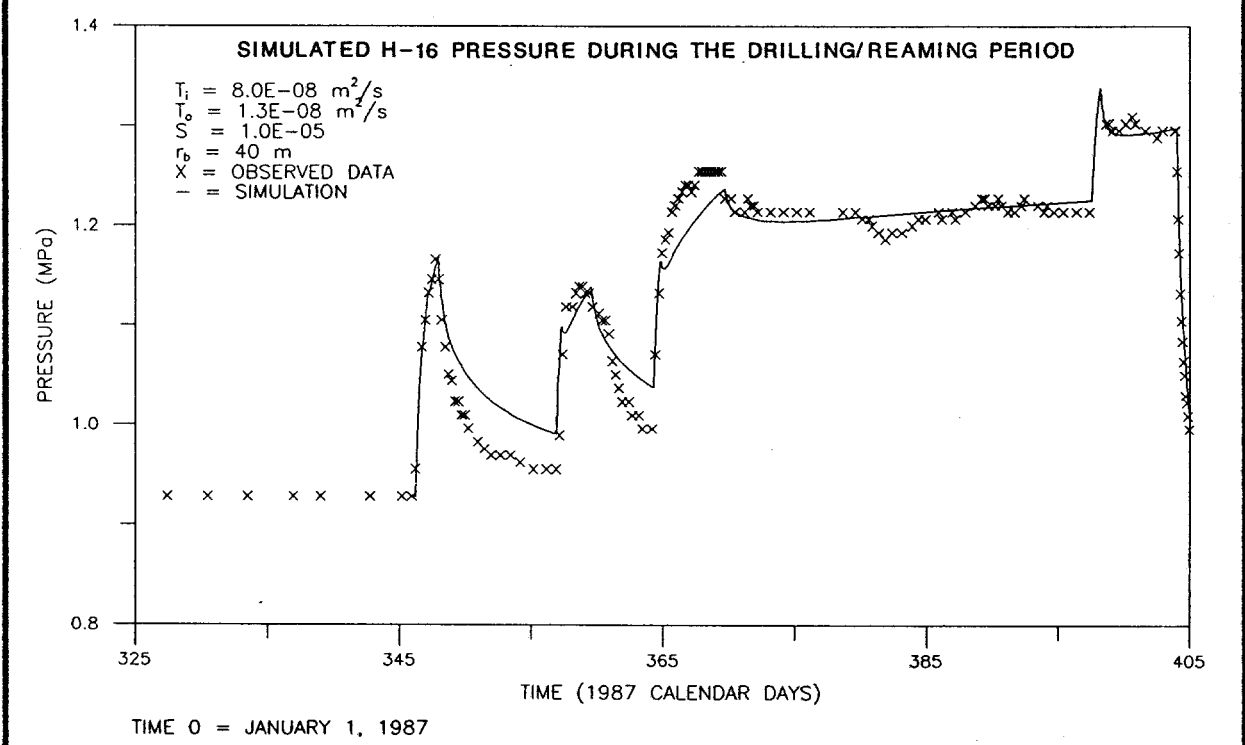
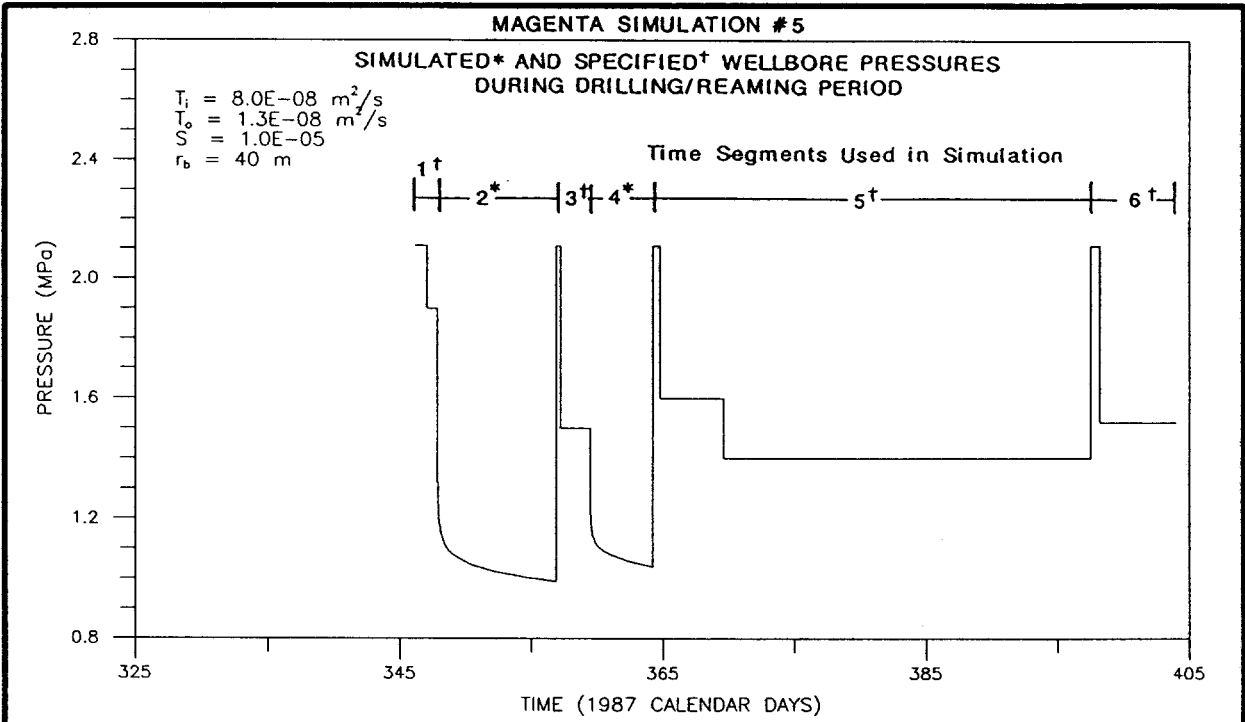
Figure A.8



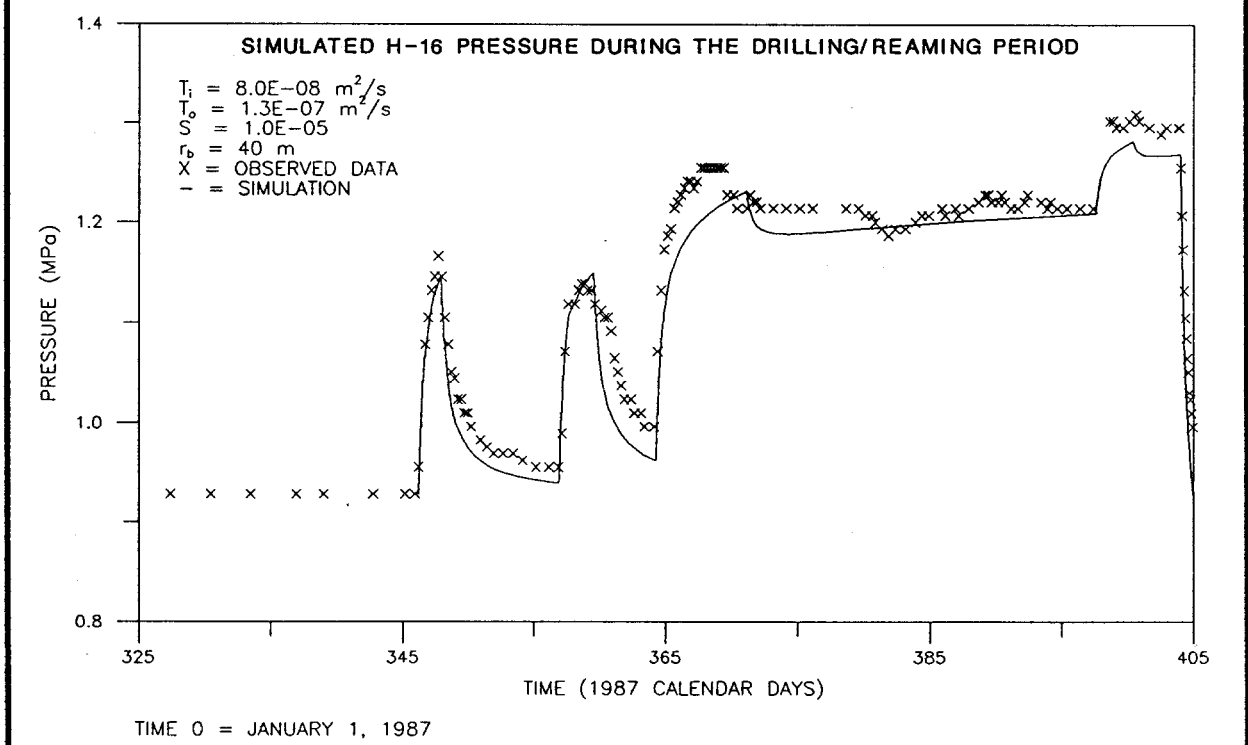
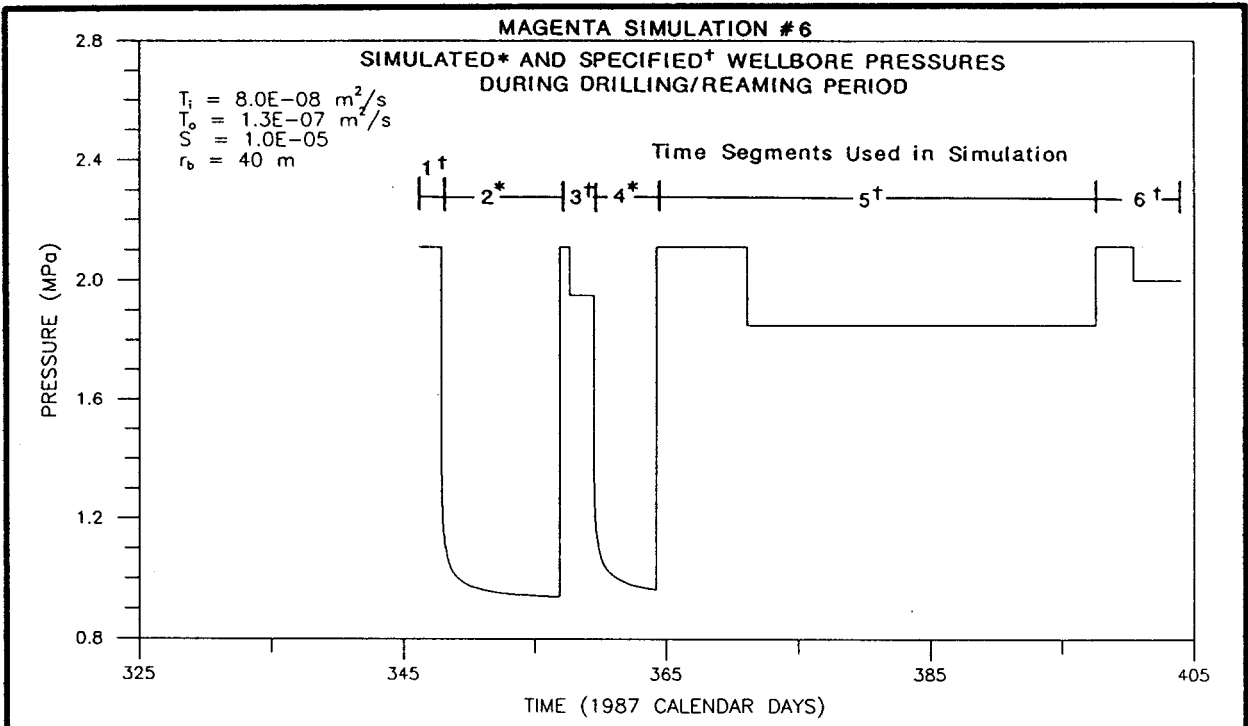
Drawn by J.D.A.	Date 2/23/89	SPECIFIED AND SIMULATED WELLBORE PRESSURES AND SIMULATED AND OBSERVED FORMATION FLUID PRESSURES FOR THE MAGENTA DOLOMITE DRILLING/REAMING PERIOD USING A FORMATION-HETEROGENEITY BOUNDARY AND $T_i = 2.5 \times 10^{-8} \text{ m}^2/\text{s}$
Checked by G.S.	Date 2/23/89	
Revisions ABW	Date 6/23/89	
H09700R876	2/23/89	
<b>INTERA Technologies</b>		Figure A.9



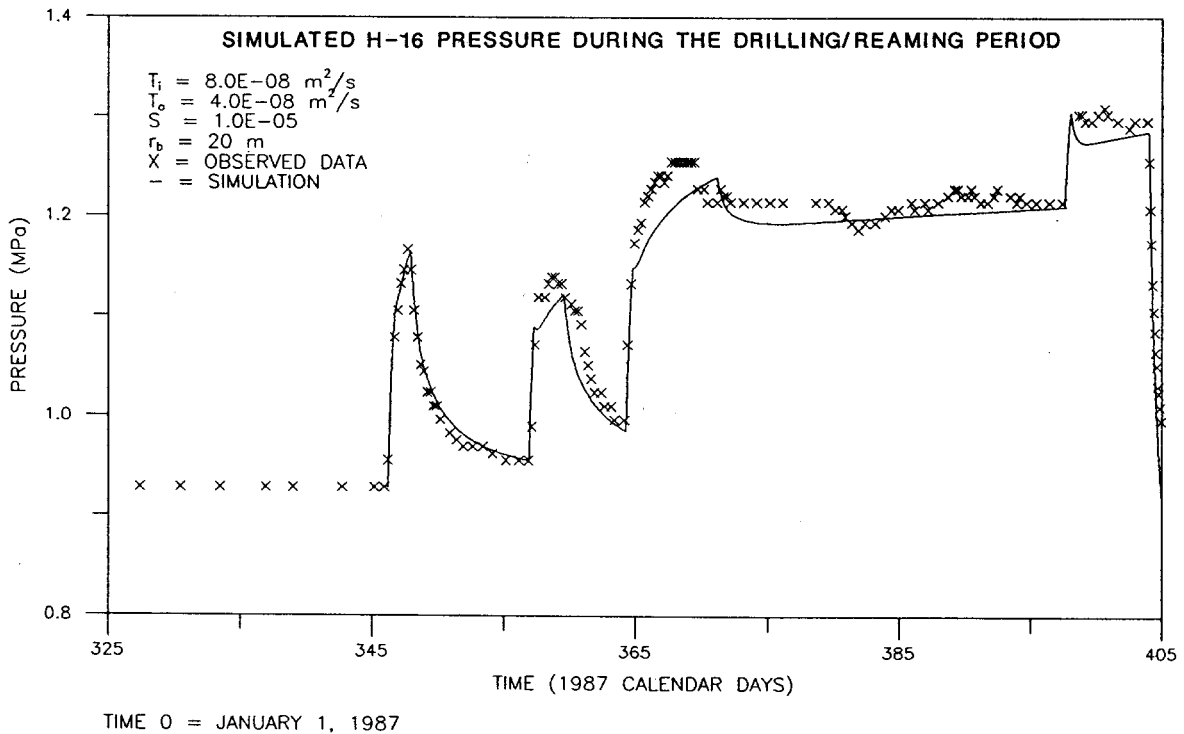
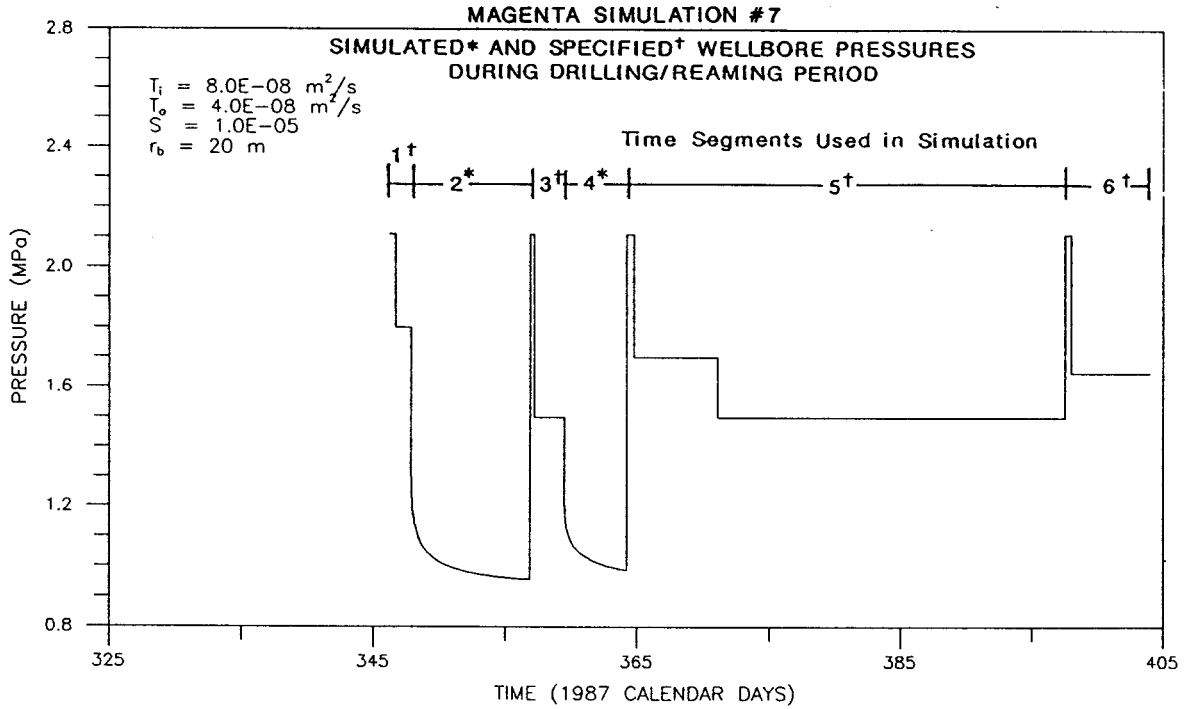
Drawn by	J.D.A.	Date	2/23/89	SPECIFIED AND SIMULATED WELLBORE PRESSURES AND SIMULATED AND OBSERVED FORMATION FLUID PRESSURES FOR THE MAGENTA DOLOMITE DRILLING/REAMING PERIOD USING A FORMATION-HETEROGENEITY BOUNDARY AND $T_i = 2.5 \times 10^{-7} \text{ m}^2/\text{s}$
Checked by	G.S.	Date	2/23/89	
Revisions	ABW	Date	6/23/89	
H09700R876			2/23/89	
<b>INTERA Technologies</b>				Figure A.10



Drawn by J.D.A.	Date 2/23/89	SPECIFIED AND SIMULATED WELLBORE PRESSURES AND SIMULATED AND OBSERVED FORMATION FLUID PRESSURES FOR THE MAGENTA DOLOMITE DRILLING/REAMING PERIOD USING A FORMATION-HETEROGENEITY BOUNDARY AND $T_o = 1.3 \times 10^{-8} \text{ m}^2/\text{s}$
Checked by G.S.	Date 2/23/89	
Revisions ABW	Date 6/23/89	
H09700R876	2/23/89	
<b>INTERA Technologies</b>		Figure A.11



Drawn by J.D.A.	Date 2/23/89	SPECIFIED AND SIMULATED WELLBORE PRESSURES AND SIMULATED AND OBSERVED FORMATION FLUID PRESSURES FOR THE MAGENTA DOLOMITE DRILLING/REAMING PERIOD USING A FORMATION-HETEROGENEITY BOUNDARY AND $T_o = 1.3 \times 10^{-7} \text{ m}^2/\text{s}$
Checked by G.S.	Date 2/23/89	
Revisions ABW	Date 6/23/89	
H09700R876	2/23/89	
<b>INTERA Technologies</b>		Figure A.12

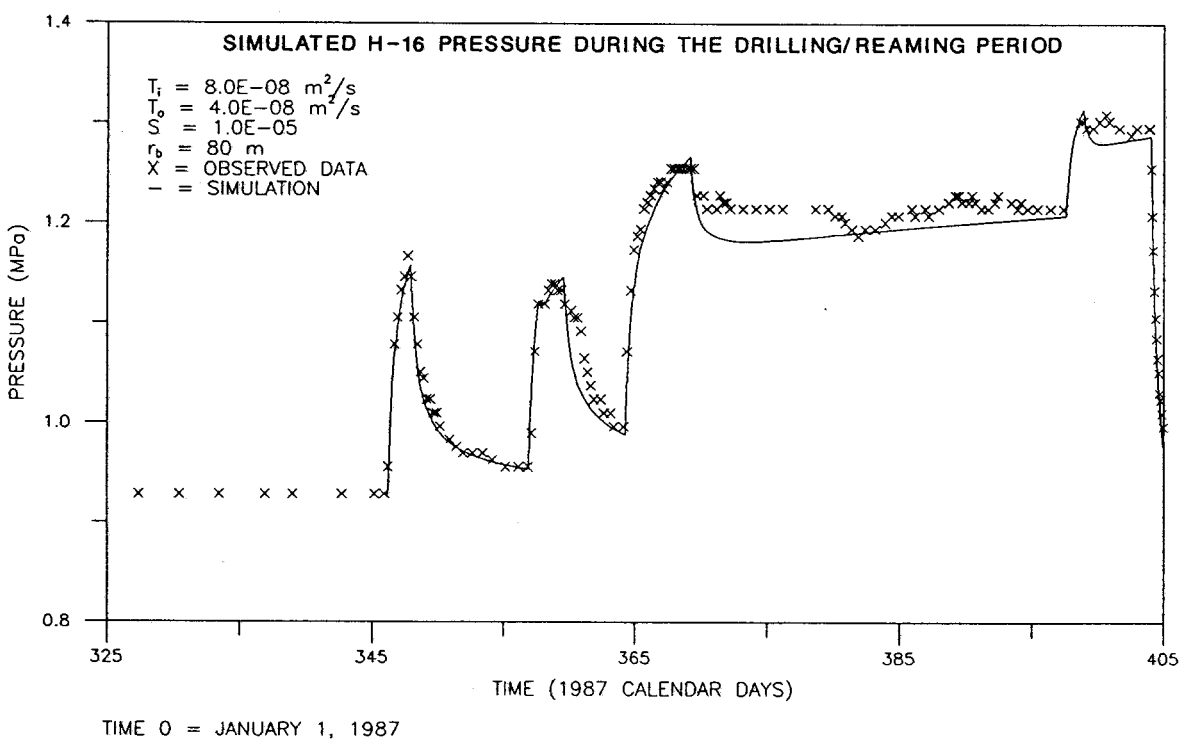
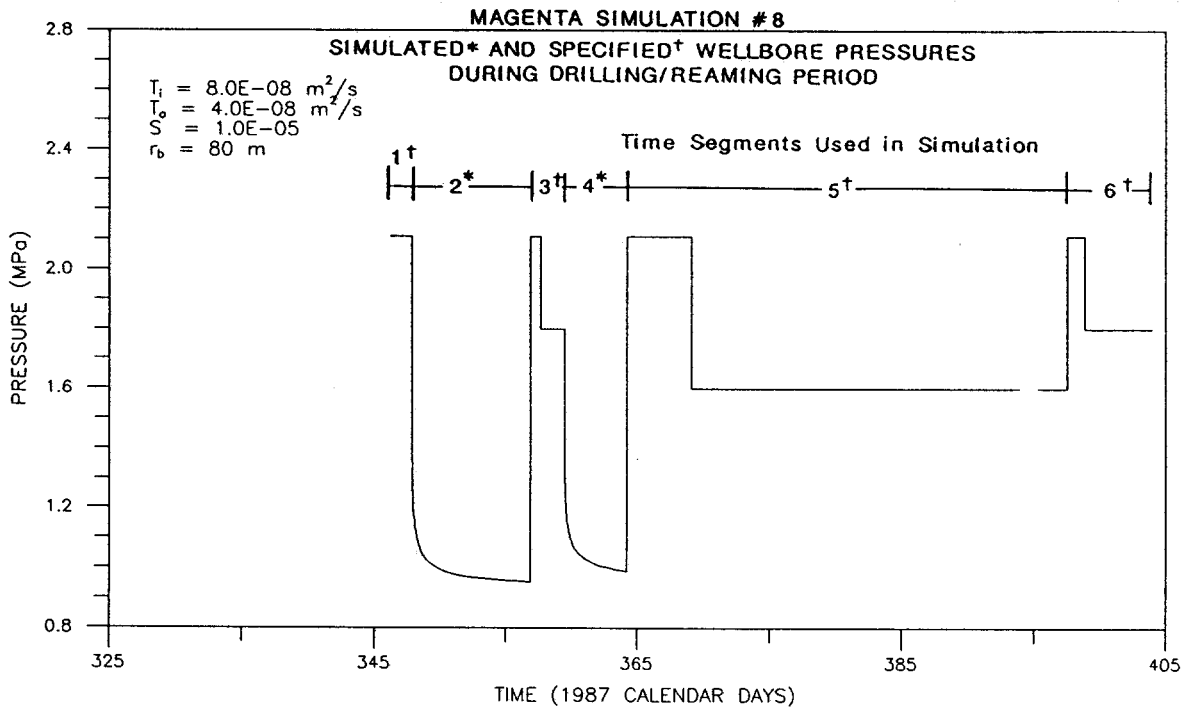


Drawn by	J.D.A.	Date	2/23/89
Checked by	G.S.	Date	2/23/89
Revisions	ABW	Date	6/23/89
H09700R876		Date	2/23/89

SPECIFIED AND SIMULATED WELLBORE PRESSURES AND SIMULATED AND OBSERVED FORMATION FLUID PRESSURES FOR THE MAGENTA DOLOMITE DRILLING/REAMING PERIOD USING A FORMATION-HETEROGENEITY BOUNDARY AND  $r_b = 20 \text{ m}$

**INTERA Technologies**

Figure A.13

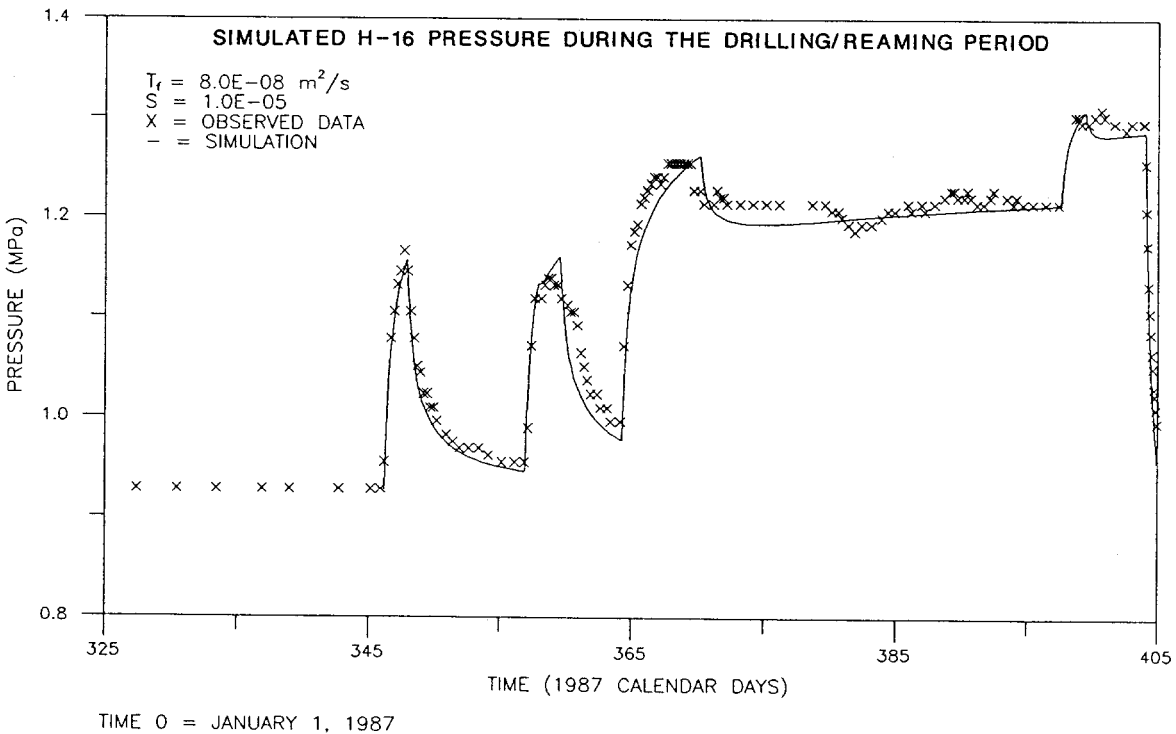
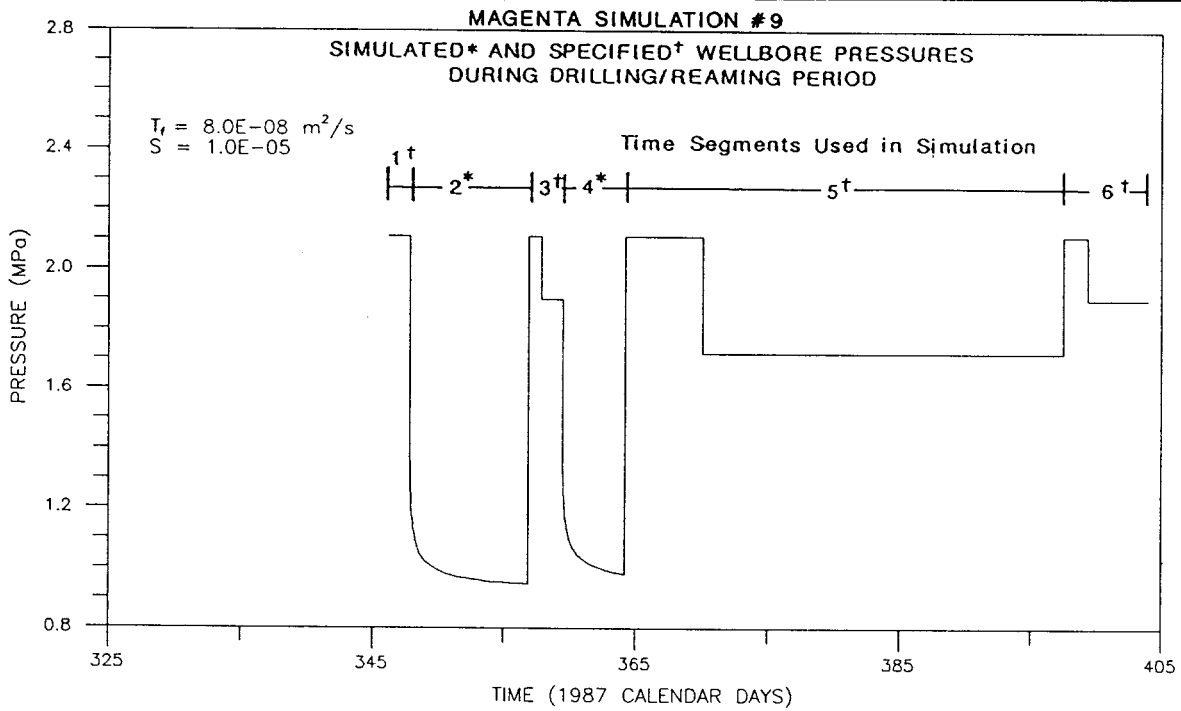


Drawn by J.D.A.	Date 2/23/89
Checked by G.S.	Date 2/23/89
Revisions ABW	Date 6/23/89
H09700R876	2/23/89

SPECIFIED AND SIMULATED WELLBORE PRESSURES AND SIMULATED AND OBSERVED FORMATION FLUID PRESSURES FOR THE MAGENTA DOLOMITE DRILLING/REAMING PERIOD USING A FORMATION-HETEROGENEITY BOUNDARY AND  $r_b = 80 \text{ m}$

**INTERA Technologies**

Figure A.14

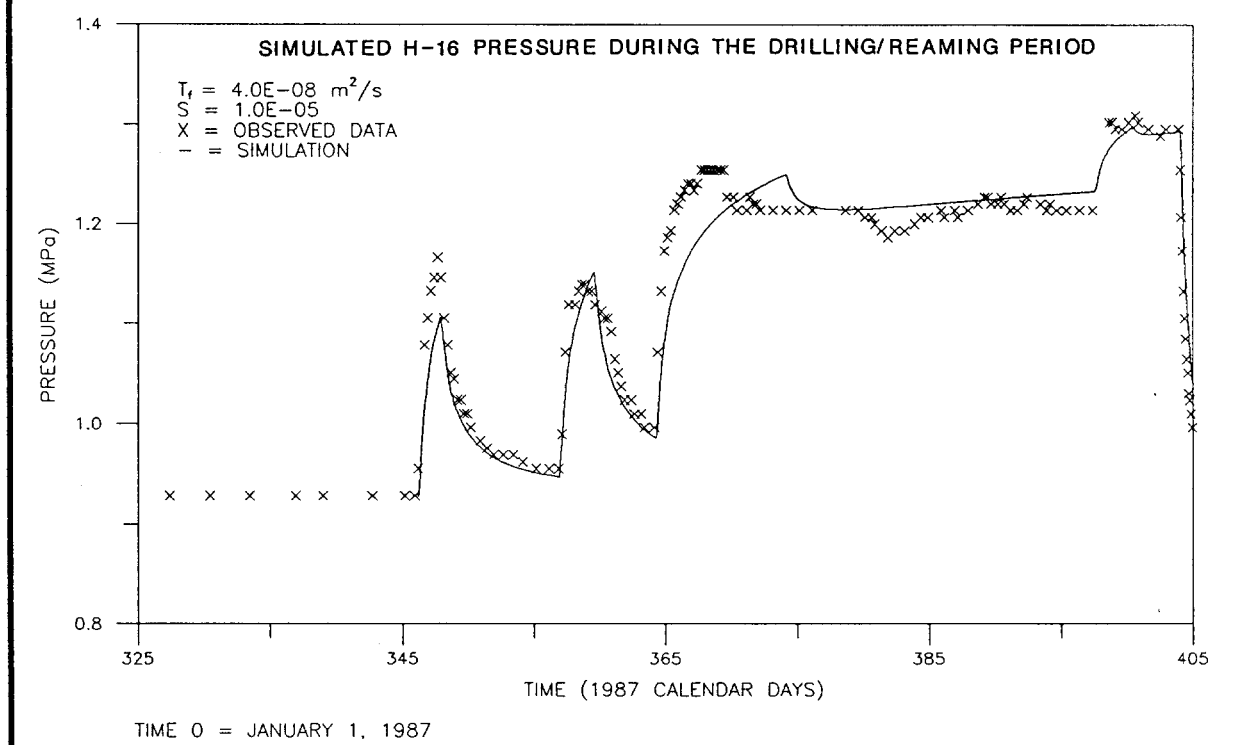
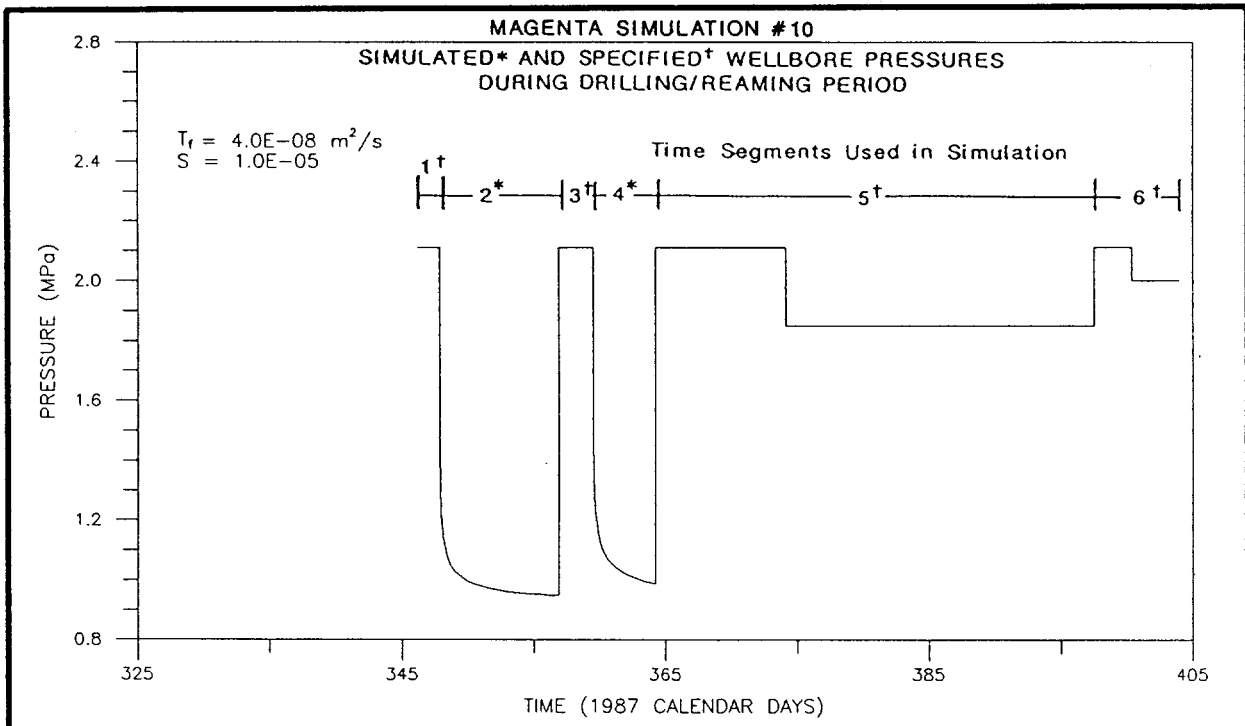


Drawn by	J.D.A.	Date	2/23/89
Checked by	G.S.	Date	2/23/89
Revisions	ABW	Date	6/23/89
H09700R876			2/23/89

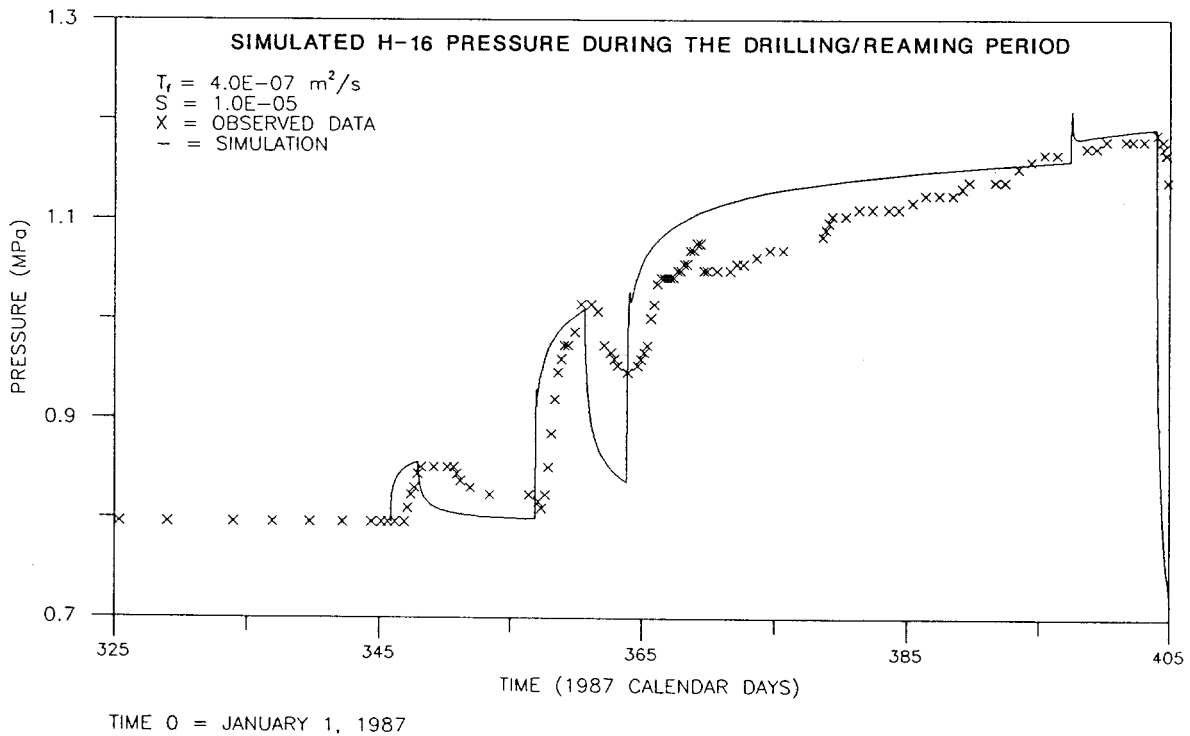
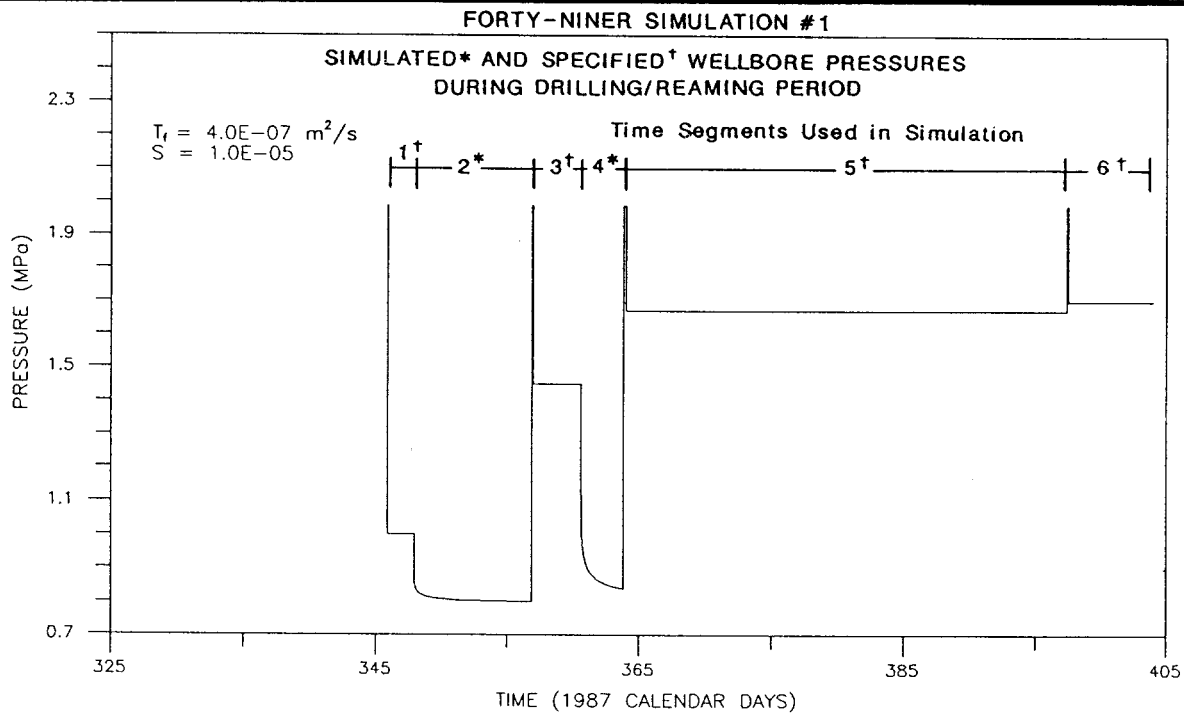
SPECIFIED AND SIMULATED WELLBORE PRESSURES AND SIMULATED AND OBSERVED FORMATION FLUID PRESSURES FOR THE MAGENTA DOLOMITE DRILLING/REAMING PERIOD WITHOUT A FORMATION-HETEROGENEITY BOUNDARY AND  $T_f = 8.0 \times 10^{-8} \text{ m}^2/\text{s}$

**INTERA** Technologies

Figure A.15



Drawn by J.D.A.	Date 2/23/89	SPECIFIED AND SIMULATED WELLBORE PRESSURES AND SIMULATED AND OBSERVED FORMATION FLUID PRESSURES FOR THE MAGENTA DOLOMITE DRILLING/REAMING PERIOD WITHOUT A FORMATION-HETEROGENEITY BOUNDARY AND $T_f = 4.0 \times 10^{-8} \text{ m}^2/\text{s}$
Checked by G.S.	Date 2/23/89	
Revisions ABW	Date 6/23/89	
H09700R876	2/23/89	
<b>INTERA Technologies</b>		Figure A.16



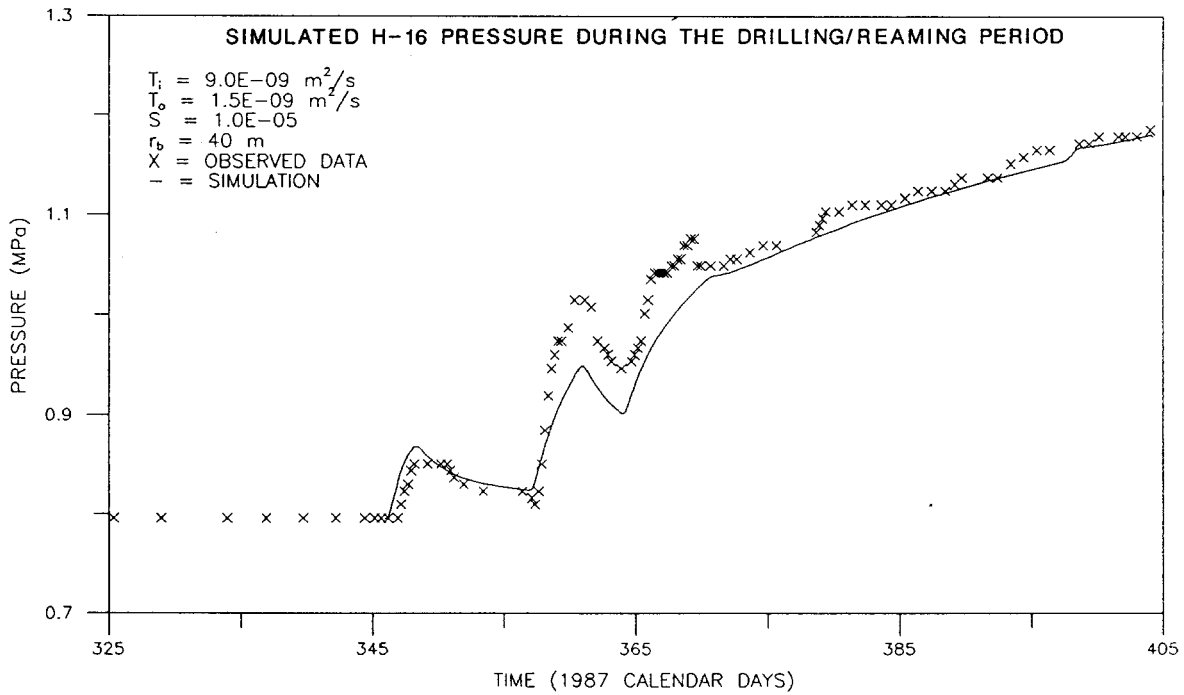
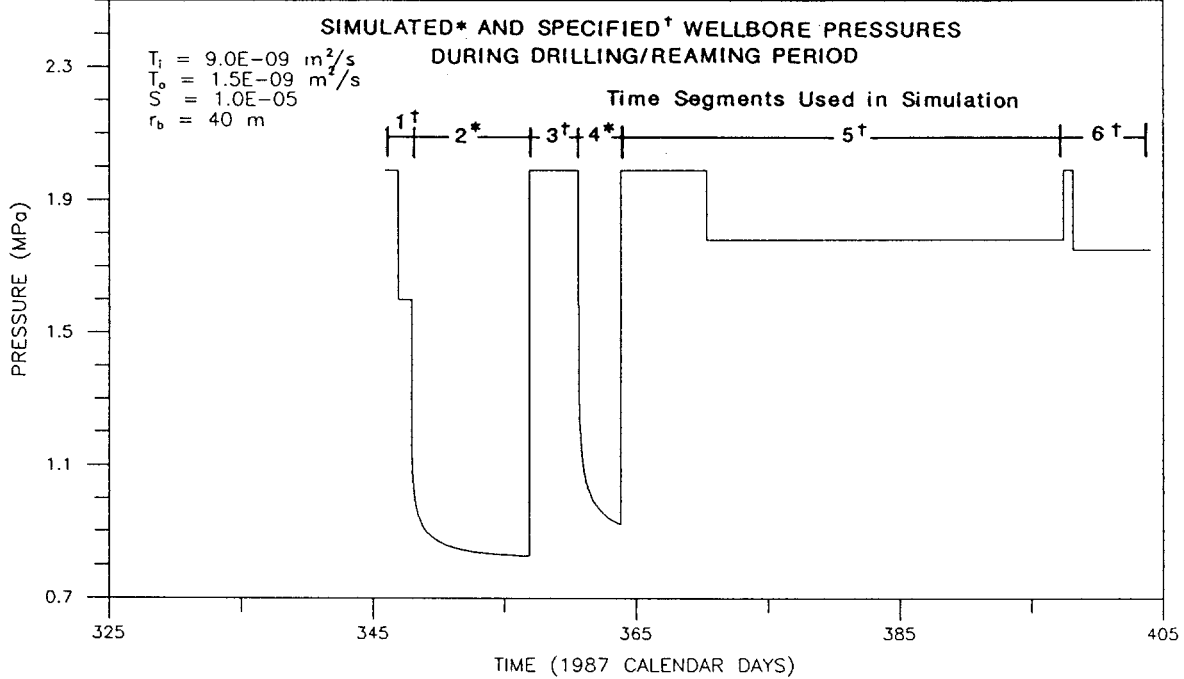
Drawn by J.D.A.	Date 2/23/89
Checked by G.S.	Date 2/23/89
Revisions ABW	Date 6/23/89
H09700R876	2/23/89

SPECIFIED AND SIMULATED WELLBORE PRESSURES AND SIMULATED AND OBSERVED FORMATION FLUID PRESSURES FOR THE FORTY-NINER CLAYSTONE DRILLING/REAMING PERIOD USING A HOMOGENEOUS-FORMATION CHARACTERIZATION

**INTERA Technologies**

Figure A.17

FORTY-NINER SIMULATION #2



TIME 0 = JANUARY 1, 1987

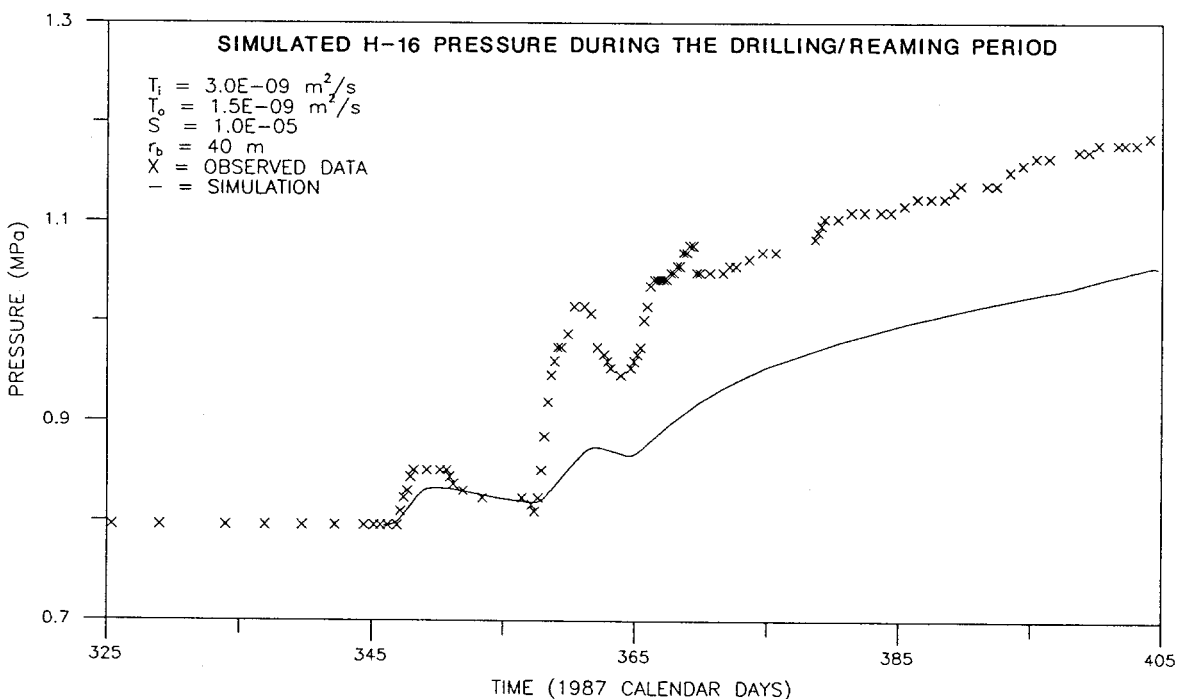
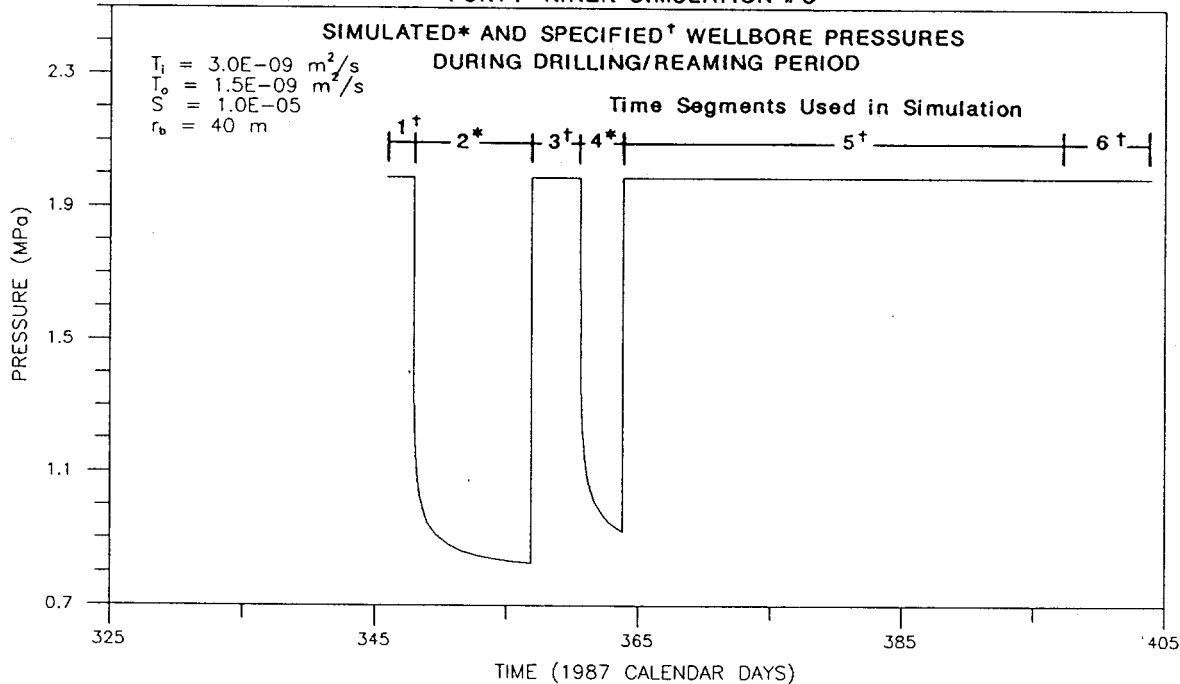
Drawn by J.D.A.	Date 2/23/89
Checked by G.S.	Date 2/23/89
Revisions ABW	Date 6/23/89
H09700R876	2/23/89

SPECIFIED AND SIMULATED WELLBORE PRESSURES AND  
SIMULATED AND OBSERVED FORMATION FLUID PRESSURES  
FOR THE FORTY-NINER CLAYSTONE DRILLING/REAMING  
PERIOD USING A FORMATION-HETEROGENEITY BOUNDARY

**INTERA** Technologies

Figure A.18

FORTY-NINER SIMULATION #3



TIME 0 = JANUARY 1, 1987

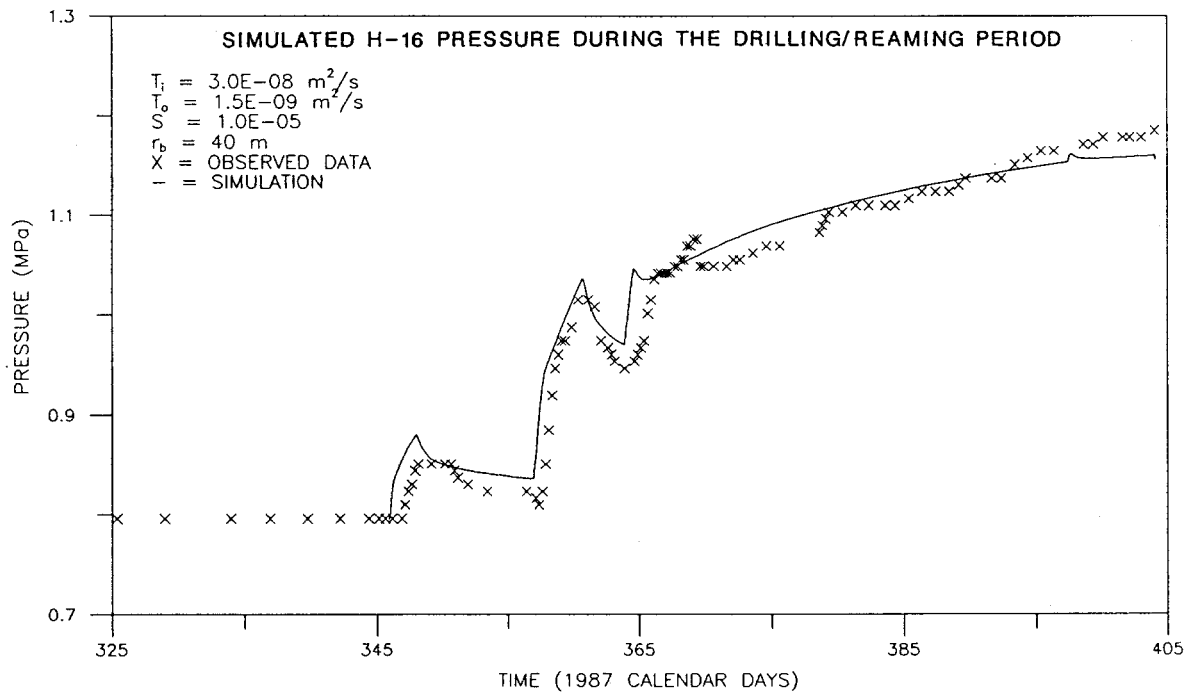
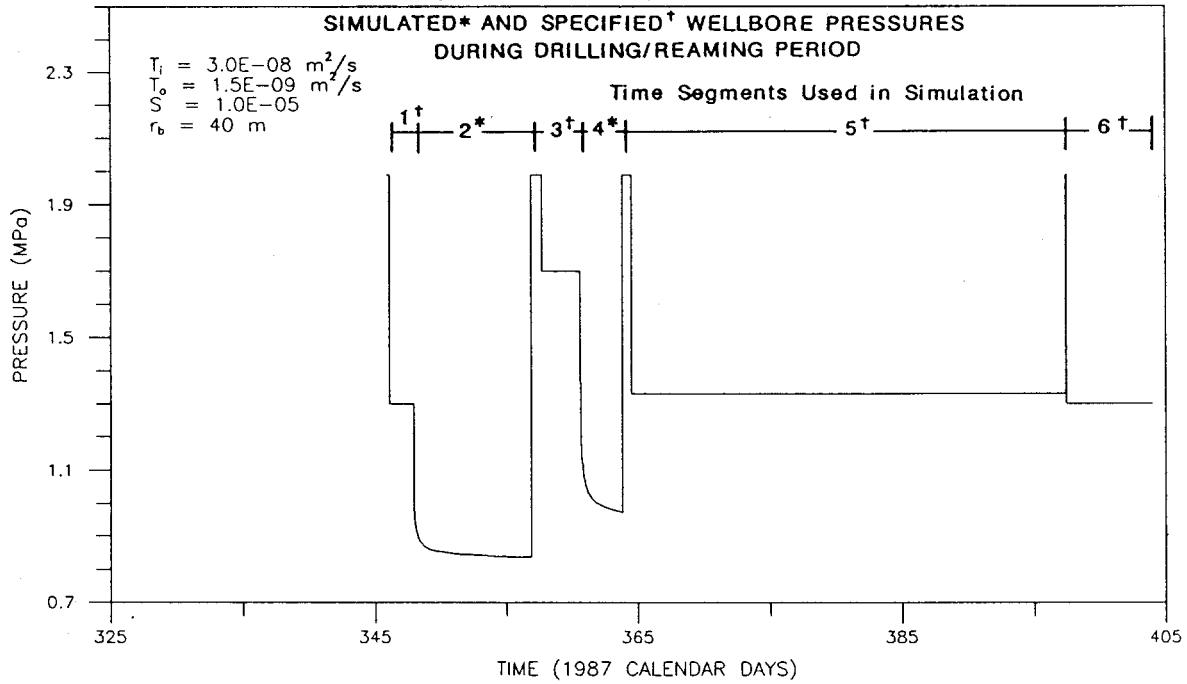
Drawn by J.D.A.	Date 2/23/89
Checked by G.S.	Date 2/23/89
Revisions ABW	Date 6/23/89
H09700R876	2/23/89

SPECIFIED AND SIMULATED WELLBORE PRESSURES AND SIMULATED AND OBSERVED FORMATION FLUID PRESSURES FOR THE FORTY-NINER CLAYSTONE DRILLING/REAMING PERIOD USING A FORMATION-HETEROGENEITY BOUNDARY AND  $T_i = 3.0 \times 10^{-9} \text{ m}^2/\text{s}$

**INTERA Technologies**

Figure A.19

FORTY-NINER SIMULATION #4



TIME 0 = JANUARY 1, 1987

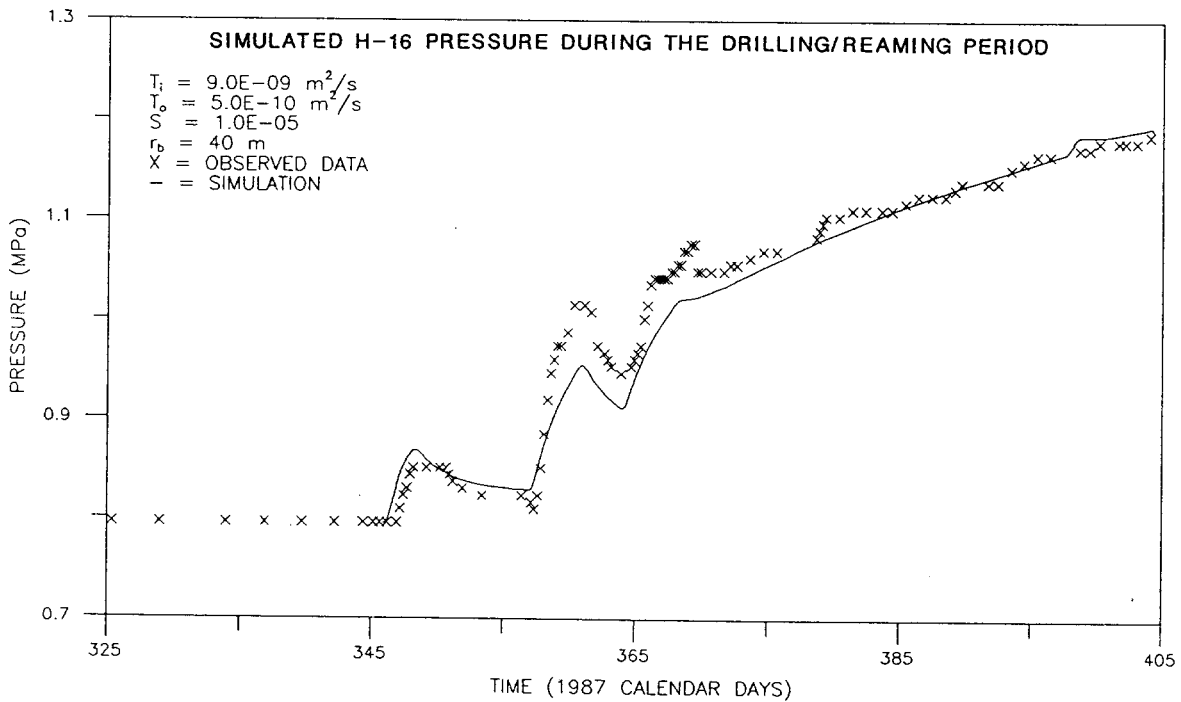
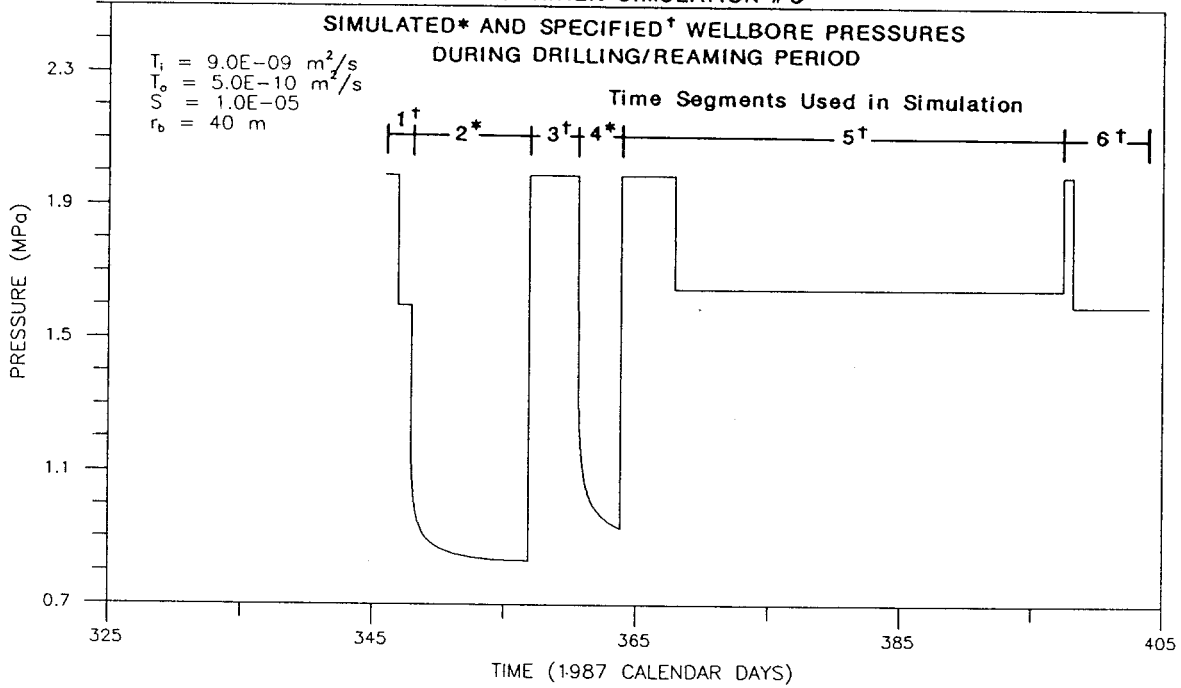
Drawn by	J.D.A.	Date	2/23/89
Checked by	G.S.	Date	2/23/89
Revisions	ABW	Date	6/23/89
H09700R876			2/23/89

SPECIFIED AND SIMULATED WELLBORE PRESSURES AND SIMULATED AND OBSERVED FORMATION FLUID PRESSURES FOR THE FORTY-NINER CLAYSTONE DRILLING/REAMING PERIOD USING A FORMATION-HETEROGENEITY BOUNDARY AND  $T_i = 3.0 \times 10^{-8} \text{ m}^2/\text{s}$

**INTERA Technologies**

Figure A.20

**FORTY-NINER SIMULATION #5**



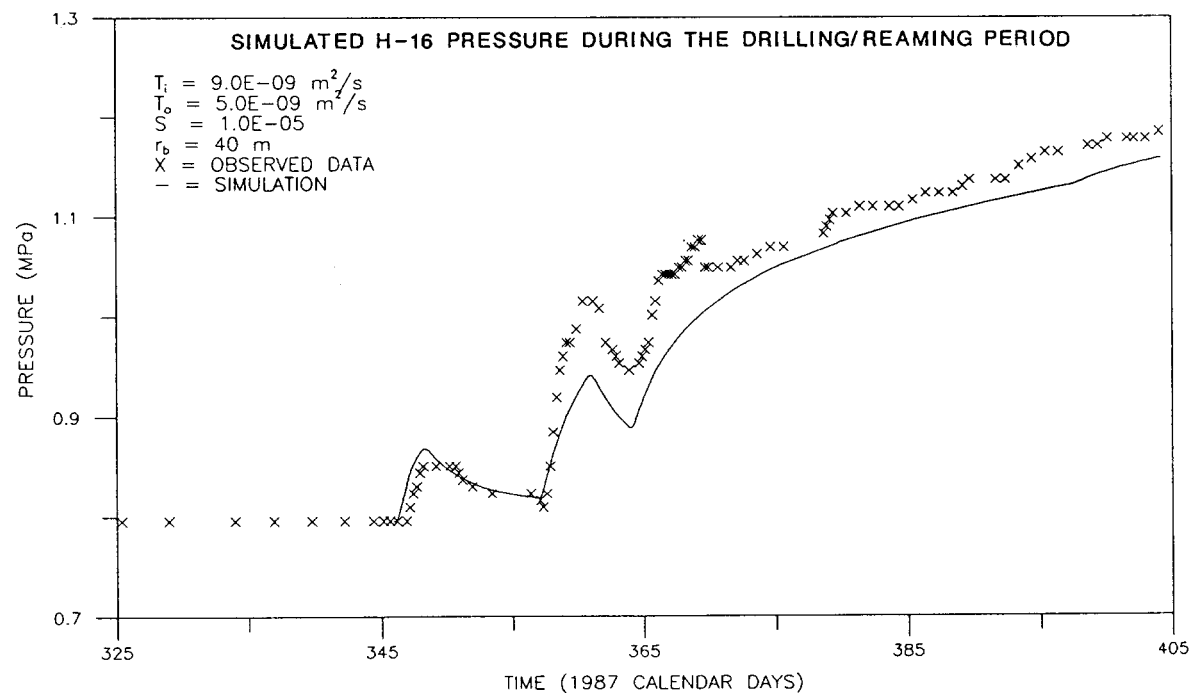
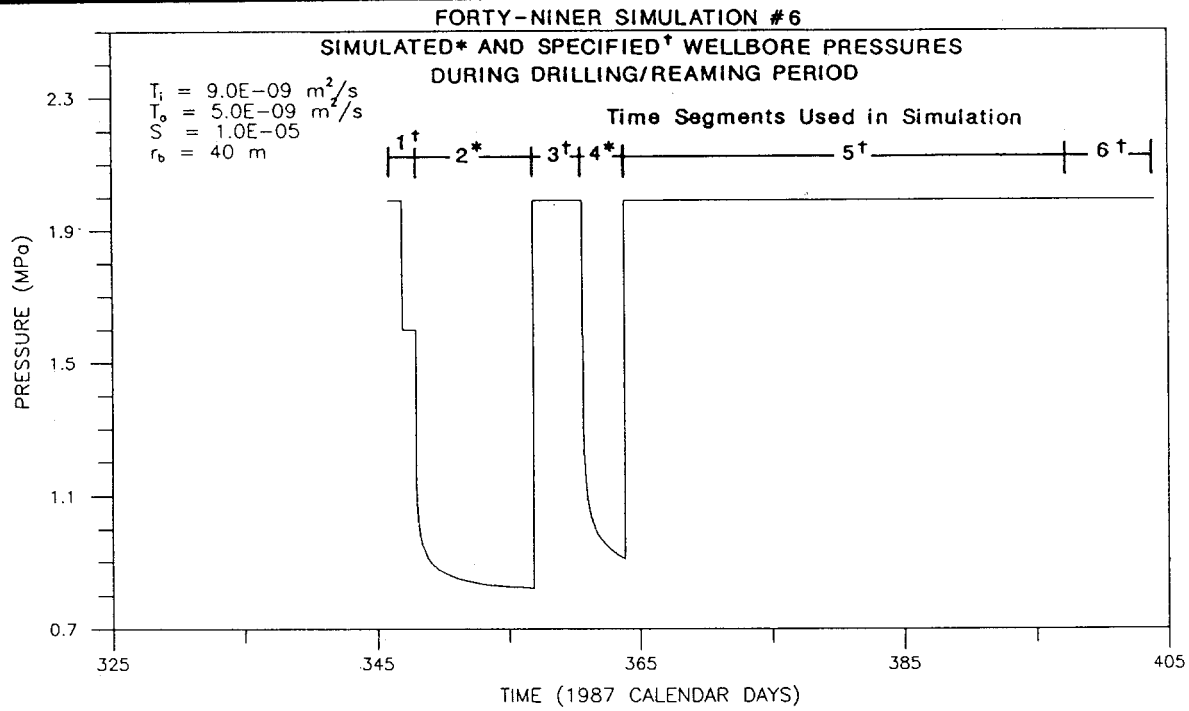
TIME 0 = JANUARY 1, 1987

Drawn by	J.D.A.	Date	2/23/89
Checked by	G.S.	Date	2/23/89
Revisions	ABW	Date	6/23/89
H09700R876			2/23/89

SPECIFIED AND SIMULATED WELLBORE PRESSURES AND SIMULATED AND OBSERVED FORMATION FLUID PRESSURES FOR THE FORTY-NINER CLAYSTONE DRILLING/REAMING PERIOD USING A FORMATION-HETEROGENEITY BOUNDARY AND  $T_o = 5.0 \times 10^{-10} \text{ m}^2/\text{s}$

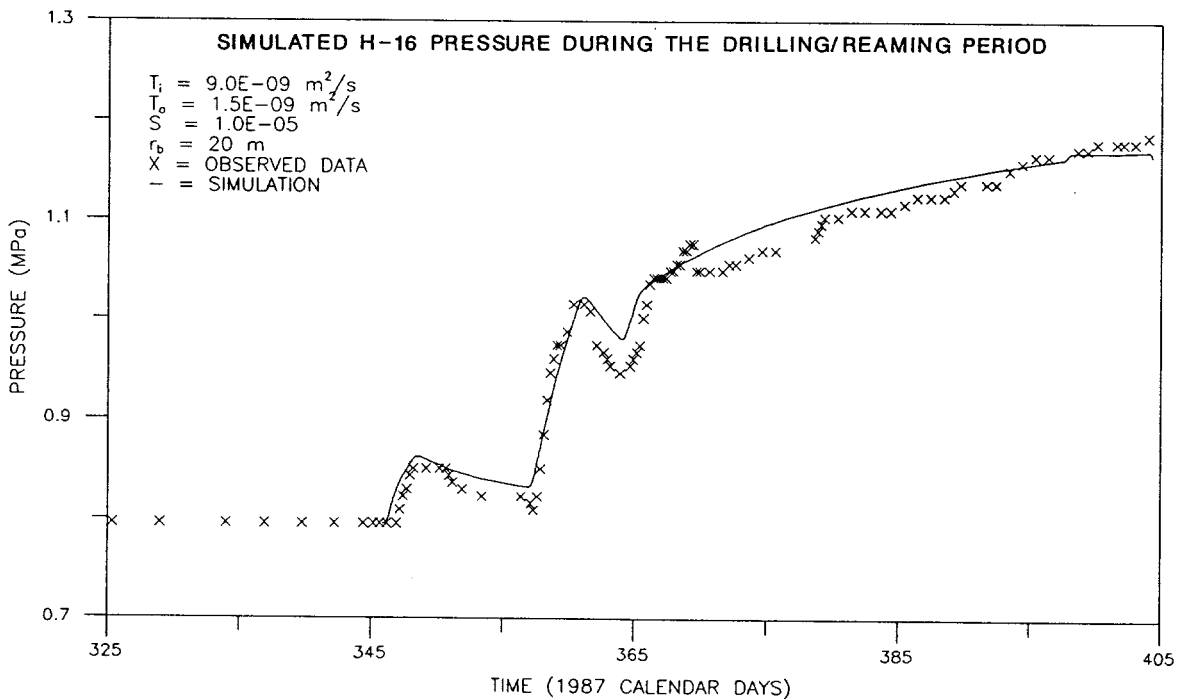
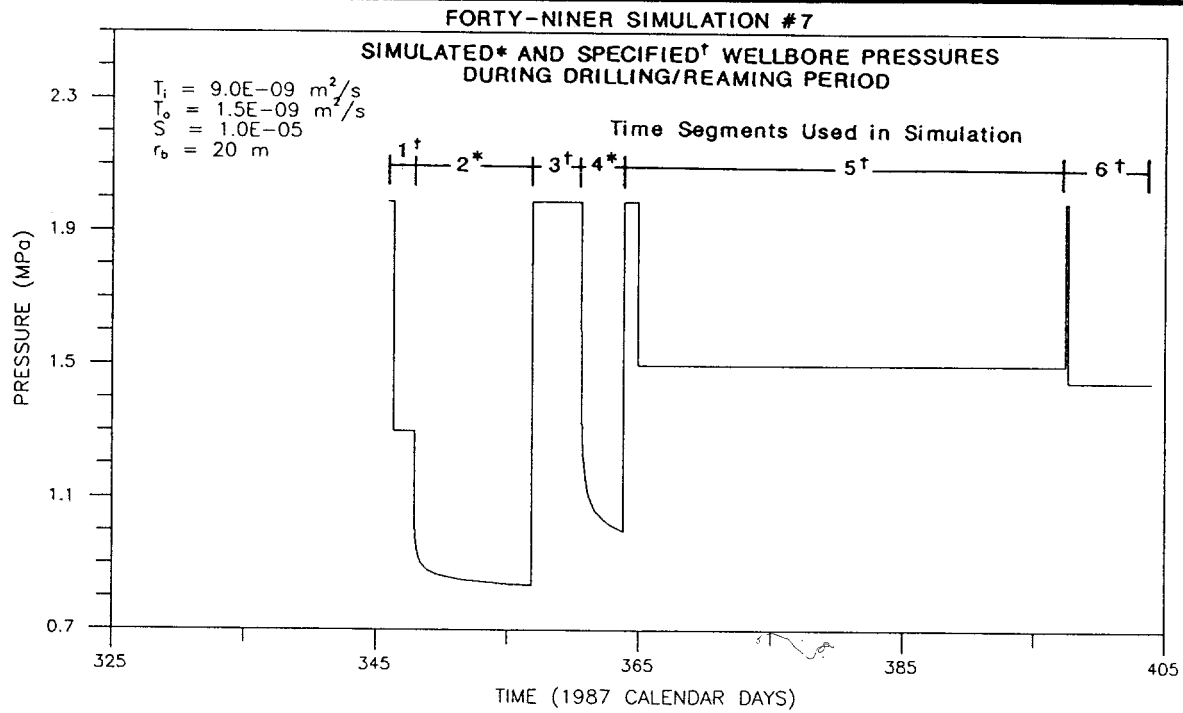
**INTERA Technologies**

Figure A.21



TIME 0 = JANUARY 1, 1987

Drawn by J.D.A.	Date 2/23/89	SPECIFIED AND SIMULATED WELLBORE PRESSURES AND SIMULATED AND OBSERVED FORMATION FLUID PRESSURES FOR THE FORTY-NINER CLAYSTONE DRILLING/REAMING PERIOD USING A FORMATION-HETEROGENEITY BOUNDARY AND $T_o = 5.0 \times 10^{-9} \text{ m}^2/\text{s}$
Checked by G.S.	Date 2/23/89	
Revisions ABW	Date 6/23/89	
H09700R876	2/23/89	
<b>INTERA Technologies</b>		Figure A.22



TIME 0 = JANUARY 1, 1987

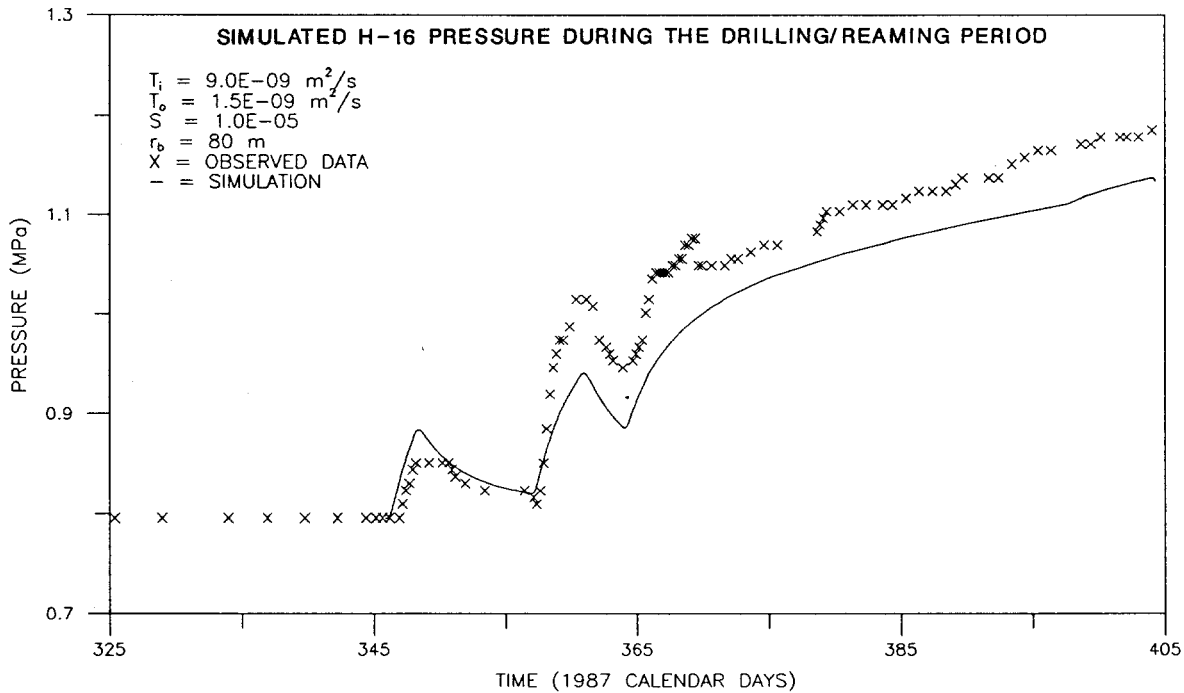
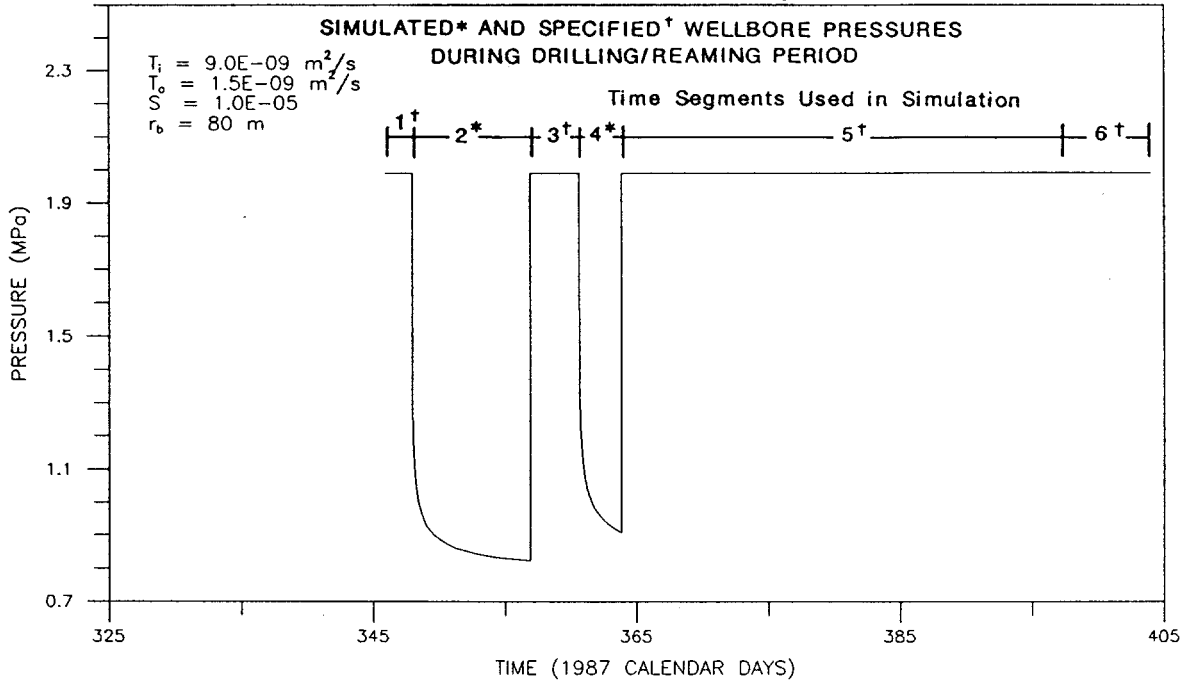
Drawn by J.D.A.	Date 2/23/89
Checked by G.S.	Date 2/23/89
Revisions ABW	Date 6/23/89
H09700R876	2/23/89

SPECIFIED AND SIMULATED WELLBORE PRESSURES AND SIMULATED AND OBSERVED FORMATION FLUID PRESSURES FOR THE FORTY-NINER CLAYSTONE DRILLING/REAMING PERIOD USING A FORMATION-HETEROGENEITY BOUNDARY AND  $r_b = 20 \text{ m}$

**INTERA Technologies**

Figure A.23

FORTY-NINER SIMULATION #8



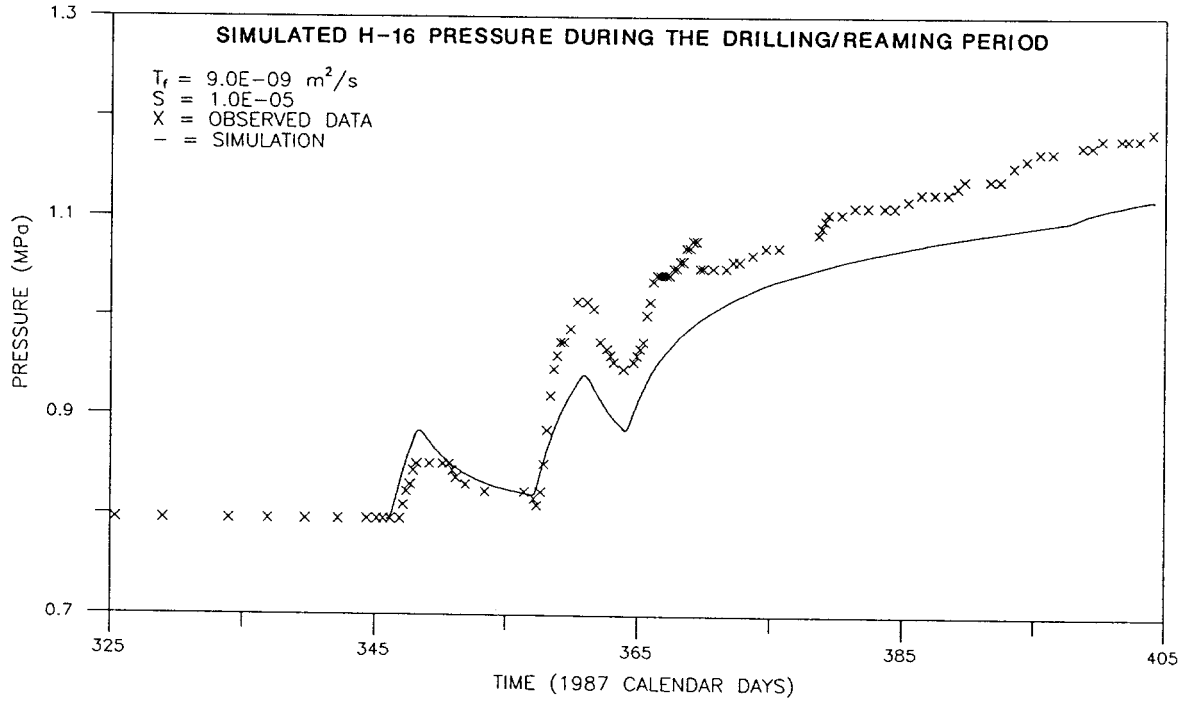
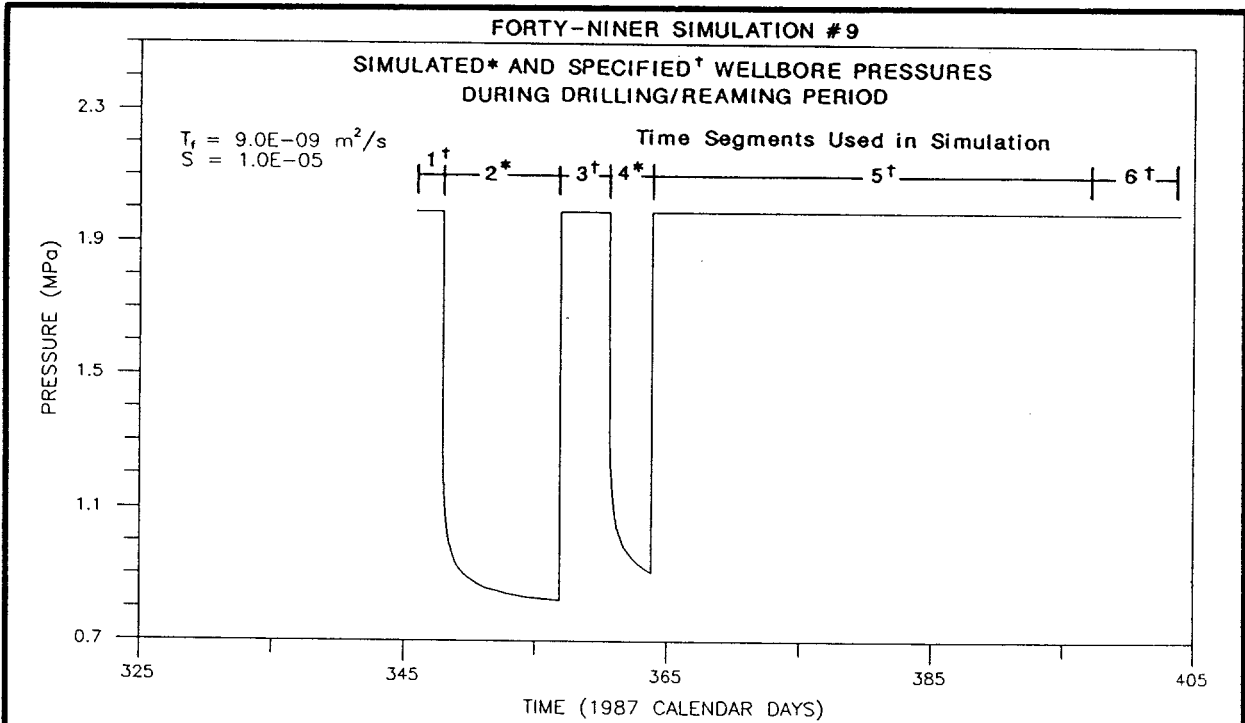
TIME 0 = JANUARY 1, 1987

Drawn by J.D.A.	Date 2/23/89
Checked by G.S.	Date 2/23/89
Revisions ABW	Date 6/23/89
H09700R876	2/23/89

SPECIFIED AND SIMULATED WELLBORE PRESSURES AND SIMULATED AND OBSERVED FORMATION FLUID PRESSURES FOR THE FORTY-NINER CLAYSTONE DRILLING/REAMING PERIOD USING A FORMATION-HETEROGENEITY BOUNDARY AND  $r_b = 80 \text{ m}$

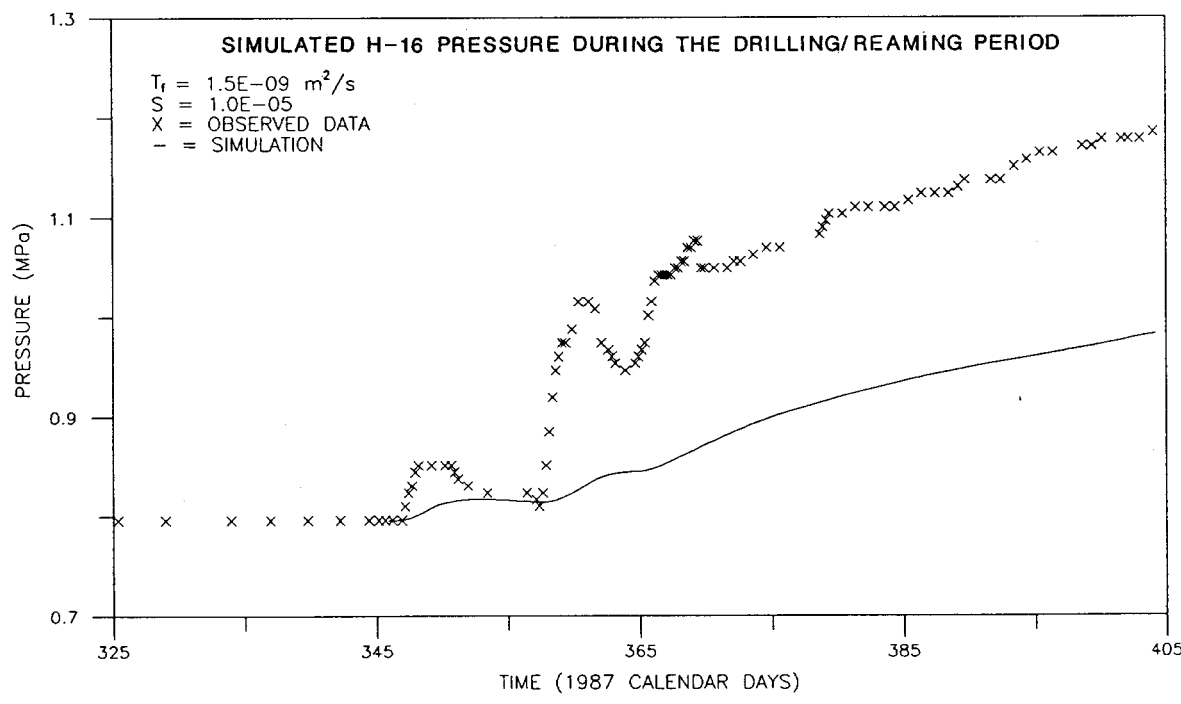
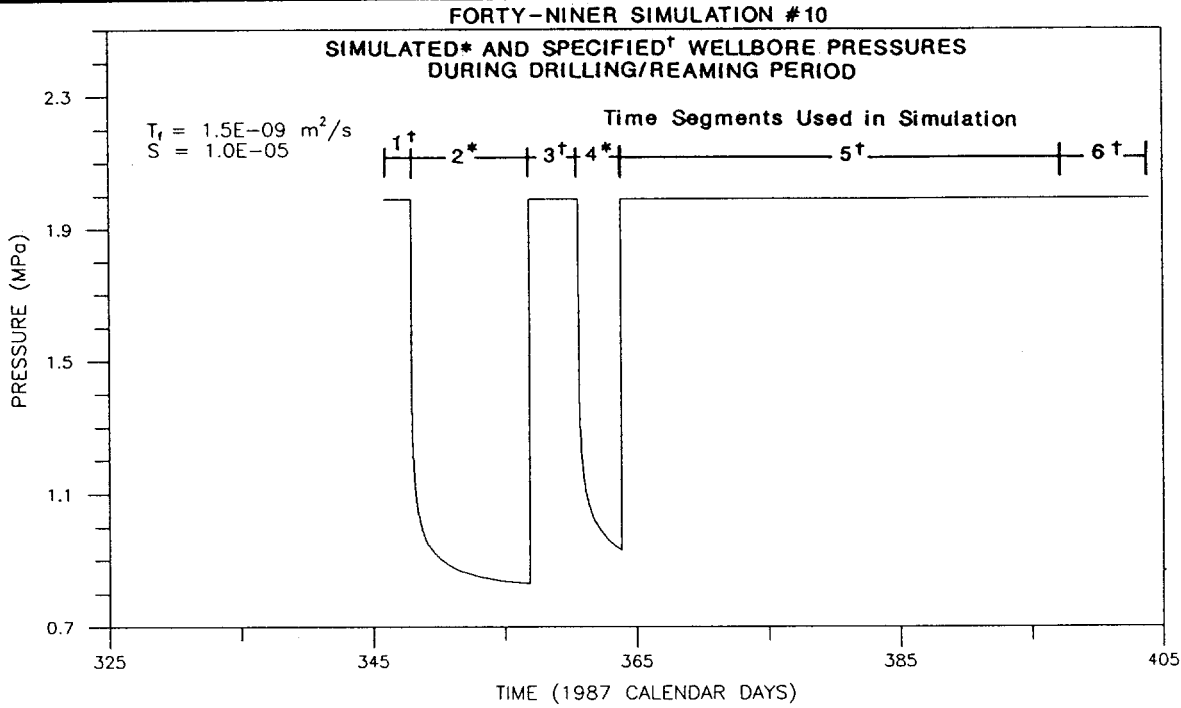
**INTERA Technologies**

Figure A.24



TIME 0 = JANUARY 1, 1987

Drawn by	J.D.A.	Date	2/23/89	SPECIFIED AND SIMULATED WELLBORE PRESSURES AND SIMULATED AND OBSERVED FORMATION FLUID PRESSURES FOR THE FORTY-NINER CLAYSTONE DRILLING/REAMING PERIOD WITHOUT A FORMATION-HETEROGENEITY BOUNDARY AND $T_f = 9.0 \times 10^{-9} \text{ m}^2/\text{s}$
Checked by	G.S.	Date	2/23/89	
Revisions	ABW	Date	6/23/89	
H09700R876		Date	2/23/89	
<b>INTERA Technologies</b>				Figure A.25



TIME 0 = JANUARY 1, 1987

Drawn by J.D.A.	Date 2/23/89
Checked by G.S.	Date 2/23/89
Revisions ABW	Date 6/23/89
H09700R876	2/23/89

SPECIFIED AND SIMULATED WELLBORE PRESSURES AND SIMULATED AND OBSERVED FORMATION FLUID PRESSURES FOR THE FORTY-NINER CLAYSTONE DRILLING/REAMING PERIOD WITHOUT A FORMATION-HETEROGENEITY BOUNDARY AND  $T_r = 1.5 \times 10^{-9} \text{ m}^2/\text{s}$

**INTERA Technologies**

Figure A.26

## DISTRIBUTION:

U. S. Department of Energy (5)  
Office of Civilian Radioactive Waste  
Management  
Office of Geological Repositories  
Forrestal Building  
Washington, DC 20585  
Deputy Director, RW-2  
Associate Director, RW-10  
Office of Program Administration  
and Resources Management  
Associate Director, RW-20  
Office of Facilities Siting and  
Development  
Associate Director, RW-30  
Office of Systems Integration  
and Regulations  
Associate Director, RW-40  
Office of External Relations and  
Policy

U. S. Department of Energy (3)  
Albuquerque Operations Office  
P.O. Box 5400  
Albuquerque, NM 87185  
B. G. Twining  
J. E. Bickel  
R. Marquez, Director  
Public Affairs Division

U. S. Department of Energy/AL  
Attn: National Atomic Museum Librarian  
P.O. Box 5400  
Albuquerque, NM 87185

U. S. Department of Energy (9)  
WIPP Project Office (Carlsbad)  
P.O. Box 3090  
Carlsbad, NM 88221  
A. Hunt (4)  
T. Lukow  
V. Daub (2)  
R. Batra  
J. Carr

U. S. Department of Energy  
Research & Waste Management Division  
P.O. Box E  
Oak Ridge, TN 37831  
W. R. Bibb, Director

U. S. Department of Energy  
Richland Operations Office  
Nuclear Fuel Cycle & Production  
Division  
P.O. Box 500  
Richland, WA 99352  
R. E. Gerton

U. S. Department of Energy (5)  
Office of Defense Waste and  
Transportation Management  
Washington, DC 20545  
T. B. Hindman ---- DP-12  
C. H. George ---- DP-124  
M. Duff ----- DP-123  
A. Follett ----- DP-122  
J. Mather ----- DP-123

U. S. Department of Energy (2)  
Idaho Operations Office  
Fuel Processing and Waste  
Management Division  
785 DOE Place  
Idaho Falls, ID 83402

U. S. Department of Energy (4)  
Savannah River Operations Office  
Waste Management Project Office  
P.O. Box A  
Aiken, SC 29802  
S. Cowan  
W. J. Brumley  
J. R. Covell  
D. Fulmer

U. S. Environmental Protection Agency  
Office of Radiation Programs (ANR460)  
Washington, DC 20460  
D. J. Egan, Jr.  
M. Cotton

U. S. Nuclear Regulatory Commission (4)  
Division of Waste Management  
Mail Stop 623SS  
Washington, DC 20555  
M. Bell  
H. Miller  
J. Philip  
NRC Library

U. S. Geological Survey  
Branch of Regional Geology  
MS913, Box 25046  
Denver Federal Center  
Denver, CO 80225  
R. Snyder

U. S. Geological Survey (2)  
Water Resources Division  
Suite 200  
4501 Indian School, NE  
Albuquerque, NM 87110  
C. Peters

New Mexico Institute of Mining and  
Technology (3)  
Environmental Evaluation Group  
7007 Wyoming Blvd., NE, Suite F-2  
Albuquerque, NM 87109  
R. H. Neill, Director

NM Department of Energy & Minerals  
P.O. Box 2770  
Santa Fe, NM 87501  
K. LaPlante, Librarian

New Mexico State Engineers Office  
District II, 909 E. Second  
P.O. Box 1717  
Roswell, NM 88201  
A. Mason

U. S. Geological Survey  
Conservation Division  
P.O. Box 1857  
Roswell, NM 88201  
W. Melton

New Mexico Bureau of Mines  
and Mineral Resources (2)  
Socorro, NM 87801  
F. E. Kottolowski, Director  
J. Hawley

Battelle Pacific Northwest  
Laboratories (6)  
Battelle Boulevard  
Richland, WA 99352  
D. J. Bradley  
J. Relyea  
R. E. Westerman  
S. Bates  
H. C. Burkholder  
L. Pederson

Bechtel Inc. (2)  
P.O. Box 3965  
45-11-B34  
San Francisco, CA 94119  
E. Weber  
H. Taylor

Westinghouse Electric Corporation (8)  
P.O. Box 2078  
Carlsbad, NM 88221  
Library  
A. L. Trego  
W. P. Poirer  
W. R. Chiquelin  
V. F. Likar  
R. F. Kehrman  
K. Broberg  
R. F. Cook

Oak Ridge National Laboratory (4)  
Box Y  
Oak Ridge, TN 37830  
R. E. Blanko  
E. Bondiotti  
C. Claiborne  
G. H. Jenks

INTERA Inc. (17)  
6580 Austin Center Blvd., #300  
Austin, TX 78731  
G. E. Grisak  
J. F. Pickens  
G. J. Saulnier (5)  
J. L. Lolcama  
A. Haug  
J. D. Avis (5)  
M. Reeves  
T. L. Cauffman  
Library

INTERA Inc. (4)  
P.O. Box 2123  
Carlsbad, NM 88221  
W. A. Stensrud  
P. S. Domski  
R. Roberts  
J. B. Palmer

IT Corporation (2)  
P.O. Box 2078  
Carlsbad, NM 88221  
D. Deal

IT Corporation (4)  
5301 Central Ave., NE  
Suite 700  
Albuquerque, NM 87108  
R. F. McKinney  
M. E. Crawley  
R. M. Holt  
J. Myers

RE/SPEC, Inc. (5)  
P.O. Box 725  
Rapid City, SD 57709  
L. L. Van Sambeek  
T. Pfeifle  
G. Callahan  
J. L. Ratigan  
J. D. Osnes

RE/SPEC, Inc. (2)  
P.O. Box 14984  
Albuquerque, NM 87191  
W. E. Coons  
P. F. Gnirk

S-Cubed (3)  
P.O. Box 1620  
La Jolla, CA 92038  
E. Peterson  
P. Lagus  
K. Lie

University of Arizona  
Department of Nuclear Engineering  
Tucson, AZ 85721  
J. G. McCray

University of Wisconsin-Madison  
Department of Geology and Geophysics  
1215 W. Dayton St.  
Madison, WI 53706  
M. P. Anderson

The Pennsylvania State University  
Materials Research Laboratory  
University Park, PA 16802  
D. Roy

Texas A&M University  
Center of Tectonophysics  
College Station, TX 77840  
J. Handin

University of Texas at El Paso  
Department of Geological Sciences  
El Paso, TX 79968  
D. W. Powers

University of New Mexico (3)  
Geology Department  
Albuquerque, NM 87131  
D. G. Brookins  
M. Campana  
Library

New Mexico Tech (3)  
Department of Geoscience  
Socorro, NM 87801

J. Wilson  
F. Phillips  
C. S. Chen

Argonne National Laboratory  
9700 South Cass Avenue  
Argonne, IL 60439  
D. Hambeley

Los Alamos National Laboratory  
Los Alamos, NM 87545  
B. Erdal, CNC-11

Brookhaven National Laboratory  
Associated Universities, Inc.  
Upton, NY 11973  
P. W. Levy, Senior Scientist

National Academy of Sciences,  
WIPP Panel:

Dr. Charles Fairhurst, Chairman  
Department of Civil and  
Mineral Engineering  
University of Minnesota  
500 Pillsbury Dr., SE  
Minneapolis, MN 55455

Dr. Frank L. Parker  
Department of Environmental and  
Water Resources Engineering  
Vanderbilt University  
Nashville, TN 37235

Dr. John O. Blomeke  
Route 3  
Sandy Shore Drive  
Lenoir City, TN 37771

Dr. John D. Bredehoeft  
Western Region Hydrologist  
Water Resources Division  
U. S. Geological Survey  
345 Middlefield Road  
Menlo Park, CA 94025

Dr. Karl P. Cohen  
928 N. California Avenue  
Palo Alto, CA 94303

Dr. Fred M. Ernsberger  
250 Old Mill Road  
Pittsburgh, PA 15238

Dr. Rodney C. Ewing  
Department of Geology  
University of New Mexico  
200 Yale, NE  
Albuquerque, NM 87131

Dr. George M. Hornberger  
Department of Environmental Sciences  
Clark Hall  
University of Virginia  
Charlottesville, VA 22903

Dr. D'Arcy A. Shock  
233 Virginia  
Ponca City, OK 74601

Dr. Christopher G. Whipple  
Electric Power Research Institute  
3412 Hillview Avenue  
Palo Alto, CA 94303

Dr. Peter B. Meyers, Staff Director  
National Academy of Sciences  
Committee on Radioactive Waste  
Management  
2101 Constitution Avenue  
Washington, DC 20418

Ina Alterman  
National Academy of Sciences  
Board on Radioactive Waste  
Management  
GF462  
2101 Constitution Avenue  
Washington, DC 20418

Hobbs Public Library  
509 N. Ship Street  
Hobbs, NM 88248  
M. Lewis, Librarian

New Mexico Tech  
Martin Speere Memorial Library  
Campus Street  
Socorro, NM 87810

New Mexico State Library  
P.O. Box 1629  
Santa Fe, NM 87503  
I. Vollenhofer

Zimmerman Library  
University of New Mexico  
Albuquerque, NM 87131  
Z. Vivian

WIPP Public Reading Room  
Atomic Museum  
Kirtland East AFB  
Albuquerque, NM 87185  
G. Schreiner

WIPP Public Reading Room  
Carlsbad Municipal Library  
101 S. Halagueno St.  
Carlsbad, NM 88220  
L. Hubbard, Head Librarian

British Nuclear Fuels, PLC  
Risley, Warrington, Cheshire  
WA3 6AS 1002607 GREAT BRITAIN  
D. R. Knowles

Institut für Tieflagerung (4)  
Theodor-Heuss Strasse 4  
D-3300 Braunschweig  
FEDERAL REPUBLIC OF GERMANY  
K. Kuhn

Bundesanstalt für  
Geowissenschaften  
und Rohstoffe (3)  
Postfach 510 153  
D-3000 Hannover 51  
FEDERAL REPUBLIC OF GERMANY  
M. Langer  
P. Vogel  
K. Schelkes

Hahn-Meitner Institut für  
Kernforschung  
Glienicke Strasse 100  
100 Berlin 39  
FEDERAL REPUBLIC OF GERMANY  
W. Lutze

Bundesministerium für Forschung  
und Technologie  
Postfach 200 706  
D-5300 Bonn 2  
FEDERAL REPUBLIC OF GERMANY  
Rolf-Peter Randl

Physikalisch-Technische  
Bundesanstalt  
Postfach 33 45  
D-3300 Braunschweig  
FEDERAL REPUBLIC OF GERMANY  
P. Brenneke

Kernforschung Karlsruhe  
Postfach 3640  
D-7500 Karlsruhe  
FEDERAL REPUBLIC OF GERMANY  
K. D. Closs

Japan Atomic Energy Research Institute  
Tokai-Muri, Naka-Gun  
Ibaraki-Ken 319-11, JAPAN  
Shingo Tashiro

Svensk Kärnbränsleforsörjning AB  
Project KBS  
Kärnbränslesakerhet  
Box 5864  
S-102 48 Stockholm, SWEDEN  
F. Karlsson

Svensk Kärnbränslehantering AB (2)  
Box 5864  
S-102 48 Stockholm, SWEDEN  
A. Ström  
K.-E. Almén

Atomic Energy of Canada, Ltd. (4)  
Whiteshell Nuclear Research  
Establishment  
Pinewa, Manitoba, CANADA  
ROE 1L0  
P. Haywood  
J. Tait  
C. C. Davison  
D. Stevenson

Studiecentrum Voor Kernenergie  
Centre D'Energie Nucleaire  
SCK/CEN  
Boeratang 200  
B-2400 Mol, BELGIUM  
A. Bonne

Ontario Hydro Research Lab (2)  
800 Kipling Avenue  
Toronto, Ontario, CANADA  
M8Z 5S4  
D. K. Mukerjee  
A. T. Jakubick

Centre D'Etudes Nucleaires  
De La Vallee Rhone  
CEN//VALRHO  
S.D.H.A. BP 171  
30205 Bagnols-Sur-Ceze, FRANCE  
C. Sombret

OECD Nuclear Energy Agency  
Division of Radiation Protection  
and Waste Management  
38, Boulevard Suchet  
75016 Paris, FRANCE  
J-P Olivier

Netherlands Energy Research  
Foundation ECN (2)  
3 Westerduinweg  
P.O. Box 1  
1755 ZG Petten, THE NETHERLANDS  
T. Deboer, Mgr.  
L. H. Vons

Rijksinstituut voor Volksgezondheid en  
Milieuhygiene (2)  
Antonie van Leeuwenhoeklaan 9  
P.O. Box 1  
3720 BA Bilthoven, THE NETHERLANDS  
P. Glasbergen  
S. M. Hassanizadeh

Nationale Genossenschaft für die  
Lagerung Radioaktiver Abfälle (3)  
Parkstrasse 23  
CH-5401 Baden, SWITZERLAND  
P. Hufschmied  
C. McCombie  
M. Thury

Sveriges Geologiska AB  
Pusterviksgatan 2  
S-413 01 Goteborg, SWEDEN  
A. Winberg

Environment Canada  
National Water Research Institute  
Canada Centre for Inland Lakes  
867 Lakeshore Road  
P.O. Box 5050  
Burlington, Ontario  
L7R 4A6 CANADA  
K. S. Novakowski

Energy, Mines and Resources Canada  
Geological Survey of Canada  
601 Booth St.  
Ottawa, Ontario  
K1A 0E8 CANADA  
D. Boyle

Technical Research Center of Finland  
Nuclear Engineering Laboratory  
P.O. Box 169  
SF-00181 Helsinki, FINLAND  
V. Taivassalo

Gartner-Lee Limited  
140 Renfrew Drive  
Markham, Ontario  
L3R 6B3 CANADA  
K. G. Kennedy

University of British Columbia  
Department of Geological Sciences  
Vancouver, British Columbia  
V6T 1W5 CANADA  
R. A. Freeze

ANDRA  
31 Rue de la Federation  
75015 Paris, FRANCE  
D. Alexandre, Deputy Director

Oak Ridge National Laboratory  
Building 2001  
Ecological Sciences Information  
Center  
P.O. Box X  
Oak Ridge, TN 37830  
C. S. Fore

Princeton University  
Department of Civil Engineering  
Princeton, NJ 08504  
G. Pinder

Rockwell International  
Rocky Flats Plant  
Golden, CO 80401  
C. E. Wickland

National Ground Water  
Information Center  
6375 Riverside Drive  
Dublin, OH 43017  
J. Bix

University of California (3)  
Lawrence W. Berkeley Laboratory  
Berkeley, CA 94720  
P. A. Witherspoon  
J. C. S. Long  
S. M. Benson

Kansas Geological Survey  
University of Kansas  
1930 Constant Avenue, Campus West  
Lawrence, KS 66046  
J. Butler

Roswell Public Library  
301 N. Pennsylvania Avenue  
Roswell, NM 88201  
N. Langston

U. S. Geological Survey  
Water Resources Division  
521 W. Seneca St.  
Ithaca, NY 14850  
R. M. Yager

U. S. Geological Survey (2)  
Water Resources Division  
345 Middlefield Rd.  
Menlo Park, CA 94025  
P. Hsieh  
A. F. Moench

Texas A&M University  
Department of Geology  
College Station, TX 77843  
P. A. Domenico

Pannell Library  
New Mexico Junior College  
Lovington Highway  
Hobbs, NM 88240  
R. Hill

Government Publications Dept.  
General Library  
University of New Mexico  
Albuquerque, NM 87131

Savannah River Laboratory (6)  
Aiken, SC 29801  
N. Bibler  
E. L. Albenisius  
M. J. Plodinec  
G. G. Wicks  
C. Jantzen  
J. A. Stone

Savannah River Plant  
Building 704-S  
Aiken, SC 29808  
R. G. Baxter

Arthur D. Little, Inc.  
Acorn Park  
Cambridge, MA 01240-2390  
C. R. Hadlock

Emcon Associates  
1921 Ringwood Avenue  
San Jose, CA 95131  
F. W. Fenzel

University of Arizona  
Department of Hydrology  
Tucson, AZ 85721  
S. P. Neuman

L. Lehman and Associates, Inc.  
1103 W. Burnsville Parkway  
Suite 209  
Minneapolis, MN 55337  
L. Lehman

S. S. Papadopoulos and Assoc., Inc.  
12596 W. Bayaud Ave., Suite 290  
Lakewood, CO 80228  
J. W. Anthony

Golder Associates  
4104 148th Avenue NE  
Redmond, WA 98052  
T. W. Doe

Scientific Software-Intercomp  
1801 California, 2nd Floor  
Denver, CO 80202  
J. M. Sofia

SAIC  
10260 Campus Point Drive  
San Diego, CA 92121  
H. R. Pratt

SAIC  
Suite 1250  
160 Spear St.  
San Francisco, CA 94105  
M. B. Gross

SAIC  
101 Convention Center Dr.  
Las Vegas, NV 89109  
G. Dymmel

Thomas Brannigan Library  
106 W. Hadley St.  
Las Cruces, NM 88001  
D. Dresp, Head Librarian

Sandia Internal:

1510	J. W. Nunziato	6342	K. Brinster
1511	D. F. McTigue	6342	M. G. Marietta
1520	C. W. Peterson	6342	R. P. Rechard
1521	R. D. Krieg	6343	T. M. Schultheis
1521	H. S. Morgan	6344	E. D. Gorham
3141	S. A. Landenberger (5)	6344	R. L. Beauheim (5)
3151	W. I. Klein (3)	6344	P. B. Davies
3154-1	C. L. Ward, for DOE/OSTI (8)	6344	S. J. Finley
6000	D. L. Hartley	6344	A. L. Jensen
6200	V. L. Dugan	6344	A. M. LaVenue
6232	W. R. Wawersik	6344	R. Z. Lawson
6233	T. M. Gerlach	6344	M. D. Siegel
6253	D. A. Northrup	6344	S. W. Webb
6253	N. R. Warpinski	6345	A. R. Lappin
6300	R. W. Lynch	6345	L. H. Brush
6310	T. O. Hunter	6345	K. L. Robinson
6311	A. L. Stevens	6346	J. R. Tillerson
6312	F. W. Bingham	6416	E. J. Bonano
6313	T. E. Blejwas	9300	J. E. Powell
6315	L. E. Shephard	9310	J. D. Plimpton
6316	R. P. Sandoval	9320	M. J. Navratil
6317	S. Sinnock	9325	R. L. Rutter
6340	W. D. Weart	9325	J. T. McIlmoyle
6340	S. Y. Pickering	9330	J. O. Kennedy
6341	R. C. Lincoln	9333	O. L. Burchett
6341	R. L. Hunter	9333	J. W. Mercer
6341	Sandia WIPP Central Files (5)	9335	P. D. Seward
	(700HIND)	8524	J. A. Wackerly (SNLL Library)
6342	D. R. Anderson		



8232-2/070179



00000001 -



8232-2/070179



00000001 -



8232-2/070179



00000001 -